ANISOTROPIC SUPERCONDUCTORS AND ELASTIC IMPURITY SCATTERING

ANISOTROPIC SUPERCONDUCTORS AND ELASTIC IMPURITY SCATTERING

By

JOHANNA MARIA DAAMS, M.SC.

A Thesis

Submitted to the School of Graduate Studies

in Partial Fulfilment of the Requirements

for the Degree

Doctor of Philosophy

McMaster University

November 1977

DOCTOR OF PHILOSOPHY (1977)
(Physics)

McMASTER UNIVERSITY
Hamilton, Ontario.

TITLE: Anisotropic Superconductors and Elastic Impurity Scattering

AUTHOR: Johanna Maria Daams B.Sc. 1973 Queen's
M.Sc. 1974 McMaster

SUPERVISOR: Professor J. P. Carbotte

NUMBER OF PAGES: xi,241

SCOPE AND CONTENTS:

ABSTRACT

The thermodynamic properties of a number of simple metals in the superconducting state are calculated from the numerical solution of the isotropic Eliashberg equations on the imaginary axis and comparison is made with experiment. The functional derivatives of these properties with respect to change in the electron-phonon interaction are calculated and used in a detailed analysis of the interaction in superconducting Nb. Anisotropy in the electron-phonon interaction is also investigated numerically for some metals using a simple model for the anisotropy. The functional derivative in an anisotropic superconductor is found to be qualitatively different at low frequencies from that of an isotropic system. The difference is shown to be caused by the washing out of anisotropy by thermal phonons. Some comparison with experiment and with previous approximate solutions of the same model is made. For some quantities the previous approximate estimates of the effect of gap anisotropy are shown to be inadequate. A useful expression relating the amount of anisotropy with the impurity dependence of the critical temperature is developed independent of any such model or approximation.

Another calculation is done with a realistic calculated interaction for lead that includes anisotropy in the phonons

and Fermi surface. An orthonormal basis set for the expansion of this interaction is enumerated and tested, but is found unnecessary for lead because the interaction is very close to separable. It is shown that the anisotropy in the interaction can be approximated by a very simple separable model without significantly affecting the thermodynamic properties. Also, the gap anisotropy on the imaginary axis is found to be identical to that of the gap edge at T=0 calculated on the real axis from the same interaction.

ACKNOWLEDGEMENTS

I would like to thank my research supervisor, Dr. J. P. Carbotte for his guidance and encouragement in this work.

I wish to thank Dr. C. R. Leavens, and Dr. F. W. Kus for helpful discussions and aid with the programming.

The financial assistance of the National Research Council of Canada is gratefully acknowledged.

Finally, I want to thank Mrs. Helen Kennelly for patiently and accurately typing a chaotic manuscript.

TABLE OF CONTENTS

LIST OF FIGURES

LIST OF TABLES

CHAPTER 1

INTRODUCTION

Because the BCS theory of superconductivity and its extension by Eliashberg to systems with a strong electron-phonon interaction have been so successful, it is possible to relate the small remaining discrepancies between theory and experiment to the details of the electron-phonon interaction in a particular material. The detail being investigated here is the anisotropy in the electron-phonon interaction, which can easily be taken care of, formally at least, by the addition of another subscript for the sums over the Fermi surface. Predicting the effects of this anisotropy on the gap or other measurable quantities is not so easy, either with an analytical expression or by numerical calculation. Since previous work has focused on approximate solutions of model anisotropic interactions (for weak-coupling superconductors) and incompletely iterated solutions with a realistic interaction, an attempt will be made here to get exact solutions for the model interaction in both weak and strong coupling systems and a completely converged solution for a realistic calculated interaction in Pb. Both calculations are done numerically but on the imaginary axis, thus limiting the discussion to thermodynamic properties except in Pb, where a comparison will be

made between gap anisotropy on the real and imaginary axis. For that metal also an expansion of the interaction in terms of a recently suggested set of orthonormal basis functions suitable for anisotropic quantities defined on the Fermi surface will be tested. Another calculation with a simple but justifiable model anisotropy will show how the previously mentioned approximate solution compares with the exact numerical results, and whether the experimental data is consistent with a small amount of anisotropy or not. One other possible cause for the small discrepancy between theory and experiment, an error in the average interaction (not in the anisotropy) will be investigated by means of the functional derivatives of some thermodynamic properties with respect to the interaction. Niobium will serve as an example for this kind of analysis.

Elastic scattering by non-magnetic impurities usually forms a part of any discussion of anisotropy effects because it controls the amount of gap anisotropy by disrupting the pair formation. The part of the thermodynamic properties due to anisotropy in the electron-phonon interaction can therefore be found indirectly by comparing measurements in the pure material and in a dilute alloy. This relationship between gap anisotropy and impurity concentration will be investigated numerically, and a simple expression relating the rate of change of T_c to the amount of gap anisotropy will be derived. The next chapter presents the theory on which all these calculations are based.

CHAPTER 2

THE ELECTRON-PHONON INTERACTION, ANISOTROPIC SUPERCONDUCTORS, AND ELASTIC IMPURITY SCATTERING

1. Necessary Theoretical Background

In this section the equations used throughout the rest of the thesis will be presented, but with relatively little discussion because strong-coupling theory is well-established and hardly new. Since a detailed understanding of superconductivity, as is essential for calculating anisotropy effects because they are usually so small, requires knowledge of the electron-phonon interaction, that is the best place to start.

Although the potentials near the positively-charged ions in a metal are large and rapidly varying, the conduction electrons behave very much like free electrons, because the effective ionic potentials are relatively weak for the following reasons. First, the Pauli exclusion principle keeps the conduction electrons away from the core region where the already-filled atomic orbitals are localized. Secondly, some conduction electrons are attracted to the positive charge and therefore screen it from more distant electrons. These two factors permit the replacement of the strong field around each ion by the pseudopotential, a much weaker non-singular effective interaction that has these two effects built into it.

The pseudopotential can then be treated as a perturbation to second order for the conduction electrons. From this description it should be clear that the pseudopotential is a rather complicated function, not necessarily unique, and will in general be non-local. However, even if a local approximation is made, the resulting function turns out to be quite adequate for certain calculations, for example phonons in simple metals, and of course the electron-phonon interaction itself. The Fourier transform of the pseudopotential $W(\underline{q})$ is, at least for the nearly-free electron metals, a flat-bottomed well of depth $2/3\ E_F$ and radius of order $2k_F$ which falls off rapidly for large $\underline{q}$. An impurity atom can also be assigned a pseudopotential, or rather the difference $\Delta W(\underline{q})$ between host and impurity, (although the pseudopotential of an impurity of different valence than the host may be too strong for perturbative treatment). The impurity pseudopotential will depend on the host through the influence of the electron density on the screening. The $2/3\ E_F$ rule still holds though, implying that $\Delta W(0) = 0$ for isovalent impurities. The current state of the art for impurity pseudopotentials does not seem to be quite as good as for the host, for which the Fermi surface determined by $W(\underline{q})$ can be checked against de Haas-van Alphen data. The perturbation caused by the pseudopotentials is not carried past second order (the first order change in the energy is absorbed in a Fermi energy redefinition) and is important only for electrons near the intersection of the Fermi surface with the

Bragg planes because these are the only degenerate states between which the periodic array of ions can cause transitions. This periodicity ensures that the only possible momentum transfers are of reciprocal lattice vectors $\underline{\kappa}_n$, and that the new wave function; the pseudo-wave function, is, outside the core, a linear combination of plane wave states:

$$|\text{pseudo-wave function}\rangle_{\underline{k}} = |\underline{k}\rangle - \sum_n a_{\underline{\kappa}_n}(\underline{k})\,|\underline{k}+\underline{\kappa}_n\rangle \qquad (2\text{-}1)$$

where the $a_{\underline{\kappa}_n}$ are the plane wave mixing coefficients and $|\underline{k}\rangle$ is a plane wave state. A one plane-wave approximation (no sum over n) will therefore be just a spherical Fermi surface, while for a multi plane-wave solution the $a_{\underline{\kappa}_n}(\underline{k})$ determine the shape of the Fermi surface, the weight $dS_{\underline{k}}/|v_{\underline{k}}|$ of a given point $\underline{k}$, the Fermi velocity $\underline{v}_{\underline{k}}$ and the band mass renormalization. The $a_{\underline{\kappa}_n}(\underline{k})$ need only be specified over a small fraction of the Fermi surface, the irreducible 48th, (defined by $k_y \geq 0$, $k_x \geq k_y$, $k_z \geq k_x$), if there is cubic symmetry; the velocities and weights elsewhere can be found by applying group operations.

In principle the phonons could also be calculated from first principles by screening the plasma oscillations of the bare ions; but this procedure has only been done for the simplest metals - a category, which for this particular calculation, excludes Pb. For others force constants have been fitted to dispersion curves for high symmetry directions obtained from neutron scattering. These constants are sufficient to determine the frequencies $\omega_{q\lambda}$ and, polarization vectors $\underline{\xi}^{\lambda}(\underline{q})$ for

any wave vector $\underline{q}$ and branch λ, the density $F(\omega)$ of phonon states and the density of states $F(\underline{q},\omega)$ for a particular momentum $\underline{q}$.

The electron-phonon matrix element between two plane-wave states is, with

$$\delta W(\underline{r}) \equiv \Sigma\, W(\underline{r}-\underline{R}_\ell) - W(\underline{r}-\underline{R}^o_\ell) ,$$

being the pseudopotential,

$$\langle\underline{k}|\delta W|\underline{k}'\rangle = \frac{1}{\Omega}\sum_\ell \int d^3\underline{r}\; e^{i(\underline{k}-\underline{k}')\cdot\underline{r}}[W(\underline{r}-\underline{R}_\ell)-W(\underline{r}-R^o_\ell)] \qquad (2\text{-}2)$$

where $\underline{R}^o_\ell$ is the equilibrium position of ion ℓ, $\underline{R}_\ell$ the displaced position, and Ω the crystal volume. For small displacements $\underline{R}_\ell-\underline{R}^o_\ell$ may be expanded in phonon annihilation and creation operators after the transformation to normal modes is made. The matrix element $g_{\underline{kk}'\lambda}$ for the transition between the multi-plane wave states $\underline{k}$ and $\underline{k}'$ brought about by the phonon $\underline{q}\lambda$ is then

$$g_{\underline{kk}'\lambda} = \frac{-i}{\sqrt{2MN\omega_{\lambda\underline{k}-\underline{k}'}}}\,\underline{\xi}^\lambda(\underline{k}'-\underline{k}) \;. \qquad (2\text{-}3)$$

$$\sum_{nn'} a^*_{\underline{\kappa}_{n'}}(\underline{k}')\,a_{\underline{\kappa}_n}(\underline{k})\,(\underline{k}'+\underline{\kappa}_{n'}-\underline{k}-\underline{\kappa}_n)\,\langle\underline{k}'+\underline{\kappa}_{n'}|\delta W|\underline{k}+\underline{\kappa}_n\rangle \;.$$

where M is the ionic mass and N the total number of atoms in the crystal. This together with the Fermi surface data is all the information needed to see how the phonons modify the behaviour of the electrons, although later it will be rearranged in a more convenient form.

Since the thermodynamic properties and dynamical response of interacting particles can be expressed in terms of the expectation values of certain combinations of second quantized operators, the Green's functions which are closely related to such averages, are sufficient to describe the system. Evaluated at a discrete set of points on the imaginary axis, they give only the thermodynamics, evaluated on the real axis they give that and the dynamic properties. Actually it is not so much the electron Green's functions that are required as the self-energies (Σ), which embody the changes caused by many-body effects. These changes may be determined self-consistently through the following choice of diagrams:

Σ = 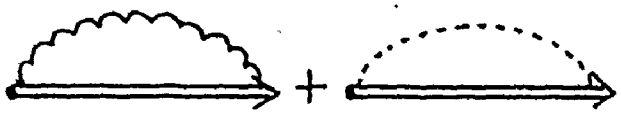

The first is the emission and reabsorption of a phonon, the second the Coulomb interaction. No further vertex corrections for the phonons are necessary, thanks to Migdal's theorem which is connected to the adiabatic approximation stated in terms of Green's functions. The Coulomb interaction is of course not so easily disposed of, but in a superconductor a very detailed treatment turns out to be unnecessary, since much of the interaction can be absorbed by suitable renormalization[56]; also the attractive force responsible for superconductivity, the electron-phonon interaction, is limited to a very small frequency interval (of order ω_D, the Debye temperature) over which the Coulomb interaction, (which extends to frequencies

of the order E_F, the Fermi energy) can be treated as a constant. In fact, in order to cut off frequency sums at ω_c, usually taken as 5 or 10 times the maximum phonon frequency rather than E_F, the Coulomb interaction below ω_c is replaced by an effective interaction, which takes into account the omitted frequency range above ω_c. As mentioned earlier, the Coulomb interaction is nearly constant over this small interval, so that a single frequency-independent constant μ^* turns out to be quite adequate. There is no $\underline{k}$- or frequency dependence because the effective interaction is instantaneous and very short range, the long range part being screened out. The theory is good enough to give an order of magnitude estimate for μ^*, but since this is far less than the accuracy with which the electron-phonon interaction is known, μ^* is customarily fitted to some measurable property. Since it is a pseudopotential, it will depend somewhat on ω_c and the method of summation, i.e. on the real or imaginary axis[78]. This situation justifies to a large extent the sort of manipulation done later to obtain numerical results.

Returning to eqn. (2-3), and writing it out in terms of the phonon propagator $D_\lambda(\underline{q}, i\omega_n)$, the vertex element $|g_{\underline{k}\underline{k}',\lambda}|^2$, the electron Green's function, $G(\underline{k}, i\omega_n)$ and its self-energy $\Sigma(\underline{k}, i\omega_n)$, one finds

$$\Sigma(\underline{k}, i\omega_n) = k_B T \sum_{\underline{k}' m \lambda} \{\Sigma |g_{\underline{k}\underline{k}',\lambda}|^2 D_\lambda(\underline{k}-\underline{k}', i\omega_n - i\omega_m) - \mu^*\} \tau_3 G(\underline{k}', i\omega_m) \tau_3 \tag{2-4}$$

In this equation the electron Green's functions are being evaluated on the imaginary axis at the Matsubara frequencies ω_n, where $i\omega_n = i\pi k_B T(2n-1)$ and the phonon propagators at even multiples of $i\pi k_B T$. The Matsubara frequencies also determine the number of terms in the summation, which is truncated for $\omega_n > \omega_c$. The phonon propagator here is not an unknown to be found, but is identical to the free phonon Green's function

$$D_\lambda(\underline{q}, z) = \frac{2\omega_{\underline{q}\lambda}}{\omega^2_{\underline{q}\lambda} - z^2} \quad . \tag{2-5}$$

since the phonon frequencies are almost unaffected by the superconducting transition. The electron Green's functions are greatly changed; in fact eqn. (2-4) is a 2×2 matrix equation with the diagonal terms corresponding to the normal part of the electron-phonon interaction and the off-diagonal terms to the gap. It can however be reduced to only two independent equations, which are, after the following definitions

$$G(\underline{k}, i\omega_n) \equiv \frac{1}{i\omega_n 1 - \varepsilon_{\underline{k}}\tau_3 - \Sigma(\underline{k}, i\omega_n)} \tag{2-6}$$

$$\Sigma(\underline{k}, i\omega_n) \equiv i(\tilde{\omega}_{\underline{k}}(n) - \omega_n)1 + i\tilde{\Delta}_{\underline{k}}(n)\tau_1 \tag{2-7}$$

(the τ are the Pauli spin matrices) eqns. (2-8) and (2-9):

$$\tilde{\Delta}_{\underline{k}}(n) = \frac{(2\pi)^3}{\Omega} k_B T \sum_{\underline{k}', m} (\lambda_{\underline{k}\underline{k}'}(m-n) - \mu^*) \frac{\tilde{\Delta}_{\underline{k}'}(m)}{\tilde{\omega}^2_{\underline{k}'}(m) + \varepsilon^2_{\underline{k}'} + \tilde{\Delta}^2_{\underline{k}'}(m)} \tag{2-8}$$

$$\tilde{\omega}_{\underline{k}}(n)-\omega_n = \frac{(2\pi)^3}{\Omega} k_B T \sum_{\underline{k}',m} \lambda_{\underline{k}\underline{k}'}(m-n) \frac{\tilde{\omega}_{\underline{k}'}(m)}{\tilde{\omega}^2_{\underline{k}'}(m)+\varepsilon^2_{\underline{k}'}+\tilde{\Delta}^2_{\underline{k}'}(m)}. \quad (2\text{-}9)$$

These are the Eliashberg equations. Here $\varepsilon_{\underline{k}}$ is the single-particle energy measured from the Fermi energy and $\lambda_{\underline{k}\underline{k}'}(m)$ contains the phonon propagator:

$$\lambda_{\underline{k}\underline{k}'}(m) = \sum_{\lambda} |g_{\underline{k}\underline{k}'\lambda}|^2 D_{\lambda}(\underline{k}-\underline{k}', 2m\pi i k_B T) \quad (2\text{-}10)$$

which can be rewritten as (see footnote, pg. 12).

$$\lambda_{\underline{k}\underline{k}'}(m) = \int \frac{2\omega d\omega}{\omega^2 + \omega_m^2} (\alpha^2 F(\omega))_{\underline{k}\underline{k}'} \quad (2\text{-}11)$$

where $\underline{q} = \underline{k}-\underline{k}'$

$$(\alpha^2 F(\omega))_{\underline{k}\underline{k}'} \equiv \sum_{\lambda} \frac{\Omega}{(2\pi)^3} |g_{\underline{k}\underline{k}'\lambda}|^2 \delta(\omega-\omega_{\underline{q}\lambda}) \quad (2\text{-}13)$$

is seen to be the phonon density of states $F(\underline{k}-\underline{k}',\omega)$ weighted by the effectiveness of these particular phonons for causing a transition between electron states $\underline{k}$ and $\underline{k}'$.

Equations (2-8) and (2-9) can be simplified in the conventional way by using the fact that $\Sigma(\underline{k}, i\omega_n)$ has very little $\varepsilon_{\underline{k}}$ dependence, which allows, when the summation $\sum_{\underline{k}'}$ is rewritten as $\frac{\Omega}{(2\pi)^3} \int \frac{dS_{\underline{k}'}}{|v_{\underline{k}'}|} \int d\varepsilon$, the treatment of the upper k' belongs to the top line, not to $\tilde{\omega}_{\underline{k}}(m)$ as constants during the ε-integration. If the limits of integration are extended to $\pm \infty$ (which is permissible because $E_F >> \tilde{\omega}_{\underline{k}}$ or $\tilde{\Delta}_{\underline{k}}$) equations (2-8) and (2-9) become

$$\tilde{\Delta}_{\underline{k}}(n) = \pi k_B T \sum_m \int \frac{dS_{\underline{k}'}}{|v_{\underline{k}'}|} (\lambda_{\underline{k}\underline{k}'}(m-n) - \mu^*) \frac{\tilde{\Delta}_{\underline{k}'}(m)}{\sqrt{\tilde{\Delta}^2_{\underline{k}'}(m) + \tilde{\omega}^2_{\underline{k}'}(m)}} \qquad (2\text{-}13)$$

$$\tilde{\omega}_{\underline{k}}(n) = \omega_n + \pi k_B T \sum_m \int \frac{dS_{\underline{k}'}}{|v_{\underline{k}'}|} \lambda_{\underline{k}\underline{k}'}(m-n) \frac{\tilde{\omega}_{\underline{k}'}(m)}{\sqrt{\tilde{\Delta}^2_{\underline{k}'}(m) + \tilde{\omega}^2_{\underline{k}'}(m)}} \qquad (2\text{-}14)$$

It is sometimes more convenient to write these two equations in terms of $\bar{\Delta}_{\underline{k}}(n) \equiv \tilde{\Delta}_{\underline{k}}(n)/|\tilde{\omega}_{\underline{k}}(n)|$:

$$\frac{|\tilde{\omega}_{\underline{k}}(n)|\bar{\Delta}_{\underline{k}}(n)}{\pi k_B T} = \sum_m \int \frac{dS_{\underline{k}'}}{|v_{\underline{k}'}|} (\lambda_{\underline{k}\underline{k}'}(m-n) - \mu^*) \frac{\bar{\Delta}_{\underline{k}'}(m)}{\sqrt{1+\bar{\Delta}^2_{\underline{k}'}(m)}} \qquad (2\text{-}15)$$

$$\frac{|\tilde{\omega}_{\underline{k}}(n)|}{\pi k_B T} = 2n-1 + \sum_m \int \frac{dS_{\underline{k}'}}{|v_{\underline{k}'}|} \lambda_{\underline{k}\underline{k}'}(m-n) \frac{\mathrm{sgn}(\omega_n \omega_m)}{\sqrt{1+\bar{\Delta}^2_{\underline{k}'}(m)}} \qquad (2\text{-}16)$$

The factor $\mathrm{sgn}(\omega_n \omega_m)$ appears in eqn. (2-16) but not (2-15) because $\bar{\Delta}_k(n)$ and $\tilde{\Delta}_{\underline{k}}(n)$ are even functions of n while $\tilde{\omega}_{\underline{k}}(n)$ is not.

These non-linear equations have non-trivial solutions only for $T < T_c$. At T_c they can be linearized by setting the $\tilde{\Delta}_{\underline{k}'}(m)$ or $\bar{\Delta}_{\underline{k}'}(m)$ under the square root to zero. The transition temperature could be found by extrapolating the gap $\bar{\Delta}_{\underline{k}}(n)$ to the temperature where it vanishes, but in practice it is easier to find T_c as the temperature where the linearized equation

$$\tilde{\Delta}_{\underline{k}}(n) = \pi k_B T \sum_m \int \frac{dS_{\underline{k}'}}{|v_{\underline{k}'}|} (\lambda_{\underline{k}\underline{k}'}(m-n) - \mu^*) \frac{\tilde{\Delta}_{\underline{k}'}(m)}{|\tilde{\omega}_{\underline{k}'}(m)|} \qquad (2\text{-}17)$$

has a non-trivial solution. Here

$$\tilde{\omega}_{\underline{k}}(n) = \omega_n + \pi k_B T \sum_m \lambda_{\underline{k}}(m-n)\,\mathrm{sgn}(\omega_m) \quad , \tag{2-18}$$

and

$$\lambda_{\underline{k}}(m) = \int \frac{dS_{\underline{k}'}}{|v_{\underline{k}'}|} \lambda_{\underline{k}\underline{k}'}(m) \tag{2-19}$$

is a partial average of $\lambda_{\underline{k}\underline{k}'}$, which can also be written as

$$\lambda_{\underline{k}}(m) = \int \frac{d\omega\ \omega}{\omega^2+\omega_m^2} \left(\alpha^2 F(\omega)\right)_{\underline{k}}^{\dagger} \tag{2-20}$$

where

$$\left(\alpha^2 F(\omega)\right)_{\underline{k}} \equiv \int \frac{dS_{\underline{k}'}}{|v_{\underline{k}'}|} \left(\alpha^2 F(\omega)\right)_{\underline{k}\underline{k}'} \quad . \tag{2-21}$$

If an approximate solution in which the $\underline{k}$-dependence of $\tilde{\Delta}_{\underline{k}}(n)$ and $\tilde{\omega}_{\underline{k}}(n)$ is ignored is desired, then equations (2-15), (2-16), (2-17) and (2-18) become:

$$\frac{|\tilde{\omega}(n)|}{\pi k_B T}\,\bar{\Delta}(n) = \sum_m \left(\lambda(m-n)-\mu^*\right) \frac{\bar{\Delta}(m)}{\sqrt{1+\bar{\Delta}^2(m)}} \tag{2-22}$$

$$\frac{|\tilde{\omega}(n)|}{\pi k_B T} = |2n-1| + \sum_m \lambda(m-n) \frac{\mathrm{sgn}(\omega_n \omega_m)}{\sqrt{1+\bar{\Delta}^2(m)}} \tag{2-23}$$

$$\tilde{\Delta}(n) = \pi k_B T \sum \left(\lambda(m-n)-\mu^*\right) \frac{\tilde{\Delta}(m)}{|\tilde{\omega}(m)|} \tag{2-24}$$

In this expression ω_m is an even, not an odd multiple of $\pi k_B T$ as in (2-18). It should be clear henceforth from the context how the ω_m is to be interpreted - always even when they appear with $\lambda(m)$.

and

$$\tilde{\omega}(n) = \omega_n + \pi k_B T \sum_m \lambda(m-n)\,\mathrm{sgn}\omega_m \qquad (2\text{-}25)$$

where the $\lambda(m)$ which are the average of $\lambda_{\underline{k}}(m)$ can also be written as

$$\lambda(m) = \int \frac{2\omega d\omega}{\omega^2+\omega_m^2}\,\alpha^2F(\omega) \qquad (2\text{-}26)$$

with $\alpha^2F(\omega)$ being the obvious average:

$$\iint \frac{dS_{\underline{k}}}{|v_{\underline{k}}|}\frac{dS_{\underline{k}'}}{|v_{\underline{k}'}|}\,(\alpha^2F(\omega))_{\underline{k}\underline{k}'} \Big/ \int \frac{dS_{\underline{k}''}}{|v_{\underline{k}''}|} \quad . \qquad (2\text{-}27)$$

If the Fermi surface is spherical, then $(\alpha^2F(\omega))_{\underline{k}\underline{k}'}$ is a function of $\underline{k}-\underline{k}'$ only and a purely geometrical identity may be used to rewrite eqns. (2-27) and (2-3) as

$$\alpha^2F(\omega) = \frac{\Omega}{N}\int_{|q|<2k_F} d^3\underline{q}\,\frac{m}{32\pi^3\hbar^2Mk_F}\sum_\lambda \frac{|\underline{q}\cdot\underline{\xi}^\lambda(\underline{q})|}{|q|\omega_{\underline{q}\lambda}}\,W^2(\underline{q})\,\delta(\omega-\omega_{\underline{q}\lambda}) \quad . \qquad (2\text{-}28)$$

(m is the electron mass, $\hbar$ Planck's constant over 2π).

$\alpha^2F(\omega)$ is, like its antecedent $(\alpha^2F(\omega))_{\underline{k}\underline{k}'}$, therefore a phonon density of states weighted according to the effectiveness of the phonons of frequency ω for causing transitions between any two states on the Fermi surface. The original notation, $\alpha^2(\omega)F(\omega)$, reflects this interpretation, $\alpha^2(\omega)$ being the weight factor, but became too unwieldy when 2 or 4 subscript $\underline{k}$'s were added and functional derivatives were taken with respect to it, hence the peculiar compromise $\alpha^2F(\omega)$ used

Because the gap on the imaginary axis is not directly measurable, but its analytic continuation on the real axis is, the relationship is worth writing out. Since $i\tilde{\Delta}_{\underline{k}}(n)$ and $i\tilde{\omega}_{\underline{k}}(n)$ are both Green's functions, (or rather integrals over energy of Green's functions) they must satisfy certain spectral relations such as

$$G(\underline{k},i\omega_n) = \frac{1}{\pi}\int_{-\infty}^{\infty} d\omega' \frac{\rho(\underline{k},\omega')}{i\omega_n-\omega'} \qquad (2\text{-}29)$$

where $\rho(\underline{k},\omega)$, a real function, is given by the difference in the imaginary part of $G(k,Z)$ across the branch cut on the real axis:

$$\begin{aligned} 2i\rho(\underline{k},\omega) &= \lim_{\delta\to 0}[G(\underline{k},\omega+i\delta)-G(\underline{k},\omega-i\delta)] \\ &= 2i\ \mathrm{Im}G(\underline{k},\omega+i\delta) \end{aligned} \qquad (2\text{-}30)$$

When a similar substitution is made for the phonon Green's functions, and the sums over discrete frequencies are converted using Poisson's formula to integrals on the real axis, the Eliashberg equations become

$$\Delta_{\underline{k}}(\omega)Z_{\underline{k}}(\omega) = \int \frac{dS_{\underline{k}'}}{|v_{\underline{k}'}|}\int_0^{\omega_c} d\omega' \mathrm{Re}\left[\frac{\Delta_{\underline{k}'}(\omega')}{\sqrt{\omega'^2-\Delta^2_{\underline{k}'}(\omega')}}\right]\left[\int d\Omega K_+(\omega,\underline{k},\omega',\underline{k}',\Omega)\right.$$

$$\left. - \mu^* \tanh\frac{\omega'}{2k_BT}\right] \qquad (2\text{-}31)$$

$$\omega(1-Z_{\underline{k}}(\omega)) = \int \frac{dS_{\underline{k}'}}{|v_{\underline{k}'}|} \int_0^{\omega_c} d\omega' \mathrm{Re}\left\{\frac{\omega'}{\sqrt{\omega'^2-\Delta^2_{\underline{k}'}(\omega')}}\right\} \int d\Omega K_- (\omega,\underline{k},\omega',\underline{k}',\Omega) \tag{2-32}$$

where $K_{\pm}(\omega,\underline{k},\omega',\underline{k}',\Omega) \equiv (\alpha^2 F(\Omega))_{\underline{k}\underline{k}'}[(n(\Omega)+f(-\omega'))(\frac{1}{\omega'+\omega+\Omega+i\delta} \pm \frac{1}{\omega'-\omega+\Omega-i\delta}) \mp (n(\Omega)+f(\omega'))(\frac{1}{-\omega'+\omega+\Omega+i\delta} \pm \frac{1}{\omega'-\omega+\Omega-i\delta})]$ and $f(\omega')$ and $n(\Omega)$ are the usual fermion and boson occupation numbers.

$Z_{\underline{k}}(\omega)$ and $\Delta_{\underline{k}}(\omega)$ are related to the self energy of the matrix Green's function on the real axis by

$$\Sigma(\underline{k},\omega) = -\omega(Z_{\underline{k}}(\omega)-1)1 + \varepsilon_{\underline{k}}\tau_3 + \omega Z_{\underline{k}}(\omega)\Delta_{\underline{k}}(\omega)\tau_1. \tag{2-33}$$

Hence $\omega Z_{\underline{k}}(\omega)$ and $\Delta_{\underline{k}}(\omega)$ are therefore the real-axis analogues of $\tilde{\omega}_{\underline{k}}(n)$ and $\bar{\Delta}_{\underline{k}}(n)$.

Another directly measurable quantity is the free energy difference between the normal and superconducting states. Being a perfect diamagnet, a superconductor in an applied magnetic field $\underline{B}$ acquires a magnetic moment $M = -B/4\pi$, which will increase its free energy per unit volume by

$$\Delta F = \frac{1}{8\pi} B^2 = \frac{1}{8\pi} H_c^2 . \tag{2-34}$$

When this quantity becomes greater than the free energy difference in the absence of an applied field between the normal and superconducting states, a transition occurs and the system switches back to the normal state, hence the term critical field ($H_c(T)$). Since this field has a nearly parabolic temperature dependence for all superconductors, the details of a particular sytem are best displayed in the deviation D(t) from a parabola:

$H_c(T)$

where t is the reduced temperature T/T_c. As this equation shows, the superconducting transition is second-order (since $H_c(T_c) = 0$), corresponding to a finite specific heat jump at T_c. Since $H_c(T)$ is linear in $T_c - T$ just below T_c, the specific heat difference $\Delta C_v(T_c)$ at T_c can be expressed in terms of $(dH_c/dT)_{T_c}$ by an obvious thermodynamic relationship which is usually referred to as Rutger's equation:

$$\Delta C_v(T_c) = k_B T_c (dH_c/dT)^2_{T_c}/4\pi \quad . \qquad (2\text{-}36)$$

The following discussion is largely based on a paper by Wada[79]. He finds the free energy difference between the normal and superconducting states by expressing in terms of Green's functions the difference in the expectation value of the operator

$$K \equiv H_0 + H_{ep} + H_{ee} \qquad (2\text{-}37)$$

where H_0 is the Hamiltonian for the non-interacting electrons and phonons, H_{ep} the electron-phonon interaction and H_{ee} the Coulomb interaction between the electrons. In terms of Green's functions,

$$\langle K \rangle = k_B T \sum_{\underline{k}n} \mathrm{tr}\{G(\underline{k}, i\omega_n)\varepsilon_{\underline{k}}\tau_3 + \frac{1}{2}\Sigma(\underline{k}, i\omega_n)G(\underline{k}, i\omega_n)\} + 2\langle K_M \rangle \qquad (2\text{-}38)$$

where tr stands for the trace and K_M is the ion kinetic energy, which must somehow be eliminated from eqn. (2-38) in favour of electron Green's functions. This is done using the so-called

Chester's relation[20], another quite general thermodynamic relationship

$$K_M = -M(\partial F/\partial M)_T = -\frac{\Omega}{4\pi} H_c M \frac{\partial H_c}{\partial M} \qquad (2\text{-}39)$$

(here M is the atomic mass)

through which certain assumptions about the isotope effect will enter into the derivation. So far no approximations have been made, but now, in order to remove the unknown, the free energy, from the right side of eqn. (2-38) and get a closed expression, it becomes necessary to assume some sort of mass dependence for the critical field. The obvious assumption, based on eqn. (2-3), that $H_c \propto M^{-1/4}$, is only approximately true because the Coulomb pseudopotential depends on the choice of ω_c, which is in turn proportional to the maximum phonon frequency. It is also necessary to assume that $H_c(T)/H_c(0)$ is independent of M, another approximation that would be exact only if μ^* were independent of M. With these assumptions, eqn. (2-38) becomes

$$\Delta F = -N(0)k_B T\Delta \sum_{\underline{k},n} \frac{\omega_n \tilde{\omega}_{\underline{k}}(n)+\varepsilon_{\underline{k}}^2}{\tilde{\omega}_{\underline{k}}^2(n)+\varepsilon_{\underline{k}}^2+\tilde{\Delta}_{\underline{k}}^2(n)} \qquad (2\text{-}40)$$

where N(0) is the single-spin density of states at the Fermi surface, and the Δ means that the difference between normal and superconducting states is being considered, a necessary precaution because expression (2-40) would otherwise diverge. To put this differently, it is impossible to split eqn. (2-41)

(to follow) into normal and superconducting free energies. Performing the usual integration over energy leads to

$$\frac{\Delta F}{N(0)} = (\pi k_B T)^2 \sum_n \int \frac{dS_{\underline{k}}}{|v_{\underline{k}}|} [\omega_n(-1 + \frac{1}{\sqrt{1+\bar{\Delta}^2_{\underline{k}}(n)}}) - (\tilde{\omega}^o_{\underline{k}}(n) - \tilde{\omega}_{\underline{k}}(n)\sqrt{1+\bar{\Delta}^2_{\underline{k}}(n)})]\,\mathrm{sgn}(\omega_n) \tag{2-41}$$

where $\tilde{\omega}^o_{\underline{k}}(n)$, which refers to the normal state, is defined as in eq. (2-18).

It is sometimes useful to rewrite this, using eqn. (2-22), as

$$\frac{\Delta F}{N(0)} = (2(\pi k_B T)^2 \int \frac{dS_{\underline{k}}}{|v_{\underline{k}}|} \sum_n |\omega_n| (\frac{1}{\sqrt{1+\bar{\Delta}^2_{\underline{k}}(n)}} - 1) + (\pi k_B T)^2 \sum_{nm} \iint \frac{dS_{\underline{k}}}{|v_{\underline{k}}|} \frac{dS_{\underline{k}'}}{|v_{\underline{k}'}|} [(\frac{1}{\sqrt{1+\bar{\Delta}^2_{\underline{k}}(n)}} \frac{1}{\sqrt{1+\bar{\Delta}^2_{\underline{k}'}(m)}} - 1)\lambda_{\underline{k}\underline{k}'}(m-n)\,\mathrm{sgn}(\omega_n\omega_m) + \frac{\bar{\Delta}_{\underline{k}}(n)}{\sqrt{1+\bar{\Delta}^2_{\underline{k}}(n)}} \frac{\bar{\Delta}_{\underline{k}'}(m)}{\sqrt{1+\bar{\Delta}^2_{\underline{k}'}(m)}} (\lambda_{\underline{k}\underline{k}'}(m-n) - \mu^*)]. \tag{2-42}$$

By using eqn. (2-29) it is possible to get an expression in terms of the gap on the real axis:

$$\Delta F = N(0) \int_0^\infty d\omega \int \frac{dS_{\underline{k}}}{|v_{\underline{k}}|} \mathrm{Re}[(1 + Z^o_{\underline{k}}(\omega))\omega - \frac{\omega^2}{\sqrt{\omega^2 - \bar{\Delta}^2_{\underline{k}}(\omega)}} - Z_{\underline{k}}(\omega)\sqrt{\omega^2 - \bar{\Delta}^2_{\underline{k}}(\omega)}]\tanh\frac{\omega}{2k_B T}$$

with $Z_{\underline{k}}^{o}(\omega)$ being the corresponding quantity in the normal state.

Bardeen and Stephens[14] claim to present a slightly different formula, but it is shown without difficulty (at least on the imaginary axis) that the two are equivalent.

Equation (2-38) can also be used to obtain the part of the normal state specific heat caused by the electron-phonon interaction through the free energy difference:

$$\frac{\Delta F}{N(0)} = \pi k_B T \sum_n |\tilde{\omega}(n) - \omega_n| \qquad (2\text{-}44)$$

which is valid for both isotropic and anisotropic systems.

This is equivalent to the formula quoted by Grimvall[95] on the real axis. If the electron-phonon interaction is ignored then the normal-state specific heat of the electrons at low temperature is $C_{en} = \gamma k_B T$ where

$$\gamma = \frac{2\pi^2 k_B^2}{3} N(0) \qquad (2\text{-}45)$$

The simplest correction for the electron-phonon interaction to this formula is the addition of a factor of $1+\lambda(0)$ to γ. But this is exact only at $T=0$; evaluation of expression (2-44) instead would replace γ by a temperature-dependent quantity, but the effect is small.

The discussion of the normal state was necessary because eqn. (2-41) gives only the difference $\Delta C_v \equiv C_S - C_N$ between the normal and superconducting state specific heat. Besides the term $C_{en} \sim \gamma k_B T$, C_N also comprises a lattice contribution C_L propor-

tional to T^3, which requires no renormalization and is unaffected by the superconducting transition. Figure 2-1 taken from Ref. 109 shows roughly the relative contributions of these terms for a medium-coupling system, Sn:

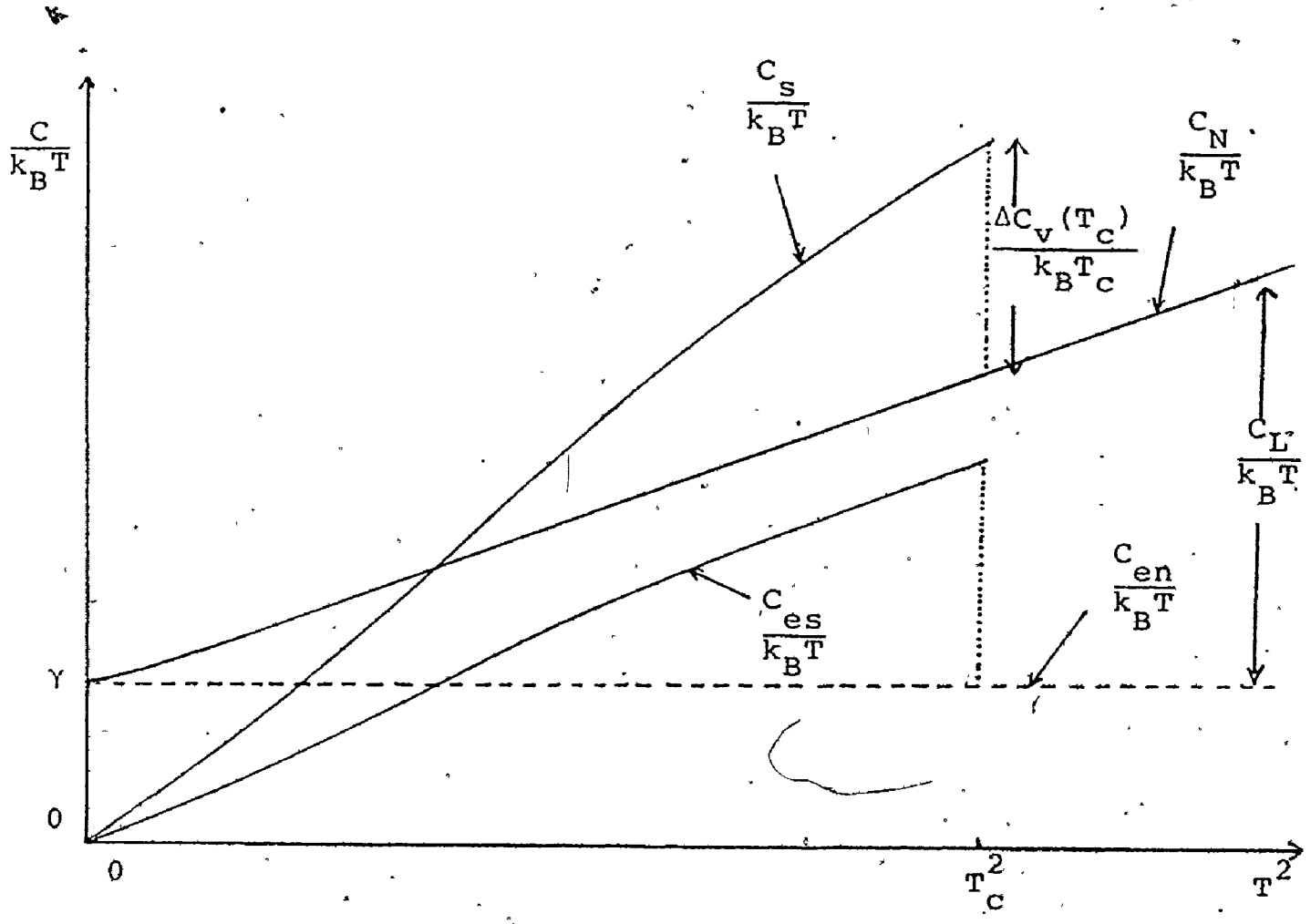

Fig. 2-1 Contributions to the specific heat

For stronger coupling the lattice contribution is proportionately larger. Since C_L is unchanged by the transition the quantity usually calculated and compared with experiment is $C_{es} \equiv C_S - C_L \approx \Delta C_v + \gamma k_B T$.

This section closes with a brief discussion of BCS theory, which is a special case of the strong coupling theory expounded here. It is appropriate when the electron-phonon coupling is so weak that retardation effects (which required the use of the phonon Green's function) and quasi-particle damping (corresponding to an imaginary part of $\Delta_{\underline{k}}(\omega)$) can be ignored. These criteria are not quantitative, but in practice it is not difficult to classify a system as weak or strong coupling; in Figures 5-5 and 5-6 for example, Nb_3Sn, Pb, and Hg fall into one group, Nb, In, Sn, Tl and Ta in the intermediate coupling group, while Al, for which BCS theory is appropriate, is an extreme set apart from all the others. The value of $\lambda(0)$ (compare Table 5-3) is often enough to classify a superconductor.

The criteria just mentioned permit not an analytical solution of the gap equations written here but the use of a simpler Hamiltonian, in which the coupling strength is represented by a single parameter $N(0)V$, $N(0)$ being the usual density of states and V a measure of the attraction between the electrons. The phonon cut off is taken care of through a vaguely defined "typical phonon frequency", of order ω_D, the Debye temperature, which allows T_c and H_c to be scaled up and down as in

$$k_B T_c = 1.14\ \omega_D\ e^{-\frac{1}{N(0)V}} . \qquad (2\text{-}46)$$

Since the combination $\omega_D e^{-\frac{1}{N(0)V}}$ appears in all calculated quantities, this theory predicts that certain dimensionless ratios should be universal. The chief ones are $D(t)$, $C_{es}(T)/\gamma k_B T$ (which includes the specific heat jump at T_c, $\Delta C_v(T_c)/\gamma k_B T_c$ (= 1.43), and $\gamma(k_B T_c)^2/H_c^2(0)$ (= .168). Others such as $(T_c/H_c(0))(dH_c/dT)_{T_c}$ are derivable from these. Deviations from these ratios are to be interpreted as a measure of the coupling strength. One more BCS relation will prove useful:

$$\xi_0 = v_F/\pi\Delta \ . \qquad (2\text{-}47)$$

Here V_F is some average Fermi velocity, Δ is the gap at T=0 ($\sim 2k_B T_c$), and ξ_0 the coherence length, the distance over which the electrons are correlated. This completes the listing of formulas for later reference.

2. Elastic Impurity Scattering and Anisotropic Superconductors

The difference in the properties of a dilute alloy and the pure metal are in general expected to be linear in the impurity concentration. When this does not happen, when there is something like saturation occurring, then the impurities are changing the properties of the system in some more fundamental way than just adding or subtracting a little to the parameters that still determine the properties of the metal. Such is the case when non-magnetic impurities are added to an

anisotropic superconductor. The behaviour of the critical temperature is typical:

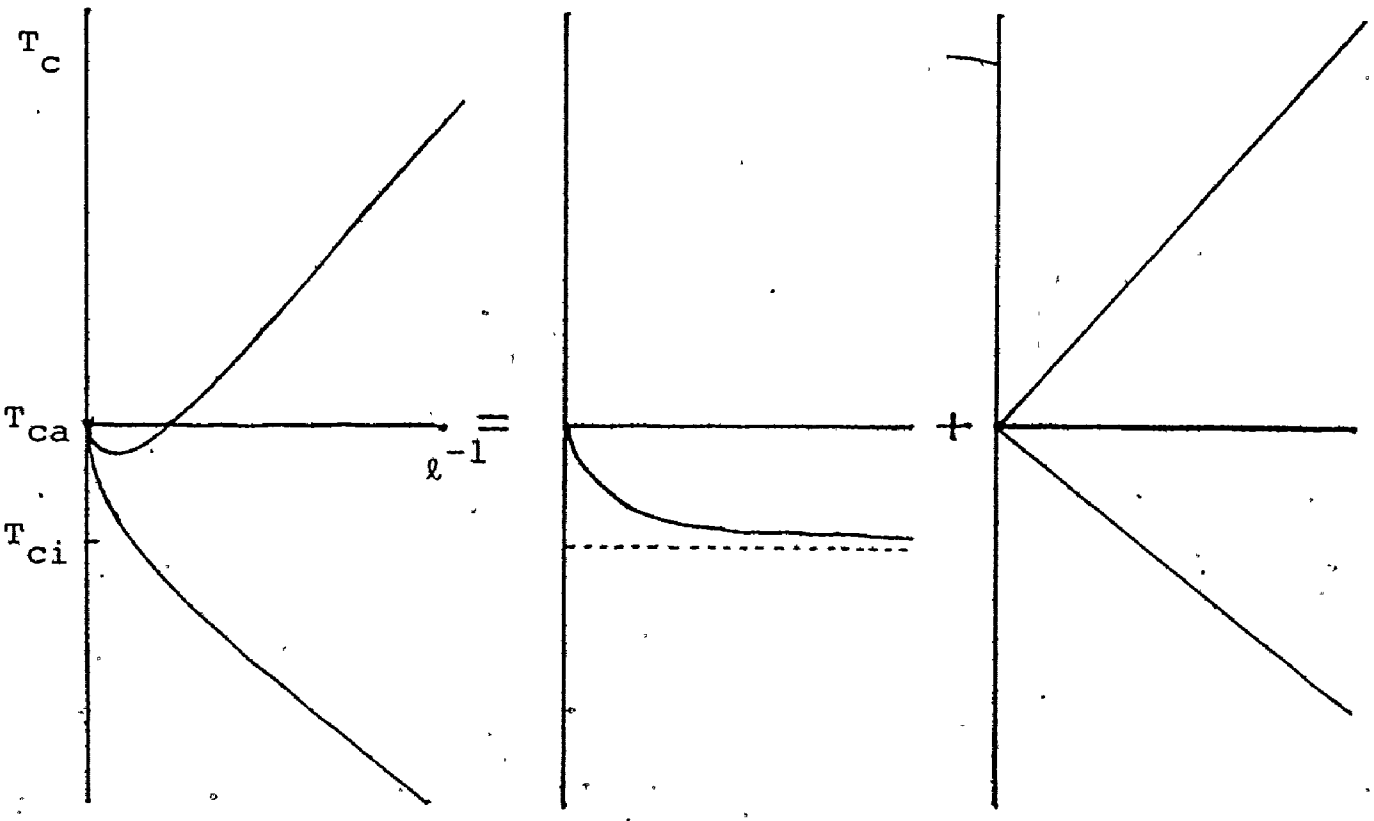

Fig. 2-2 Valence effect and mean free path effect.

Different impurities in the same host cause a change in T_c that may be separated into a linear part depending on the choice of the impurity and a saturating part which is approximately independent of the particular impurity when plotted against ℓ^{-1}, the mean free path. The linear term, called the valence effect because its sign is nearly always determined by the valence difference between host and impurity, although other factors may influence it, is not difficult to understand.

Impurities cause certain gross changes in the host; the number of electrons may change, so that the Fermi surface is altered, the phonon spectrum changes if there is a large mass difference between host and impurity, plus more subtle effects. The other term, called the mean free path effect because saturation occurs when $\ell >> \xi_0$, the coherence length cannot be explained in this way. The fundamental change first suggested by P. W. Anderson[10] that it reflects is the change in the pairing, from a correlation between $|\underline{k}\uparrow>$ and $|-k\underline{\downarrow}>$ to a correlation between an eigenstate of the alloy and its time reverse. These two states cannot be labelled with momentum any more because they are linear combinations of states from all over the Fermi surface. This mixing of states is the cause of the initial drop, for when the electrons are being scattered all over, they cannot take advantage of the anisotropy as they do in the pure metal to enhance their attractive interaction, because these electrons see only an isotropic averaged interaction. This last idea is important enough to restate in different words: When the interaction in an anisotropic superconductor is replaced by the averaged interaction, T_c, $H_c(0)$ and other indices of coupling strength drop, typically by a few percent. The averaged superconductor is what will be termed the corresponding isotropic system, and its properties will be labelled with subscript i, as opposed to subscript a for the pure anisotropic system. The phrase "corresponding isotropic system" is preferred here over the more widely used "dirty limit" because its

behaviour is in theory and in practice determined by solving the isotropic gap equations in which nothing referring to impurities appears, rather than the anisotropic equations with a large impurity term. Not even in principle can the latter equations be solved because the eigenstates of the impure system are not known. The only possible approach is the usual procedure with an alloy, to do a configuration average, thus recovering $\underline{k}$ as a conserved quantity and then to treat the impurities as an additional term in the Hamiltonian or self-energy. There is more than one possible way of doing this [69,108], but the method followed here is that of Markowitz and Kadanoff [36], who provided not just a suitable set of diagrams, but also, with the help of a model interaction, an analytical expression for the change in T_c. The validity of their model will be discussed in considerable detail in Chapters 3 and 5, but their expression for the self-energy should be discussed first. It is simply

$\Sigma =$ 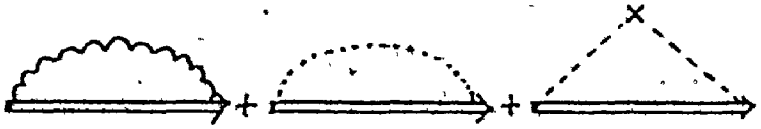 (2-48)

which treats the impurity scattering on the same footing as the attractive interaction that causes superconductivity. That does not seem quite right, and there is indeed a price to pay, namely the appearance of an imaginary part to the gap on the real axis even when the electron-phonon interaction is very weak [67,21] and no quasi-particle damping by phonons is

happening. But this is only to be expected when the state $|\underline{k}>$ being used as labels have finite lifetimes. Markowitz and Kadanoff consider other diagrams linear in the concentration, such as

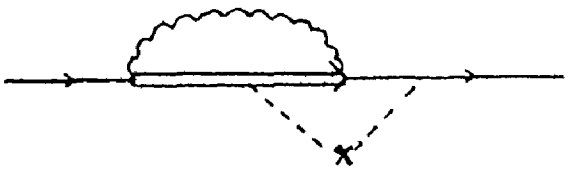

but dismiss these as small and belonging to the valence term. The smallness may be proved by an adaptation of Migdal's proof, while the justification for relegating all other contributions to the valence effect is provided by the fact that the one impurity diagram shown earlier is sufficient to wash out gap anisotropy and saturate T_c at T_{ci}. They manage also to relate the difference $T_{ca}-T_{ci}$ to the amount of gap anisotropy, but that is more a feature of their model interaction, although their estimates of both quantities are of the right order. Improving these estimates, connecting them to a realistic electron-phonon interaction, and extending them to other thermodynamic properties is one of the major goals of this thesis. The emphasis is however very much on the thermodynamic properties, which are much easier to handle, as a comparison of eqns. (2-31) and (2-22) makes plain. One more term in the self-energy hardly complicates eqns. (2-22) and (2-17):

$$\tilde{\omega}_{\underline{k}}(n) = \omega_n + c\pi\tau_{\underline{k}}^{-1}\mathrm{sgn}(\omega_n) + \pi k_B T_c \sum_m \lambda_{\underline{k}}(m-n)\,\mathrm{sgn}\omega_m \qquad (2\text{-}49)$$

$$\tilde{\Delta}_{\underline{k}}(n) = \pi k_B T_c \sum_m \int \frac{dS_{\underline{k}'}}{|v_{\underline{k}'}|}(\lambda_{\underline{k}\underline{k}'}(m-n) - \mu^*) + c\tau^{-1}_{\underline{k}\underline{k}'}/k_B T_c) \frac{\tilde{\Delta}_{\underline{k}'}(m)}{|\tilde{\omega}_{\underline{k}'}(m)|} \qquad (2\text{-}50)$$

$$\tau^{-1}_{\underline{k}\underline{k}'} = \sum_R |\Delta W(\underline{k}-R\underline{k}')|^2 \,. \qquad (2\text{-}51)$$

Here c is the fraction of impurities, and R is a sum over group operations appropriate to the system. A single Fermi surface average of $\tau^{-1}_{\underline{k}\underline{k}'}$ defines $\tau^{-1}_{\underline{k}}$, and a second average gives τ^{-1}, the inverse of the impurity lifetime. The use of $\tau^{-1}_{\underline{k}\underline{k}'}$ instead of $|\Delta W(\underline{k}-\underline{k}')|^2$ is intended to emphasize the way crystal symmetry creates an effective impurity interaction much smoother than the actual pseudopotential. This point will be discussed more later.

As a quick and non-trival illustration of the convenience of working on the imaginary axis, consider the expected null effect of elastic impurities on an isotropic system, often called Anderson's theorem. When eqn. (2-50) is rewritten in terms of $\bar{\Delta}(n)$, the impurity term, like $\lambda(0)$, cancels from both sides. The next chapter will have more significant changes to show.

CHAPTER 3

THE APPLICATION OF FUNCTIONAL DERIVATIVES TO ANISOTROPIC IMPURE SYSTEMS

This chapter covers a range of diverse topics, with the common thread being the effect on thermodynamic quantities (mainly T_c) of infinitesimal changes in the electron-phonon interaction and the amount of elastic impurity scattering. Section 1 is devoted to isotropic systems and is largely a review of work done by previous authors on the subject. In section 2 these methods are generalized to anisotropic systems (a far richer field) and in section 3 applied to elastic scattering from non-magnetic impurities.

1. Functional Derivatives in Isotropic Systems

It is of great interest to know how the changes in the electron phonon interaction or the phonon spectrum induced by alloying, pressure or phase changes will affect T_c and H_c. To study these changes, the natural method is to add an infinitesimal change $\delta\alpha^2F(\omega)$ or $\delta F(\omega)$ onto the original quantity and obtain the resulting change δT_c or δH_c. The rates of change $\delta T_c/\delta\alpha^2F(\omega)$, $\delta T_c/\delta F(\omega)$, $\delta H_c/\delta\alpha^2F(\omega)$ or $\delta H_c/\delta F(\omega)$ are the functional derivatives. Their functional forms will depend on the type of change made in $\alpha^2F(\omega)$ or $F(\omega)$ and the choice of the real axis, or the imaginary axis, since the solution of the gap equations appears explicitly in the func-

tional derivative. In this discussion only two types of infinitesimal changes are considered: the delta function of infinitesimal weight centred on some phonon frequency ω_0, and the infinitesimal shifts of all the frequencies by some amount $\delta\omega_{q\lambda}$. The former reveals the relative importance of different phonon frequencies, while the latter shows the effect of gross changes in $F(\omega)$, such as those caused by the application of pressure, or the effect of a drop in a single phonon frequency associated with phase transitions.

The simplicity of the functional form of the functional derivative on the imaginary axis and the fact that the solution of the gap equations is required for its evaluation implies that the imaginary axis is the more natural place to work. In addition, the symmetry of eqn. (2-24) in the indices m and n makes a further simplification possible. This is the transformation of eqn. (2-24) to an eigenvalue equation with a symmetric kernel, allowing the perturbation methods appropriate for Hermitian operators to be used in evaluating the functional derivative. This transformation, first used by Bergmann and Rainer[15], is the elimination of $\tilde{\Delta}(n)$ in favour of

$$\bar{\Delta}(n) \equiv \tilde{\Delta}(n)/(\rho + |\tilde{\omega}(n)|) \qquad (3\text{-}1)$$

so that eqn. (2-24) becomes

$$\rho\bar{\Delta}(n) = \pi k_B T \sum_m (\lambda(m-n) - \mu^* - \frac{\delta_{mn}|\tilde{\omega}(n)|}{\pi k_B T})\bar{\Delta}(m). \qquad (3\text{-}2)$$

For systems with magnetic impurities, $\rho(T)$ is the pair-breaking parameter and as such has physical meaning. Here it is used

for mathematical convenience only. The $\bar{\Delta}(n)$ just defined is clearly different from the one discussed in Chapter 2, but this should not create confusion because the only solution of eqn. (3-2) with physical meaning is the one with zero eigenvalue at T_c. At a given temperature eqn. (3-2) will have more than one eigenvalue. The eigenvalue that passes through zero as T approaches T_c is the only one of interest; henceforth ρ will always refer to that particular one. In fact T_c could be defined as the maximum of the roots (if any) of all the eigenvalues of eqn. (3-2). It is the change in that special eigenvalue which yields the functional derivative. From first order perturbation theory,

$$\delta T_c = -\left(\frac{\partial \rho}{\partial T}\right)^{-1}_{T_c} \sum_{m,n} \delta K_{mn}\, \bar{\Delta}(m)\bar{\Delta}(n) \Big/ \sum_n \bar{\Delta}^2(n) \qquad (3\text{-}3)$$

where δK_{mn} is the change in the kernel of eqn. (3-2) evaluated at T_c caused by $\delta\alpha^2 F(\omega)$, the $\bar{\Delta}(n)$ are the solution of eqn. (2-24), and

$$\left(\frac{\partial \rho}{\partial T}\right)_{T_c} \equiv -\sum_{m,n} \left(\frac{\partial K_{mn}}{\partial T}\right)_{T_c} \bar{\Delta}(m)\bar{\Delta}(n) \Big/ \sum_n \bar{\Delta}^2(n) \qquad (3\text{-}4)$$

The minus sign in eqn. (3-3) is best explained by the following diagram:

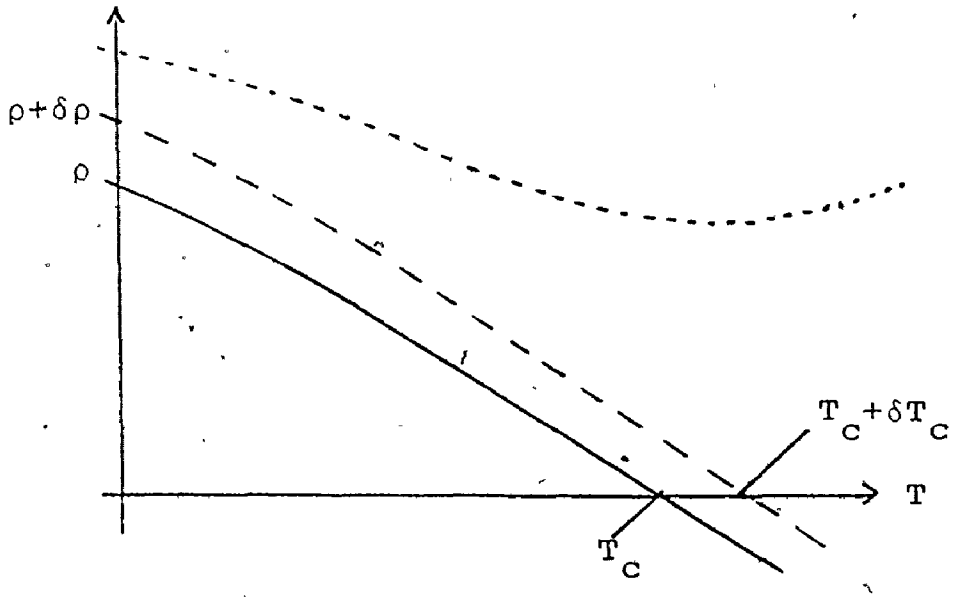

Fig. 3-1 Behaviour of $\rho(T)$ near T_c. The dotted line is later shown to be impossible.

The transition temperature of the system with the infinitesimal change added to the kernel is the point where the new eigenvalue $\rho + \delta\rho$ passes through zero. Hence $\delta T_c \doteq -(\frac{\partial\rho}{\partial T})^{-1}_{T_c} \delta\rho$. Later it will be shown that $(\partial\rho/\partial T)_{T_c} < 0$.

Since the partial derivatives are always evaluated at T_c, that subscript will henceforth be dropped. Table 5-3 lists values for $\partial\rho/\partial T$ showing it is insensitive to large differences in $\alpha^2F(\omega)$.

It is convenient at this point to prove a property of ρ that will prove useful in section 2, namely that ρ is the maximum eigenvalue of eqn. (3-2) at $T = T_c$. This property is not obvious; there could be an eigenvalue of eqn. (3-2) above ρ that is a positive increasing quantity for $T > T_c$ (such as the dotted line in the preceding diagram). A formal proof requires a transformation suggested by Rainer[105]. First rewrite eqn. (2-24) as

$$\bar{\Delta}(n)\left[\left|\tilde{\omega}(n)\right| - \pi k_B T_c(\lambda(0) - \mu^*)\right]$$

$$= \pi k_B T_c \sum_{m\neq n} (\lambda(m-n) - \mu^*)\bar{\Delta}(m).$$

Defining $\pi k_B T_c \hat{\omega}(n) \equiv \left[\left|\tilde{\omega}(n)\right| - \pi k_B T_c(\lambda(0)-\mu^*)\right]$ and $g(n) \equiv \sqrt{\hat{\omega}(n)\bar{\Delta}(n)}$, then this equation becomes

$$g(n) = \sum_{m\neq n} \frac{\lambda(m-n)-\mu^*}{\sqrt{\hat{\omega}(n)\hat{\omega}(m)}}\, g(m) \ .$$

It is convenient to introduce an eigenvalue $E(T)$ while letting T vary and to replace μ^* by a function $\mu(T)$ which has a constant value μ^* below some arbitrarily defined temperature above which it decreases to zero as $T \to \infty$.

$$E(T)g(n) = \sum_{m\neq n} \frac{(\lambda(m-n)-\mu(T))}{\sqrt{\hat{\omega}(n)\hat{\omega}(m)}}\, g(m) \qquad (3\text{-}5)$$

Analogously to eqn. (3-2), the maximum value of T for which there exists an eigenvalue of unity is T_c. Unlike the situation with eqn. (3-2), it <u>is</u> possible to prove that the maximum eigenvalue E_M at T_c is unity, because the kernel of eqn. (3-5) is completely continuous (or compact) - it is obviously bounded <u>and</u> goes to zero as $T \to \infty$ because as $T \to \infty$, $\lambda(n\neq 0) \propto T^{-2}$ while $\hat{\omega}(n) \to 2n-1$. Hence a well-known theorem[106] about completely continuous kernels can be applied, which states that the only possible limit point of the eigenvalues is zero, ie as $T \to \infty$, <u>all</u> the $E(T) \to 0$. The desired result, that ρ is the maximum eigenvalue of eqn. (3-2) at T_c now

follows trivially. Suppose there were an eigenvalue E' greater than unity at T_c. Then since E' eventually falls to zero, it must pass through unity at some temperature T' greater than T_c, implying that eqn. (2-24) has a non-trivial solution at T'. Therefore unity is the maximum eigenvalue of eqn. (3-5) for $T = T_c$ implying that for <u>any</u> function $\tilde{g}(n)$,

$$1 \geq \pi k_B T_c \sum_{m \neq n} \frac{(\lambda(m-n)-\mu^*)}{(\hat{\omega}(m)\hat{\omega}(n))^{1/2}} \tilde{g}(m)\tilde{g}(n) / \sum_n \tilde{g}^2(n) \qquad (3\text{-}6)$$

Rewriting eqn. (3-6) in terms of $g'(n) \equiv \tilde{g}(n)/\sqrt{\hat{\omega}(n)}$ yields

$$0 \geq -\sum_n |\hat{\omega}(n)| g'^2(n) + \pi k_B T_c \sum_{m,n} (\lambda(m-n)-\mu^*) g'(n) g'(m)$$

with equality holding for $g'(n) = \bar{\Delta}(n)$, which establishes that $\rho(=0)$ is indeed the maximum eigenvalue at T_c of eqn. (3-2), and is therefore stationary with respect to variations in $\bar{\Delta}(n)$.

The next result to be proved is $\partial\rho/\partial T < 0$. Since the maximum eigenvalue $E_M(T)$ is stationary with respect to variations in g(n) and is a decreasing function of T at T_c,

$$0 > \sum_n g^2(n) \left(\frac{\partial E_M}{\partial T}\right)_{T_c} = \sum_{\substack{m,n \\ m\neq n}} g(n)g(m) \frac{\partial}{\partial T} \left\{\frac{\lambda(m-n)-\mu^*}{(\hat{\omega}(n)\hat{\omega}(m))^{1/2}}\right\}_{T_c}$$

$$= \sum_{m,n} \bar{\Delta}(n)\bar{\Delta}(m) \frac{\partial}{\partial T} (\lambda(m-n)-\mu^*)$$

$$- \frac{1}{2} \sum_{\substack{m,n \\ m\neq n}} (\lambda(m-n)-\mu^*) \frac{\bar{\Delta}(m)\bar{\Delta}(n)}{\sqrt{\hat{\omega}(m)\hat{\omega}(n)}} \left(\sqrt{\frac{\hat{\omega}(n)}{\hat{\omega}(m)}} \frac{\partial \hat{\omega}_m}{\partial T} + \sqrt{\frac{\hat{\omega}(m)}{\hat{\omega}(n)}} \frac{\partial \hat{\omega}_n}{\partial T}\right)$$

In going to the second line, the identity $g(n)/\sqrt{\hat{\omega}(n)} = \bar{\Delta}(n)$

was used. The second term may be simplified using the fact

$$\sum_{m\neq n} (\lambda(m-n)-\mu^*)\bar{\Delta}(m) = \hat{\omega}(n)\bar{\Delta}(n)$$

so that it reduces to

$$-\sum_n \bar{\Delta}^2(n) \frac{\partial\hat{\omega}(n)}{\partial T} = -\sum_n \bar{\Delta}^2(n) \frac{\partial}{\partial T}\left(\frac{|\tilde{\omega}(n)|}{\pi k_B T}\right) .$$

Combining the first and second terms gives

$$0 > \sum_{m,n} \bar{\Delta}(m)\bar{\Delta}(n) \frac{\partial}{\partial T}\{\lambda(m-n)-\mu^*-\delta_{mn}\frac{|\tilde{\omega}(n)|}{k_B T}\}_{T_c}$$

Comparison with eqns. (3-2) and (3-4) shows that this is the desired result.

The mathematical formalities are out of the way, now the tools can be used to see how $\alpha^2F(\omega)$ and $F(\omega)$ influence T_c. If $\delta\alpha^2F(\omega)$ is a δ-function at frequency ω_0 and weight ϵ, the effectiveness of the different frequency parts of $\alpha^2F(\omega)$ for enhancing T_c can be obtained from eqn. (3-3):

$$\delta T_c = \epsilon\left(\frac{\partial\rho}{\partial T}\right)^{-1}\pi k_B T_c \sum_{m,n} \frac{2\omega_0}{\omega_0^2+\omega_{n-m}^2}\left(\bar{\Delta}(m)\bar{\Delta}(n)-\bar{\Delta}^2(n)\,\mathrm{sgn}(\omega_n\omega_m)\right)/\sum_n \bar{\Delta}^2(n) \quad (3\text{-}7)$$

Some plots of $\delta T_c/\delta\alpha^2F(\omega)$ are shown in Fig. 5-3. It is easily seen that the curves for different superconductors have almost the same shape with a maximum near $\omega_0 = 7\ k_B T_c$, the difference in scale being due almost entirely to differences in $\partial\rho/\partial T$. The universality in the shapes is almost certainly due to the fact that $\bar{\Delta}(n) \approx \bar{\Delta}(1)/(2n-1)$ for small n, and approaches some negative constant at large n

for all superconductors. Slight deviations in shape between weak and strong coupling curves are probably due to the inadequacy of the formula just quoted to describe strong coupling systems. For strong coupling systems, the maximum in the curves could be explained by assuming that the dominant terms in the sum are those with $|m-n| = 1$ (the m=n terms cancel), so that $\delta T_c/\delta\alpha^2F(\omega)$ would be proportional to $\omega_0/(\omega_0^2+(2\pi k_B T_c)^2)$, which does have a maximum at $\omega_0 = 2\pi k_B T_c$, but the assumption does not hold so well for weak coupling where $\bar{\Delta}(n)$ decreases more slowly, and it seems necessary to to invoke the following physical explanation given by Carbotte[107]: An ion vibrating with a frequency $7k_BT_c$ moves through a quarter of its period (ie from equilibrium to its maximum displacement) during the time an electron stays within a coherence length of it; thus $7k_BT_c$ is the optimum frequency for the lattice's polarization response to the electron. But this polarization is just the origin of the attraction between electrons that leads to superconductivity, therefore $7k_BT_c$ is the best frequency to enhance.

Looking ahead to anisotropic systems, and back to Anderson's theorem, one finds that the really interesting feature of these curves is their linearity and positive sign at low frequency. It seems plausible that phonons of very low frequency (the only ones that could be excited thermally) would disrupt the pairing interaction and therefore the functional derivative at small ω_0 should be negative. In fact, the lowest

frequency phonons play no role whatever, since they contribute significantly only to $\lambda(0)$, which cancels out of eqn. (2-24). Bergmann and Rainer[15] supply a physical interpretation: to the electrons, the very slowly moving thermal phonons, with their low energy which makes the electron-phonon scattering nearly elastic, are hardly distinguishable from static lattice defects and therefore by Anderson's theorem do not affect T_c. In fact, they were able to prove strictly that for $\mu^*=0$, $\delta T_c/\delta\alpha^2F(\omega_0) \geq 0$ at any frequency. If $\mu^* \neq 0$, no inequality could be established, but all systems studied had positive definite functional derivatives.

For future reference, the coefficient of ω_0 in $\lim_{\omega_0 \to 0} \frac{\delta\rho}{\delta\alpha^2F(\omega_0)}$ is required. In principle, this coefficient could be obtained analytically by substituting $\bar{\Delta}(n) = 1/|2n-1|$ in eq. (3-7), but in practice it is more easily obtained from Fig. 5-3 and Table 5-3. Thanks to the universal shape of the curves, the coefficient is very nearly the same for all materials. The resulting expression is

$$\lim_{\omega_0 \to 0} \frac{\delta\rho}{\delta\alpha^2F(\omega_0)} \approx .09 \frac{\omega_0}{k_B T_c} . \qquad (3-8)$$

The existence of a maximum in $\delta T_c/\delta\alpha^2F(\omega)$ suggested to C.R. Leavens that it is possible to construct an $\alpha^2F(\omega)$ of optimal shape for maximizing T_c. Such a construction makes sense only if it is subject to some constraint - for example eqn. (2-24) trivially implies that under the transformation

$\alpha^2F(\omega) \rightarrow \alpha^2F(r\omega)$, $T_c \rightarrow T_c/r$, so that T_c could be increased indefinitely. The constraint Leavens chose was to keep the following quantity fixed;

$$A \equiv \int_0^\infty \alpha^2F(\omega)\,d\omega \quad . \tag{3-9}$$

This leads to an optimal spectrum of the form

$$\alpha^2F(\omega) = A\delta(\omega - \omega_E^*) \tag{3-10}$$

and a least upper bound on T_c. The optimal frequency ω_E^* is a function of A and μ^*:

$$\omega_E^* = 1.75\ A\ d(\mu^*) \tag{3-11}$$

where $d(0) = 1$ and $d(\mu^*)$ decreases linearly to about .5 at $\mu^* = .20$. The least upper bound is

$$k_B T_c \leq .23\ c(\mu^*)A \tag{3-12}$$

where $c(\mu^*)$ falls from unity at $\mu^* = 0$ to .65 at $\mu^* = .20$ and equality holds for the delta-function spectrum eqn. (3-10). He also found that for $\alpha^2F(\omega)$ near the optimum shape (ie with $\lambda(0)$ deviating from the optimum value $2A/\omega_E^*$, or with a rectangular $\alpha^2F(\omega)$), T_c remained very close to its least upper bound, so that his result is of practical use even though $\alpha^2F(\omega)$ of real materials are nothing like delta-functions. It might seem that similar inequalities could be obtained by constraining other integer moments of $\alpha^2F(\omega)$, such as the

more accessible $\lambda(0)$, but Leavens[34] showed that with the exception of the first moment, proportional to the McMillan-Hopfield parameter η, (which turned out to be relevant only for systems with unrealistically large $\lambda(0)$), the resulting optimal spectra were unphysical and led to meaningless inequalities for T_c. The paramount importance of A and its inequality is most convincingly displayed in Fig. 3-2, which shows that all experimental T_c for which data was available satisfy eqn. (3-12) and some in fact lie just below the least upper bound.

The position of the optimal spectrum at such high frequency appears to contradict the experimental result that T_c in certain strong-coupling alloys increases as the composition approaches the critical value for a structural phase transition, when it is believed that one phonon softens considerably while the other phonon frequencies shift but by a smaller amount. To examine this effect, consider the following infinitesimal change in the phonon frequencies:

$$\omega_{q\lambda} \rightarrow \omega_{q\lambda} + \delta\omega_{q\lambda} \quad . \qquad (3\text{-}13)$$

(This particular variation was chosen instead of a delta-function added to $F(\omega)$ because of the complications caused by the normalization condition on $F(\omega)$. In addition this gives a better description of structural phase transitions which occur when the frequency of one phonon $q\lambda$ drops abruptly.) A one-plane-wave approximation can be used here for simplicity without changing the conclusions to be drawn.

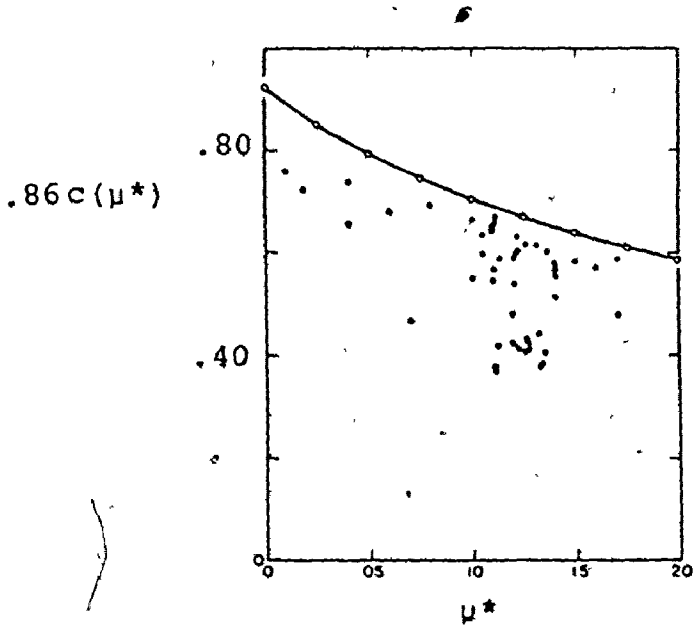

Fig. 3-2 The function $c(\mu^*)$ occurring in the relation $k_B T_c < .23 c(\mu^*) A$ is shown as a function of μ^* by the solid curve. The open circles (o) are calculated values of $c(\mu^*)$; the solid circles (•) indicate experimental values of $k_B T_c / .23A$ and μ^* for all the materials for which this data is available. This figure is taken from Ref. 33.

Then from eqn. (2-28), the change in $\alpha^2F(\omega)$ is

$$\delta\alpha^2F(\omega) \propto \int_{|q|<2k_F} \frac{d^3q}{|q|} W^2(q) \sum_\lambda (\underline{q}\cdot\underline{\varepsilon}^\lambda(q))^2 \delta\omega_{\underline{q}\lambda} \delta(\omega-\omega_{\underline{q}\lambda}) \left(\frac{\partial}{\partial\omega}\,\omega^{-1}\right) \qquad (3\text{-}14)$$

where $\left(\frac{\partial}{\partial\omega}\,\omega^{-1}\right)$ is to be regarded as an operator, and the proportionality constant is related to FS constants. To see why an operator is necessary, consider for an arbitrary function $T(\omega)$ the integral

$$\int d\omega T(\omega)\,\delta\alpha^2F(\omega) = \int_{|q|<2k_F} \frac{d^3q}{|q|} W^2(q) \sum_\lambda (\underline{q}\cdot\underline{\varepsilon}^\lambda(\underline{q}))^2 \int d\omega T(\omega) \left\{ \frac{\delta(\omega-\omega_{\underline{q}\lambda}-\delta\omega_{\underline{q}\lambda})}{\omega_{\underline{q}\lambda}+\delta\omega_{\underline{q}\lambda}} - \frac{\delta(\omega-\omega_{\underline{q}\lambda})}{\omega_{\underline{q}\lambda}} \right\} .$$

The integral over ω is simply $T(\omega_{\underline{q}\lambda}+\delta\omega_{\underline{q}\lambda})/(\omega_{\underline{q}\lambda}+\delta\omega_{\underline{q}\lambda}) - T(\omega_{\underline{q}\lambda})/\omega_{\underline{q}\lambda} = \delta\omega_{\underline{q}\lambda} \frac{\partial}{\partial\omega} \left(\frac{T(\omega)}{\omega}\right)_{\omega_{\underline{q}\lambda}}$. It follows that

$$\delta\lambda(n) \propto -\int_{|q|<2k_F} \frac{d^3q}{|q|} W^2(q) \sum_\lambda (\underline{q}\cdot\underline{\varepsilon}^\lambda(\underline{q}))^2 \frac{\omega_{\underline{q}\lambda}\delta\omega_{\underline{q}\lambda}}{(\omega_{\underline{q}\lambda}^2+\omega_n^2)^2} \qquad (3\text{-}15)$$

and

$$\delta A \propto -\int_{|q|<2k_F} \frac{d^3q}{|q|} W^2(q) \sum_\lambda (\underline{q}\cdot\underline{\varepsilon}^\lambda(\underline{q}))^2 \frac{\delta\omega_{\underline{q}\lambda}}{\omega_{\underline{q}\lambda}^2} . \qquad (3\text{-}16)$$

Although Bergmann and Rainer proved it rigorously only for $\mu^*=0$, their numerical results make it plausible that whenever $\delta\lambda(n)$[†] > 0, $\delta T_c > 0$ as well. Therefore eqn. (3-15)

[†]Their proof was based on the assumption that $\delta\lambda(n)$ and $\bar{\Delta}(n)$ were positive and monotonically decreasing functions of n.

implies that for $\delta\omega_{q\lambda} < 0$, T_c should increase. There is no contradiction with the previous results, because eqn. (3-16) shows that A increases as well. It is true that $\lambda(0)$ also changes, possibly in a direction away from the optimal value, but in strong coupling systems A is the more important parameter and T_c is relatively insensitive to $\lambda(0)$[56]. Some caution should be used in applying the preceding reasoning to amorphous systems, where the functional form of $\alpha^2F(\omega)$ may be different[49], and it should also be kept in mind that the pseudopotential and the phonon frequencies are not fully independent, as is implicitly assumed in taking this functional derivative.

In closing this section two functional derivatives bypassing ρ altogether will be discussed. To obtain $\delta T_c/\delta\alpha^2F(\omega_0)$, standard first-order perturbation theory applied to homogeneous Fredholm equations of the second kind with T_c playing the role of an eigenvalue, could have been used. This procedure was in fact carried out by Appel by taking the real part of both sides of the linearized form of eqn. (2-31). Evaluation of the functional derivative required solving not just the resulting integral equation but its adjoint as well, a difficulty which again underlines the advantages of working on the imaginary axis. However, his method does allow the influence of thermal and virtual phonons to be separated, as will be shown in Appendix IV. The second functional derivative where ρ plays no part is $\delta H_c(T)/\delta\alpha^2F(\omega_0)$. Since ΔF is stationary with respect to $\bar{\Delta}(n)$, eqn. (2-42) immediately gives[49]

$$\delta\alpha^2F(\omega) = \varepsilon\delta(\omega-\omega_0),$$

$$\frac{\delta H_c(T)}{\delta\alpha^2F(\omega_0)} = \frac{4\pi}{H_c(T)}\frac{\delta\Delta F}{\delta\alpha^2F(\omega_0)}$$

where

$$\frac{\delta\Delta F}{\delta\alpha^2F(\omega_0)} = N(0)(\pi k_B T)^2 \sum_{n,m} \frac{1}{\sqrt{1+\bar{\Delta}^2(n)}}\frac{1}{\sqrt{1+\bar{\Delta}^2(m)}}\{1-\sqrt{1+\bar{\Delta}^2(n)}\sqrt{1+\bar{\Delta}^2(m)} + \bar{\Delta}^2(m)\bar{\Delta}^2(n)\}\frac{\mathrm{sgn}(\omega_n\omega_m)2\omega_0}{\omega_0^2+\omega_{n-m}^2} \qquad (3\text{-}17)$$

Because the terms n=m cancel out of this expression, there is no term proportional to ω_0^{-1}; hence $\lambda(0)$ and the low-lying thermal phonons play no role here either. The shape of $\delta\Delta F/\delta\alpha^2F(\omega_0)$ is similar to that of $\delta T_c/\delta\alpha^2F(\omega_0)$ in being linear at small ω_0. In the next section the situation will turn out to be quite different.

2. Functional Derivatives in Anisotropic Superconductors

In this section, all the methods discussed in section 1 will be generalized to pure anisotropic systems. Defining $\bar{\Delta}_{\underline{k}}$ and ρ as in eqn. (3-2), and substituting in eqn. (2-17) obtains

$$\rho\bar{\Delta}_{\underline{k}}(n) = \pi k_B T_c \sum_m \int \frac{dS_{\underline{k}'}}{|v_{\underline{k}'}|}\{\lambda_{\underline{k}\underline{k}'}(m-n)-\mu^*+\delta_{mn}c\tau_{\underline{k}\underline{k}'}^{-1}\}/k_B T_c$$

$$-\delta(\underline{k}-\underline{k}')\delta_{mn}\{|\tilde{\omega}_{\underline{k}}(n)|/\pi k_B T_c\}\bar{\Delta}_{\underline{k}'}(m) \qquad (3\text{-}18)$$

In this section, references to eqn. (3-18) will assume c=0. As an immediate illustration of the power of the methods

outlined in the last chapter, a rigorous and simple proof is presented of the fact that an anisotropic superconductor has a higher T_c than the corresponding isotropic system. Consider the following infinitesimal change in $(\alpha^2F(\omega))_{\underline{k}\underline{k}'}$ which leaves $\alpha^2F(\omega)$ unaffected but augments the anisotropy (Note that this is not a delta- function - the interaction is being changed at all frequencies):

$$\delta(\alpha^2F(\omega)_{\underline{k}\underline{k}'}) = \varepsilon[(\alpha^2F(\omega))_{\underline{k}\underline{k}'} - \alpha^2F(\omega)] \quad . \tag{3-19}$$

Then the change in the kernel $K_{\underline{k}\underline{k}'}(m-n)$ of eqn. (3-18) is

$$\varepsilon\pi k_B T \{[\lambda_{\underline{k}\underline{k}'}(m-n) - \mu^* - \delta(\underline{k}-\underline{k}')\delta_{mn} \frac{|\tilde{\omega}_{\underline{k}}(n)|}{\pi k_B T_c}]$$

$$- [\lambda(m-n) - \mu^* - \delta(\underline{k}-\underline{k}')\delta_{mn} \frac{<|\tilde{\omega}_{\underline{k}}(n)|>}{\pi k_B T_c}]\}$$

where $<\ >$ denotes an FS average, so that

$$\delta\rho =$$

$$0 - \varepsilon k_B T_c \sum_{m,n} \{<\bar{\Delta}_{\underline{k}}(n)><\bar{\Delta}_{\underline{k}'}(m)>\lambda(m-n) - \delta_{mn} \frac{<|\tilde{\omega}_{\underline{k}}(n)|>}{\pi k_B T_c} <\bar{\Delta}^2_{\underline{k}}(n)>\}$$

$$/\sum_n <\bar{\Delta}^2_{\underline{k}}(n)> \quad . \tag{3-20}$$

The first term vanishes because $\bar{\Delta}_{\underline{k}}(n)$ is the solution of eqn. (3-18). Since $<\Delta^2_{\underline{k}}(n)> \geq <\Delta_{\underline{k}}(n)>^2$, eqn. (3-20) becomes

$$\frac{\delta\rho}{\delta(\alpha^2F(\omega))_{\underline{k}\underline{k}'}} \geq -\pi k_B T_c \sum_{m,n} \{\langle\bar{\Delta}_{\underline{k}}(n)\,X\bar{\Delta}_{\underline{k}'}(m)\rangle\lambda(m-n) - \delta_{mn}\langle|\tilde{\omega}_{\underline{k}}(n)|\rangle$$

$$(\pi k_B T_c)^{-1}\langle\bar{\Delta}^2_{\underline{k}}(n)\rangle\} \Big/ \sum_n \langle\bar{\Delta}^2_{\underline{k}}(n)\rangle$$

$$= -\pi k_B T_c \iint_{48} \frac{dS_{\underline{k}}}{|v_{\underline{k}}|}\frac{dS_{\underline{k}'}}{|v_{\underline{k}'}|}\langle\bar{\Delta}_{\underline{k}}(n)\rangle\langle\bar{\Delta}_{\underline{k}}(m)\rangle K_{\underline{k}\underline{k}'}(m-n)\Big/\sum_n \langle\bar{\Delta}^2_{\underline{k}}(n)\rangle \quad . \qquad (3\text{-}21)$$

But $\langle\bar{\Delta}_{\underline{k}}(n)\rangle$ is not the solution of eqn. (3-18), whose maximum eigenvalue is zero. (The proof for isotropic systems can easily be generalized by defining

$$g_{\underline{k}}(n) \equiv \bar{\Delta}_{\underline{k}}(n)|\tilde{\omega}_{\underline{k}}(n)| - \pi k_B T_c\langle\bar{\Delta}_{\underline{k}'}(n)(\lambda_{\underline{k}\underline{k}'}(0)-\mu^*)\rangle$$

and

$$\hat{\omega}_{\underline{k}}(n) \equiv [g_{\underline{k}}(n)/(\bar{\Delta}_{\underline{k}}(n)\pi k_B T_c)]^2$$

so that no terms independent of T will appear in the numerator of the transformed equation written in terms of $g_{\underline{k}}$, $\hat{\omega}_{\underline{k}}$ and $\mu(T)$).

Therefore $\delta\rho/\delta(\alpha^2F(\omega))_{\underline{k}\underline{k}'} \geq 0$, and so $\delta T_c \geq 0$, with equality holding only for isotropic systems. Analogous reasoning, making use of the fact that ΔF, like ρ, is stationary with respect to variations in $\bar{\Delta}_{\underline{k}}$ leads to the conclusion that ΔF can also be increased by augmenting the anisotropy according to eqn. (3-19). $\delta\Delta F$, the expression obtained by substituting $\varepsilon(\lambda_{\underline{k}\underline{k}'}(n)-\lambda(n))$ for $\lambda_{\underline{k}\underline{k}'}(n)$ in eqn. (2-42) is

$$\varepsilon\Delta F^{*}-\varepsilon(\pi k_B T)^2 N(0)\sum_{nm}\operatorname{sgn}(\omega_n\omega_m)\Big\{\Big[\Big\langle\frac{1}{\sqrt{1+\bar{\Delta}_{\underline{k}}^2(n)}}\Big\rangle\Big\langle\frac{1}{\sqrt{1+\bar{\Delta}_{\underline{k}}^2(m)}}\Big\rangle-1\Big]\lambda(m-n)$$

$$+\Big\langle\frac{\bar{\Delta}_{\underline{k}}(n)}{\sqrt{1+\bar{\Delta}_{\underline{k}}^2(n)}}\Big\rangle\Big\langle\frac{\bar{\Delta}_{\underline{k}}(m)}{\sqrt{1+\bar{\Delta}_{\underline{k}}^2(m)}}\Big\rangle(\lambda(m-n)-\mu^{*})\Big\}$$

where $\Delta F^{*} \equiv \Delta F - 2\pi k_B T N(0)\sum_n|\omega_n|\Big(\Big\langle\frac{1}{1+\bar{\Delta}_{\underline{k}}^2(n)}\Big\rangle-1\Big)$ appears for the same reason as the zero in eqn. (3-20). The remaining terms can be expressed as

$$-\varepsilon(\pi k_B T)^2 N(0)\sum_{nm}\iint\frac{dS_{\underline{k}}}{|v_{\underline{k}}|}\frac{dS_{\underline{k}'}}{|v_{\underline{k}'}|}\{\operatorname{sgn}(\omega_n\omega_m)$$

$$\Big[\Big\langle\frac{1}{\sqrt{1+\bar{\Delta}_{\underline{k}}^2(n)}}\Big\rangle\Big\langle\frac{1}{\sqrt{1+\bar{\Delta}_{\underline{k}}^2(m)}}\Big\rangle-1\Big]\lambda_{\underline{k}\underline{k}'}(m-n)+\Big\langle\frac{\bar{\Delta}_{\underline{k}}(n)}{\sqrt{1+\bar{\Delta}_{\underline{k}}^2(n)}}\Big\rangle\Big\langle\frac{\bar{\Delta}_{\underline{k}}(m)}{\sqrt{1+\bar{\Delta}_{\underline{k}}^2(m)}}\Big\rangle$$

$$(\lambda_{\underline{k}\underline{k}'}(m-n)-\mu^{*})\}$$

which must be less than ΔF^{*} since eqn. (2-42) is stationary with respect to variations in $\bar{\Delta}_{\underline{k}}(n)$. Therefore $\delta\Delta F \geq 0$.

In these proofs, where isotropic and anisotropic superconductors are being compared, it seems at first thought more natural to start with an isotropic superconductor and add infinitesimal anisotropy onto it, but then one will always find $\delta\rho = 0$. This occurs because the anisotropic eigenvectors of eqn. (3-21) cannot be expressed as linear combinations of the eigenvectors of eqn. (3-2). Perturbation theory therefore fails, making it necessary to work backwards, always subtrac-

ting anisotropy from an anisotropic superconductor to make comparisons between them.

The infinitesimal variation of eqn. (3-19) differs from those used for isotropic superconductors in not being a delta-function; either in frequency or in $\underline{k}$. With only two exceptions it is impossible to prove general results with infinitesimal variations of the latter type, because there are several complicating, competing factors present in anisotropic superconductors. For example, adding

$$\varepsilon \sum_{i,j} [\delta(\underline{k}-\underline{k}_i)\delta(\underline{k}'-\underline{k}_j)+\delta(\underline{k}'-\underline{k}_i)\delta(\underline{k}-\underline{k}_j)]\delta(\omega-\omega_0) \quad , \tag{3.22}$$

where $\{\underline{k}_i\}$ and $\{\underline{k}_j\}$ are sets each of 48 symmetry-related directions, to $(\alpha^2F(\omega)_{\underline{kk}'}$ will increase A and $\lambda(0)$, but on the other hand, an unlucky choice of $\{\underline{k}_i\}$ and $\{\underline{k}_j\}$ may reduce the anisotropy of the interaction. The same arguments apply to variations of the type $\varepsilon\delta(\omega-\omega_0)$, variations in the phonon spectrum, and to the changes caused by small amounts of inelastic impurity scattering.

Recall that $\lambda(0)$ does not cancel out of the anisotropic equations, implying that m=n terms <u>will</u> appear in the functional derivative and be proportional to ω_0^{-1}. The remaining terms for $\delta(\alpha^2F(\omega))_{\underline{kk}'} = \varepsilon\delta(\omega-\omega_0)$ will still have the same shape as in Fig. 5-3, since for small anisotropy $\langle\bar{\Delta}_{\underline{k}}(n)\rangle$ has very much the same n dependence as the isotropic solution, and its magnitude will increase by an amount of the order of R_0^2 (thanks to the correlation between $\bar{\Delta}_{\underline{k}}(n)$ and $\lambda_{\underline{k}}(0)$), where

$$R_0^2 \equiv [\Sigma_n \langle\bar{\Delta}_{\underline{k}}^2(n)\rangle - \langle\bar{\Delta}_{\underline{k}}(n)\rangle^2]/\Sigma_n \langle\bar{\Delta}_{\underline{k}}^2(n)\rangle \qquad (3.23)$$

which will be small in realistic calculations. Therefore, at small ω_0, eqn. (3-8) still describes the linear contribution of the m≠n terms.

The contribution to $\delta T_c/\delta(\alpha^2F(\omega))_{\underline{kk}'}$ of the m=n terms for arbitrary $\delta(\alpha^2F(\omega))_{\underline{kk}'}$ is proportional to

$$\Sigma_n \{\iint_{48} \frac{dS_{\underline{k}}}{|v_{\underline{k}}|}\frac{dS_{\underline{k}'}}{|v_{\underline{k}'}|}\bar{\Delta}_{\underline{k}}(n)\delta\lambda_{\underline{kk}'}(0)\bar{\Delta}_{\underline{k}'}(n) - \int_{48}\frac{dS_{\underline{k}}}{|v_{\underline{k}}|}\bar{\Delta}_{\underline{k}}^2(n)\delta\lambda_{\underline{k}}(0)\}/\Sigma_n\langle\bar{\Delta}_{\underline{k}}^2(n)\rangle$$

$$= \Sigma_n \{\iint_{48} \frac{dS_{\underline{k}}}{|v_{\underline{k}}|}\frac{dS_{\underline{k}'}}{|v_{\underline{k}'}|}\delta\lambda_{\underline{kk}'}(0)[\bar{\Delta}_{\underline{k}}(n)\bar{\Delta}_{\underline{k}'}(n) - \tfrac{1}{2}(\bar{\Delta}_{\underline{k}}^2(n)+\bar{\Delta}_{\underline{k}'}^2(n))]\}$$

$$/\ \Sigma\langle\bar{\Delta}_{\underline{k}}^2(n)\rangle \qquad (3.24)$$

which is clearly negative if $\delta\lambda_{\underline{kk}'}(0) > 0$. In the particular case $\delta(\alpha^2F(\omega))_{\underline{kk}'} = \varepsilon\delta(\omega-\omega_0)$, implying $\delta\lambda_{\underline{kk}'}(0) = 2\varepsilon/\omega_0$, expression (3-24) reduces to $-2R_0^2/\omega_0$. The functional derivative of an anisotropic superconductor is therefore qualitatively different only at low frequency; it turns negative when $-2R_0^2/\omega_0$ dominates the linear term described by eqn. (3-8) (see Fig. 5-16 for example). If R_0 is of the same order as the root mean square anisotropy of the gap edge on the real axis (some

evidence will be presented in Chapter 5 in support of this assumption), then eqns. (3-24) and (3-8) imply that the frequency where the functional derivative turns negative is of order $.5\ k_B T_c$, thus only a very small fraction of $\alpha^2F(\omega)$ decreases T_c. Coefficients of $-\omega_0^{-1}$ greater than $2R_0^2$ can be obtained by choosing a $\delta(\alpha^2F(\omega))_{\underline{k}\underline{k}'}$ which is roughly correlated with $\bar{\Delta}_{\underline{k}}(n)\bar{\Delta}_{\underline{k}'}(n)$, and since $\bar{\Delta}_{\underline{k}}(n)$ is correlated with $\lambda_{\underline{k}}(0)$, a likely candidate is

$$\varepsilon \frac{(\alpha^2F(\omega))_{\underline{k}\underline{k}'}}{\alpha^2F(\omega)}\,\delta(\omega-\omega_0). \qquad (3.25)$$

Because the double FS average of expression (3-25) minus $\varepsilon\delta(\omega-\omega_0)$ vanishes, it follows that the most effective way of augmenting T_c while keeping $\alpha^2F(\omega)$ fixed is to exaggerate the anisotropy of $(\alpha^2F(\omega))_{\underline{k}\underline{k}'}$ at as low a frequency as possible because the difference between the δT_c generated by variation (3-25) and the δT_c obtained from $\varepsilon\delta(\omega-\omega_0)$ is inversely proportional to ω_0.

To prove that the thermal phonons are the cause of the change in sign, the functional derivatives must be evaluated on the real axis, where they appear explicitly in the kernel as the $n(\Omega)$ of eqn. (2-31). The proof that the $n(\omega_0)$ are the sole origin of the ω_0^{-1} term in the functional derivative and that it vanishes without gap anisotropy is rather tedious and has been relegated to Appendix IV, together with some other comments about the functional derivative

on the real axis.

It will come as no surprise that $\delta\Delta F/\delta\alpha^2F(\omega_0)$ also has a functional derivative dominated by a negative ω_0^{-1} term at low frequency when anisotropy is present while the remaining terms resemble the isotropic functional derivative. Although similar to eqn. (3-24), the proof requires a longer chain of inequalities than that for $\delta T_c/\delta\alpha^2F(\omega_0)$, thus it is worth writing out. The simplest possible $\delta(\alpha^2F(\omega))_{\underline{k}\underline{k}'} = \varepsilon\delta(\omega-\omega_0)$ is used, and only the terms m=n are considered. Their contribution is

$$(\delta\Delta F)_{m=n} = \varepsilon(\pi k_B T)^2 N(0)\frac{2}{\omega_0}\sum_n\left\{\int\frac{dS_{\underline{k}}}{|v_{\underline{k}}|}\int\frac{dS_{\underline{k}'}}{|v_{\underline{k}'}|}\right.$$

$$\left\{\frac{1}{\sqrt{1+\Delta_{\underline{k}}^{-2}(n)}}\frac{1}{\sqrt{1+\bar{\Delta}_{\underline{k}'}^2(n)}} - 1 + \frac{\bar{\Delta}_{\underline{k}}(n)}{\sqrt{1+\bar{\Delta}_{\underline{k}}^2(n)}}\frac{\bar{\Delta}_{\underline{k}'}(n)}{\sqrt{1+\bar{\Delta}_{\underline{k}}^2(n)}}\right\}$$

$$= \varepsilon(\pi k_B T)^2 N(0)\frac{2}{\omega_0}\sum_n\left\{\left\langle\frac{1}{\sqrt{1+\bar{\Delta}_{\underline{k}}^2(n)}}\right\rangle^2 - 1 + \left\langle\frac{\bar{\Delta}_{\underline{k}}(n)}{\sqrt{1+\bar{\Delta}_{\underline{k}}^2(n)}}\right\rangle^2\right\} \quad (3.26)$$

By the Schwarz inequality,

$$\left\langle\frac{1}{\sqrt{1+\bar{\Delta}_{\underline{k}}^2(n)}}\right\rangle^2 \leq \left\langle\frac{1}{1+\bar{\Delta}_{\underline{k}}^2(n)}\right\rangle$$

and

$$\left\langle\frac{\bar{\Delta}_{\underline{k}}(n)}{\sqrt{1+\bar{\Delta}_{\underline{k}}^2(n)}}\right\rangle^2 \leq \left\langle\frac{\bar{\Delta}_{\underline{k}}^2(n)}{1+\bar{\Delta}_{\underline{k}}^2(n)}\right\rangle$$

so that the quantity in braces is less than or equal to

$$\left\langle \frac{1}{1+\bar{\Delta}_{\underline{k}}^{2}(n)} \right\rangle + \left\langle \frac{\bar{\Delta}_{\underline{k}}^{-2}(n)}{1+\bar{\Delta}_{\underline{k}}(n)} \right\rangle - 1 = 0 \,.$$

It follows that $(\delta\Delta F)_{m=n} \leq 0$ with equality holding for isotropic systems. To prove that thermal phonons are the origin, eqn. (2-43) would have to be rewritten in a form analogous to eqn. (2-42), so that the thermal phonons appear explicitly in the functional derivative as $n(\omega_0)$. In Appendix IV this same procedure of isolating $n(\omega_0)$ is carried out in great detail for δT_c, also showing that the only source of terms inversely proportional to ω_0 as $\omega_0 \to 0$ is the thermal phonons. Since $\lim_{\omega_0 \to 0} n(\omega_0) = \frac{k_B T}{\omega_0}$, and the functional derivative on the real axis has no explicit factors of T like eqn. (3-26), while the coefficient of ω_0^{-1} must be the same whichever way it is obtained, on the real axis or imaginary axis, it follows that $(\delta\Delta F)_{m=n}$ is proportional to T/ω_0. (A corollary is that the quantity in the braces is proportional to T^{-1}.) But $(\delta H_c/\delta\alpha^2 F(\omega_0))_{T=0}$ for isotropic systems is linear, positive, and vanishes as $\omega_0 \to 0$, therefore as $T \to 0$ the contribution of the $m \neq n$ terms to $\delta\Delta F$ is finite and approaches a finite constant. Hence the frequency where the functional derivative changes sign is proportional to T.

Allowing anisotropy adds another dimension to the search for an optimum spectrum and least upper-bound on T_c. The great difficulty lies in the many degrees of freedom even for fixed $\alpha^2 F(\omega)$ or A of the anisotropic electron-phonon interaction - it is unignorably frequency-dependent as a

glance at any $(\alpha^2F(\omega))_{\underline{k}}$ (Fig. 5-21) will show - and in the absence or inconvenience of constraints on the anisotropy. Eqn. (3-21) shows how T_c may be increased indefinitely by exaggerating the already existing anisotropy, while keeping $\alpha^2F(\omega)$ fixed, thus showing the need for a constraint. A constraint on the anisotropy, however defined, that is averaged over frequency does not pin matters down enough, for it would not preclude wild anisotropy at isolated frequencies. That difficulty at least can be avoided by looking only at an anisotropic delta-function in frequency; one expects on the basis of Leavens' work that the optimal spectrum will have the form:

$$(\alpha^2F(\omega))_{\underline{k}\underline{k}'} = A\delta(\omega-\omega_E)V_{\underline{k}\underline{k}'} \qquad (3\text{-}27)$$

where

$$\langle\langle V_{\underline{k}\underline{k}'}\rangle\rangle = 1 \quad \text{and} \quad \langle V_{\underline{k}\underline{k}'}\rangle \equiv 1 + V_{\underline{k}} \,. \qquad (3\text{-}28)$$

Now comes the difficulty of constraining the anisotropy, which first requires defining it. Even the simplest choice, fixing $\langle V_{\underline{k}}^2\rangle$, turns out to be a useless constraint, because the FS weights $dS_{\underline{k}}/|v_{\underline{k}}|$ are also free to vary (but without changing their mean value), thus making the variational equations impossibly complicated. It is more realistic to abandon the idea of constraints on the anisotropy altogether and guess at an optimum interaction with fixed $\alpha^2F(\omega)$ or A.

Consider a spherical FS with

$$V^{\phi}_{\underline{k}\underline{k}'} = S^{-2}\ \phi(\underline{k}-\underline{k}') \qquad (3\text{-}29)$$

where $\phi(\underline{q})$ vanishes unless $\pm\underline{q}$ lies inside the neighbourhood of some wave-vector $\tilde{\underline{q}}$, with the size of the neighbourhood determined by S as follows:

$$\int \frac{dS_{\underline{k}}}{|v_{\underline{k}}|}\ \phi(\underline{k}-\underline{k}') = S \qquad (3\text{-}30)$$

so that only a fraction S assumed to be very small, of the states participate in the electron-phonon interaction. (This interaction does not satisfy crystal symmetry. That defect could be remedied by replacing $\phi(\underline{q})$ by $\sum_R \phi(R\underline{q})$ where the sum is over group operations. The inclusion of symmetry only complicates the equations without altering the proof to follow.) The states between which the interaction occurs are shown in the following diagram:

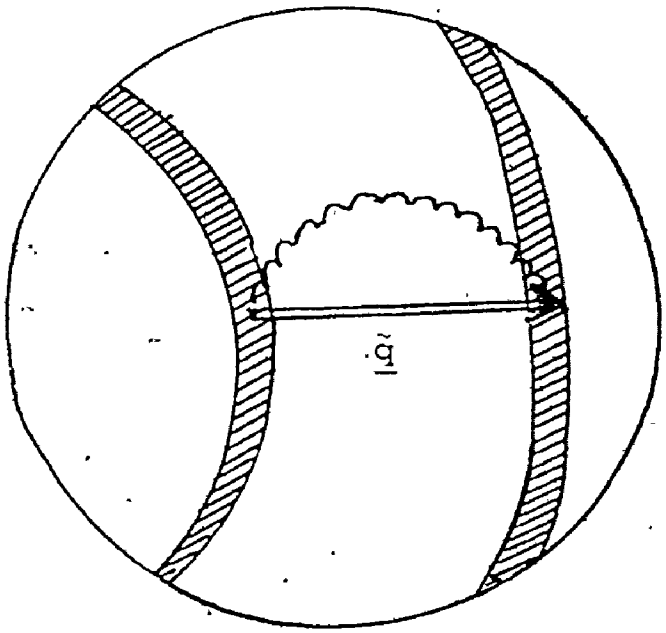

In regions where $\phi(\underline{k}-\underline{k}') = 0$ for any $\underline{k}'$, the $\bar{\Delta}_{\underline{k}}$ vanishes. Elsewhere, the gap is independent of $\underline{k}$ and satisfies the same equation as an isotropic system having $\alpha^2F(\omega) = S^{-1}A\delta(\omega-\omega_E)$. Therefore, if $\mu^* = 0$, T_c has been increased by a factor of S^{-1} over that of the corresponding isotropic system. Because the anisotropic equation has the same form as the isotropic one, where the gap exists, even if $\mu^* \neq 0$, it is possible to determine the optimal frequency for the anisotropic system from Leavens' eqn. (3-11). The new ω_E^* is clearly $1.75\ S^{-1}Ad(\mu^*)$. This rise in ω_E^* can be explained by considering the occupation numbers defined in BCS theory. The ω_E^* for an isotropic system is proportional to A; in an anisotropic system, one expects it to be proportional to the average weighted by the occupation numbers of the areas under the $(\alpha^2F(\omega))_{\underline{k}}$, which is more than the unweighted average by a factor of S^{-1}, since the pairs are formed only from states where the interaction is non-zero, just where the interaction is greater than the usual average by a factor of S^{-2}. Consider the following infinitesimal addition to $(\alpha^2F(\omega))_{\underline{k}\underline{k}}$, which leaves $\alpha^2F(\omega)$ fixed, but distributes the interaction:

$$\varepsilon(\delta(\omega-\omega_E)\phi'(\underline{k}-\underline{k}')-\delta(\omega-\omega_E)\phi(\underline{k}-\underline{k}')) \qquad (3-31)$$

where $\phi'(\underline{q})$ is defined like $\phi(\underline{q})$ but centred on some different wave-vector $\tilde{\underline{q}}'$ such that its neighbourhood does not overlap

with the one defined by $\underline{q}$. Then the first term of (3-31) contributes nothing to $\delta\rho$, since the lack of overlap ensures that $\tau_{\underline{k}}$ vanishes wherever $\phi'(\underline{k}-\underline{k}')$ is non-zero, and the second term therefore makes $\delta\rho$ negative. The conclusion is that the optimum spectrum for fixed A is

$$(\alpha^2F(\omega))_{\underline{k}\underline{k}'} = \lim_{S\to 0} AS^{-2}\phi(\underline{k}-\underline{k}')\delta(\omega-1.75\ S^{-1}\ Ad(\mu^*)). \quad (3-32)$$

Unlike Leavens' optimum spectrum, this resembles nothing seen in nature. However, the steps leading up to it do suggest how, for fixed A, the electron-phonon interaction should be adjusted to maximize T_c: firstly, $\lambda(0) = 2A/\omega_E^*$ should be less than the optimum value quoted by Leavens, since ω_E^* is larger, and secondly, the electron-phonon interaction should be concentrated between as few states as possible.

This section on pure anisotropic superconductors will close with a comparison between a weak coupling and strong coupling superconductor having the same amount of anisotropy (i.e. roughly the same root mean square deviation in $\lambda_{\underline{k}}(0)$), by means of eqn. (2-17). To begin with, it is necessary to make quantitative the distinction between weak coupling and strong coupling. The criterion is not A or T_c but the size of $\lambda(0)$. Compare two isotropic superconductors having spectral densities differing only by a stretch factor r: $\alpha^2F(\omega)$ and $\alpha^2F(r\omega)$. The areas under these distributions are respectively A and A/r, but they have the <u>same</u> $\lambda(0)$. Substitution into eqn. (2-24) shows that their transition temperatures are

T_c and T_c/r, and most importantly, that they have identical $\bar{\Delta}(n)$. Below T_c, eqn. (2-22) implies that at temperatures T and T/r they will have the same $\bar{\Delta}(n)$ so that the analytic continuations $\Delta(\omega)$ and $Z(\omega)$ will be identical except for the same stretch factor as in $\alpha^2F(\omega)$, implying that the ratio of the gap edge at T=0 to the transition temperature and the deviation of $Z(\omega)$ from unity, two of the criteria distinguishing weak coupling from strong coupling, will be the same for the two systems.

Returning to anisotropic superconductors, first, consider the situation with $\mu^* = 0$. Because the λ's are larger, one expects $\tilde{\omega}_{\underline{k}'}(m)$ to be more anisotropic for a strong coupling than a weak coupling superconductor. Since the $\underline{k}'$ dependence of $\lambda_{\underline{k}\underline{k}'}(m-n)$ is positively correlated with $\lambda_{\underline{k}'}(m-n)$ and therefore with $\tilde{\omega}_{\underline{k}'}(m)$ as well, the kernel $\lambda_{\underline{k}\underline{k}'}(m-n)/|\tilde{\omega}_{\underline{k}'}(m)|$ of a strong coupling superconductor will have less $\underline{k}$ dependence than that of a weak coupling superconductor. In addition, since $\tilde{\Delta}_{\underline{k}}(n)$ is positively correlated with $|\tilde{\omega}_{\underline{k}}(n)|$ even if $\tilde{\Delta}_{\underline{k}}(n)$ were equally anisotropic for the two systems, the strong coupling superconductor will have less anisotropy in $\bar{\Delta}_{\underline{k}}(n)$, the quantity of physical interest. If $\mu^* > 0$, then the difference in anisotropy of $\bar{\Delta}_{\underline{k}}(n)$ between the two systems is even greater, because the relative size of μ^* and $\lambda(0)$ is so different. If $\mu^* << \lambda(0)$, then the anisotropy of the kernel is hardly affected by the subtraction of the isotropic

quantity μ^*, but if μ^* and $\lambda(0)$ are of comparable magnitude (in Al, for example $\lambda(0) \sim .4$ and $\mu^* \sim .13$) then $\lambda_{\underline{kk}'}(0)-\mu^*$ is far more anisotropic than $\lambda^*_{\underline{kk}'}(0)$. All these facts suggest that for the same amount of anisotropy in $\lambda_{\underline{k}}(0)$, a weak coupling superconductor will will have a larger R_0^2 than the strong coupling superconductor. In general, for a system with as strong a coupling as Pb, R_0 is less than the root mean square deviation of $\lambda_{\underline{k}}(0)$, while in systems as weak as Al, the inequality is reversed. As yet there is no basis for assuming that $(T_{ca}-T_{ci})/T_{ci}$ will also be larger for the weak coupling superconductor. That, however will be proved true by using elastic impurity scattering to obtain T_{ci}.

3. Elastic Impurity Scattering

In this section, the functional derivative will be used to examine in detail the impurity dependence of ΔF, and the anisotropy, with occasional use of a separable model for the potential. The appropriateness of ρ for such investigation is immediately seen by using eqn. (3-18) to get $\partial T_c/\partial c$:

$$\frac{\partial T_c}{\partial c} = -\frac{\partial T}{\partial \rho}\sum_n \Big\{ \int_{48} \frac{dS_{\underline{k}}}{|v_{\underline{k}}|} \int_{48} \frac{dS_{\underline{k}'}}{|v_{\underline{k}'}|}\, \bar{\Delta}_{\underline{k}}(n)\, \tau^{-1}_{\underline{kk}'}\, \bar{\Delta}_{\underline{k}'}(n)$$

$$- \int_{48} \frac{dS_{\underline{k}}}{|v_{\underline{k}}|}\, \bar{\Delta}^2_{\underline{k}}(n)\, \tau^{-1}_{\underline{k}} \Big\} / \sum_n \langle \bar{\Delta}^2_{\underline{k}}(n) \rangle \ ,$$

Since

$$\int_{48} \frac{dS_{\underline{k}}}{|v_{\underline{k}}|} \bar{\Delta}^2_{\underline{k}}(n)\,\tau^{-1}_{\underline{k}} = \frac{1}{2}\int_{48} \frac{dS_{\underline{k}}}{|v_{\underline{k}}|}\int_{48} \frac{dS_{\underline{k}'}}{|v_{\underline{k}'}|}\,(\bar{\Delta}^2_{\underline{k}}(n)+\bar{\Delta}^2_{\underline{k}'}(n))\tau^{-1}_{\underline{k}\underline{k}'},$$

$\partial T_c/\partial c$ is clearly negative and increases with the amount of gap anisotropy. It is useful to define for later reference

$$R_E^2 \equiv \tau \sum_n \langle\langle \tau^{-1}_{\underline{k}\underline{k}'} [\tfrac{1}{2}(\bar{\Delta}^2_{\underline{k}}(n)+\bar{\Delta}^2_{\underline{k}'}(n))-\bar{\Delta}_{\underline{k}}(n)\bar{\Delta}_{\underline{k}'}(n)]\rangle\rangle / \sum_n \langle\bar{\Delta}^2_{\underline{k}}(n)\rangle. \quad (3\text{-}33)$$

Because $(\Delta W(\underline{q}))^2$ varies smoothly over a scale of k_F in contrast to $\bar{\Delta}_{\underline{k}}$ which repeats itself on every 48th (a region whose maximum dimension is $k_F/\sqrt{2}$) and because the definition (2-50) of $\tau^{-1}_{\underline{k}\underline{k}'}$ probably makes $\tau^{-1}_{\underline{k}\underline{k}'}$ a smoother function of $\underline{k}$ and $\underline{k}'$ than $(\Delta W(\underline{k}-\underline{k}'))^2$ it seems reasonable to replace $\tau^{-1}_{\underline{k}\underline{k}'}$ by τ^{-1} in eqn. (3-33). (The approximation is tested numerically in Chapter 5 for two typical pseudopotentials.) The resulting simplification is

$$\frac{\partial T_c}{\partial c} = \frac{\partial T}{\partial p}\,\tau^{-1} R^2, \quad (3\text{-}34)$$

where R^2 is defined like R_0^2 by eqn. (3-23); the absence of the subscript indicates the presence of elastic impurity scattering. It is unfortunately impossible to prove that this is an over or under estimate; model $\Delta_{\underline{k}}$ and $\tau^{-1}_{\underline{k}\underline{k}'}$ can be invented that lead to $R_E > R$ and $R_E < R$, but there is reason to believe that $R_E \sim R$, which is consistent with the observed fact that the initial slopes of T_c curves for different impurities in the same material are almost the same when plotted as a function

of inverse mean free path.

It is important to realize that eqn. (3-34) is valid at all concentrations, not just in the limit $c \to 0$. Also, since $\rho=0$ is a maximum eigenvalue, it follows from second-order perturbation theory that $\partial^2\rho/\partial c^2 > 0$, so that R^2 decreases with c and being positive, must eventually saturate. It will be proved that when $c\tau^{-1}_{\underline{kk}'} >> k_B T_c$, eqn. (2-50) reduces to eqn. (2-24), so that the expected result, $R^2 \to 0$ at high impurity concentration, does indeed follow from the diagrams chosen in Chapter 2.

The starting point of the proof is eqn. (2-49). With the definitions $a_{\underline{k}}(n) \equiv \bar{\Delta}_{\underline{k}}(n) - \langle \bar{\Delta}_{\underline{k}}(n) \rangle$ and $\bar{\Delta}_0(n) \equiv \langle \bar{\Delta}_{\underline{k}}(n) \rangle$, and for simplicity omitting μ^* and using τ^{-1} instead of $\tau^{-1}_{\underline{kk}'}$, eqn. (2-49) becomes

$$(\Delta_0(n) + a_{\underline{k}}(n))\,|\tilde{\omega}_{\underline{k}}(n)| = \pi k_B T_c \sum (\lambda_{\underline{k}}(m-n)\bar{\Delta}_0(m) + \langle \lambda_{\underline{kk}'}(m-n)\, a_{\underline{k}'}(n)\rangle) + \frac{c\pi}{\tau}\bar{\Delta}_0(n) \quad (3\text{-}35)$$

Taking the FS average of both sides of eqn. (3-35), one obtains

$$\bar{\Delta}_0(n)\left(|\tilde{\omega}(n)| - \frac{c\pi}{\tau}\right) + \left\langle a_{\underline{k}}(n)\left(|\tilde{\omega}_{\underline{k}}(n)| - \frac{c\pi}{\tau}\right)\right\rangle = \pi k_B T_c \sum (\lambda(m-n)\bar{\Delta}_0(m) + \langle \lambda_{\underline{k}}(m-n)\, a_{\underline{k}}(m)\rangle) \quad (3\text{-}36)$$

in which c/τ cancels out, and which reduces to the T_c equation of an isotropic system when $a_{\underline{k}}(n) \to 0$.

Subtracting eqn. (3-36) from eqn. (3-35), one obtains

$$\bar{\Delta}_0(n)\left(|\tilde{\omega}_{\underline{k}}(n)|+|\tilde{\omega}(n)|\right) + a_{\underline{k}}(n)|\tilde{\omega}_{\underline{k}}(n)|+<a_{\underline{k}}(n)\left(|\tilde{\omega}_{\underline{k}}(n)|-\pi\frac{c}{\tau}\right)>$$

$$=\pi k_B T_c \sum\{(\lambda_{\underline{k}}(m-n)-\lambda(m-n))\bar{\Delta}_0(m)+<(\lambda_{\underline{kk}'}(m-n)-\lambda_{\underline{k}'}(m-n))a_{\underline{k}'}(m)>\}. \quad (3.37)$$

In this equation c/τ appears only in the term $\pi a_{\underline{k}}(n)c/\tau$. All other quantities have no explicit dependence on c/τ. T_c may be divided out on both sides of the equation so that it is present only buried in the λ's. It follows that as c/τ becomes the dominant term in $|\tilde{\omega}_{\underline{k}}(n)|$, (i.e. $\frac{c}{\tau} >> k_B T_c$), $a_{\underline{k}}(n)/\bar{\Delta}_0(n)$ is proportional to c^{-1}. Hence for large c, eqn. (3-36) reduces to the isotropic limit.

Now an argument will be presented that $\partial\rho/\partial T$ changes by an amount of order R_0^2 as T_c falls from T_{ca} to T_{ci}. Since $\partial\lambda_{\underline{kk}'}(0)/\partial T = 0$, there is no term inversely proportional to frequency as in $\delta\rho/\delta\alpha^2F(\omega)$. Also, $<\bar{\Delta}_{\underline{k}}(n)>^2$ changes by an amount of order R_0^2. Finally, Table 5-3 shows that $\partial\rho/\partial T$ varies by a factor of 2.5 over all the range of systems studied, showing a gradual decrease with T_c and $\lambda(0)$, suggesting that $\partial\rho/\partial T$ is quite insensitive to T_c as well. Numerical verification of this assertion is provided in Chapter 5.

Since the washing out of anisotropy depends on $c/\tau\ k_B T_c$, one expects R^2 to decrease faster as a function of $c\tau^{-1}$ for weak coupling than strong coupling systems, and since $|\partial T/\partial\rho|$ is larger for weak coupling than strong coupling superconductors, the inescapable conclusion is that for a given amount of anisotropy in the interaction, the weak coupling system will have not just more gap anisotropy but a larger $(T_{ca}-T_{ci})/T_{ci}$.

This means that on experimental curves such as fig. 2-1, the initial dip will be shallower and have a smaller initial slope, thus making the valence effect obscure the mean free path effect. Anisotropy effects are in general smaller in strong superconductors.

Since $a_{\underline{k}}(n) \propto c^{-1}$ for large c, eqn. (3-34) implies that for that limit $T_c(c)-T_{ci} \propto c^{-1}$. For other values of c, eqn. (3-34) gives little information about $T_c(c)$; all the c-dependence is hidden in the eigenvectors, and when nothing is known about the other eigenvalues or eigenvectors of eqn. (3-18), no perturbation expansion of the $\bar{\Delta}_{\underline{k}}(n)$ is feasible. The way around this obstacle is to use a model interaction that makes c/τ appear explicitly in R^2. But models will be used only as a last resort at the end of this section. It is still possible to make some headway with R^2, and $\partial\Delta F/\partial c$ remains to be examined.

In both strong and weak coupling superconductors, R_0^2 can be approximated to a very good degree by

$$R_0^2 \approx 1 - <\bar{\Delta}_{\underline{k}}(1)>^2/<\bar{\Delta}_{\underline{k}}^2(1)> \qquad (3-38)$$

because $\bar{\Delta}_{\underline{k}}^2(n)$ is a very rapidly decreasing function of n, and changes relatively little in shape for the first few n. The approximation turns out to be slightly worse for weak coupling. Now, a connection can be made between R and an observable, the gap edge at T=0. It can be shown that for a weak coupling superconductor the real part of the gap can be

approximated at low frequency by a frequency-independent constant[101], the gap edge, and that the anisotropy in the gap edge is nearly temperature-independent. It follows from eqn. (2-29) that R is very close to the root mean square deviation of the gap edge at T=0. For strong coupling, Re $\Delta_{\underline{k}}(\omega)$ shows much more structure, and there is no evidence, for or against, that the anisotropy of the gap edge is temperature-independent. Nevertheless, if it could be shown numerically that if the shape and therefore the anisotropy of $\bar{\Delta}_{\underline{k}}(n)$ is temperature independent down to very low temperatures implying the same property in Re $\bar{\Delta}_{\underline{k}}(\omega)$, then R could be identified with the anisotropy of the zero-temperature gap edge, since the dominant contribution to $\bar{\Delta}_{\underline{k}}(1)$ at very low temperature is from the low frequency part of Re $\Delta_{\underline{k}}(\omega)$. But at low frequency near the gap edge, Re $\Delta_{\underline{k}}(\omega)$ is slowly varying (it is a constant + a term quadratic in ω) and is therefore close to the value at the gap edge. Accordingly, the root mean square anisotropy in $\bar{\Delta}_{\underline{k}}(k)$ would be identified with the root mean square anisotropy of the zero-temperature gap edge, finally making the connection between R^2 and a measurable quantity. This is verified in Chapter 5.

Another method of connecting R^2 with the gap on the real axis is purely mathematical - using Poisson's formula and the analytic properties of Green's functions. According to Poisson's formula

$$\sum_{\text{odd } n} G(\underline{k},i\omega_n)G(\underline{k}',i\omega_n) = -\frac{1}{2\pi i k_B T}\int_C dz f(z)G(\underline{k},z)G(\underline{k}',z) \quad (3\text{-}39)$$

where the contour C is shown in Fig. 3-3(a).

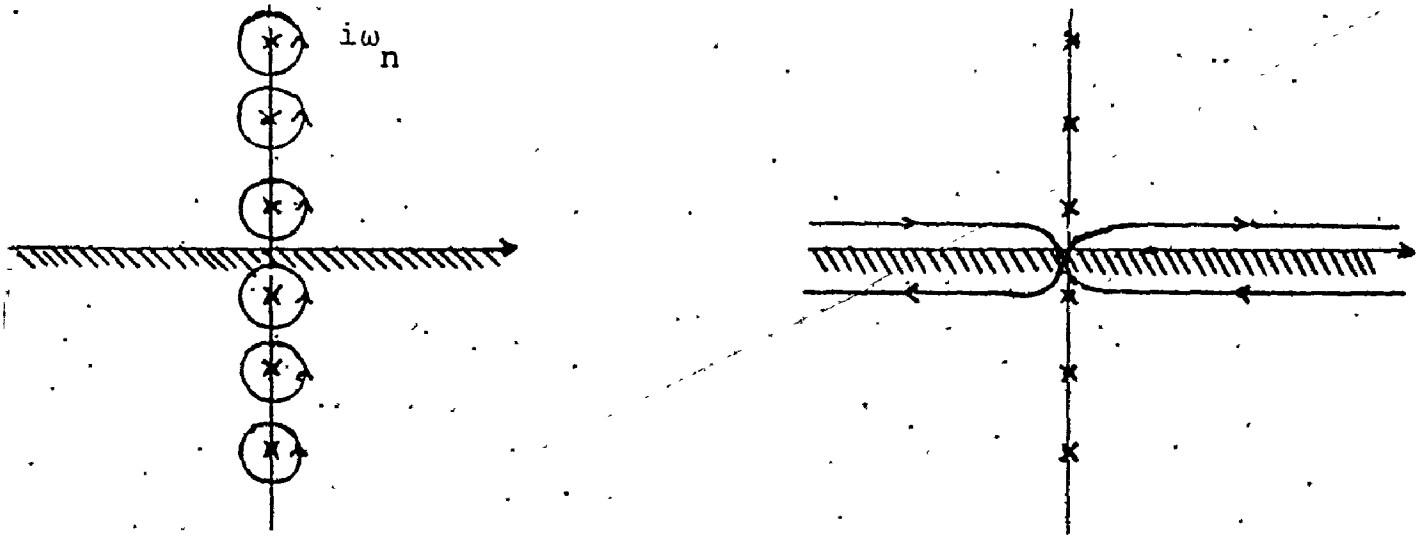

Fig. 3-3(a) Contour C (b) Contour C'

Since $G(\underline{k},z)$ has no poles but only a branch cut on the real axis, the contour C may be deformed to C' shown in Fig. 3-3(b), so that eqn. (3-39) becomes

$$\sum_{\text{odd } n} G(\underline{k},i\omega_n)G(\underline{k}',i\omega_n) = -\frac{1}{2\pi i k_B T}\int_{C'} dz f(z)G(\underline{k},z)G(\underline{k}',z)$$

$$= -\frac{1}{2\pi i k_B T}\int_{-\infty}^{\infty} d\omega f(\omega)\pi^{-2}\int_{-\infty}^{\infty} d\omega'\int_{-\infty}^{\infty} d\omega'' \rho(\underline{k},\omega')\rho(\underline{k}',\omega'')$$

$$\left(\frac{1}{\omega+i\delta-\omega'}\frac{1}{\omega+i\delta-\omega''} - \frac{1}{\omega-i\delta-\omega'}\frac{1}{\omega-i\delta-\omega''}\right)$$

$$= \frac{1}{2\pi i k_B T}\int_{-\infty}^{\infty} d\omega 2i\ \mathrm{Im}(G(\underline{k},\omega+i\delta)G(\underline{k}',\omega+i\delta)) \quad (3\text{-}40)$$

using the identities $f(\omega)+f(-\omega)=1$, $\mathrm{Im}\frac{1}{\omega+i\delta} = i\pi\delta(\omega)$, and $-G(\underline{k},-\omega+i\delta) = G(\underline{k},\omega+i\delta) = G^*(\underline{k},\omega-i\delta)$.

Now specializing to the case of the gap on the real axis at T_c, and performing the standard $\int d\varepsilon_{\underline{k}} \int d\varepsilon_{\underline{k}'}$ integration on both sides of eqn. (3-40), one obtains

$$\Sigma\, \bar{\Delta}_{\underline{k}}(n)\bar{\Delta}_{\underline{k}'}(n) = \frac{1}{\pi k_B T_c} \int_{-\infty}^{\infty} \mathrm{Im}\left(\frac{\Delta_{\underline{k}}(\omega)}{\omega} \frac{\Delta_{\underline{k}'}(\omega)}{\omega}\right) . \qquad (3\text{-}41)$$

Therefore

$$R^2 = \int_{-\infty}^{\infty} \frac{d\omega}{\omega^2} \mathrm{Im}\{\langle\Delta_{\underline{k}}^2(\omega)\rangle - \langle\Delta_{\underline{k}}(\omega)\rangle^2\}$$

$$/\int_{-\infty}^{\infty} \frac{d\omega}{\omega^2} \mathrm{Im}\langle\Delta_{\underline{k}}^2(\omega)\rangle . \qquad (3\text{-}42)$$

(The integral does not diverge because at T_c, $\lim_{\omega\to 0} \mathrm{Re}\,\Delta(\omega) \propto \omega^2$ and $\mathrm{Im}\,\Delta(\omega)$ is odd.) Even though it could be expressed in terms of $\mathrm{Re}\,\Delta_{\underline{k}}(\omega)$ alone, eqn. (3-42) is not informative unless the gap anisotropy is temperature-independent. That question will be answered in Chapter 5 by examining the temperature dependence of the anisotropy of the solutions on the imaginary axis.

$\partial\Delta F/\partial c$ for a system with s-wave elastic scattering ($\tau_{\underline{k}\underline{k}'}^{-1} = \tau^{-1}$) will, not surprisingly, be identical to eqn. (3-26), except that $\pi(\tau k_B T)^{-1}$ replaces $2\varepsilon/\omega_0$. Knowing the temperature dependence of the quantity in braces, one finds that $\lim_{T\to 0} \frac{\partial\Delta F}{\partial c}$ is a constant depending on the anisotropy. Since ΔF, like ρ, is stationary with respect to variations in $\bar{\Delta}_{\underline{k}}(n)$,

results similar to those for T_c can be proved: $\partial\Delta F/\partial c < 0$, and $\partial^2\Delta F/\partial c^2 > 0$ so that the quantity in braces in (3-26) (the analogue of R^2) decreases to zero as c increases.

To obtain T_c as a function of c, a separable model for the anisotropy first used by Markowitz and Kadanoff[36] will be introduced. They applied it to the BCS model on the real axis and therefore limited their work to weak coupling superconductors, but set $\mu^* = 0$ (a bad approximation in weak coupling systems) and ignored anisotropy in $Z_{\underline{k}}(\omega)$ (a better approximation). Their model will be generalized to remove these faults and used on the imaginary axis, where strong coupling is easier to handle. The model consists of replacing $(\alpha^2F(\omega))_{\underline{k}\underline{k}'}$ by $\alpha^2F(\omega)(1+a_{\underline{k}})(1+a_{\underline{k}'})$ (this $a_{\underline{k}}$ has no connection with the quantity in eqn. (3-35)) where $\langle a_{\underline{k}}\rangle = 0$, and to make some contact with reality, $a_{\underline{k}}$ is shaped like $\lambda_{\underline{k}}(0)$ or the area under $(\alpha^2F(\omega))_{\underline{k}}$, (the two are very similar in lead), so that $\sqrt{\langle a_{\underline{k}}^2\rangle}$ is the root mean square deviation of $\lambda_{\underline{k}}(0)$. Substituting this kernel into eqn. (2-50) gives the one-dimensional equation expected from a separable kernel:

$$\tilde{\Delta}'(n) = \pi k_B T_c \sum (\lambda(m-n) - \mu_E^*(n)) \frac{\tilde{\Delta}'(m)}{|\tilde{\omega}(m)|} \qquad (3\text{-}43a)$$

where

$$\Delta'(n) = \langle \tilde{\Delta}_{\underline{k}}(n) \rangle_{p_n} \qquad (3\text{-}43b)$$

$$|\tilde{\omega}(n)| = p_n / [r_n + s_n + p_n(s_n + t_n)] \qquad (3\text{-}43c)$$

$$r_n = \left\langle \frac{1}{|\omega_n| + (1+a_{\underline{k}})\pi k_B T_c \sum_m \lambda(m-n)\,\mathrm{sgn}\omega_n \omega_m + c\pi/\tau} \right\rangle \qquad (3\text{-}43d)$$

$$s_n = \langle a_{\underline{k}}/\text{same denominator}\rangle \tag{3-43e}$$

$$t_n = \langle a_{\underline{k}}^2/\text{same denominator}\rangle \tag{3-43f}$$

$$p_n = \frac{1 - \frac{c\pi}{\tau} r_n}{1 + \frac{c\pi}{\tau} s_n} \tag{3-43g}$$

$$\mu_E^*(n) = \mu^* E_n/S \tag{3-43h}$$

$$S = \pi k_B T_c \mu^* \Sigma_m s_m/(1 + \frac{c\pi}{\tau} s_m) \tag{3-43i}$$

$$E_n = \pi k_B T_c \Sigma_m \lambda(m-n)(t_m+s_m)/(1+c\pi s_m/\tau) \tag{3-43j}$$

$$+ \frac{\pi c}{\tau} s_n/(1 + \frac{\pi c}{\tau} s_n) .$$

If the FS is treated as spherical (that can be done when the Fermi surface anisotropy is already built into the $a_{\underline{k}}$ through their resemblance to the $\lambda_{\underline{k}}(0)$) then the FS averages in (3-43d), (e) and (f) can be replaced by integrals over the probability density P(a) defined as follows: P(a)da = probability that $a_{\underline{k}}$ lies between a and a+da. The use of a probability density necessitated the approximation of $\tau'_{\underline{k}\underline{k}}$, by τ^{-1}. It also means that less will be known about $\bar{\Delta}_{\underline{k}}(n)$; only the probability density $P_\Delta(a)$ that $\bar{\Delta}_{\underline{k}}(n)$ deviates by a fraction a from its mean value. That probability density, together with the T_c obtained from eqn. (3-43) can be compared with the solution generated from a more accurate method described in the next chapter.

For a strong coupling superconductor, with s-wave scattering, $T_{ca}-T_c(c)$ may be approximated as follows:

$$T_{ca}-T_c(c) = \int_c^0 dc\, \frac{\partial T_c}{\partial c} \approx \tau^{-1}\left|\frac{\partial T}{\partial \rho}\right| \int_c^0 dc\,(1-<\bar{\Delta}_{\underline{k}}(1)>^2/<\bar{\Delta}^2_{\underline{k}}(1)>) \qquad (3\text{-}44)$$

since R^2 can be approximated by the first term in the sum. Although for weak coupling R^2 may also be approximated by one term, the non-zero μ^* makes the expression for $\tilde{\Delta}_{\underline{k}}(1)$ excessively complicated. In addition, because $\frac{c}{\tau}$ is larger in comparison to the rest of $\tilde{\omega}_{\underline{k}}(n)$, the remaining terms in R^2 have a relatively greater dependence on $\frac{c}{\tau}$ and cannot be neglected.

For $\mu^*=0$, a reasonable approximation for very strong coupling, and which should not affect the R^2 when $<a^2_{\underline{k}}>$ is small, eqns. (3-43) and the definition of $(\alpha^2F(\omega))_{\underline{kk}}$, imply

$$\tilde{\Delta}_{\underline{k}}(1) = <\tilde{\Delta}_{\underline{k}}(1)>(1 + p_1 a_{\underline{k}})$$

so that

$$<\bar{\Delta}_{\underline{k}}(1)> = <\frac{<\tilde{\Delta}_{\underline{k}}(1)>(1+a_{\underline{k}}p_1)}{\pi k_B T_c(1+(1+a_{\underline{k}})\lambda(0)+c\tau^{-1}/k_BT_c)}>$$

$$<\bar{\Delta}^2_{\underline{k}}(1)> = <(\frac{<\tilde{\Delta}_{\underline{k}}(1)>(1+a_{\underline{k}}p_1)}{\pi k_B T_c(1+(1+a_{\underline{k}})\lambda(0)+c\tau^{-1}/k_BT_c)})^2>.$$

Assuming small anisotropy, so that terms of order higher than $<a^2_{\underline{k}}>$ can be neglected, an expression for R^2 as a function of c can be obtained after some tedious algebra from

$$R^2 \approx 1 - \langle \bar{\Delta}_{\underline{k}}(1)\rangle^2 / \langle \bar{\Delta}^2_{\underline{k}}(1)\rangle$$
$$\approx \frac{\langle a^2_{\underline{k}}\rangle (\lambda^2(0)-1)}{(1+\lambda(0) + \frac{c}{\tau k_B T_c})^2} \quad (3\text{-}45)$$

Note that as expected in a strong coupling system, $R_0^2 < \langle a^2_{\underline{k}}\rangle$:

$$R_0^2 = \langle a^2_{\underline{k}}\rangle (\lambda(0)-1)/(\lambda(0)+1). \quad (3\text{-}46)$$

Integrating eqn. (3-45) while treating T_c as a constant (it varies by only a few percent) gives .

$$T_{ca} - T_c(c) \approx -k_B T_{ca} \frac{\partial T}{\partial \rho} \langle a^2_{\underline{k}}\rangle (\lambda^2(0)-1)\{\frac{1}{1+\lambda(0)} - \frac{1}{1+\lambda(0) + \frac{c}{\tau k_B T_{ca}}}\}. \quad (3\text{-}47)$$

In contrast, Markowitz and Kadanoff predict for weak coupling .

$$T_{ca} - T_c(c) = \langle a^2_{\underline{k}}\rangle T_c I_c \ (\frac{c}{k_B T_c \tau}) \quad (3\text{-}48a)$$

where

$$\lim_{c\to 0} I_c \sim -\frac{\pi}{8} \frac{c}{k_B T_{ca} \tau} \quad (3\text{-}48b)$$

and

$$\lim_{\frac{c}{\tau} >> k_B T_c} I_c \sim \ell n(\frac{1}{2 k_B T_c \tau}) \quad (3\text{-}48c)$$

If more terms had been retained in the expression for R^2, then eqn. (3-47) would reduce for $\lambda(0) << 1$ (ie no anisotropy in $Z_{\underline{k}}(\omega)$ and very weak coupling) to digamma functions and a function similar to I_c. Taking the limit $c\tau^{-1} >> k_B T_{ca}$ in eqn. (3-47) gives

$$\frac{T_{ca}-T_{ci}}{T_{ca}} \sim -\frac{\partial T}{\partial \mu} \langle a_{\underline{k}}^2 \rangle (\lambda(0)-1)/(\lambda(0)+1) . \qquad (3\text{-}49)$$

This is to be compared with Markowitz and Kadanoff's result for weak coupling

$$\frac{T_{ca}-T_{ci}}{T_{ci}} = \frac{1}{N(0)V} \langle a_{\underline{k}}^2 \rangle \qquad (3\text{-}50)$$

where $N(0)V$ is defined by the standard result of BCS theory

$$k_B T_{ci} = \omega_D \exp(-1/N(0)V) . \qquad (2\text{-}46)$$

It is important to realize that these last two results are the difference in T_c between the pure strong coupling and the dirty limit strong coupling only if the diagrams of eqn. 2-48) are correct. Otherwise they are only the difference between the anisotropic and corresponding isotropic systems.

The separable model with the assumption of small anisotropy has already been applied by Clem[22] to other thermodynamic properties of weak coupling superconductors. Since the convergence of eqn. (2-41) for an isotropic system already presents difficulties because the three terms cancel to about .0001% (see Chapter 5), it seems unwise to apply approximations such as those leading to eqn. (3-50) to obtain the effect of anisotropy on ΔF. In addition, properties such as C_v at very low temperatures are sensitive to the details of $P(a)$ - a few small regions where the gap is small can contribute substantially to C_v. Rather, the best possible numerical methods [illegible] be [illegible] ied to the [illegible] and the

CHAPTER 4

FERMI SURFACE HARMONICS

In realistic calculations the limitations of computer time and the fineness of the grid of k-points required for accuracy (the minimum grid square size is 2 degrees × 2 degrees) make it impossible to iterate equations (2-13) or (2-17) to convergence, either on the real or the imaginary axis. Below T_c some worthwhile results can be obtained by inserting the solution of the isotropic gap equation into the right-hand side of the anisotropic equations with the real Fermi surface, as has been done at T=0 on the real axis for Pb by Tomlinson and Carbotte[73]. This procedure was first suggested by Bennett[81]. It is not clear however, whether this one-iteration result is an over or under estimate of the gap anisotropy. A different approach by Leavens and Carbotte[101] using approximations to the part of the kernel derived from the Green's functions effectively went as far as two iterations and yielded an approximate T_{ca} and zero-temperature gap, but used approximations valid only for weak coupling superconductors and did not include Fermi surface anisotropy. A very disturbing feature pointed out by Leavens and Carbotte is that the mean value of the gap obtained after one iteration is <u>less</u> than the mean value of the gap for the corresponding isotropic system, contradicting the theory of Chapter 2.

Tomlinson and Carbotte make no such comparison in their paper; but it was still possible to average their values of the gap edge at T=0, giving a mean of 1.33 meV, in comparison to 1.38 meV for the corresponding isotropic system[102]. The reason for stressing this particular weakness of one-iteration results is two-fold: firstly, it is the only property of the anisotropic gap that is constrained, there being no such condition on the quantity of real interest, the mean square anisotropy of the gap edge, and secondly because errors in the mean value of the gap will invalidate attempts to obtain the anisotropy dependence of quantities such as the specific heat, even if the one-iteration result did have the correct mean square anisotropy. Leavens and Carbotte[101] also iterated to convergence several model interactions consisting of a sum of factorable matrix elements and found that the anisotropy changed little after the first iteration but that the mean value of the gap converged very slowly; 5 iterations brought it up only half the distance separating the isotropic gap from the average anisotropic gap. It is not clear how much of their results would carry over to strong coupling systems with Fermi surface anisotropy.

For these reasons it is desirable to write the gap equations in a form that can be iterated to convergence. This implies an expansion of the gap and the kernel in some new basis truncated to a reasonable size. On a spherical Fermi surface, the spherical harmonics would seem a natural choice,

thanks to their orthonormality and simple functional form. This choice however overlooks one of the most important themes of this chapter, that of crystal symmetry and the constraints it places on the basis. Pb is fcc at all temperature and the pairing is s-wave, therefore the gap is invariant under all operations of the full cubic group O_h, the set of proper and improper rotations and reflections which map a cube or octahedron into itself. In the language of group theory, the gap is a Γ_1 representation of O_h. Since the basis functions used to expand the gap and the kernel must obviously share all their invariance properties, the basis functions are also Γ_1 representations. The group O_h is large (48 operations) and therefore reduces greatly (all odd orders are thrown out for example) the number of basis functions that can be constructed from suitable linear combinations of the spherical harmonics, ie the Kubic harmonics, which are usually expressed as real polynomial functions of the Cartesian coordinates, not as trigonometric functions. Individual terms of a Kubic harmonic have the form $x^p y^q z^r$ where $p, q, r \geq 0$ and $p+q+r$ = order of Kubic harmonic. The Kubic harmonics of type Γ_1 a given order are therefore less numerous than the spherical harmonics (see Table II-3). This is a liability when an orthonormal set of polynomials is to be used to expand a relatively smooth function. The orthogonality of a given polynomial to all the ones of lower order implies that it must have more changes of sign, and the higher the order the more violent these oscillations w[illegible]

in fitting one-dimensional functions it is better practice to divide up the domain of the function into smaller regions and fit each region independently with only a few polynomials of low order subject to boundary conditions that make the polynomial fit continuous and smooth at the boundaries of the regions (cubic splines are a familiar example). Something analogous can be done when the Fermi surface is non-spherical and consists of disjoint pieces (see Fig.5-22), only here there are no boundary conditions to worry about. One can define new basis functions in terms of the old global ones that covered the entire surface by setting the global polynomial to zero everywhere except in the chosen region and its symmetry-related "partners", that is the pieces of the Fermi surface related to the chosen region by some group operation. At one stroke the number of polynomials of a given order is quadrupled, since the four regions in Fig. 5-22 are not symmetry-related. But that is not the only gain in numbers. A polynomial that is zero everywhere except in region 1, say, need not be invariant under as many group operations as the global polynomial. Hence x^4+y^4 is an acceptable basis function if confined to region 1. But in such cases, when the local function is defined differently from the global functions, a complication arises because then the local functions must have different functional forms on the other symmetry-related pieces of Fermi surface. In this example, the basis function is defined as

$x^4 + y^4$ near (001), (00$\bar{1}$)

y^4+z^4 near ($\bar{1}$00), ($\bar{1}$00)

$z^4 + x^4$ near (010), (0$\bar{1}$0)

to have full cubic symmetry. Fortunately this multiplicity of functional forms does not complicate the numerical work, where only the values on the 48th are of interest. An additional reason for using local rather than global basis functions for the gap equations is that the local average values of the directional $\lambda_{\underline{k}}(0)$ and of the one-iteration gap vary considerably among the four regions. In fact, there is more variation between than within the regions.

On a non-spherical Fermi surface the Kubic harmonics and the local basis functions derived therefrom will not be orthogonal with the weight function $dS_{\underline{k}}/|v_{\underline{k}}|$. This could be corrected by performing Gram-Schmidt orthogonalization on the polynomial functions of Cartesian coordinates, using $\frac{dS_{\underline{k}}}{|v_{\underline{k}}|}$ as the weight function for the inner product. The Gram-Schmidt recursion formula is

$$\psi_0 = \phi_0/\sqrt{<\phi_0|\phi_0>}$$

$$\psi_\ell = (\phi_\ell - \sum_{\ell'=1}^{\ell-1} <\phi_\ell|\psi_{\ell'}>)/N_\ell$$

Here the ϕ_ℓ are the non-orthogonal polynomials, ψ_ℓ the orthonormal set generated from them, $<\ |\ >$ denotes the inner product, and N_ℓ is a constant determined by the condition

$\langle \psi_\ell | \psi_\ell \rangle = 1.$

According to P.B. Allen[1], more suitable arguments for polynomial basis functions are the components of the velocity. He argues that the kind of functions that need expansion are usually slowly varying in the nearly-free-electron like parts of the Fermi surface and vary rapidly near the intersection of the Fermi surface with the Brillouin zone, just where the velocity deviates from its nearly free electron values (see Fig. 5-20). In fact the deviations of $\lambda_{\underline{k}}$ and the one-iteration gap from their local mean value correlate well with the deviations of $v_{\underline{k}}^2$ from its mean value. That the correlation goes the wrong way - $v_{\underline{k}}^2$ decreases where $\lambda_{\underline{k}}$ and $\Delta_{\underline{k}}$ increase - is not a serious objection, since a linear combination of polynomials that goes up near the edge of the Fermi surface can always be constructed by subtracting the upward-curling polynomials from the zeroth order (constant) basis functions. This supposition is confirmed numerically in the next chapter. Therefore, basis functions with velocity components as arguments already have some of the shape of the functions that they are meant to expand built right in to them, so that convergence should be rapid compared to the expansion mentioned in the previous paragraph. Finally, the use of $\underline{v}_{\underline{k}}$ rather than Cartesian coordinates increases the number of linearly independent basis functions when there is Fermi surface anisotropy. As an illustrative example, consider the three polynomials 1, z^2, x^2+y^2, which

satisfy the symmetry constraints for region 1. In contrast to 1, $v_z^2 + v_x^2 + v_y^2$, the former set is linearly dependent whereas the latter is not because $v_x^2 + v_y^2 + v_z^2$ is not a constant.

P.B. Allen named these promising functions Fermi surface harmonics (FSH). Throughout the main body of this thesis that name will be reserved for the Gram-Schmidt orthogonalized functions, to be denoted by ψ_ℓ. It is convenient to define a function $i(\ell)$, i being the region where ψ_ℓ is non-zero. The symbols ℓ, ℓ', ℓ'' etc. and i, i' will be reserved as basis and region labels. The subscripts on the ϕ_ℓ, the functions from which the ψ_ℓ are derived by Gram-Schmidt orthogonalization have the same meaning. (Note that Gram-Schmidt orthogonalization does not mix functions from different regions.) Chapter 5 lists the ϕ_ℓ actually used in the numerical calculations, and Appendices I, II and III provide a longer list as well as describing systematic methods of obtaining the ϕ_ℓ by means of group theory.

To rewrite equations (2-15) and (2-17) in the new basis, the Clebsch-Gordan coefficients of the FSH are needed. Define

$$C_{\ell\ell'\ell''} \equiv \int_{48} \frac{dS_{\underline{k}}}{|v_{\underline{k}}|} \psi_\ell(\underline{v}_{\underline{k}})\psi_{\ell'}(\underline{v}_{\underline{k}})\psi_{\ell''}(\underline{v}_{\underline{k}})$$

It follows immediately that a product of two FSH can be written as

$$\psi_\ell(\underline{v}_{\underline{k}})\psi_{\ell'}(\underline{v}_{\underline{k}}) = \sum_{\ell''} C_{\ell\ell'\ell''}\psi_{\ell''}(\underline{v}_{\underline{k}})$$

By inspection, the Clebsch-Gordan coefficients are symmetric in all three subscripts and vanish unless $i(\ell) = i(\ell') = i(\ell'')$. A less obvious pert

ψ_0 -

polynomials, is that $C_{\ell\ell'\ell''}$ also vanishes if the orders of ψ_ℓ, $\psi_{\ell'}$ and $\psi_{\ell''}$ fail to satisfy the triangle inequality. Therefore the number of terms in the above expansion is finite.

In translating equations (2-15) and (2-17) into the FSH basis, the question of the completeness of the FSH comes up, because the equations are unmanageable without the assumption

$$\sum_{\ell} \psi_\ell(\underline{v}_{\underline{k}}) \psi_\ell(\underline{v}_{\underline{k}'}) = \delta(\underline{k}-\underline{k}') \ .$$

P.B. Allen[1,18] has considered the completeness of the FSH in some detail, concluding that if there are no pairs of wavevectors $\underline{k}_1$ and $\underline{k}_2$ such that $\underline{v}_{\underline{k}_1} = \underline{v}_{\underline{k}_2}$ then the set is complete. That such an equality should occur accidentally is unlikely, but the higher symmetry of $\underline{v}_{\underline{k}}$ compared to $\underline{k}$ makes such an occurrence possible at a few points or lines of measure zero. If the FSH are used to expand only functions having as much as or more symmetry than the $\underline{v}_{\underline{k}}$, then there is no problem, because if symmetry implies $\underline{v}_{\underline{k}_1} = \underline{v}_{\underline{k}_2}$, then it also implies that the gap, for example, is the same at $\underline{k}_1$ and $\underline{k}_2$. The FSH are therefore for all practical purposes a complete set because the probability of accidental degeneracy of $\underline{v}_{\underline{k}}$ is negligible.

With the following definitions

$$\bar{\Delta}_\ell(n) \equiv \int_{48} \frac{dS_{\underline{k}}}{|\underline{v}_{\underline{k}}|} \psi_\ell(\underline{v}_{\underline{k}}) \bar{\Delta}_{\underline{k}}(n) \qquad (4\text{-}1)$$

$$\tau_{\ell\ell'} \equiv \int\int_{48} \frac{dS_{\underline{k}}}{|\underline{v}_{\underline{k}}|} \frac{dS_{\underline{k}'}}{|\underline{v}_{\underline{k}'}|} \psi_\ell(\underline{v}_{\underline{k}}) \psi_{\ell'}(\underline{v}_{\underline{k}'}) \tau^{-1}_{\underline{k}\underline{k}'}$$

$$\hat{\tau}_{\ell\ell'} \equiv \int_{48} \frac{dS_{\underline{k}}}{|v_{\underline{k}}|} \psi_\ell(\underline{v}_{\underline{k}})\psi_{\ell'}(\underline{v}_{\underline{k}})\tau_{\underline{k}}^{-1}$$

$$= \sum_{\ell''} C_{\ell\ell'\ell''} \int_{48} \frac{dS_{\underline{k}}}{|v_{\underline{k}}|} \psi_{\ell''}(\underline{v}_{\underline{k}})\tau_{\underline{k}}^{-1}$$

$$\mu^*_{\ell\ell'} = \begin{cases} \mu^* \sqrt{W_{i(\ell)}}\sqrt{W_{i(\ell')}} & \text{Order of } \psi_\ell = \text{order of } \psi_{\ell'} = 0 \\ 0 & \text{otherwise} \end{cases}$$

W_i = weight of region i.

$$\lambda_{\ell\ell'}(n) \equiv \iint_{48} \frac{dS_{\underline{k}}}{|v_{\underline{k}}|} \frac{dS_{\underline{k}'}}{|v_{\underline{k}'}|} \psi_\ell(\underline{v}_{\underline{k}})\psi_{\ell'}(\underline{v}_{\underline{k}'})\lambda_{\underline{k}\underline{k}'}(n)$$

$$\hat{\omega}_{\ell\ell'}(n) \equiv \int_{48} \frac{dS_{\underline{k}}}{|v_{\underline{k}}|} \psi_\ell(\underline{v}_{\underline{k}})\psi_{\ell'}(\underline{v}_{\underline{k}})[\tilde{\omega}_{\underline{k}}(n) - c\pi\tau_{\underline{k}}^{-1}\mathrm{sgn}(\omega_n)]/\pi k_B T$$

$$= \sum_{\ell''} C_{\ell\ell'\ell''} \int_{48} \frac{dS_{\underline{k}}}{|v_{\underline{k}}|} \psi_{\ell''}(\underline{v}_{\underline{k}})[\tilde{\omega}_{\underline{k}}(n) - c\pi\tau_{\underline{k}}^{-1}\mathrm{sgn}(\omega_n)]/\pi k_B T$$

the transition temperature equation can be written

$$[\frac{c\hat{\tau}_{\ell\ell}}{k_B T_c} + |\hat{\omega}_{\ell\ell}(n)|]\bar{\Delta}_\ell(n) = \sum_{\ell' m} [\lambda_{\ell\ell'}(m-n) - \mu^*_{\ell\ell'} + \delta_{mn}\frac{c\tau_{\ell\ell'}}{k_B T_c}]\bar{\Delta}_{\ell'}(m)$$

$$- \sum_{\ell' \neq \ell} [|\hat{\omega}_{\ell\ell'}(n)| + \frac{c\hat{\tau}_{\ell\ell'}}{k_B T_c}]\bar{\Delta}_{\ell'}(n). \qquad (4\text{-}2)$$

If $\hat{\Delta}_\ell(n)$ is defined as

$$\hat{\Delta}_\ell(n) \equiv [\frac{c\hat{\tau}_{\ell\ell}}{k_B T_c} + |\hat{\omega}_{\ell\ell}(n)|]\bar{\Delta}_\ell(n)$$

and $\bar{\Delta}$ is eliminated in favour of $\hat{\Delta}$, then equation (4-2) has the same form as equation (3-43(a)), so that Leavens' method of

iteration may be applied for rapid numerical solution.

The gap equations below T_c are more difficult to transform because of their nonlinearity. Defining

$$\lambda_{\ell,\ell'\ell''}(n) \equiv \sum_{\ell'''} C_{\ell'\ell''\ell'''}\lambda_{\ell\ell'''}(n)$$

$$\tau_{\ell,\ell'\ell''} = \sum_{\ell'''} C_{\ell'\ell''\ell'''}\tau_{\ell\ell'''}$$

$$\mu_{\ell,\ell'\ell''} = \begin{cases} \mu^*\delta_{\ell'\ell''}\sqrt{W_i(\ell)} & \psi_\ell \text{ of order zero} \\ 0 & \psi_\ell \text{ of order} > \text{zero} \end{cases} \tag{4-3}$$

$$\bar{\Delta}_\ell(n) = \int_{48} \frac{dS_{\underline{k}}}{|v_{\underline{k}}|}\psi_\ell(\underline{v}_{\underline{k}})\bar{\Delta}_{\underline{k}}(n)$$

$$h_\ell(n) = \int_{48} \frac{dS_{\underline{k}}}{|v_{\underline{k}}|}\psi_\ell(\underline{v}_{\underline{k}})\frac{\mathrm{sgn}(\omega_n)}{\sqrt{1+\bar{\Delta}^2_{\underline{k}}(n)}}$$

the resulting equations are

$$\hat{\omega}_{\ell\ell}\bar{\Delta}_\ell(n) = \sum_{\ell',\ell'',m}(\lambda_{\ell,\ell'\ell''}(m-n) - \mu^*_{\ell,\ell'\ell''} + \frac{\delta_{mn}}{k_BT}c\tau_{\ell,\ell'\ell''})h_{\ell'}(m)\bar{\Delta}_{\ell''}(m) \tag{4-4}$$

$$- \sum_{\ell'\neq\ell}\hat{\omega}_{\ell\ell'}(n)\bar{\Delta}_{\ell'}(n)$$

$$\hat{\omega}_{\ell\ell'}(n) = (2n-1)\delta_{\ell\ell'} + \mathrm{sgn}(\omega_n)\sum_{m\ell''}(\lambda_{\ell'',\ell\ell'}(m-n) + \delta_{mn}\frac{c\tau_{\ell'',\ell\ell'}}{k_BT})h_{\ell''}(m) \tag{4-5}$$

Substituting equation (4-5) into the right hand side of equation (4-4) and defining $\hat{\Delta}$ as before changes (4-4) into a form that can be solved by the same method as (4-2), except that here the magnitude of the gap is the quantity which is adjusted at each iteration, instead of the trial T_c.

In the new basis the familiar quantities R_E^2 and ΔF appear as (see original definitions, equations (3-33), (3-23) and (2-41).

$$R_E^2 = \tau \sum_{n\ell\ell'} \bar{\Delta}_\ell(n)(\hat{\tau}_{\ell\ell'} - \tau_{\ell\ell'})\bar{\Delta}_{\ell'}(n) / \sum_{n\ell} \bar{\Delta}_\ell^2(n) \qquad (4\text{-}6a)$$

$$R^2 = \{\sum_n [\sum_\ell \bar{\Delta}_\ell^2(n) - \sum_i W_i \bar{\Delta}_i^2]\} / \sum_{n\ell} \bar{\Delta}_\ell^2(n) \qquad (4\text{-}6b)$$

$$\Delta F = 2(\pi k_B T)^2 N(0) \sum_{n>0} [-\sum_i (\tilde{\omega}_i^0(n) + \tilde{\omega}_i(n)) + \sum_\ell (\tilde{\omega}_\ell^0(n) + \tilde{\omega}_\ell(n)) h_\ell(n)$$

$$+ \sum_{\ell,\ell',\ell'',\ell'''} C_{\ell\ell'\ell''} \bar{\Delta}_{\ell'}(n) \bar{\Delta}_{\ell''}(n) h_{\ell'''}(n) \hat{\omega}_{\ell\ell'''}(n)] \qquad (4\text{-}7)$$

where

$$\tilde{\omega}_\ell(n) = \int_{48} \frac{dS_{\underline{k}}}{|v_{\underline{k}}|} \psi_\ell(\underline{v}_{\underline{k}}) \tilde{\omega}_{\underline{k}}(n) / \pi k_B T$$

and $\tilde{\omega}_\ell(n)$ is the corresponding quantity for the normal state. $\bar{\Delta}_i(n)/\sqrt{W_i}$ is the mean value of $\Delta_{\underline{k}}(n)$ in region i, similarly $\tilde{\omega}_i(n)/\sqrt{W_i}$.

This chapter opened with a critique of one- and two-iteration solutions of the gap equations. Changing to the FSH basis not only changes the nature of the approximation but improves the user's ability to estimate quantitatively the magnitude of the error caused by some of the approximations and makes it feasible to calculate thermodynamic quantities. There are three approximations made in solving

the equations numerically: (a) the sampling of only a finite number of points on the Fermi surface to obtain the $(\alpha^2F(\omega))_{\underline{k}\underline{k}'}$, (b) the truncation of the sums over ℓ and (c) (applying only to the nonlinear equations) the use of a very coarse grid to evaluate some of the $h_\ell(n)$.

Approximation (a) is common to both methods of solution. It is impractical at present on our computer for a multi-OPW Fermi surface to evaluate $(\alpha^2F(\omega))_{\underline{k}\underline{k}'}$ for $\underline{k}'$ points separated by intervals $\Delta\theta$ and $\Delta\phi$ (polar and azimuth angles) of less than 2° and for more than 35 $\underline{k}$-points on the 48th. Although $(\alpha^2F(\omega)_{\underline{k}}$ is a reasonably smooth function of $\underline{k}$, $(\alpha^2F(\omega))_{\underline{k}\underline{k}'}$ for fixed $\underline{k}$ is a very rapidly varying function of $\underline{k}'$, hence a fairly fine mesh of $\underline{k}'$ points is needed to get a good sample. There is some evidence that a 2°×2° mesh is fine enough, at least in Al, a more anisotropic system than Pb. Leavens and Carbotte[101] calculated $(\alpha^2F(\omega))_{\underline{k}}$ in one-plane-wave approximation using $\underline{k}'$ points chosen at random within each 2°×2° grid square. Leung et al.[96] recalculated this quantity with a multi-plane-wave Fermi surface and the same number of $\underline{k}'$ points but located at the centre of each grid square. In those directions where the one-plane-wave approximation is expected to agree with the multi-plane-wave result, the agreement between the two calculations is excellent, which suggests that the number of $\underline{k}'$ points used is actually quite adequate. From the point of view of the FSH, the $\underline{k}'$ mesh is certainly fine - even the highest order FSH used in the computations has the same sign over regions much larger

than the 2°×2° unit area. Therefore it seems reasonable that

$$(\alpha^2F(\omega))_{\underline{k}\ell'} \equiv \int_{FS} \frac{dS_{\underline{k}'}}{|v_{\underline{k}'}|} (\alpha^2F(\omega))_{\underline{k}\underline{k}'} \psi_{\ell'}(\underline{v}_{\underline{k}'}) \qquad (4\text{-}8)$$

can be calculated to the same degree of accuracy as $(\alpha^2F(\omega))_{\underline{k}}$ on the 2°×2° $\underline{k}'$ mesh. The sum over the $\underline{k}$-points necessary to generate

$$(\alpha^2F(\omega))_{\ell\ell'} \equiv \int_{48} \frac{dS_{\underline{k}}}{|v_{\underline{k}}|} (\alpha^2F(\omega))_{\underline{k}\ell'} \psi_{\ell}(\underline{v}_{\underline{k}}) \qquad (4\text{-}9)$$

is actually more problematical, because the mesh is so much coarser - only 31 $\underline{k}$ points were used in the numerical work. These points were chosen by inspection only. They are not in high-symmetry directions. On a non-spherical Fermi surface with the $\underline{v}_{\underline{k}}$ as arguments there is no way of choosing special points for Gaussian quadrature as is done by Fehlner and Vosko[29]. In principle, it is possible by interpolation to obtain $(\alpha^2F(\omega))_{\underline{k}\ell}$ on a 2°×2° mesh, but this procedure would still generate asymmetric $(\alpha^2F(\omega))_{\ell\ell'}$. From the structure of equations (4-2), (4-4) and (4-5) it is clear that the $\lambda_{\ell\ell'}(m)$ must be symmetric in ℓ and ℓ'. Therefore either the "upper diagonal" or " lower diagonal" elements of $(\alpha^2F(\omega))_{\ell\ell'}$ must be used to obtain a symmetric $\lambda_{\ell\ell'}(m)$. Since $\psi_{\ell}(\underline{v}_{\underline{k}})$ for ℓ of high order may vary rapidly between two of the sparse $\underline{k}$ points, $(\alpha^2F(\omega))_{\ell\ell'}$ for $\ell' > \ell$ is the more reliable of the two choices. As the region within which $(\alpha^2F(\omega))_{\underline{k}\ell'}$ remains nearly (to of the

around each $\underline{k}$ point, the accuracy of the $(\alpha^2F(\omega))_{\ell\ell'}$ declines. Since the Gram-Schmidt orthogonalization process forces each function to have more wriggles than its predecessors in order to be orthogonal to all of them, implying that $(\alpha^2F(\omega))_{\underline{k}\ell'}$ may not be smooth for large ℓ', the number of $\underline{k}$ points places a natural limit on the number of FSH that can be used. Another limit, of more importance in weak coupling superconductors, is that the total number of $\lambda_{\ell,\ell'\ell''}(m)$ is

$$n_c\left(\sum_i L_i\right)\sum_i L_i(L_i+1)$$

where L_i is the number of FSH in region i, and n_c is the number of Matsubara frequencies summed over (defined in Chapter 2). This does not turn out to be a problem in Pb, at least with four FSH.

Truncation of the basis introduces a qualitatively different error from stopping after one or two iterations over the Fermi surface. For one thing, the mean value of the gap will increase from the isotropic limit and be consistent with the anisotropy, so that it becomes feasible to calculate thermodynamic quantities, which are sensitive to the magnitude of the gap as well as its anisotropy. Also, since the basis functions of higher order are rapidly fluctuating, their absence should mean that only some of the finer structure of $\bar{\Delta}_{\underline{k}}$, of little relevance in the context of present experimental difficulties, is lost. It should be kept in mind that most of the gap anisotropy is caused by differences in the mean of

the gap for the four regions, and that the four zeroth order basis functions are sufficient to describe a system with constant gaps within each region. Most important, however, is that the degree of convergence can be checked by plotting T_c, H_c and C_v as functions of the number of basis functions. Such results are shown in Chapter 5.

The evaluation of the h_ℓ (defined in equation (4-3)) is a special problem posed by nonlinearity. If $\bar{\Delta}_{\underline{k}}(n) \ll 1$ as occurs near T_c for all n, and at lower temperatures for large n, then $1/\sqrt{1 + \bar{\Delta}_k^2(n)}$ can be expressed as a power series in $\bar{\Delta}_\ell(n)\psi_\ell(\underline{v}_{\underline{k}})$, so that $h_\ell(n)$ can be obtained directly from the $\bar{\Delta}_\ell(n)$ without explicitly performing a Fermi surface integration. Also if the gap anisotropy within each region is small, then for any value of $<\bar{\Delta}_{\underline{k}}(n)>$ the square root can be expanded as a power series in $\bar{\Delta}_\ell(n)\psi_\ell(\underline{v}_{\underline{k}})$ where the ψ_ℓ are of greater than zeroth order. But if $\bar{\Delta}_{\underline{k}}(n) \gtrsim 1$ and the anisotropy is large, then during iteration the integration must be done so often that it is impractical to perform it on a 2°×2° mesh. Instead, the integral (really a sum over the 2°×2° mesh) is replaced by a sum over the 31 $\underline{k}$ points of quantities averaged in neighbourhoods of the $\underline{k}$-points:

$$h_\ell(m) \approx \sum_{j=1}^{31} \left\langle \int \frac{dS_{\underline{k}}}{|v_{\underline{k}}|} \right\rangle_j \langle \psi_\ell(\underline{v}_{\underline{k}}) \rangle_j / \sqrt{1 + \langle \bar{\Delta}_{\underline{k}}(n) \rangle_j^2} \quad . \qquad (4\text{-}9)$$

Here $\left\langle \int \frac{dS_{\underline{k}}}{|v_{\underline{k}}|} \right\rangle_j$ = weight of $\underline{k}$-point j

$\langle \psi_\ell(\underline{v}_{\underline{k}}) \rangle_j$ = average value of ψ_ℓ near point j

and

$$\langle \bar{\Delta}_{\underline{k}}(n) \rangle = \sum_{\ell} \langle \psi_{\ell}(\underline{v}_{\underline{k}}) \rangle_j \bar{\Lambda}_{\ell}(n) \ .$$

The approximation should be valid if the $\bar{\Delta}_{\underline{k}}(n)$ do not vary much within each neighbourhood j.

An objection related to the truncation of the basis is that the kernel of the integral equation $(\alpha^2 F(\omega))_{\underline{k}\underline{k}'}$ behaves more like a function of $\underline{q} \equiv \underline{k}-\underline{k}'$ than a product of functions of $\underline{k}$ and $\underline{k}'$. In the one-OPW approximation, $(\alpha^2 F(\omega))_{\underline{k}\underline{k}'}$ is indeed a function of $\underline{q}$ only, and it is unlikely that the addition of more OPW's will make $(\alpha^2 F(\omega))_{\underline{k}\underline{k}'}$ more like a separable potential. An expansion of $(\alpha^2 F(\omega))_{\underline{k}\underline{k}'}$ as the sum of a finite number of separable terms, as is implied in equation (4-9), would therefore seem to be a poor approximation despite the existence of the addition theorem for the spherical harmonics, which expresses the Legendre polynomial $P_{\ell}(|\underline{q}|)$ as a finite sum of products of spherical harmonics with $\underline{k}$ and $\underline{k}'$ as arguments. A useful addition theorem is impossible to formulate for the FSH because they are functions of $\underline{v}_{\underline{k}}$ whereas an identity involving $\underline{k}$ and $\underline{k}'$ is required. Nevertheless the existence of the identity for spherical harmonics indicates that the distance between a function of $\underline{q}$ and a sum of separable terms is not so great. The real tests of expansions in FSH are numerical and will be discussed in the next chapter.

In Chapter 3 a separable model for the electron-phonon interaction was discussed in which $(\alpha^2F(\omega))_{\underline{k}\underline{k}'}$ was approximated by $(1+a_{\underline{k}})\ (1+a_{\underline{k}'})\ \alpha^2F(\omega)$, where $(1+a_{\underline{k}})$ was defined as $\lambda_{\underline{k}}(0)/\lambda(0)$ or $\int d\omega(\alpha^2F(\omega))_{\underline{k}}\ /A$. The FSH offer a way of seeing how well $\lambda_{\underline{k}\underline{k}'}(0)$ or $\int d\omega(\alpha^2F(\omega))_{\underline{k}\underline{k}'}$ can be approximated in this way.

Given that:

$$\lambda_{\underline{k}\underline{k}'}(0) = \sum_{\ell\ell'} \lambda_{\ell\ell'}(0)\,\psi_\ell(\underline{v}_{\underline{k}})\,\psi_{\ell'}(\underline{v}_{\underline{k}'}) \tag{4-10}$$

then

$$\lambda_{\underline{k}}(0) = \sum_{\ell i} \lambda_{\ell i}(0)\,\psi_\ell(\underline{v}_{\underline{k}})\sqrt{W_i} \tag{4-11}$$

and

$$\lambda(0) = \sum_{ij} \lambda_{ij}(0)\sqrt{W_iW_j} \tag{4-12}$$

where the substitution of i or j for the usual subscripts ℓ or ℓ' indicates the coefficient of the zeroth order FSH in region i or j. It follows that:

$$\begin{aligned}
&\lambda(0)\,(1+a_{\underline{k}})\,(1+a_{\underline{k}'}) \\
&= \lambda_{\underline{k}}(0)\,\lambda_{\underline{k}'}(0)/\lambda(0) \\
&= \sum_{\ell\ell' ij} \lambda_{\ell i}(0)\,\lambda_{\ell' j}(0)\sqrt{W_iW_j}\,\psi_\ell(\underline{v}_{\underline{k}})\,\psi_{\ell'}(\underline{v}_{\underline{k}'}) \Big/ \sum_{ij} \lambda_{ij}(0)\sqrt{W_iW_j}
\end{aligned} \tag{4-13}$$

This expression can be compared with $\lambda_{\underline{k}\underline{k}'}(0)$ by picking out the coefficient of $\psi_\ell(\underline{v}_{\underline{k}})\,\psi_{\ell'}(\underline{v}_{\underline{k}'})$, which is

$$\sum_{ij} \lambda_{\ell i}(0)\lambda_{\ell' j}(0)\sqrt{W_i W_j} \Big/ \sum_{ij} \lambda_{ij}(0)\sqrt{W_i W_j} \qquad (4\text{-}14)$$

and comparing it to $\lambda_{\ell\ell'}(0)$. Since most of the anisotropy occurs between rather than within the regions, this comparison is most meaningful when ℓ and ℓ' are zeroth order functions. In Table 5-12 this is done for $\lambda_{\underline{k}\underline{k}'}(0)$ and $\int d\omega(\alpha^2 F(\omega))_{\underline{k}\underline{k}'}$.

CHAPTER 5

RESULTS AND DISCUSSION OF NUMERICAL CALCULATIONS

In this chapter calculations are presented of the functional derivatives mentioned in the previous chapter, the thermodynamics of several isotropic and model anisotropic superconductors and the exact solution of Markowitz and Kadanoff's separable model; also preliminary results for the application of Fermi surface harmonics to anisotropic Pb are discussed. The emphasis is however somewhat different from that of the preceding two chapters in that the thermodynamics of the important elemental superconductors are stressed, although no new formalism has been developed there. These numerical results - the first of their kind for the specific heat - showing the effects of strong coupling and anisotropy on the specific heat and deviation function are of sufficient interest in themselves, since in the past only semi-empirical formulas, or expressions properly restricted to weak coupling have been used to deduce the gap anisotropy from experiment. No such deductions will be made here, but a fairly detailed comparison with experiment is done with the results of isotropic calculations.

1. The Functional Derivative of the Deviation Function

Since the shape of the deviation function D(t) says more about the type of coupling in a superconductor than the magnitudes of H_c and T_c, it would be very useful to know how D(t) responds to changes in $\alpha^2F(\omega)$ and μ^* The required functional derivative, $\delta D(t)/\delta\alpha^2F(\omega)$, defined by

$$\Delta D(t) = \int d\omega\, \Delta\alpha^2F(\omega)\,[\delta D(t)/\delta\alpha^2F(\omega)]\,, \qquad (5\text{-}1)$$

and $\partial D(t)/\partial\mu^*$, can be expressed in terms of other functional derivatives and $dH_c(T)/dT$ as follows:

$$\Delta D(t)/\delta\alpha^2F(\omega) = \{H_c(0)\,\delta H_c(T)/\delta\alpha^2F(\omega) - H_c(T)\,\delta H_c(0)/\delta\alpha^2F(\omega) + tH_c(C)\,(dH_c(T)/dT)\,\delta T_c/\delta\alpha^2F(\omega)\}/H_c^2(0)\,. \qquad (5\text{-}2)$$

The third term appears because the differentiation with respect to $\alpha^2F(\omega)$ of $H_c(T)$ is done keeping T/T_c fixed but allowing T and T_c to vary. The derivative of $H_c(0)$ is obtained the same way that $H_c(0)$ is found in imaginary-axis calculations, by straightforward extrapolation; since the height of the maximum of $\delta H_c(T)/\delta\alpha^2F(\omega)$ changes only by a few percent, while its position shifts down from $7k_BT_c$ to about $2.6\ k_BT_c$ as t goes all the way from 0 to 1 (see Fig. 5-13) the extrapolation should be reliable.

Figures 5-1, 5-8 and 5-14 show $\delta D(t)/\delta\alpha^2F(\omega)$ and $\partial D(t)/\partial\mu^*$ for lead and for a weak and medium coupling system. The surprising amount of structure and temperature dependence compared to the two parent functional derivatives occur be-

$\frac{\delta D(t)}{\delta \alpha^2 F(\omega)}$ $\frac{\partial D(t)}{\partial \mu^*}$

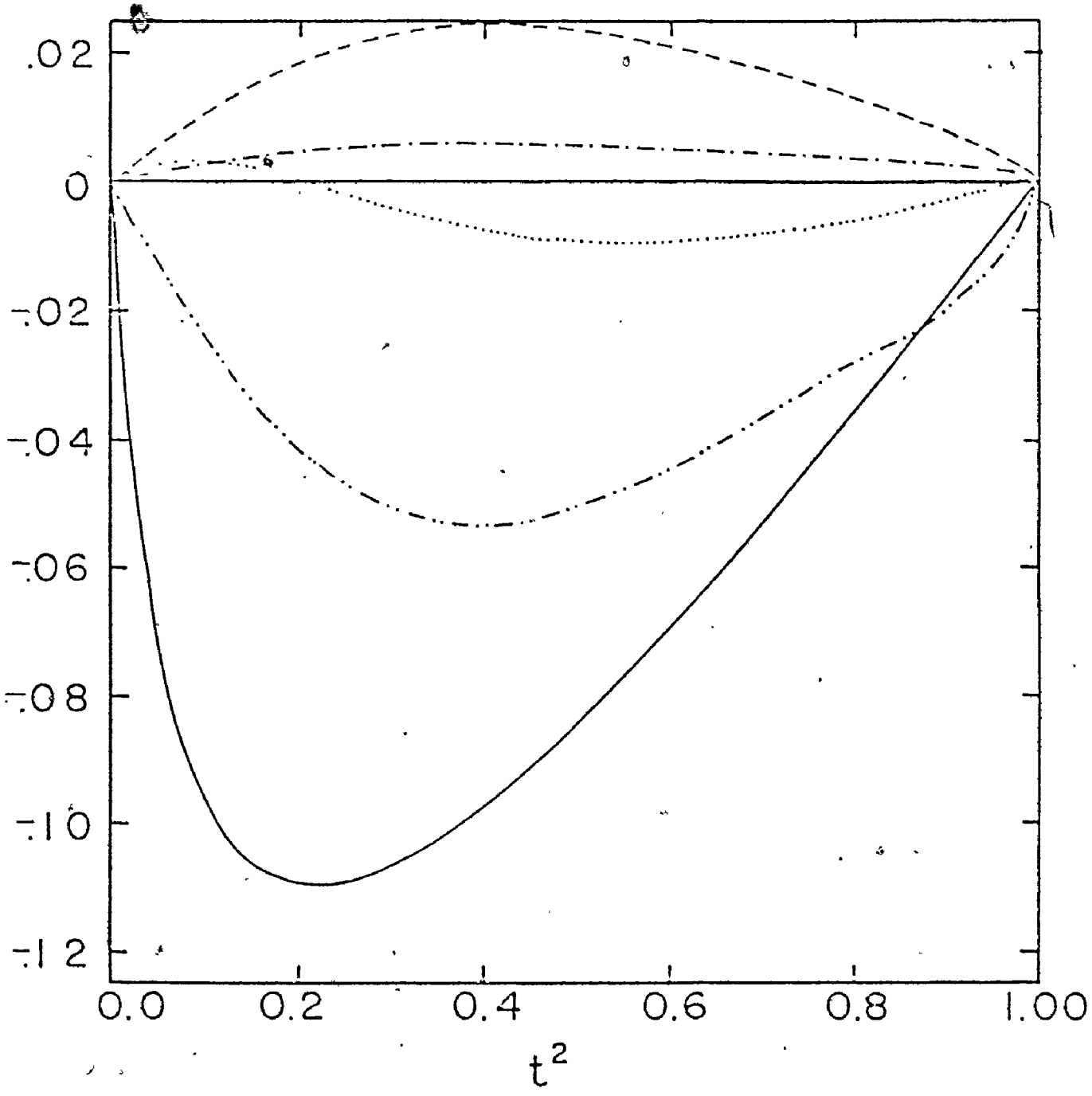

Fig. 5-1 Functional derivative of D(t) for Pb. This is for the isotropic tunneling $\alpha^2F(\omega)$ with ω_c = 110 meV.

——— ω/k_BT_c = .4 ····· ω/k_BT_c = 2.6,

– – – – ω/k_BT_c = 5.0, – · – · – ω/k_BT_c = 17.0

– · · – · · $\partial D(t)/\partial \mu^*$.

cause of the degree of cancellation in (5-2) and the difference in the position of the maxima of $\delta T_c/\delta\alpha^2F(\omega)$ and $\delta H_c(T)/\delta\alpha^2F(\omega)$. If there were a simple physical explanation for the position of the maximum of $\delta H_c(0)/\delta\alpha^2F(\omega)$ at 2.6 T_c, more could be said about that negative region. Rainer and Bergmann[49] found similar negative regions in the functional derivatives of dimensionless ratios such as $T_c/H_c(0)(dH_c/dT)_{T_c}$ and conclude that increasing $\alpha^2F(\omega)$ in this frequency range actually decreases any strong coupling effects. But it is in any case not important because it lies below most of $\alpha^2F(\omega)$, at least in the crystalline elements studied here, with the possible exception of Hg. Because $\delta D(t)/\delta\alpha^2F(\omega)$ indicates whether a given change in $\alpha^2F(\omega)$ moves the system towards weak or strong coupling, a better explanation would be valuable. The difference between Figures 5-1 and 5-14, weak and strong coupling, is not just in magnitude but proportion as well, since the relative sizes of $\partial D(t)/\partial\mu^*$ and $\delta D(t)/\delta\alpha^2F(\omega)$ are very different, so that these shapes are far from universal.

There are many applications of this functional derivative, for example to alloy series, the effects of pressure[104], the isotope effect (through $\partial T_c/\partial\mu^*$, as done by Leavens[88]), or the modification of an $\alpha^2F(\omega)$ to improve agreement with experiment, as is done in section 4 for Nb. One obvious limitation of the method is that it cannot handle large changes in the interaction, especially in μ^*, as the relative sizes of $\partial T_c/\partial\mu^*$ and $\partial^2T_c/\partial\mu^{*2}$ in Table 5-3 indicate. Another

arises from the truncation of the Matsubara frequency sums. Table 5-1 compares the changes predicted by functional derivatives in T_c, $H_c(0)$, and $D(t)$ with the changes obtained by direct calculation. In columns (a) and (c) the starting point $\alpha^2F(\omega)$ was that obtained by Rowell and in (b) was the modified $\alpha^2F(\omega)$ described in Fig. 5-8, so that slightly different functional derivatives had to be used in column (b). The changes used to test the functional derivative were in μ^* ((a) and (b)) and in $\alpha^2F(\omega)$ (column (c)). The change in $\alpha^2F(\omega)$, which decreased A and λ by about 5 and 10% respectively, is the same one shown in Fig. 5-8.

One sees immediately that the error in predicting $\Delta D(t)$ is much larger than that for ΔT_c and $\Delta H_c(0)$. This is to be expected because the three terms in equation (5-2) cancel out to about 80%, thus magnifying any error in ΔT_c and ΔH_c. But not even a correction from the second derivative can improve the ΔT_c predicted in columns (b) and (c); there the error is 3 or 4 times greater than the error in H_c, in contrast to column (a) where the error is about the same. Poor convergence of the numerical solution is not the problem. In fact, iterating the equations to the limit set by machine accuracy only verifies that for small changes in the kernel, ΔT_c and $\Delta H_c(T)$ are predicted by the functional derivative to better than 1%, while for larger changes the discrepancy remains. The problem occurs because the functional derivative has a discontinuity when the number of Matsubara frequencies summed over

Table 5-1

Comparison of the changes predicted by functional derivative with the results of direct computation in Nb.

Column (a) $\lambda = .98$, μ^* increased from .1091 to .11725

(b) $\lambda = .89$, μ^* decreased from .1091 to .092

(c) .03 subtracted from $\alpha^2F(\omega)$ from $\omega = 3$ to 12 meV, λ changes from .98 to .89, μ^* constant

	(a)	(b)	(c)
ΔT_c direct calculation	-.32	.73	-.97
functional derivative	-.32	.67	-.82
$\Delta H_c(0)$ direct calculation	-75.	165.	-235.
functional derivative	-76.	168.	-248.
$\Delta D(.7)$ direct calculation	-.00076	.0015	-.0054
functional derivative	-.00081	.0018	-.0045

Initial $T_c \sim 9.2$ K, $H_c(0) \sim 1980$ G, $D(.7) \sim -.010$ (values are approximate).

changes, with the result that only changes in T_c small enough for the number of terms in the sum to remain constant, i.e. within a temperature interval of about $2\pi(k_B T_c)^2/\omega_c$, can be predicted with arbitrary accuracy. Further consequences of the truncation of the sum are discussed in the next section.

2. Difficulties in the Numerical Solution.

Apart from the need to have very well-converged solutions of the gap equation, which is easily managed by increasing the number of iterations, and the size of the arrays for the gap and the kernel, most of the problems in numerical solution of the gap equation on the imaginary axis arise from the need to truncate the sums over Matsubara frequencies. That the difficulty is partly one of interpretation is demonstrated by the following example.

At T_c the expression for $\tilde{\omega}(n)$ (eqn. (2-25)) can be simplified, if an infinite number of Matsubara frequencies are allowed, to

$$\tilde{\omega}(n) = \omega_n + \pi k_B T_c \, \mathrm{sgn}(\omega_n) \left(-\lambda(0) + 2 \sum_{m=0}^{n} \lambda(m)\right) \qquad (5\text{-}3)$$

because an infinite number of terms cancel out thanks to the factor $\mathrm{sgn}(\omega_m)$. If the sums are truncated some cancellation still occurs, but the expression does not simplify and eqn. (2-25) must be evaluated as it stands. It would seem that expression (5-3) is preferable, since there is no truncation, but it can also be argued that the sum in $\tilde{\omega}(n)$ should be cut off

just like the sum in $\tilde{\Delta}(n)$ for the sake of consistency. Moreover, expression (5-3) results in a T_c inconsistent with the non-linear gap equations, since below T_c, $\tilde{\omega}(n)$ cannot be expressed as such a finite sum even if the interaction is not truncated; hence in a numerical solution the number of Matsubara frequencies summed over to get $\tilde{\omega}(n)$ both at and below T_c must be the same as that used for $\tilde{\Delta}(n)$ because if T_c is inconsistent with the gap equation below T_c, then neither D(t), nor the specific heat jump extrapolated to T_c can be trusted, especially since the discrepancy in T_c is of the order of one percent. Although the need for numerical consistency precludes the use of expression (5-3), it is not immediately obvious how best to reinterpret the upper bound of the frequencies used on the real axis, which does have a physical meaning, in terms of truncation on the imaginary axis.

The conclusion of section 1 in Chapter 2 was that for a given ω_c the μ^* used on the imaginary axis need not be the number derived from tunneling but is a constant, depending on ω_c, chosen to fit the experimental T_c or the gap edge, or anything measurable. It is worth knowing what happens to other calculated quantities when T_c and μ^* are nailed down in this way. In the following table the effects of using different ω_c and μ^* with the same $\alpha^2F(\omega)$ and T_c are shown. The entries in brackets correspond to $\mu^* = .1257$, which leads to a T_c slightly higher than that in the neighbouring columns. Using $\partial T_c/\partial \mu^*$ to see what change $\Delta\mu^*$ is needed to bring T_c down to

Table 5-2

Effect of different ω_c while using the same $\alpha^2F(\omega)$ and fitting μ^* to T_c. The tunneling $\alpha^2F(\omega)$ was used for Pb. For both metals the maximum phonon frequency is about 10 meV

	Pb	Pb	Tl	Tl	Tl
T_c	7.1926	7.1910	2.330	2.329 (2.391)*	2.328
μ^*	.15063	.1438	.1356	.1301 (.1257)	.1400
ω_c (meV)	110.	66.	66.	32.7	15.6
H_c	819.4	818.3	173	172 (177)	
D(t=.7)	.0244	.0246	-.0190	-.0184 (-.0177)	-.0188
$(\partial H_c/\partial T)_{T_c}$	-245.	-241	-137	-137. (-136.)	-135
$\partial T_c/\partial \mu^*$	-13.1	-15.1	-11.1	-12.1 (12.4)	-11.6
$(\partial H_c/\partial \mu)_{T=0}$	-1.63×10^3	-1.82×10^3	-1.0×10^3	-1.11×10^3 (-1.14×10^3)	$-.81\times10^3$
$-\partial T_c/\partial \mu$	.79	.79	1.26	1.19	1.04

*The numbers in brackets correspond to μ^* = .1257. The other values in this column, corresponding to μ^* = .1307, were obtained from them by functional derivatives.

2.329, then $\partial H_c(T)/\partial\mu^*$ and $\partial D/\partial\mu^*$, one can get values to compare with the other two columns. These two derivatives will also prove useful later in the discussion of anisotropy effects. Right now they provide evidence that in the calculation of measurable quantities, the choice of ω_c and μ^* is unimportant, while for the derivatives with respect to μ^*, a significant difference is seen. There is no contradiction, since what is always called $\partial T_c/\partial\mu^*$ or $\partial H_c/\partial\mu^*$ does not really give the change in T_c or H_c when the Coulomb repulsion is increased, because these derivatives are taken at fixed ω_c when in fact μ^* is a function of ω_c. They should be regarded more as conveniences in fitting μ^* to experiment or comparing different calculations.

An entirely different problem resulting from truncating arises because there are inevitably discontinuities in the thermodynamic properties and their derivatives whenever the number of terms in the sum changes. This means that not only is T_c a non-smooth function of μ^* at fixed ω_c, and vice versa, but also that the free energy ΔF and its derivatives are not smooth functions of temperature. Some of this discontinuity can be smoothed out by the appropriate weighting of the last term N in the frequency sum as follows: if ω_c lies a fraction f of the distance between ω_N and ω_{N-1}, then the Nth term in any sum is multiplied by f. This procedure is intuitively appealing and does actually make T_c a monotoni-

cally decreasing function of μ^* at fixed ω_c. Unfortunately, it does not go far enough to straighten $\partial T_c/\partial \mu^*$ and $\partial T_c/\partial \rho$, both of which display a typical sloping saw-toothed pattern as a function of μ^* in which the jumps are of the order of a few percent, far larger than the increment between jumps of the mean value of $\partial T_c/\partial \mu^*$. This shape explains the behaviour of ΔT_c in Table 5-1, because the error in the predicted ΔT_c is a constant fraction (20%) of the directly calculated ΔT_c, implying that the $|\partial T_c/\partial \mu^*|$ used in the comparison was larger than the mean value over one sawtooth.

A related problem shows up in $\partial D/\partial \mu^*$ in Fig. 5-14 only now it has its origin in $\partial H_c(T)/\partial \mu^*$. But before even this curve could be calculated there were complications caused by $\partial T_c/\partial \mu^*$. Just as T_c and H_c must be consistent to get a smooth D(t), so the three derivatives in eqn. (5-2) must not contradict each other, otherwise $\partial D/\partial \mu^*$ as $t \to 1$ swings in all directions. It was in fact necessary to adjust $\partial T_c/\partial \mu^*$ by a few percent, to get $\partial D(t)/\partial \mu^*$ at the highest temperatures lying on a straight line. The remaining bumps, caused by $\partial H_c/\partial \mu^*$, are not such a problem, since they can be removed by a straightforward smoothing procedure. The reader may however wonder how D(t), or even the change in D(t), can be a smooth function of temperature when its derivative is not. The answer is of course that

$$\Delta\mu^* \frac{\partial D(t)}{\partial \mu^*} \neq \int d\mu^* \frac{\partial D(t,\mu^*)}{\partial \mu^*}$$

because the position of the bumps changes when μ^* and T_c do.

So far the difficulties have all been associated with $\partial/\partial\mu^*$, because in that derivative expressions such as

$$\sum_{mn} \bar{\Delta}(n)\bar{\Delta}(m) \qquad (5\text{-}4)$$

occur in which the large values of n and m are not weighted by factors like $2\omega/(\omega^2 + \omega_{n-m}^2)$ as in $\delta/\delta\alpha^2F(\omega)$, while $\bar{\Delta}(n)$ at large n tends to a negative constant which is often a sizeable fraction of $\bar{\Delta}(1)$. The result is that such an expression is very sensitive to changes in the number of Matsubara frequencies, especially when there are relatively few (less than 50, say) terms in the sum. Increasing ω_c and lowering the temperature therefore lessens the sensitivity, since the more terms there are in the sum, the smaller the influence of the last term. This problem disappears almost entirely for $t < .1$.

Even at very low temperature however the truncation of sums requires very careful handling to calculate a meaningful specific heat. In the first place, the free energy ΔF (eqn. 2-41) is the difference between individually divergent sums, so that the amount of cancellation may be as great as 1 part in 10^6. Moreover the triplets of temperatures at which ΔF is evaluated for the specific heat must be chosen so that they truly reflect the mean curvature of ΔF and not the local bumps due to increments in the number of Matsubara frequencies. It is easier to discuss the problem in terms of the slope of

$\partial\Delta F/\partial T$ than the curvature of ΔF. Just below T_c, most of the mean slope of $\partial\Delta F/\partial T$ comes from the slope of individual line segments, while for $t < .4$, the jumps between line segments account for most of it, as shown below.

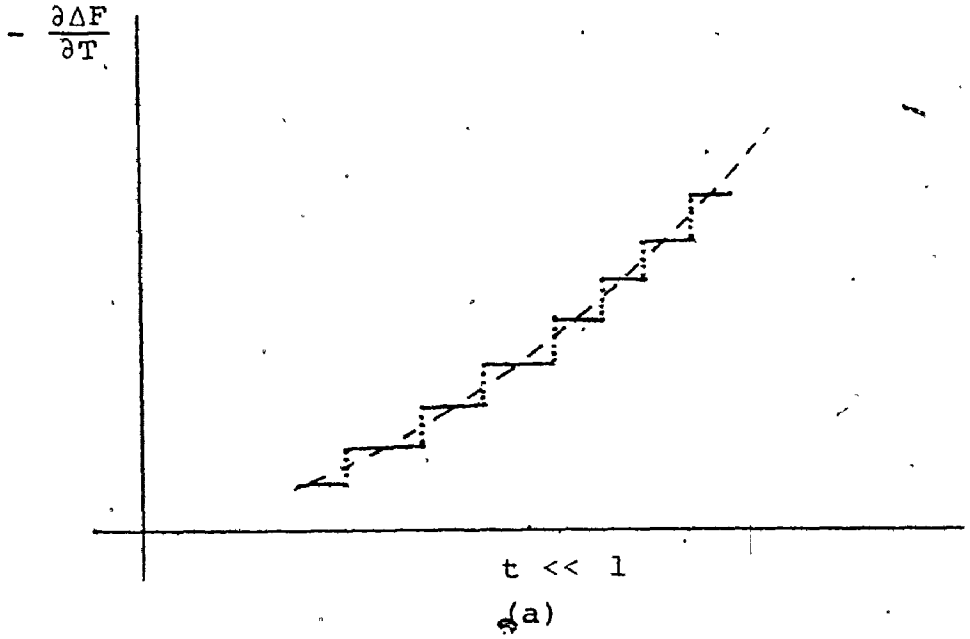

(a)

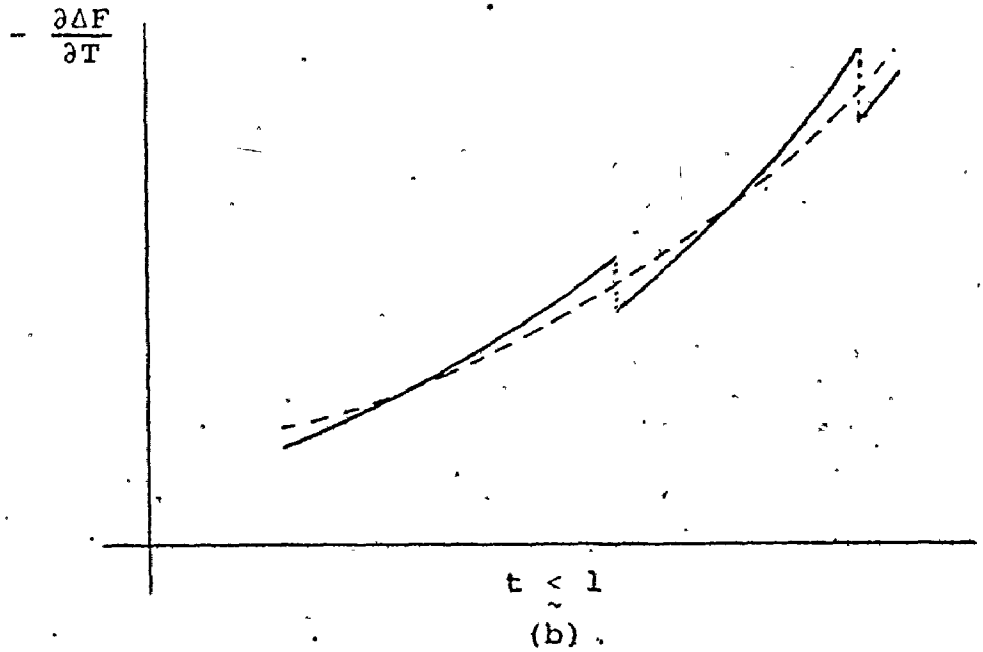

(b)

Fig. 5-2 Discontinuities in $\partial\Delta F/\partial T$ due to changes in the number of Matsubara frequencies. Dashed line is the smoothed value.

If it is conceded that the mean slope and not the slope of each segment is to be interpreted as the specific heat, a question easily answered by direct calculation, then the three adjacent temperatures where ΔF is evaluated to get the specific heat must correspond to different numbers of Matsubara frequencies and all three to the same fraction f defined several paragraphs back. Where this is not possible, as may happen, just below T_c, two of the temperatures were taken on one line segment There remains a jump in $\Delta C_v(T)$ and dH_c/dT when the middle temperature of the triplet crosses from one segment to the next, but these discontinuities, which look something like Fig. 5-2(b), can be handled by a smoothing subroutine, only not so well immediately below T_c, so that there is always an uncertainty of a percent or two in $\Delta C_v(T_c)/\gamma T_c$, and a discrepancy between that quantity and $(dH_c/dT)_{T_c}$. Nevertheless there is good reason to believe that all these precautions are effective. When the specific heat and deviation function were calculated using the $\alpha^2F(\omega)$ for Al calculated by Leung et al[96] and a μ^* of .1267 $C_{es}/\gamma T$ and D(t) lay about one percent below the BCS values tabulated by Mühlschlegel[87], and even that discrepancy could be attributed to the Coulomb parameter. One uncertainty that does remain is in the specific heat at very low temperature, $t < .2$, where C_{es} is approximately exponential. It could not be computed for Al, since there were far too many Matsubara frequencies; in any case around $t = .1$, $|\Delta C_v|$ may be as much as 99% of γT, greatly magnifying any

error. More will be said about this temperature region in section 3 when comparison with experiment is discussed.

This section closes with a description of the method of solution and the one convergence problem that occurred for large impurity concentrations. For isotropic separable frequency-independent, and arbitrary $(\alpha^2F(\omega))_{\underline{kk}'}$, T_c was calculated from modifications of an algorithm developed by Leavens[88]. The author is indebted to Dr. Leavens for the use of his program and for many helpful discussions. His procedure was to calculate at the beginning of iteration i the quantities

$$B(T_j) \equiv \pi k_B T_c^{(j)} \Sigma (\lambda^{(j)}(n-m) - \mu^*) \tilde{\Delta}^{(i)}(m) / |\tilde{\omega}_m^{(j)}| \qquad (5\text{-}6)$$

for a set of temperatures T_j centred on the $T_c^{(i)}$ of the previous iteration: $.90\ T_c^{(i)}$, $.95\ T_c^{(i)}$, $.90\ T_c^{(i)}$, $T_c^{(i)}$, $1.05\ T_c^{(i)}$, $1.10\ T_c^{(i)}$. $\tilde{\Delta}^{(i)}$ is the gap from the previous iteration, normalized so that $\tilde{\Delta}(1) = 1$. If both T_c and $\tilde{\Delta}$ are fully converged, then the $B(T_j)$ are monotonically decreasing and $B(T_3) = 1$. Therefore $T_c^{(i+1)}$ is chosen as the temperature, found by interpolation, where $B(T) = 1$. The $\lambda(m)$ are then recalculated using $T_c^{(i+1)}$, and $\tilde{\Delta}^{(i+1)}$ is obtained by putting $\tilde{\Delta}^{(i)}$ in the right-hand side of eqn. (2-24) and renormalizing $\tilde{\Delta}$. For the non-linear gap equation a very similar procedure was adopted, with the magnitude of the gap playing the role of temperature. $\tilde{\Delta}^{(j)}(1)$ is calculated for a set of C_j centred on unity with $C_j\tilde{\Delta}^{(i)}(n)$ replacing $\tilde{\Delta}(n)$ in the right

side of eqns. (2-22) and (2-23). The ratios $\tilde{\Delta}^{(j)}(1)/\tilde{\Delta}^{(i)}(1)$, like $B(T_j)$, then determine by what constant all the $\tilde{\Delta}^{(i)}(n)$ are multiplied by before going into the RHS of eqn. (2-22) to generate $\tilde{\Delta}^{(i+1)}(n)$. Both algorithms are fast, and T_c or $\tilde{\Delta}(n)$ converge to 1 part in 10^7 within 10 iterations, at least for pure systems, unless the inter-band coupling is relatively weak. When a large amount of elastic impurity scattering is put in, the linear equations (3-43) for the separable model converge as usual, but equations (2-50) and (4-2) do not, because the term $c\tau^{-1}_{\underline{kk}}$, dominates the kernel. This problem occurs only at relatively large concentrations where $T_c - T_{ci} \propto c^{-1}$, and the constant of proportionality can be obtained if $T_c - T_{ci}$ at lower concentrations is known. In any case, T_{ci} can always be found by putting the averaged $\alpha^2F(\omega)$ in the isotropic program.

3. Thermodynamics of Isotropic Superconductors

In this section calculations are presented of the critical field $H_c(T)$ and the specific heat of isotropic Hg, In, Nb, Nb_3Sn, Pb, Sn, Ta and Tl, and comparison is made with experiment. Some functional derivatives are also calculated, but they are not used for a really detailed comparison with experiment as is done in the next sections for Nb and Pb. The $\alpha^2F(\omega)$ discussed here were derived from tunneling data, except for Al which was calculated[96], and the μ^* was chosen to fit the experimental T_c. The properties of these

spectra, $\partial T_c/\partial \mu^*$, the μ^* obtained from tunneling and the μ^* needed to fit T_c, are listed in Table 5-3, while $\delta T_c/\delta \alpha^2 F(\omega)$ is shown in Fig. 5-3. The difference between the two μ^* is certainly not large, in accord with previous work by Vidberg and Serene[68]. But the main thing to notice in this table is that $\partial T/\partial \rho$ changes by only a factor of 2.4 in going from the strongest to the weakest coupling, while $\partial T_c/\partial \mu^*$ which is often very large, is roughly proportional to T_c at constant λ. In addition Table 5-3 demonstrates that the values calculated here for $\partial T/\partial \rho$ compare reasonably with those calculated by Bergmann and Rainer[15], the discrepancy being less than 25%. In the actual $\delta T_c/\delta \alpha^2 F(\omega)$ (Fig. 5-3) there is a similar problem and the discrepancy remains. Possible explanations are the difference in μ^* and ω_c (see Table 5-2) or the definition of $\tilde{\omega}(n)$ discussed in section 2 of this chapter. Although the choice of a definition for $\tilde{\omega}(n)$ matters little to T_c, it may affect $\partial T/\partial \rho$ considerably because $\partial \rho/\partial T$ and for that matter $\delta \rho/\delta \alpha^2 F(\omega)$ too are sums of terms that nearly cancel. The difference is not however significant in this context, since direct verification of $\partial T_c/\partial \mu^*$ and $\delta T_c/\delta \alpha^2 F(\omega)$ was done in Table 5-1, while $\partial T/\partial \rho$ was checked through the relationship between T_c, impurity concentration and gap anisotropy (see section 3 of Chapter 3).

For the calculation of the dimensionless ratios $D(t)$, $C_{es}(T_c)/\gamma k_B T_c$ and $\gamma (k_B T_c)^2/H_c^2$ no additional information beyond

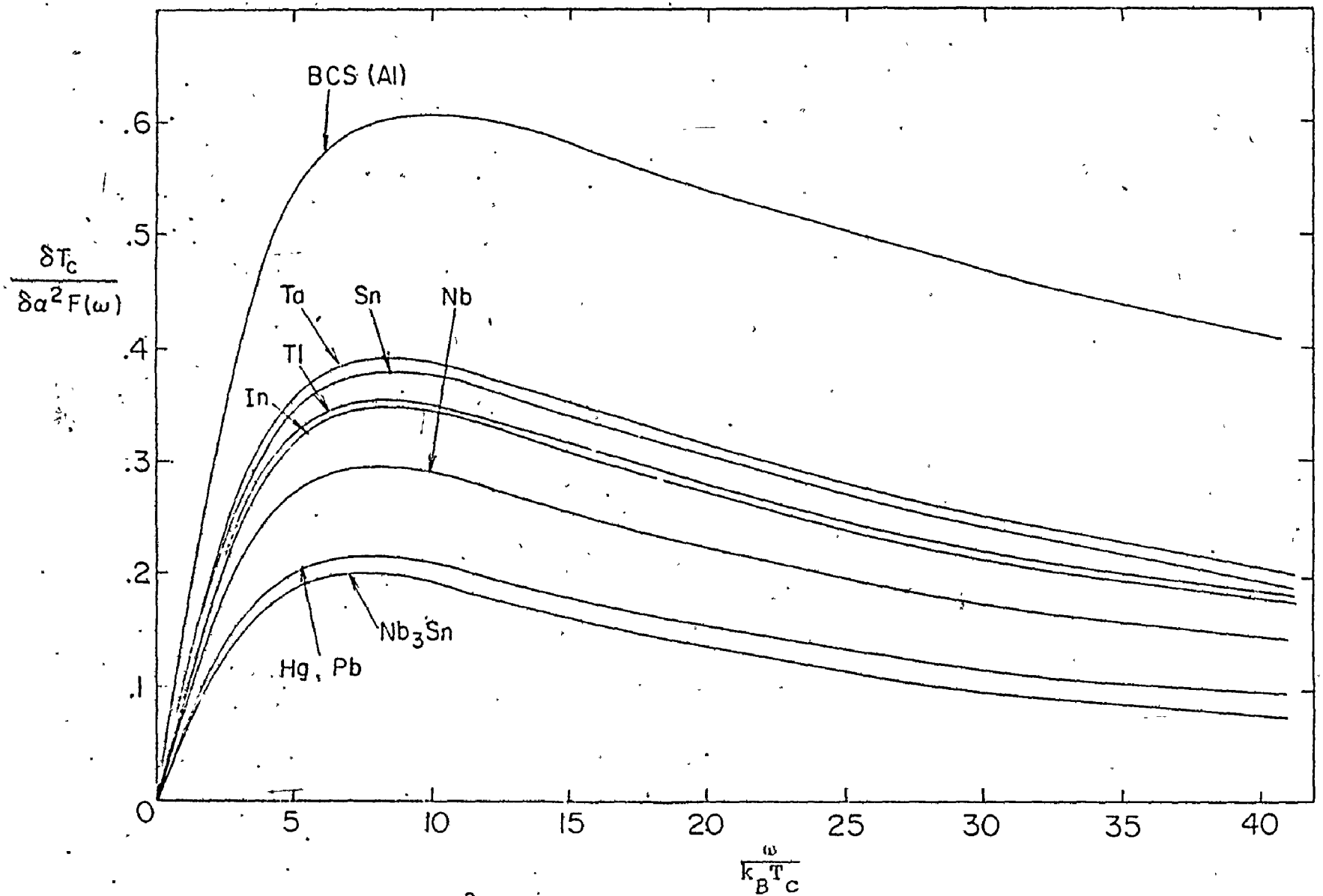

Figure 5-3 $\delta T_c/\delta \alpha^2 F(\omega)$ for several isotropic systems.

For Pb the tunneling $\alpha^2 F(\omega)$ was used, for Nb spectrum 1.

Table 5-3

Properties of $\alpha^2F(\omega)$ and T_c for the isotropic systems

The $\alpha^2F(\omega)$ were obtained from a tabulation by Rowell and Dynes (unpublished, but available from Bell Labs), except that for Al which was calculated[96].

	Hg	In	Nb	Nb_3Sn	Pb	Sn	Ta	Tl	Al
ω_M(meV)	14.3	15.9	28.5	28.7	11.	18.4	20.9	10.9	41.4
ω_c(meV)	42.9	48.	85.5	172.	66.	55.	63.	33.	124.
T_c	4.15	3.40	9.2	18.1	7.19	3.75	4.48	2.39	1.18
μ^*(tunneling)		.125	.1091	.15	.131	.111	.111	.127	-
μ^*(fitted)	.123	.115	.11725	.1575	.144	.115	.1194	.131	.1267
A (meV)	2.65	2.76	6.29	10.7	4.03	3.43	4.18	2.00	5.48
$\lambda(0)$	1.62	.804	.983	1.70	1.55	.716	.69	.795	.412
$\langle\omega\rangle$ (meV)	5.4	8.7	16.	16.	5.9	12.	14.	6.1	30.
$-\partial T_c/\partial\rho$	.79	1.16	1.03	.79	.79	1.38	1.29	1.19	1.85
$\partial T_c/\partial\mu^*$	-11.	-18.	-37.	-40.	-16.	-24.	-28.	-12.	-22.
$\partial^2 T_c/\partial\mu^{*2}$		-51.	-153.	-119.	-51.	-16.	-73.	-29.	-

Here $\langle\omega\rangle \equiv \int \omega\alpha^2F(\omega)d\omega / \int \alpha^2F(\omega)d(\omega)$

$A \equiv \int d\omega\alpha^2F(\omega)$

$\omega_c \equiv$ cut off frequency

$\omega_M \equiv$ maximum phonon frequency

$\alpha^2F(\omega)$ and μ^* is needed, but for $\Delta C_v(T_c)$, $H_c(0)$ and $(dH_c/dT)_{T_c}$ one needs $N(0)$ the Fermi surface density of states, which is obtained from γ, the coefficient of the linear term in the normal state electronic specific heat as $T \to 0$ (eqn. 2-45). Since this specific heat is not so easy to measure, nor is the deduction of γ from it straightforward in view of eqn. (2-44), it is useful to know whether a given $N(0)$ predicts both $\Delta C_v(T_c)$ and $H_c(0)$ correctly. If, for example, both the calculated quantities are larger than experiment while $D(t)$ is nearly right, and the experimental $\Delta C_v(T_c)/\gamma k_B T_c$ is too small, then the discrepancy is more likely to be in the experimental γ than in $\alpha^2F(\omega)$ or the Eliashberg equations. Although one would prefer to convert experimental results into dimensionless ratios for comparison with theory, these ratios (except $D(t)$, for which $H_c(0)$ must be obtained very accurately) contain an uncertain factor of γ. Therefore it is often better to work with $\Delta C_v(T_c)$, $(dH/dT)_{T_c}$ and $H_c(0)$, provided they are indeed the quantities being measured directly, since calorimetric data can be integrated to get $H_c(T)$, and magnetization curves can be differentiated. On surveying the various experimental results, one sees general agreement on the $\Delta C_v(T_c)$ determined calorimetrically, $(dH_c/dT)_{T_c}$, and $H_c(0)$; larger discrepancies in γ, $C_{es}(T_c)/\gamma k_B T_c$ and $D(t)$, and very large uncertainty in $\log \frac{C_{es}}{\gamma k_B T_c}$ for $t < .25$.

Table 5-4

Comparison of the results of isotropic calculations with experiment for Hg, In, Nb, Nb_3Sn, Pb, Sn, Ta and Tl

The experiments are classified according to type (magnetization or calorimetric). The numbers in brackets were obtained indirectly, from plots or from other experiments.

The entries under D(t) are the extrema of D(t).

The γ used for the theoretical work was taken from a compilation of Gladstone et al.[41] N(0) was then deduced from γ and the $\lambda(0)$ of the $\alpha^2F(\omega)$.

Hg

Experiment Type	T_c deg K	H_c Gauss	γ mJ/mole/deg^2	$\Delta C_v(T_c)$ mJ/mole/deg	$-(\partial H_c/\partial T)_{T_c}$ Gauss/deg	$\frac{C_{es}}{\gamma k_B T_c}$	$\frac{\gamma (k_B T_c)^2}{H_c^2}$	D(t)	Ref.
Mag.	4.15	408	2.22	(17.9)	196	(2.94)	(.163)		30
Mag.	4.15	412	1.91	23.2	(223)	(3.93)	(.137)	(.014)	37
Mag.	4.15	411	2.09				(.151)	(.013)	42
Mag.	4.15	426	(2.20)	(19.6)	205	(3.15)	(.148)		66
Mag.	4.15	411	1.81				(.131)	(.017)	40
Cal.	4.16	380	1.79	18.9	(201)	(3.54)	(.152)		39
Theory									
BCS						2.43	.168	-.037	
Isotropic	4.15	447	2.20	21.7	218	3.37	.134	.017	

N(0) = $.758 \times 10^{19}$ $meV^{-1}cm^{-3}$, molar volume = 14.1 cm^3

Table 5-4 (continued)

Experiment Type	T_c deg K	H_c Gauss	γ mJ/mole/deg^2	$\Delta C_v(T_c)$ mJ/mole/deg	$-(\partial H_c/\partial T)_{T_c}$ Gauss/deg	$\frac{C_{es}}{\gamma k_B T_c}$	$\frac{\gamma (k_B T_c)^2}{H_c^2}$	D(t)	Ref.
				In					
Mag	3.41	286	1.91	(10.2)	155	2.57	.176	-.026	7
Mag	3.41	285	(1.70)	(10.4)	156	2.79	(.155)		25
Mag	3.42	279	1.67	(9.6)	150	(2.68)	(.160)	-.025	30
Mag	3.41	293	(1.70)	(10.2)	155	(2.76)	(.147)		70
Mag	3.41	283	1.66					-.021 +.0005	40
Mag	3.37	269	(1.70)	14.6	(186)	(3.52)	(.170)		66
Cal	3.41	285	1.69	(9.5)	(150)	(2.66)	.157	-.021 +.0003	11
Cal	3.40	284	1.60	(9.8)	(156)	(2.80)	.149	-.017 +.0001	45
Cal	3.40	278	1.81				(.172)		65
Theory									
BCS						2.43	.168	-.037	
Isotropic	3.40	283	1.70	10.0	155	2.73	.157	-.016 +.0003	

$N(0) = .770 \times 10^{19}$ meV^{-1}cm^{-3}, molar volume = 15.7 cm^3.

Table 5-4 (continued)

Experiment Type	T_c deg K	H_c Gauss	γ mJ/mole/deg^2	$\Delta C_v(T_c)$ mJ/mole/deg	$-(\partial H_c/\partial T)_{T_c}$ Gauss/deg	$\frac{C_{es}}{\gamma k_B T_c}$	$\frac{\gamma(k_B T_c)^2}{H_c^2}$	D(t)	Ref.
				Nb					
Mag	9.20	1960	7.15				(.146)		27
Mag	9.25	1993	7.90	147	(430)	(3.01)	(.158)	$^{-.003}_{+.003}$	47
Mag	9.20	1980	7.88	127	(401)	(2.75)	(.158)		61
Cal	9.17	1944	7.53, 7.95	140	415	3.03, 2.92	(.155)	-.027	2
Cal	9.19	1994	7.80	(134)	412	2.87	(.153)	$^{-.012}_{+.0005}$	3
Cal	9.18		7.72	(144)	427	(3.03)			8
Cal	9.26	2061	7.80	140	419	(2.94)	(.146)	$^{-.015}_{+.003}$	46
Cal	8.70	2000	8.47	153	453	3.07	(.148)		51
Cal	9.28	2014	7.82	139	417	2.91	.154	$^{-.008}_{+.0004}$	53
Cal	9.23	(1975)	7.80	(135)	(413)	(2.87)	(.158)	$^{-.007}_{+.002}$	54
Cal	9.18	2038	7.74	(134)	413	(2.88)	(.157)		55
Cal	9.09		7.53	(131)	(409)				100
Theory BCS									
Isotropic* (spectrum(a))	9.20	2007	7.80	134	417	2.43 2.87	.168 .151	-.037 $^{-.008}_{+.002}$	

$N(0) = 4.64\times10^{19}$ meV^{-1}cm^{-3}, molar volume = 10.8 cm^3

*See section 4 of this chapter.

Table 5-4 (continued)

Experiment Type	T_c deg K	H_c Gauss	γ mJ/mole/deg^2	$\Delta C_v(T_c)$ mJ/mole/deg	$-(\partial H_c/\partial T)_{T_c}$ Gauss/deg	$\frac{C_{es}}{\gamma k_B T_c}$	$\frac{\gamma(k_B T_c)^2}{H_c^2}$	D(t)	Ref.
				Nb_3Sn					
Cal	18.0	5350	13.1*	(6.4×10^2) †	(634)	(3.7)	(.134)		5
				5.8×10^2	567	3.5			
Cal	17.9	5300	(13.1)*	(5.5×10^2)	590	3.3	(.136)		58
Cal ††			12.4 *						76
Theory									
BCS						2.43	.168	-.037	
Isotropic	18.1	5354	13.1	583	618	3.46	.134	.020	

$N(0) = 5.59\times10^{19}$ meV^{-1}cm^{-3}, molar volume = 11.1 cm^3

*Very uncertain. The normal state was not measured below 14 K.

†Larger value = $C_s(T_c)-C_N(T_c)$

Smaller value = $C_s(T_c-\delta/2)-C_N(T_c+\delta/2)$, where δ is the width of the transition.

Table 5-4 (continued)

Experiment Type	T_c deg K	H_c Gauss	γ mJ/mole/deg^2	$\Delta C_v(T_c)$ mJ/mole/deg	$-(\partial H_c/\partial T)_{T_c}$ Gauss/deg	$\frac{C_{es}}{\gamma k_B T_c}$	$\frac{\gamma(k_B T_c)^2}{H_c^2}$	D(t)	Ref.
				Pb					
Cal	7.19	(803)	3.00	59	(240)	3.71	(.134)	.025	6
Cal	(7.19)	(803)	(3.13)	58	(236)	(3.67)	(.140)		52
Cal	(7.19)	(803)	(3.13)	53	(227)	(3.36)	(.140)		75
Mag	7.18	803	3.06	58	238	(3.69)	(.137)	.024	74
Mag	7.20	803	3.13	60	237	(3.66)	(.140)	.021	48
Mag	7.18	803	(3.13)	(57)	237	(3.57)	(.140)		66
Theory									
BCS						2.43	.168	-.037	
Isotropic (tunneling, ω_c = 66)	7.19	818	3.13	58	241	3.60	.132	.025	

$N(0) = .86\times10^{19}$ meV^{-1}cm^{-3}, molar volume = 17.9 cm^3

Table 5-4 (continued)

Experiment Type	T_c deg K	H_c Gauss	γ mJ/mole/deg^2	$\Delta C_v(T_c)$ mJ/mole/deg	$-(\partial H_c/\partial T)_{T_c}$ Gauss/deg	$\frac{C_{es}}{\gamma k_B T_c}$	$\frac{\gamma(k_B T_c)^2}{H_c^2}$	D(t)	Ref.
				Sn					
Mag	3.72	309	1.98				(.177)	-.029	7
Mag	3.73	299	(1.78)	(9.56)	1.41	(2.44)	(.171)		28
Mag	3.72*	301*	(1.78)	(9.53)	141*	(2.44)	(.168)		
	3.63	298		(10.1)	145	(2.56)	(.163)		64
Mag	3.81†	312†	1.86	(9.63)†	140†	2.36†	(.171)†		
	3.67	298	1.86	(9.81)	144	2.44	(.174)	-.030	30
Mag	3.72	306	1.74				(.159)	-.026	40
Mag	3.73	305	(1.78)	(11.0)	151	(2.66)	(.164)		66
Mag	3.73	307	(1.78)	(10.4)	147	(2.57)	(.164)		25
Cal	(3.72)		(1.78)	(10.4)	149	(2.57)	(.163)		43
Cal	3.72	303	1.75	(10.7)	(149)	(2.64)	(.163)	-.024	19
Cal	3.70	306	1.80	(10.9)	149	(2.64)	(.162)	-.026	45
Theory									
BCS						2.43	.168	-.037	
Isotropic	3.73	307	1.78	10.8	150	2.62	.161	-.022	

$N(0) = .815\times10^{19}$ meV^{-1}cm^{-3}, molar volume = 16.2 cm^3.

†The double entries are for two different samples.

*This experiment looked at the washing out of anisotropy by impurity scattering. The upper and lower entries correspond to the clean and dirty limits respectively.

Table 5-4 (continued)

Experiment Type	T_c deg K	H_c Gauss	γ mJ/mole/deg^2	$\Delta C_v(T_c)$ mJ/mole/deg	$-(\partial H_c/\partial T)_{T_c}$ Gauss/deg	$\frac{C_{es}}{\gamma k_B T_c}$	$\frac{\gamma(k_B T_c)^2}{H_c^2}$	D(t)	Ref.
				Ta					
Mag	4.48	830	6.49				(.173)	-.030	7
Mag	4.48	825	5.99	43.4	(334)	2.62	(.162)	-.030	38
Mag	4.38	848	(5.85)	46.0	348	(2.80)	(.143)		66
Mag	4.48	838	7.83	39.3	318	(2.12)	(.201)	-.030	59
Mag	4.48	830	7.26	40.5	323	(2.25)	(.194)	-.036	63
Cal	4.36		(5.85)	(39.4)	323	(2.54)			43
Cal	4.39	780	5.69	42.3	334	(2.69)	(.165)		60
Theory									
BCS						2.43	.168	-.037	
Isotropic	4.48	812	5.85	41.2	328	2.57	.163	-.025	

$N(0) = 4.05\times10^{19}$ meV^{-1}cm^{-3}, molar volume = 10.9 cm^3.

Table 5-4 (continued)

Experiment Type	T_c deg K	H_c Gauss	γ mJ/mole/deg^2	$\Delta C_v(T_c)$ mJ/mole/deg	$-(\partial H_c/\partial T)_{T_c}$ Gauss/deg	$\frac{C_{es}}{\gamma k_B T_c}$	$\frac{\gamma(k_B T_c)^2}{H_c^2}$	D(t)	Ref.
				Tl					
Mag	2.38	177	1.50	60	137	(2.68)	(.160)	-.023	4
Mag	2.38	171	(1.46)	63	140	(2.81)	(.166)		66
Mag	2.40	171	1.53	53	128	(2.44)	(.177)	-.02	30
Mag	2.39		(1.46)	60	136	(2.72)			25
Cal	2.39	177	1.47	53	128	(2.51)	(.158)	-.03	39
Theory									
BCS						2.43	.168	-.037	
Isotropic (ω_c = 32.7)	2.39	172	1.46	57	133	2.63	.165	-.018	

$N(0) = .602\times10^{19}$ meV^{-1}cm^{-3}, molar volume = 17.2 cm^3.

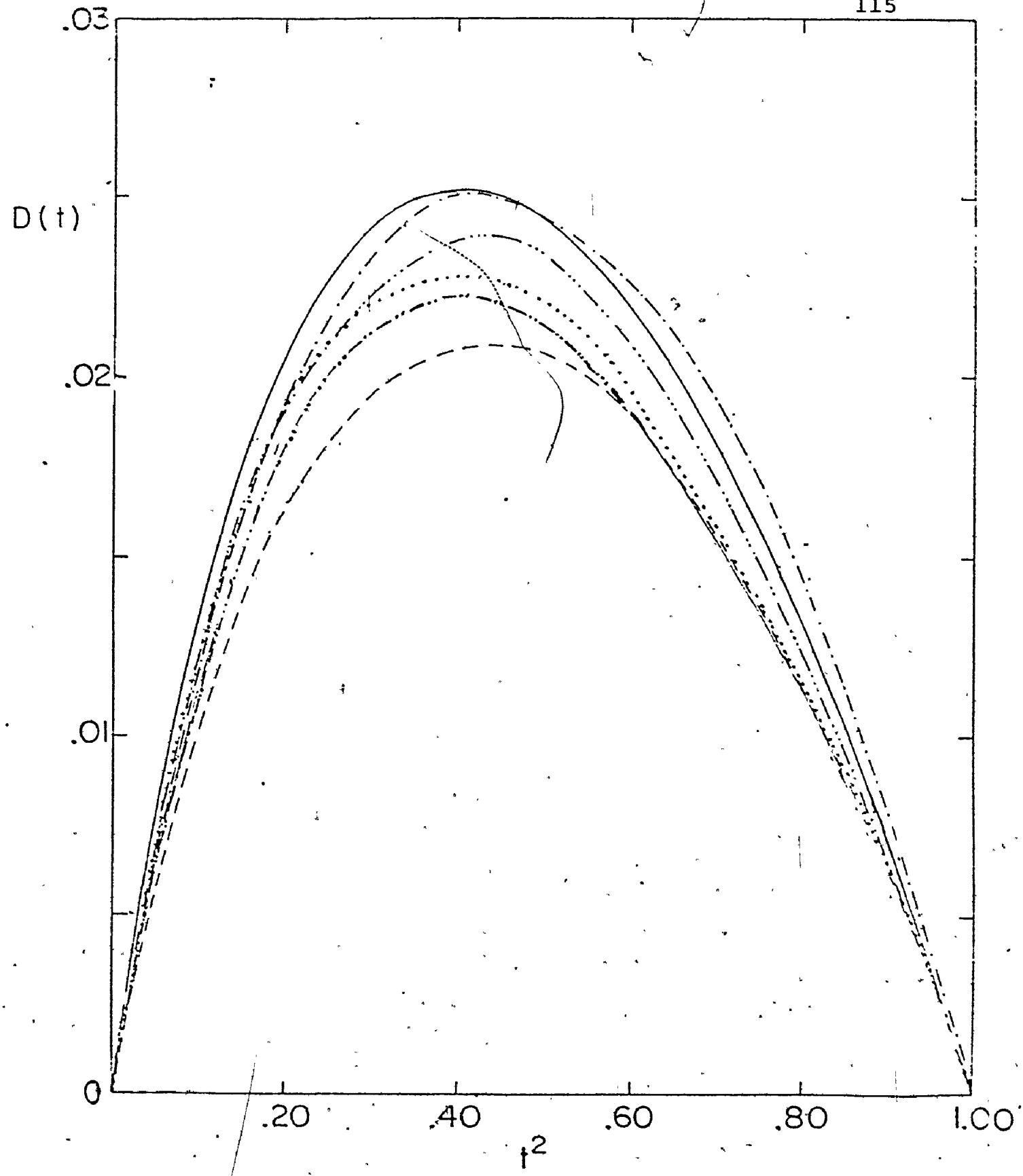

Fig. 5-4 Calculated and experimental D(t) for Pb

Experiment: - - - - - Ref. 6, ——— Ref. 48,
- · - · - · - Ref. 74.

Theory: ——— isotropic tunneling $\alpha^2F(\omega)$,
· · · · · · anisotropy added, - · - · - · anisotropy

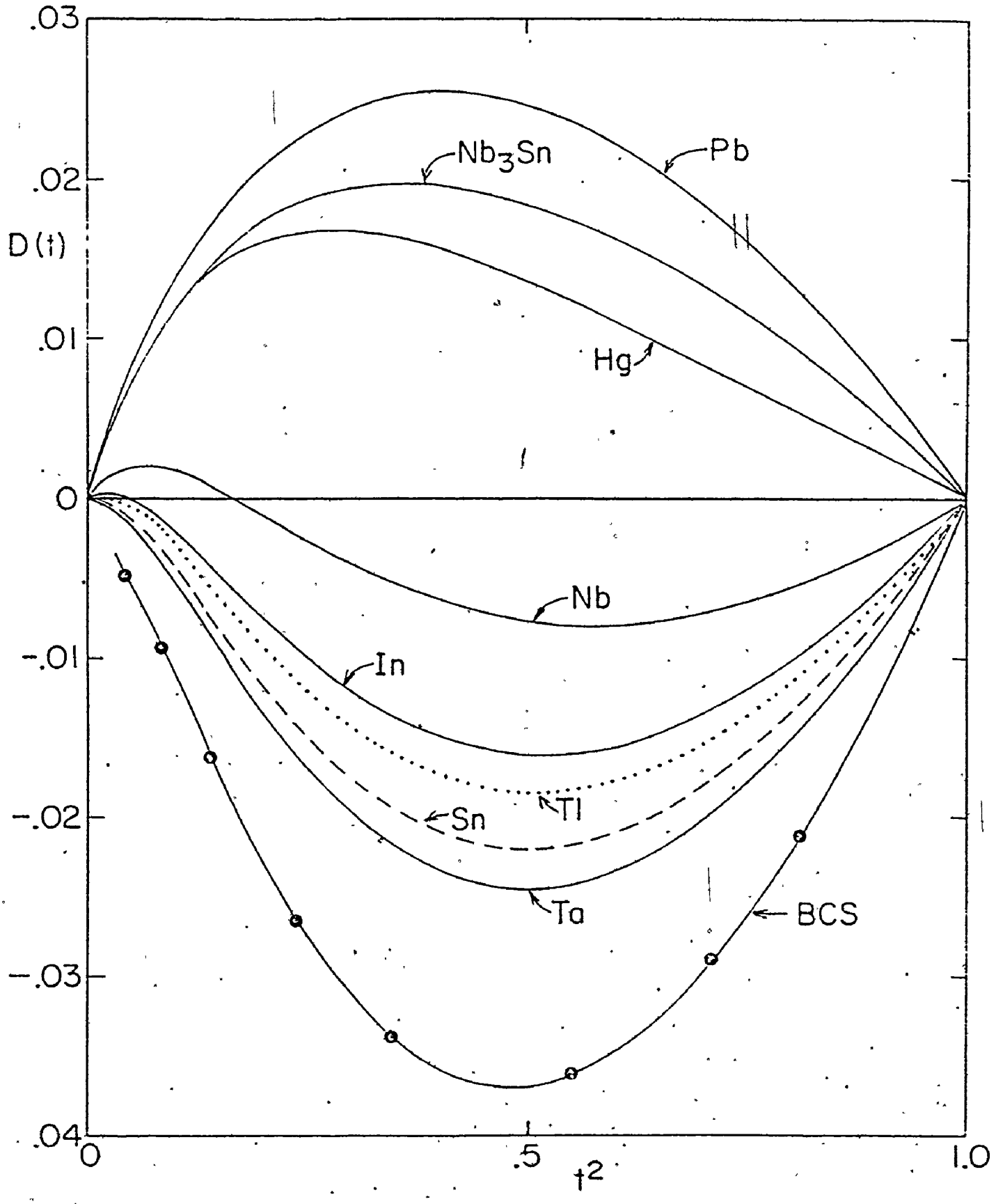

Fig. 5-5 Calculated D(t) from isotropic tunneling $\alpha^2F(\omega)$ for Pb, Nb_3Sn, Hg, Nb, In, Tl, Sn, and Ta. The curve labelled BCS is actually that calculated for Al. For all other systems D(t) and $\Delta C_v(T)$ were calculated at more closely-spaced temperatures than indicated here. For Nb spectrum (a) was used (see Table 5-5).

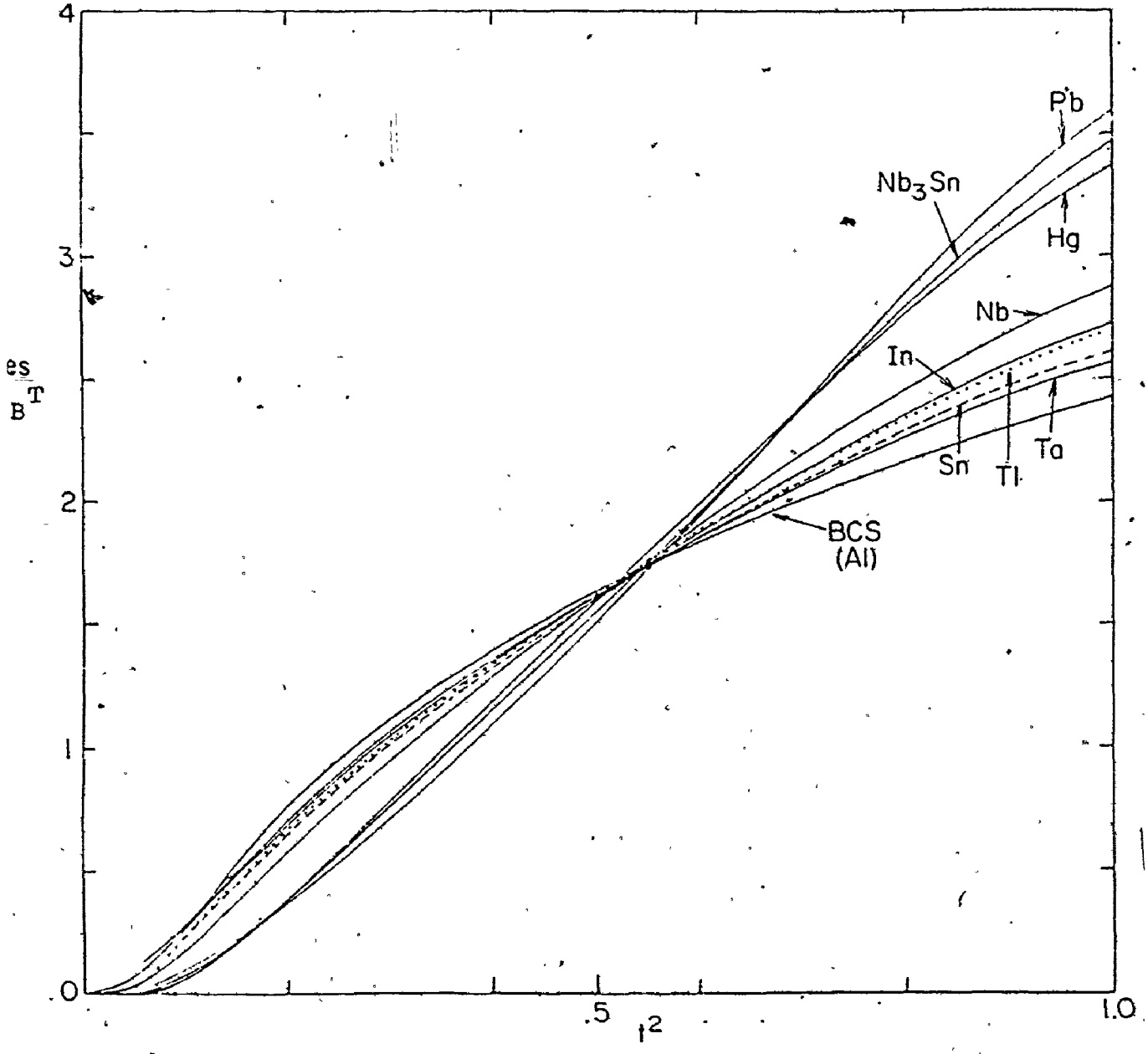

Fig. 5-6 Calculated $C_{es}/\gamma k_B T$ from isotropic tunneling $\alpha^2F(\omega)$ for Pb, Nb_3Sn, Hg, Nb, In, Tl, Sn and Ta.

This last temperature region, interesting as it may be for anisotropic systems, really lies outside the scope of this thesis, because the difficulties encountered there in this calculation can probably be removed by a better handling of the normal state electronic specific heat C_{en}. The problem is that $\gamma k_B T + (C_S - C_N)$, the quantity referred to as C_{es} throughout this thesis, actually becomes negative for the three strongest coupling cystems, Nb_3Sn, Pb and Hg around t = .2. The reader will recall that Wada's equation (2-41) gives only the difference $C_S - C_N$, with no way of getting C_S and C_N separately, so that some expression for C_N must be added to get C_S. It is of course possible that his assumption about the isotope effect is invalid, but the experimental plot of $\gamma k_B T + (C_S - C_N)$ in Figure 5-26 for Pb, also changes sign in the same place, making it more likely that the fault in the theory lies with the $\gamma k_B T$ term rather than with the expression for $C_S - C_N$. Some such negative values have been reported in In[90] and Nb[89] and attributed[24,95] to the inadequacy of $\gamma k_B T$ to describe C_N, but were not found in these calculations, at least not down to t = .15 and .045 respectively. Since C_N in Nb_3Sn has not even been measured at a low enough temperature, to see the sort of effects predicted by Grimvall[95] while in Pb and Hg γ is simply not known well enough - recall the degree of cancellation - the question is by no means settled.

The calculated D(t) and $C_{es}/\gamma k_B T_c$ for isotropic systems are shown in Figure 5-5 and 5-6, while Table 5-4 lists more

of their properties and some experimental data. Quantities not quoted directly in the references, those that were obtained from graphs or in combination with data from other references are shown in brackets. The finite width δ of the superconducting transition creates ambiguities in the definition of $\Delta C_v(T_c)$, since it is rarely made clear whether the quoted value is $C_S(T_c-\delta/2) - C_N(T_c + \delta/2)$ or the difference between $C_S(T)$ and $C_N(T)$ extrapolated to T_c. A similar difficulty arises with $(\partial H_c/\partial T)_{T_c}$, a linearly increasing function near T_c; it is rarely made clear where in the transition interval the derivative is evaluated. Another annoyance affecting the use of Rutger's formula to connect calorimetric and magnetization data is a variation of a percent or two in the quoted molar volumes. Such small points do matter, because the difference between theory and experiment is only a few percent, and the effects of anisotropy are expected to be of this order, as are the differences between experiments. In fact, there are also discrepancies where there shouldn't be any, between the calculated $\Delta C_v(T_c)$ and the calculated $(dH_c/dT)_{T_c}$. The value deduced from $(\partial H/\partial T)_{T_c}$ is larger than $\Delta C_v(T_c)$ by an amount ranging from 1% for weak coupling to 5% for strong coupling. This is another result of those discontinuities caused by changes in the number of Matsubara frequencies, and careful examination of the smoothing procedure reveals why Rutger's relation does not hold. The same analysis shows that the problem is confined to systems such that the set of temperatures ($t>.94$) from which $\Delta C_v(T_c)$ is extrapolated corresponds to the same

of f

is likely to be underestimated. A close look at the plots of the calculated C_{es} for the three strong coupling systems which satisfy the preceding conditions reveals a very slight knee around $t^2 = .80$, making the highest part of the curve slightly convex, in contrast to the experimental curves for strong coupling which are concave over the whole temperature range. The source of the problem was that for strong coupling the cutoff was taken so low that the region $t^2 > .80$ contained only one or two segments of the type shown in section 2, insufficient to allow the upper members of the triplets to have the same weight factor f as the middle temperature at which $C_v(T)$ was supposed to be evaluated. In Al, where the cutoff is already high enough, there was no difficulty - the small deviation from BCS theory decreased smoothly, without any abrupt change in the curvature - but it remains to be verified that using a very high cutoff for the upper temperature is the solution to this problem with strong coupling.

There is a great deal of information to digest in Table 5-4. A thorough discussion of only one element takes up all of the next section. Fortunately it is possible to generalize to some extent. The first observation is that the tunneling data together with the γ's quoted by Gladstone et al.[41] and the μ^* fitted to T_c predict $H_c(0)$ and $\Delta C_v(T_c)$ within a few percent, for weak and strong coupling alike. Secondly, the height of D(t) is consistently over-

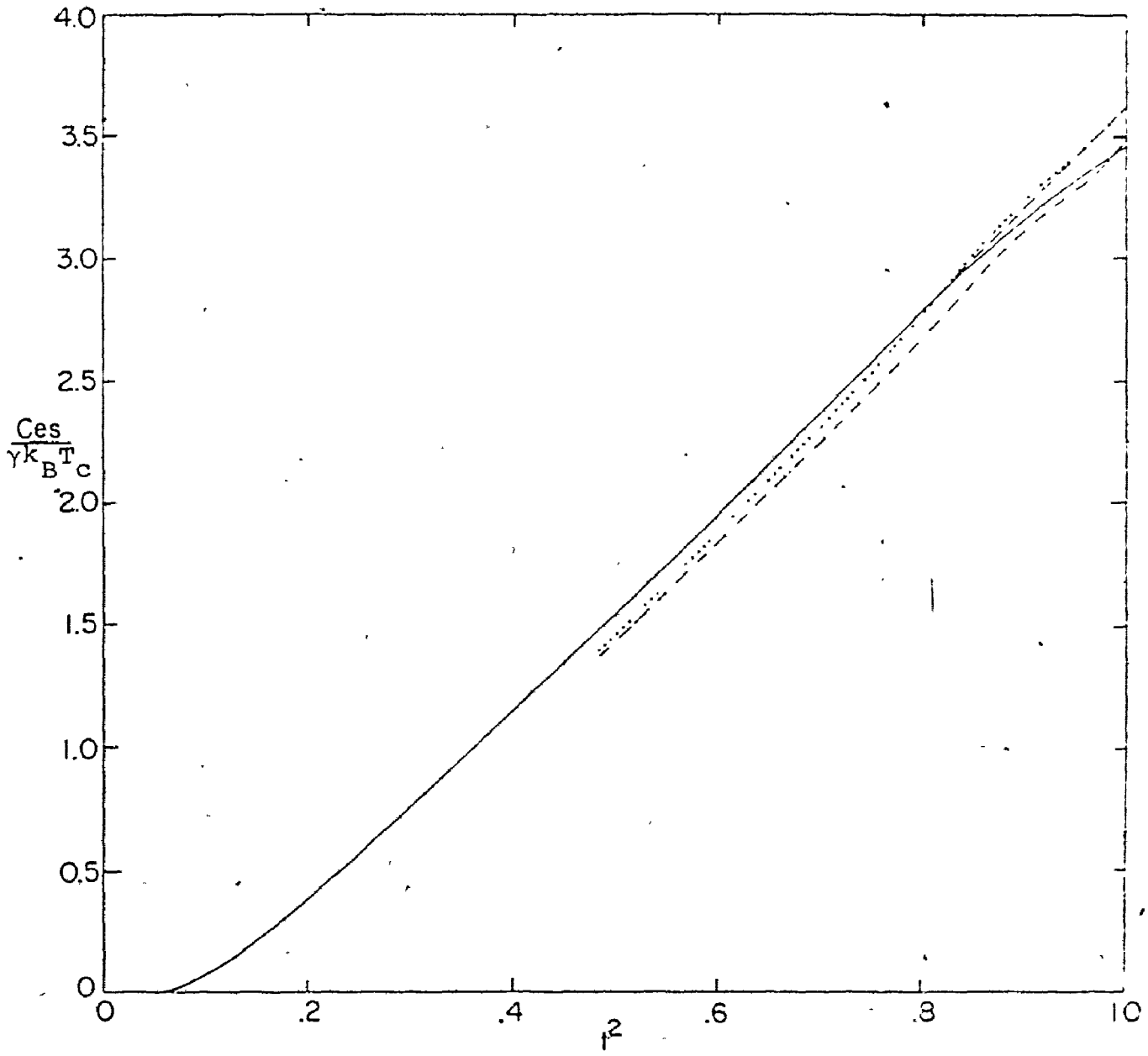

Fig. 5-7 Calculated and experimental specific heat of Nb_3Sn [4]
Calculated ———, correction to calculation ------
Experiment (Ref. 5) assuming γ = 12.5 mJ/mole/deg^2,
·····, γ = 13.1 -·-·- .

estimated by the calculations, more so in weak coupling than strong coupling. Thirdly, the ratios $C_{es}/\gamma k_B T_c$ and $\gamma(k_B T_c)^2$ derived from experiment are not at all reliable because γ is so uncertain; in fact, it is more sensible to work backwards and deduce γ from the measured $\Delta C_v(T_c)$ and the calculated jump ratio for those elements where there is agreement on $\Delta C_v(T_c)$ and $H_c(0)$. Finally, there may be a slight trend towards overestimating H_c in the four strongest coupling materials, even when the N(0) used in the calculation is adjusted to make the calculated $\Delta C_v(T_c)$ coincide with the (approximate) mean of the measured $\Delta C_v(T_c)$. This last trend may however disappear when $\Delta C_v(T_c)$ is recalculated more carefully, because then $\Delta C_v(T_c)$ can be fitted by a smaller γ.

It is worth looking in detail at Nb_3Sn, a much more complicated superconductor for the theoretician than any of the others in this table. The phonons are unignorably anharmonic because the compound is close to a structural phase transition driven by a very strong electron-phonon interaction, anomalies have been reported in the specific heat just below T_c[76], and it has been suggested[97] that the usual assumptions about the energy dependence made in deriving equation (2-13) from equation (2-9) do not hold. Yet Tables 5-3, 5-4 and Figure 5-7 demonstrate that the tunneling $\alpha^2F(\omega)$ with the unmodified Eliashberg equations describe the thermodynamics quite well; Nb_3Sn seems to behave like

Hg or Pb with the phonon frequencies scaled up. There is room for a slight improvement though, in $C_{es}(T)/\gamma k_B T$. Decreasing γ to 12.5 brings the experimental $C_{es}(T)/\gamma k_B T$ into better agreement with theory, but only at the highest temperatures, while the calculated $\Delta C_v(T_c)$, $(dH_c/dT)_{T_c}$ and $H_c(0)$ change to 557 mJ/mole/deg, -604 Gauss/deg and 5230 Gauss respectively, quite within the experimental error. The discrepancy in $C_{es}/\gamma k_B T$ remains however, and it does not resemble the effects of anisotropy to be discussed in section 5. Additional specific heat data would be helpful.

The conclusion of this section is that except for D(t) the isotropic Eliashberg equations predict the thermodynamics of weak and strong coupling superconductors within the experimental accuracy of several percent.

4. Thermodynamics of Superconducting Nb

Although superconducting Nb has been extensively studied there remains up to the time of writing considerable uncertainty about the μ^* and $\alpha^2F(\omega)$ obtained from tunneling inversion. Although there are indications that Nb is very sensitive to strain[92] and dissolved gases[86], and that tunneling experiments may not sample bulk properties[91], these considerations cannot explain a factor of three difference in the $\lambda(0)$ obtained from two different tunneling experiments. In addition, a negative μ^* was found in one experiment, which casts doubt on the applicability of the Eliashberg equations

to Nb. For these reasons it was found worthwhile to obtain several proposed $\alpha^2F(\omega)$ in order to test them and the theory by using them to calculate the thermodynamic properties. A large discrepancy between the measured values, which vary by only a few percent from one experiment to another, and the results calculated from the $\alpha^2F(\omega)$ corresponding to the negative μ^* would not in itself be conclusive; if the same inappropriate theory that generated an implausible $\alpha^2F(\omega)$ and μ^* is further used to calculate other quantities from them, one can only expect to get meaningless results. But if calculations with other $\alpha^2F(\omega)$ and μ^* give very good agreement with experiment, it seems reasonable to conclude that the theory is sound and that the anomalous $\alpha^2F(\omega)$ and μ^* are attributable to some unidentified experimental difficulty with the tunneling junction.

The three most important $\alpha^2F(\omega)$ used in these calculations, spectra 1, 2 and 3, are shown in Fig. 5-8 and described in the first three rows of Table 5-5. The factor of three difference between the $\lambda(0)$ for spectra 1 and 2, both of which were obtained from tunneling, is what motivated these calculations. The very small $\lambda(0)$, which is compensated by a negative μ^* of spectrum 2 is already a point against spectrum 2, for both theoretical calculations[91] and experiment[94] agree on a $\lambda(0)$ of order unity. Apart from an overall scale factor, spectra 1 and 2 are much the same shape:

Fig. 5-8 Several possible $\alpha^2F(\omega)$ for Nb and $\delta D(t)/\delta\alpha^2F(\omega)$ for spectrum 1.

$\alpha^2F(\omega)$

..... spectrum 1, ------ spectrum 2,

——— spectrum 3.

The modification to spectrum 1 between $\omega = 3$ and $\omega = 12$ meV is also shown.

$\delta D(t)/\delta\alpha^2F(\omega)$ is for spectrum 1.

..... t = .95, -·-·-· t = .30,

-·-·-·-·-· t = .70.

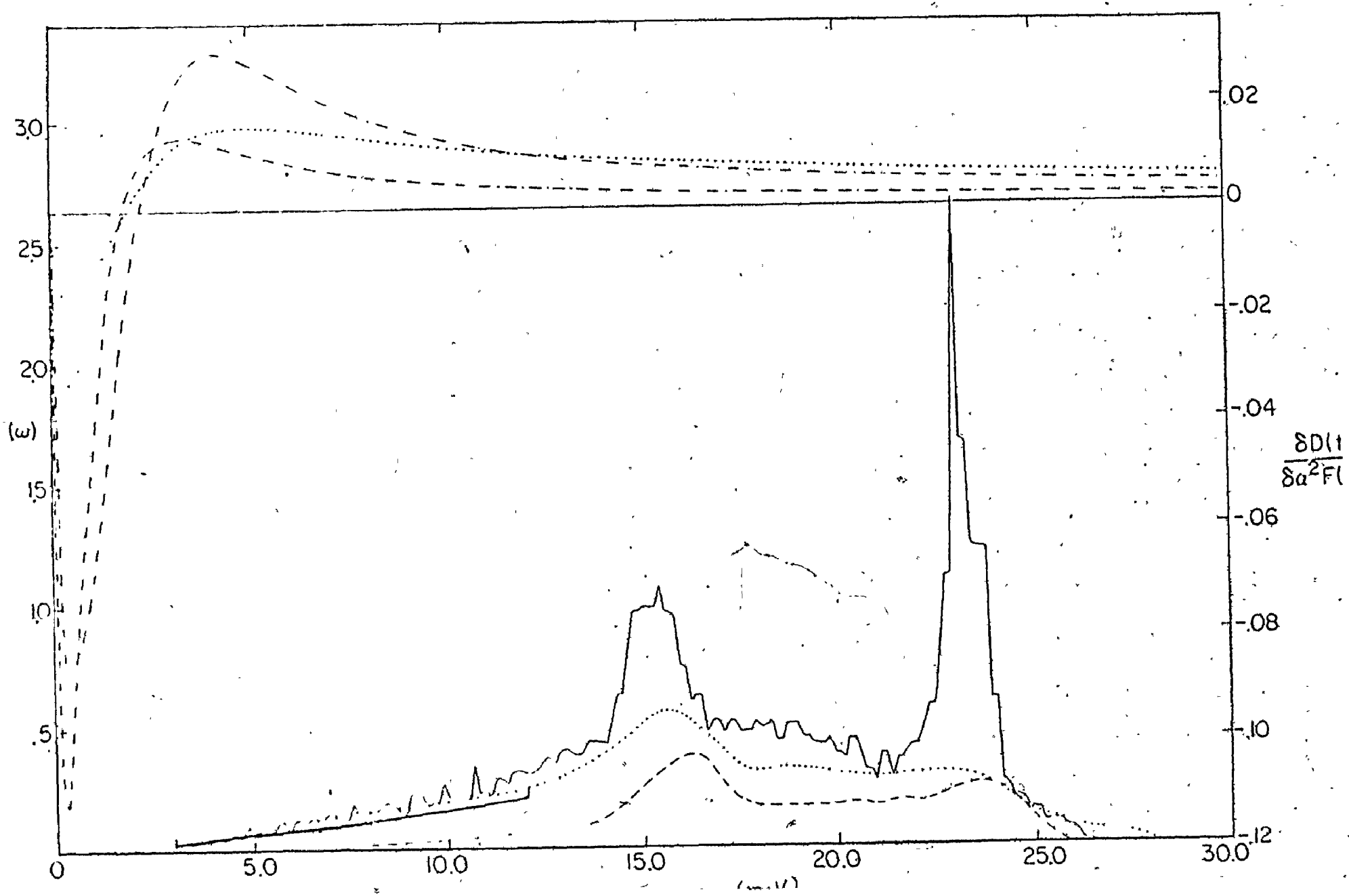
3.0
2.5
2.0
1.5
1.0
.5
(ω)
0
5.0
10.0
15.0
20.0
25.0
30.0
.02
0
-.02
-.04
-.06
-.08
-.10
-.12
δD(t
δα²F(

Table 5-5

Properties of the various $\alpha^2F(\omega)$ proposed for Nb

(a) Spectrum 1 (J. Rowell, priv. commun.)
(b) Spectrum 2 (J. Bostock, priv. commun.)
(c) Spectrum 3 (W. Butler, priv. commun.)
(d) Spectrum 3 scaled down by 2/3
(e) Spectrum 1, .03 subtracted between 3 and 12 meV
(f) Spectrum 1, delta-function of height h added at 23 meV
(g) Spectrum 1 with the model anisotropy described in the next section and μ^* the same as (a)
(h) The same as (g), but μ^* adjusted to fit T_c

$$A \equiv \int d\omega \alpha^2F(\omega) \ , \quad \langle\omega\rangle = \int d\omega \ \omega\alpha^2F(\omega)/A$$

Other derivatives for spectrum 1 are $\partial\Delta C_v(T_c)/\partial\mu^* = -664$,

$$\left(\frac{\delta D(.7)}{\delta\alpha^2F(\omega)}\right)_{\omega=23} = .0052 \ , \quad \left(\frac{\delta H_c}{\delta\alpha^2F(\omega)}\right)_{\omega=23} = 539, \quad \left(\frac{\delta T_c}{\delta\alpha^2F(\omega)}\right)_{\omega=23} = 2.11$$

	ω_c (meV)	A (meV)	λ	$\langle\omega\rangle$ (meV)	$-\left(\frac{\partial H_c}{\partial\mu^*}\right)_{T=0}$	$-\frac{\partial T_c}{\partial\mu^*}$ K	$-\frac{\partial D(.7)}{\partial\mu^*}$
(a),(g),(h)	85.5	6.29	.983	16.0	9.3×10^3	37	.10
(b)	106	2.89	.328		2.4×10^4	110	.42
(c)	80.7	9.35	1.223	17.5		29	
(d)	80.7	6.23	.816	17.5		45	
(e)	85.5	6.01	.894	16.4		42	
(f)	85.5	6.29+h	$.983 + \frac{2h}{23}$				

Table 5-6

Thermodynamic properties of Nb as calculated from various $\alpha^2F(\omega)$

For a description of the $\alpha^2F(\omega)$ see Table 5-5.
N(0) was chosen to keep γ constant at 7.80 mJ/mole/deg
$\Delta C_v(T_c)$ and $C_{es}/\gamma T_c$ are probably underestimated by about 2%

	μ^*	T_c deg K	H_c Gauss	$C_v(T_c)$ mJ/mole/deg	$-(dH_c/dT)_{T_c}$ Gauss/deg	$C_{es}/\gamma k_B T_c$	$\gamma(k_B T_c)^2/H_c^2$	D(t)
(a)	.11725	9.20	2007	134	417	2.87	.151	$-.008^{+.002}_{-}$
(b)	-.085	9.15	1866	110	375	2.54	.164	$-.027^{0.}_{-}$
(c)	.3198	9.25	1992	131	410	2.81	.155	$-.0086^{+.002}_{-}$
(d)	.0979	9.24	1794	103	364	2.74	.156	$-.014^{+.0004}_{-}$
(e)	.092	9.28	2012	131	411	2.81	.154	$-.011^{+.001}_{-}$
*(f)	.11725	$9.20^{+2.11h}_{-}$	2007^{+539h}_{-}	134	417	2.87		$-.008^{+.0052h}_{-}$
(g)	.11725	9.72	2094	136	409	2.79	.164	$-.012^{+.0005}_{-}$
*(h)	.1313	9.20	1964	127	400	2.77	.165	$-.014^{-}$

*Calculated from the derivatives quoted in Table 5-5, not directly.

in particular both lack the pronounced second peak so prominent in spectrum 3, which is a calculated $\alpha^2F(\omega)$. The huge difference in area between this $\alpha^2F(\omega)$ and the tunneling results should not be interpreted as additional evidence for Nb being somewhat anomalous, because in the transition metals such calculations are far less accurate than in a nearly-free electron metal like Pb. The existence of the second peak, which corresponds to the longitudinal phonons, has been verified by neutron-scattering studies of the phonon spectrum[93] and phonon lifetime experiments[91]; it is curious that both tunneling $\alpha^2F(\omega)$'s should lack it. The possibility that tunneling electrons do not probe the bulk properties of the junction and that this somehow makes them insensitive to the longitudinal phonons has been offered as an explanation[91].

The first three rows of Table 5-6 show the results of calculations with these three spectra. The adjustable parameters in these calculations were the same as in the previous section, namely μ^*, which was fitted to T_c for spectra 1 and 3 but left unaltered for spectrum 2, and γ, which was taken to be 7.80 mJ/mole/deg for all systems, a procedure that led to larger N(0) being used for the systems with smaller $\lambda(0)$. The fitted μ^* for spectrum 1 differed from the tunneling μ^* by 8%, a discrepancy comparable to that found previously for other elements. The improbably large μ^* (.32) needed to fit T_c for spectrum 3 suggests that a detailed discussion of this $\alpha^2F(\omega)$ should be deferred to the end of this section where possible improvements

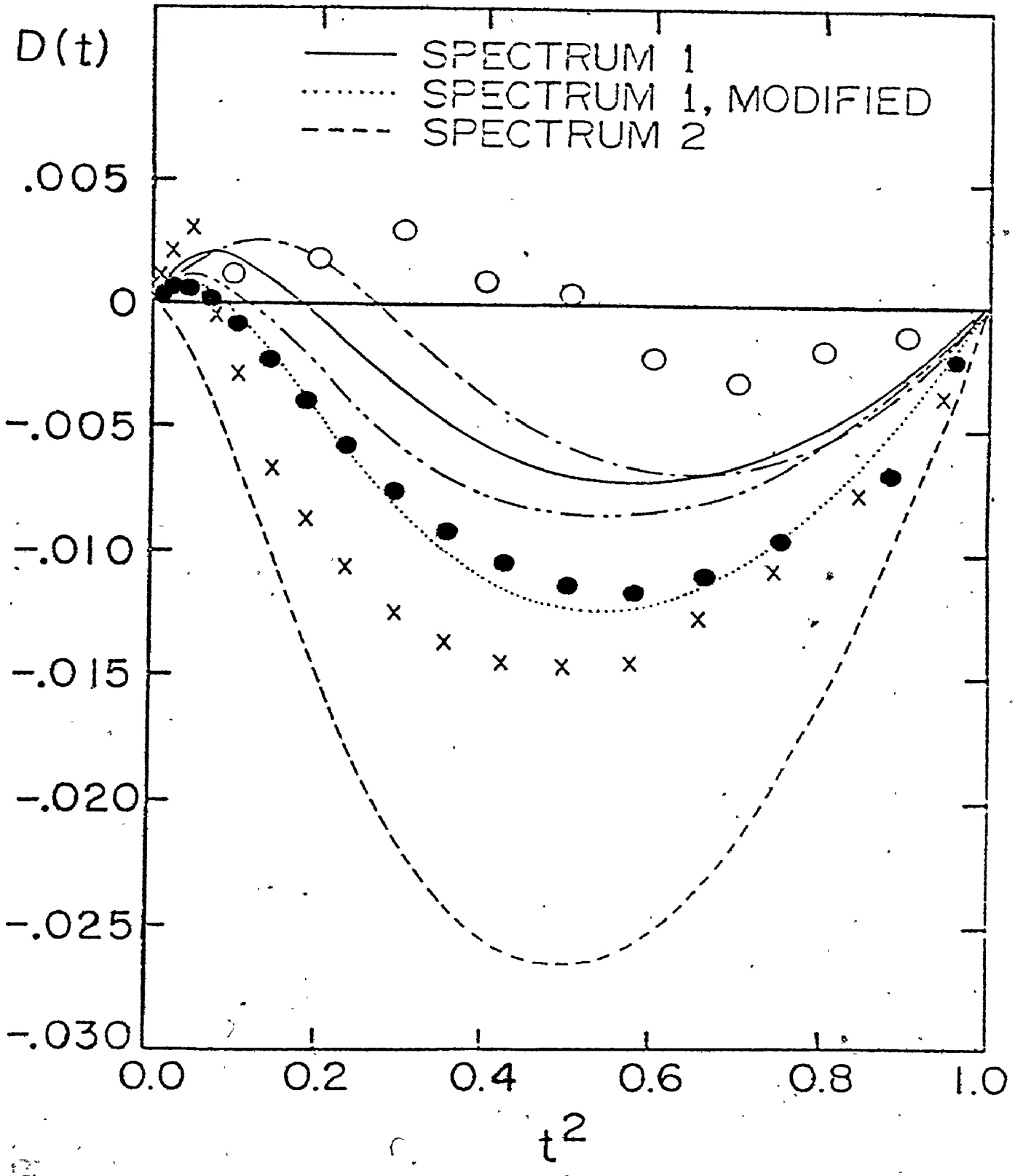

Fig. 5-9 Experimental and calculated D(t) for Nb.
Calculation: ——— spectrum 1, ·····spectrum 1 modified,
------ spectrum 2
Experiment: Ref. 3, ● Ref. 47, × Ref. 46, o Ref. 47,
-·-·-· Ref. 54, -··-··- Ref. 53.

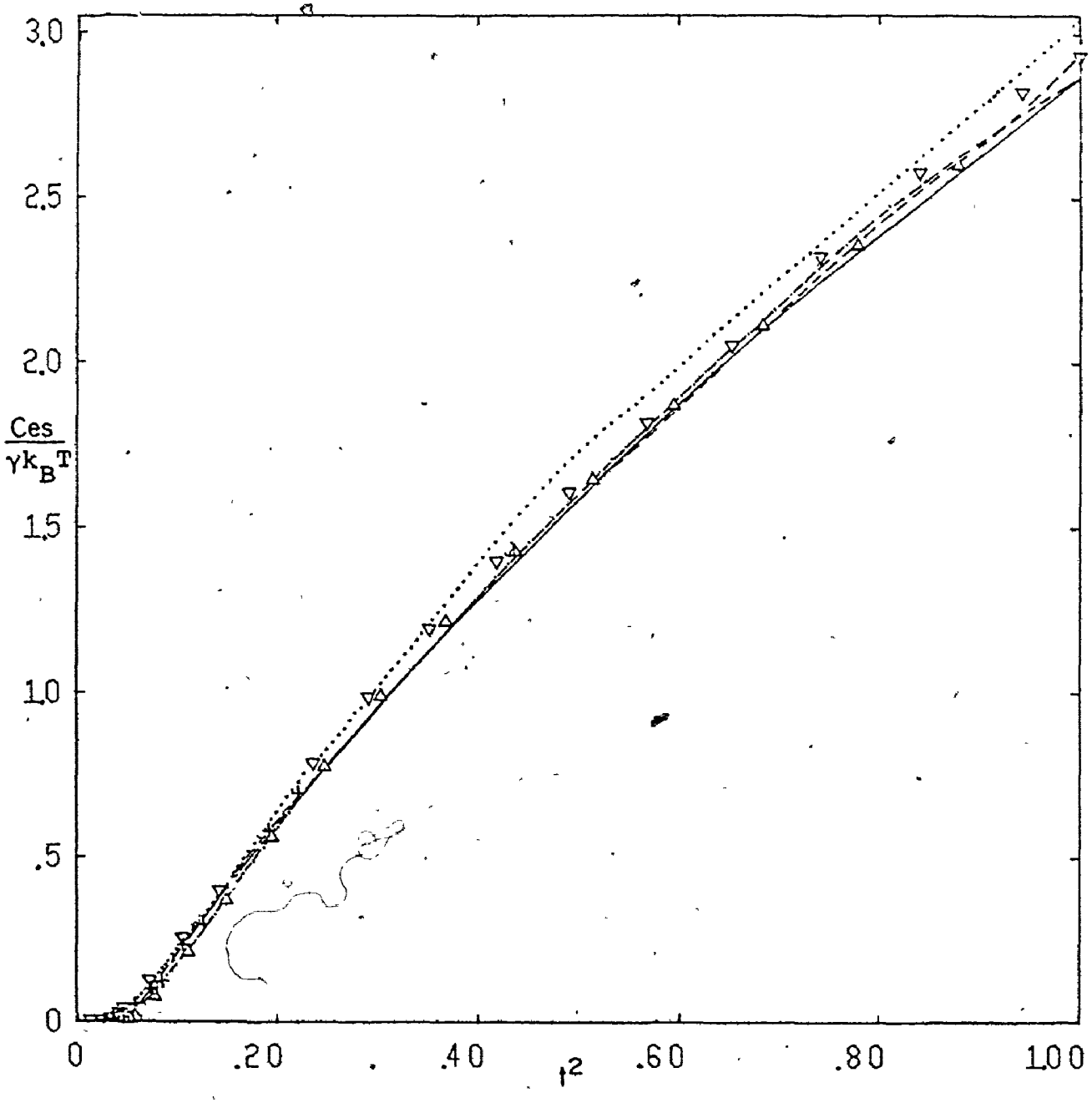

Fig. 5-10 Experimental and calculated specific heat for Nb
Experiment: ····· Ref. 8, ——— Ref. 3,
– – – – Ref. 53, Δ Ref. 100, ∇ Ref. 46, + Ref. 99.
–·–·– Calculated from spectrum 1. Note the unphysical downward turn above $t^2 = .8$.

to the three original spectra are considered.

Table 5-6 shows that the enormous differences between the three spectra are hardly reflected in the magnitudes of the $\Delta C_v(T_c)$ and H_c calculated from them; they are almost equally close to the experimental data listed in Table 5-4, except for spectrum 2 which underestimates both $\Delta C_v(T_c)$ and H_c. That last fact is not however sufficient reason to reject spectrum 2 out of hand, for a 15% increase in the N(0) used in the calculation would bring both the $\Delta C_v(T_c)$ and H_c for spectrum 2 up to the experimental values. Such an adjustment would not be consistent however with the experimental γ's which differ by only a few percent from the value used here. This kind of inconclusive juggling with numbers can be avoided by looking at the dimensionless ratios D(t) and $C_{es}(T)/\gamma k_B T$. The experimental values are shown in Table 5-4 and in Figures 5-9 and 5-10 where they are plotted together with the results from spectrum 1, while Figures 5-11 and 5-12 allow comparison of the results calculated from various $\alpha^2F(\omega)$. This additional data leaves no doubt that spectrum 2 is simply too weak coupling while spectrum 1 gives agreement almost as good as that seen in the previous section for the other elements.

The reason that these ratios are decisive when the absolute magnitudes of H_c and $\Delta C_v(T_c)$ are not is to be found in Table 5-2, and Figure 5-13 which shows $H_c^{-1}(0)\delta H_c(0)/\delta\alpha^2F(\omega)$ and $T_c^{-1}\delta T_c/\delta\alpha^2F(\omega)$. Table 5-2 demonstrates that $T_c^{-1}\partial T_c/\partial\mu^*$ and $H_c^{-1}(0)\partial H_c(0)/\partial\mu^*$ differ by less than 20%, much less than the

Fig. 5-11 D(t) calculated for Nb from various $\alpha^2 F(\omega)$.

——— spectrum 1 μ = .1091.

····· spectrum 1 modified,

------ spectrum 2,

-·-·-· spectrum 1 $\langle a_{\underline{k}}^2 \rangle$ = .04,

-·-·-·- spectrum 3

-·-·-·-·- spectrum 3 with scale factor.

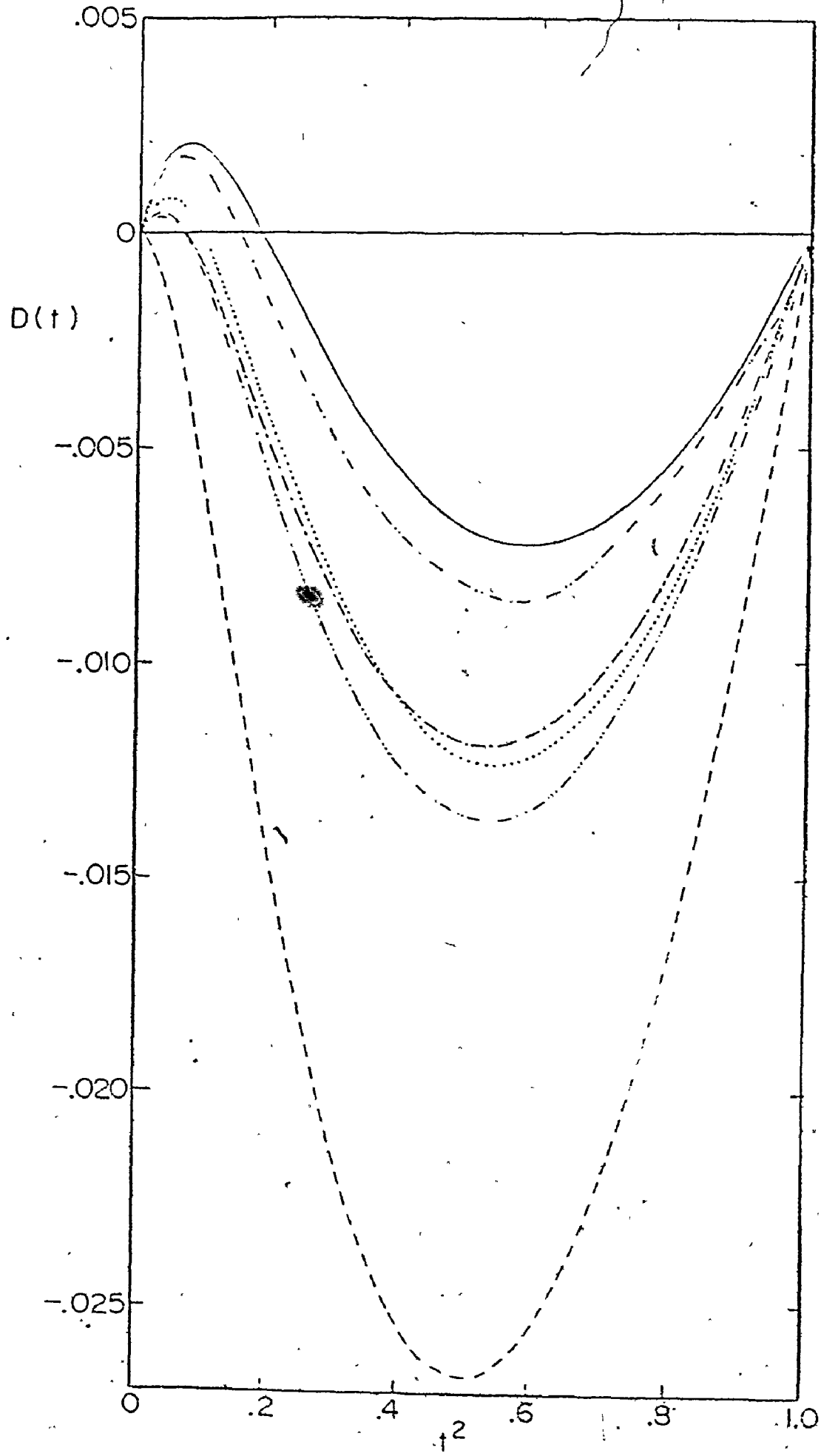
.005
0
D(t)
-.005
-.010
-.015
-.020
-.025
0
.2
.4
.6
.8
1.0
t²

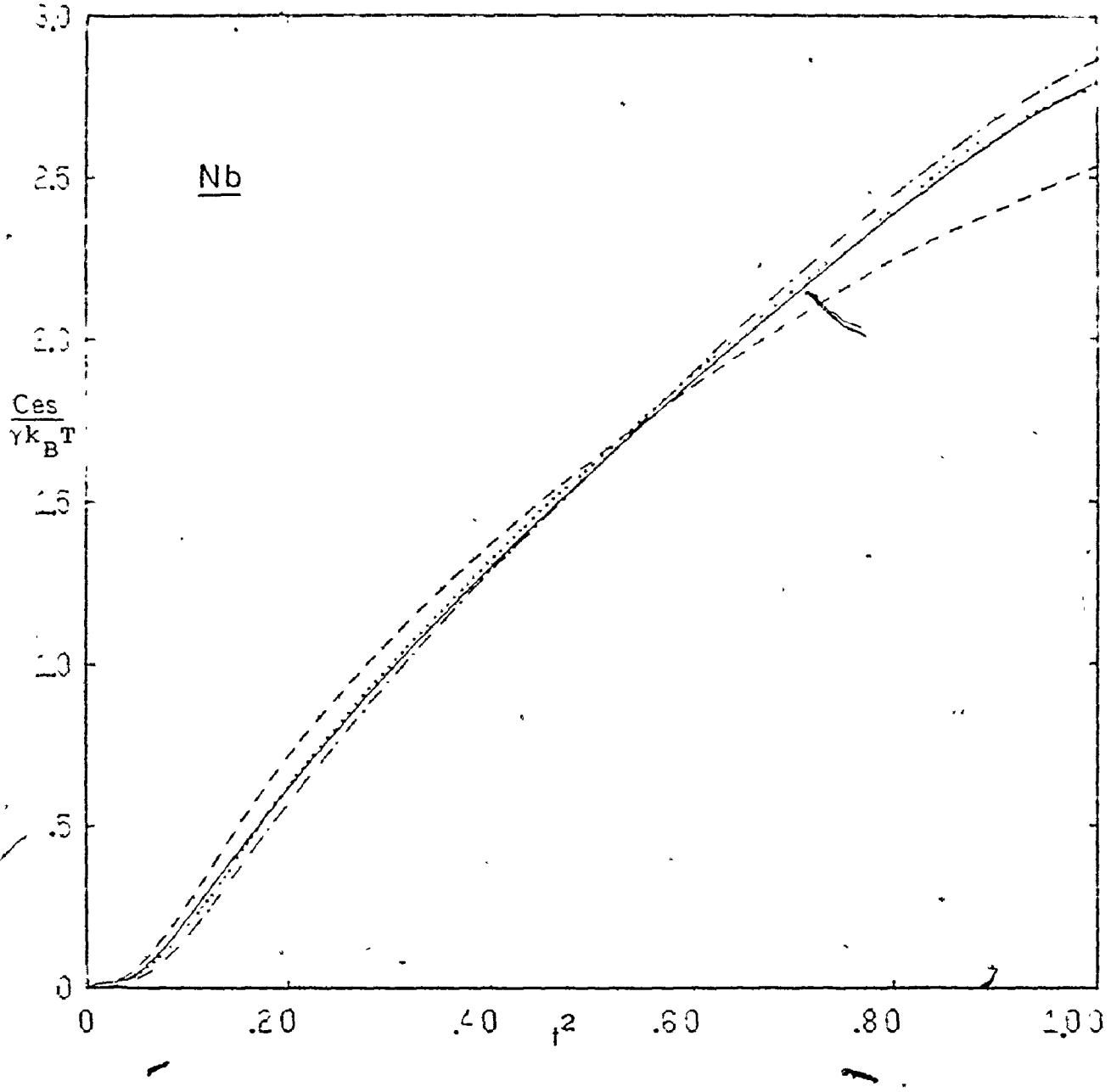

Fig. 5-12 Specific heat of Nb calculated from several different $\alpha^2F(\omega)$.

------ spectrum (a), ····· spectrum (d), but with $\mu^* = .1091$; ------ spectrum 2, ——— spectrum (g).

Note how closely the modification to spectrum 1 mimics anisotropy effects, as in Fig. 5-11.

difference between the corresponding derivatives with respect to $\alpha^2F(\omega)$ at most frequencies. What is true for $H_c(0)$ also holds for $H_c(T)$ at finite temperatures. It follows that ratios such as $\gamma T_c^2/H_c^2(0)$, $D(t)$, and $\Delta C_v(T)/\gamma T$ (which can be rewritten as

$$\frac{\Delta C_v(T)}{\gamma k_B T} = \frac{H_c^2(0)}{8\pi\gamma(k_B T_c)^2}\left[-2 + \frac{\partial^2 D(t)}{\partial t^2}\right]$$

to make explicit the ratio $T_c/H_c(0)$) are all much less sensitive to changes in μ^* than in $\alpha^2F(\omega)$. To put it more precisely: A change in $\alpha^2F(\omega)$ and a change in μ^* both chosen to increase T_c by the same amount will cause changes of quite different magnitudes in the dimensionless ratios. This is not to say that μ^* is unimportant. In Fig. 5-11 for example, the very large μ^* of spectrum 3 pulls its $D(t)$ down to that for spectrum 1, despite the considerable difference in A and $\lambda(0)$ between the two. It would be more accurate to state that adjustment of μ^* cannot compensate for deficiencies in $\alpha^2F(\omega)$ as revealed in the dimensionless ratios to the same extent that it can cover up the imperfections of $\alpha^2F(\omega)$ as revealed by the calculated T_c, $H_c(0)$ and $\Delta C_v(T_c)$.

Now that it has been established that the Eliashberg equations work for Nb and that the true $\alpha^2F(\omega)$ is quite close to spectrum 1, the functional derivatives for spectra 1 and 2 shown in Figures 5-8 and 5-14, and the directly calculated derivatives with respect to μ^* listed in Table 5-5, can be used to see how spectrum 1 might be improved. To avoid wasting time

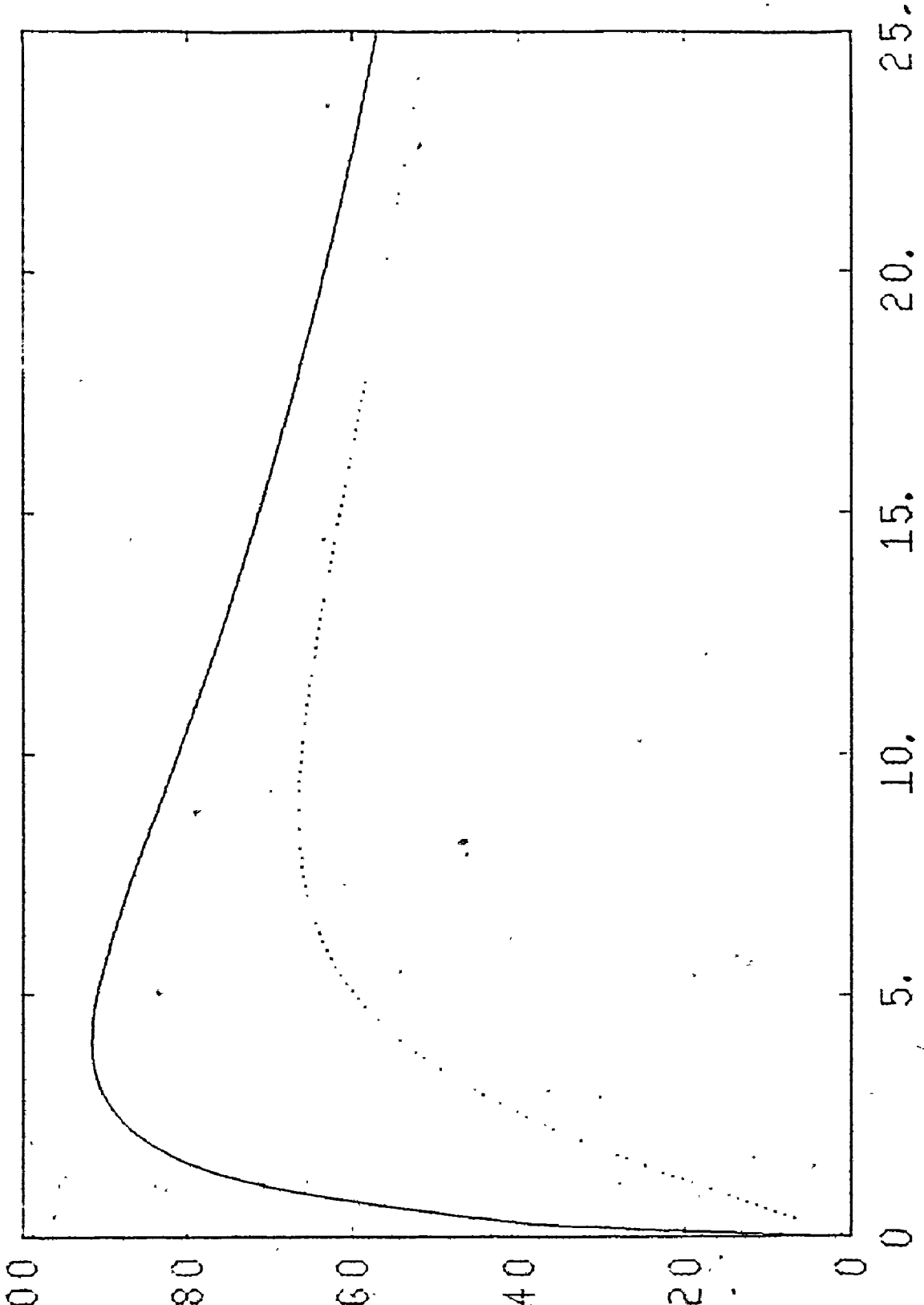

Fig. 5-13 $H_c(0)^{-1}\ \delta H_c(0)/\delta\alpha^2F(\omega)$ (———) and $T_c^{-1}\delta T_c/\delta\alpha^2F(\omega)$ (·····) for Nb, spectrum 2.

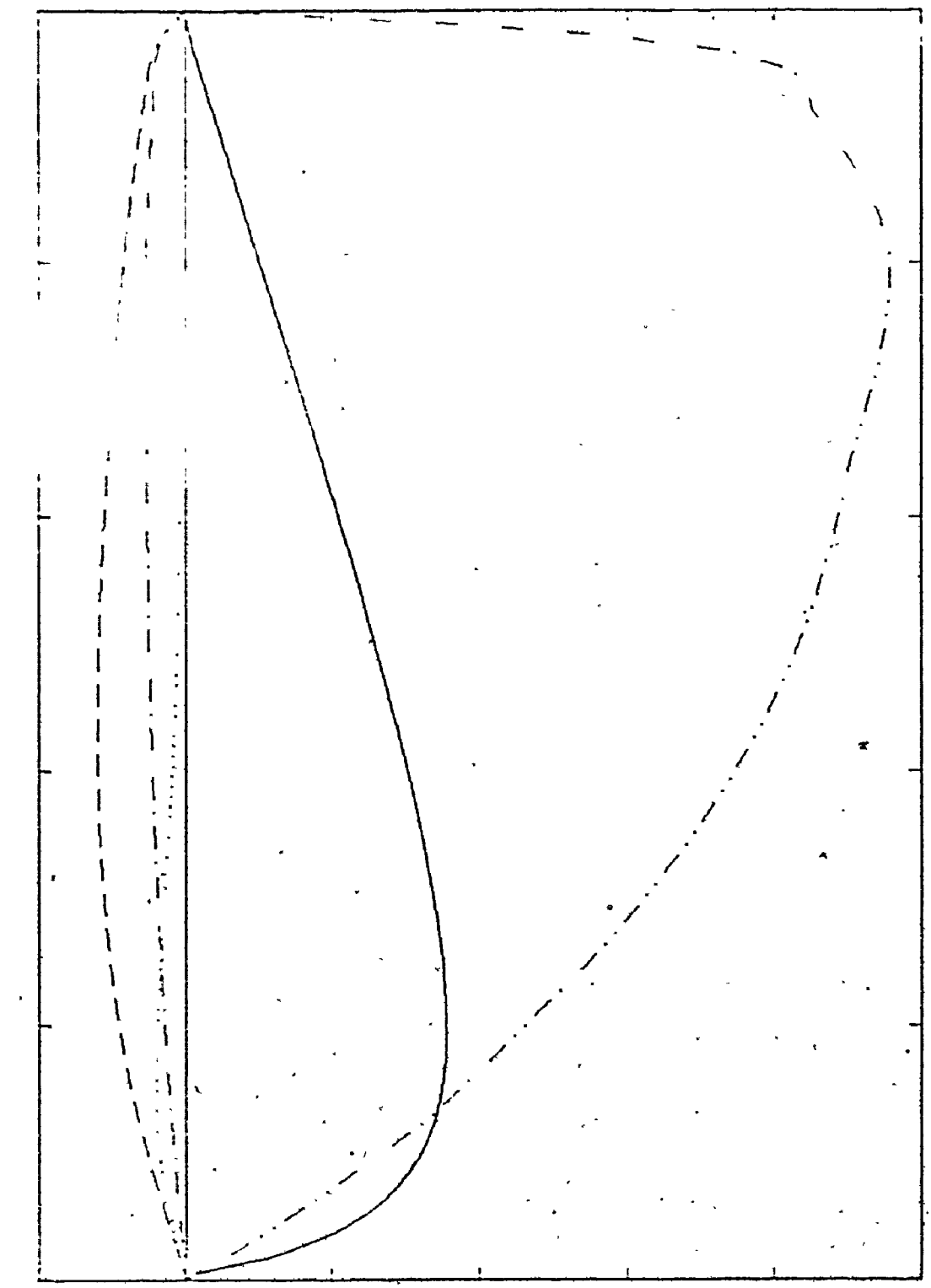

Fig. 5-14 $\delta D(t)/\delta\alpha^2F(\omega)$ and $\partial D(t)/\partial\mu^*$ for a weak coupling system. This is for Nb, spectrum 2, $\lambda = .33$
——— $\omega/k_BT_c = .4$, ····· $\omega/k_BT_c = 2.6$, --- $\omega/k_BT_c = 5.0$, -·-·- $\omega/k_BT_c = 17.0$,
-··-··- $\partial D(t)/\partial\mu^*$.

by going into too much detail it is worth finding out first how large a variation in $\alpha^2F(\omega)$ and μ^* is implied by the difference between the various experimentally measured D(t), or equivalently, how large a change is necessary to bring the calculated D(t) down to that given in Ref. 3, say, as an arbitrarily chosen example. There are many ways of doing this but some possibilities can be ruled out from the start. In the first place it is clear that the change cannot be accomplished through μ^* alone because then T_c would be reduced far below the value reported in that experiment. Adding weight to $\alpha^2F(\omega)$ below 2 meV where $\delta D(t)/\delta\alpha^2F(\omega)$ is large and negative but $\delta T_c/\delta\alpha^2F(\omega)$ is small and positive would be unrealistic because neutron scattering finds very few phonons of such low frequency. The only remaining possibility is to subtract weight from $\alpha^2F(\omega)$. The way to minimize the required reduction is to remove weight where $\delta D(t)/\delta\alpha^2F(\omega)$ is largest, between 3 and 12 meV as shown in Fig. 5-8 , thus reducing A and $\lambda(0)$ by only 5% and 10% respectively. Since T_c should stay constant during this change, μ^* is decreased at the same time. Row (e) of Table 5-6, and Fig. 5-11 display the results of a direct calculation with the altered $\alpha^2F(\omega)$ and μ^*, which compares very well with the values obtained in that particular experiment, provided allowance is made for the fact that the μ^* used was a little too small. Only the newly calculated specific heat jump is far below the value quoted in Ref. 3, but the reader will recall that these calculations underestimate the specific heat

by one to five percent.

This short aside has shown that the difference between the results reported in different experiments is consistent with a variation of about 15% in A and $\lambda(0)$. It was not intended to suggest that spectrum 1 should be modified by subtraction; quite the contrary, since the average of the other experimental data listed in Table 5-4 is somewhat higher than the values reported in Ref. 3, what spectrum 1 really needs is augmentation. The obvious place to put more weight is where the longitudinal phonons should have been, around 23 meV. Row (f) of Table 5-6 shows the effect of adding a delta-function of height h to spectrum 1 at that frequency while μ^* is held constant. Because of the previously mentioned uncertainty in $\alpha^2F(\omega)$, and because the possibility of anisotropy is being ignored for the time being, it is probably meaningless to continue this line of thought in any more detail.

Before finishing this section with a discussion of anisotropy it is worth seeing roughly how spectra 2 and 3 might be improved. The relatively large functional derivatives shown for spectrum 2 in Fig. 5-14 and Table 5-5 seem to suggest that a very small change in spectrum 2 would bring its D(t) up to experiment. Such simple reasoning grossly underestimates the required change. As $\alpha^2F(\omega)$ is augmented μ^* has to become more positive to hold T_c down to 9.2 K, with the result that part of the gain in D(t) is cancelled out. Moreover, as $\alpha^2F(\omega)$ increases, $\delta D(t)/\delta\alpha^2F(\omega)$ must decrease by at least a factor

of two to a magnitude more typical for intermediate strength coupling. From these considerations it should be clear that the necessary modification to spectrum 2 is far larger than the proposed 10 or 15 percent additions to spectrum 1.

Although spectrum 3 has the longitudinal phonon peak that was lacking in the tunneling $\alpha^2F(\omega)$, its oversized μ^* prevents that peak from showing its influence anywhere in the calculated quantities. Renormalizing the spectrum by an overall scale factor of 2/3 to make the fitting of T_c by a smaller μ^* of .10 possible has the result shown in row (d) of Table 5-6. Since $H_c(0)$, $\Delta C_v(T_c)$, and the dimensionless ratios are now all smaller even than those obtained from the unmodified spectrum 1, the guess was obviously bad. A scale factor closer to unity should have been used. It is gratifying to see that such a modification would cause spectrum 3 to approach from above the same sort of $\alpha^2F(\omega)$ that spectrum 1 seems to be converging on from below, namely an $\alpha^2F(\omega)$ resembling an average of spectra 1 and 3, with $\lambda(0) \sim 1.1$ and $A \sim 8$ meV.

The possibility of anisotropy may make it necessary to modify that conclusion. The experimental evidence in the superconducting state for anisotropy is ambiguous to say the least. One group deduced anisotropy from their tunneling experiments[85] but later redid the experiment and changed their minds[16]; another found evidence for it in the behaviour of C_{es} at low temperature[31], while it was later shown that this behaviour could be reproduced by dissolving hydrogen in the sample[35];

and so on for just about all the types of experiments where anisotropy effects were expected to be seen. But in the normal state cyclotron resonance studies[94] give clear evidence of anisotropy in $\lambda_{\underline{k}}(0)$, while other work[18] shows that the Fermi surface is far from the free-electron shape. Calculations have even been done of T_c using a supposedly realistic anisotropic interaction. One such effort, which like this work was done on the imaginary axis, included a realistic Fermi surface anisotropy and found that this source of anisotropy raised T_c by only .24 K[18]. (Unfortunately they did not quote the RMS gap anisotropy.) Another one was done on the real axis using Fermi surface harmonics to expand a calculated interaction; this computation found a 6% RMS deviation in the gap and a .07 K increase in T_c resulting from a 12% RMS anisotropy in $\lambda_{\underline{k}}(0)$. It is not at all clear why these calculated interactions should be so nearly isotropic when the Fermi surface is highly distorted, but it does seem reasonable to conclude that Nb is not one of the more anisotropic elements.

The calculation done here with a model anisotropy leads to a very similar conclusion. The model, of which more details are given in the next section, consisted simply of adding the same factor $(1+a_{\underline{k}})(1+a_{\underline{k}'})$ onto spectrum 1 at all frequencies, with $a_{\underline{k}}$ chosen to get $\langle a_{\underline{k}}^2 \rangle = .04$. The results of this change are shown in row (g) of Table 5-6. The increase in T_c of .52 K is larger than those just mentioned, but so is $\langle a_{\underline{k}}^2 \rangle$; in fact the ratio $(T_{ca}-T_{ci})/R_0^2$ where R_0^2 is the gap

anisotropy (.023 in this work) is roughly the same, verifying in one sense at least the consistency of the two calculations. The other entries in Table 5-6 show that $C_{es}/\gamma k_B T_c$ has fallen far below the experimental ratio despite the increase in $\Delta C_v(T_c)$, while D(t) is still within acceptable limits.

If there were experimental results showing the washing out of anisotropy in Nb, there would be no need to add to Table 5-6 the row (g) which shows that would happen to the properties of the anisotropic system if μ^* were increased to bring T_{ca} down to the observed value. This row is meant to answer the question: Given that the averaged interaction is close to spectrum 1, is the experimental data other than T_c more consistent with $\langle a_{\underline{k}}^2 \rangle \doteq .04$ or $\langle a_{\underline{k}}^2 \rangle = 0$? The answer must be $\langle a_{\underline{k}}^2 \rangle = 0$ because the calculated D(t) falls far too low. A very considerable increase in $\alpha^2 F(\omega)$ would be needed to compensate for that drop in D(t), which in turn calls for an increase in μ^* to hold down T_c. The upshot of it all would probably be an improbably large μ^* compensating for an $\alpha^2 F(\omega)$ that is on the average too large to be consistent with other estimates of $\lambda(0)$. If anisotropy is present then it would have to be far less than that used in this model calculation.

The conclusion drawn from these calculations is that the Eliashberg equations together with a conventional tunneling $\alpha^2 F(\omega)$ and μ^* describe the thermodynamic properties of Nb as well as they do other elements.

5. Results from the Numerical Solution of Systems with Model Anisotropies

In this section the effect of various model anisotropies together with elastic impurity scattering on the thermodynamic properties of weak and strong coupling superconductors is studied through the exact solution of the anisotropic Eliashberg equations. These model anisotropies are with one exception separable and frequency-independent: that is to say $(\alpha^2F(\omega)_{\underline{k}\underline{k}'} = (1 + a_{\underline{k}})(1 + a_{\underline{k}'})\alpha^2F(\omega)$ where $\langle a_{\underline{k}} \rangle \neq 0$, and the averaged interaction is identical to the $\alpha^2F(\omega)$ used in the preceding section. $a_{\underline{k}}$ is completely described by a frequency-independent probability density $P(a)$ defined so that $P(a)da$ is the probability of $a_{\underline{k}}$ lying between a and a+da. The impurity scattering term is also approximated by a constant, $c\tau^{-1}$, where $c^{-1}\tau$ is the impurity lifetime (not to be confused with the residual lifetime). In short, excepting the use of a retarded interaction, the model is that proposed by Markowitz and Kadanoff[36] and extended by Clem[22] to the temperatures below T_c, but with an important difference. The simplifications they found necessary to get an analytic expression for T_c, namely the use of a non-retarded interaction, the omission of μ^* and the replacement of $\tilde{\omega}_{\underline{k}}(n)$ by its average $\tilde{\omega}(n)$ were not made in these calculations. The difference between the exact and approximate solutions turns out to be significant for every realistic system studied, whether weak or strong coupling.

Since it is impractical to do calculations below T_c with a great number of shapes for P(a) and magnitudes for $\langle a_{\underline{k}}^2 \rangle$, the first thing to verify is that the properties of interest, T_c, H_c, $\Delta C_v(T_c)$ and D(t) differ from their isotropic values by an amount proportional to $\langle a_{\underline{k}}^2 \rangle$ and that the details of P(a) are unimportant to these quantities and to the gap anisotropy R_0^2. This is no more than the conclusion reached in their formal work by Markowitz and Kadanoff[36] regarding T_c, and by Clem[22] regarding T_c, H_c, $\Delta C_v(T_c)$ and D(t). The effect on R_0^2 and $T_{ca}+T_{ci}$ for Hg and Sn of different P(a) but identical $\langle a_{\underline{k}}^2 \rangle$ was a small variation in $T_{ca}-T_{ci}$ (4% for Sn, 8% for Hg) and a larger difference in R_0^2 (6% for Sn, 20% for Hg). The following P(a) were tested: $P(a) = \frac{1}{3}\delta(a \mp 2a_m) + \frac{2}{3}\delta(a \mp a_m)$, and $P(a) = .5\, a_m^{-1}\, \theta(a_m - |a|)$, where θ is the step function and a_m was adjusted to get $\langle a_{\underline{k}}^2 \rangle = .04$. This 8% variation in T_c is not significant when $T_{ca}-T_{ci}$ is 3% of T_{ci}(Hg) or 10% of T_{ci}(Sn). The sensitivity of R_0^2 to P(a) is more a problem limited to strong coupling, for the following reason. From eqn. (2-17) it follows that $\tilde{\Delta}_{\underline{k}}(n) = \langle \tilde{\Delta}_{\underline{k}}(n) \rangle (1 + C_\mu a_{\underline{k}})$, where C_μ is a constant depending on μ^*. This implies that if $\tilde{\omega}_{\underline{k}}(n)$ is very nearly isotropic then $\bar{\Delta}_{\underline{k}}(n) = \tilde{\Delta}_{\underline{k}}(n)/|\tilde{\omega}_{\underline{k}}(n)|$ will give an $R_0^2 \approx C_\mu^2 \langle a_{\underline{k}}^2 \rangle$ regardless of the shape of P(a). If however $\lambda_{\underline{k}}(0)$ is relatively large, then the anisotropy in the denominator does matter and will make R_0^2 a non-linear functional of P(a), even more so when $\langle a_{\underline{k}}^2 \rangle$ is large. The smallness of the anisotropy in the two strong coupling systems studied here makes such details unimportant for the time being.

Because the anisotropy turns out to have very little temperature dependence, it seems reasonable to generalize these results to other thermodynamic properties than T_c. (In Clem's work the gap anisotropy was necessarily temperature-independent, because it was identical to $\langle a_{\underline{k}}^2 \rangle$ at all temperatures.)

Both R_0^2 and $T_{ca}-T_{ci}$ turn out to be nearly linear in $\langle a_{\underline{k}}^2 \rangle$, at least up to $\langle a_{\underline{k}}^2 \rangle = .09$, if $\langle a_{\underline{k}}^2 \rangle$ is varied by changing a_m while keeping the functional form of P(a) fixed. In Sn, $T_{ca}-T_{ci}$ deviated by less than 4% from linearity in $\langle a_{\underline{k}}^2 \rangle$, R_0^2 by about 2%. For Hg as the previous discussion should suggest, the deviations are much larger, 6% for T_c and 14% for R_0^2 over the same range of $\langle a_{\underline{k}}^2 \rangle$.

For temperatures below T_c, there is, from the calculations with Pb described in the next section, indirect evidence of linearity in $\langle a_{\underline{k}}^2 \rangle$ of the changes in D(t) and H_c. When $\langle a_{\underline{k}}^2 \rangle$ is increased by 55% from .019 to .029, while P(a) is roughly the same shape, the difference in the maximum of D(t) increases by 51%, $T_{ca}-T_{ci}$ and $H_{ca}-H_{ci}$ both by 66%. These results should justify the use of the same $P(a) = \frac{1}{3}\,\delta(a+2a_m) + \frac{2}{3}\,\delta(a-a_m)$ with a_m chosen to get $\langle a_{\underline{k}}^2 \rangle = .04$ for all the anisotropic systems below T_c and should caution against taking the results for strong coupling too literally.

The omission of μ^* and anisotropy in $\tilde{\omega}_{\underline{k}}(n)$ has a great effect on R_0^2. Equation (2-17) shows that if both are

omitted, then $\tilde{\Delta}_{\underline{k}}(1) = \langle\tilde{\Delta}_{\underline{k}}(1)\rangle(1 + a_{\underline{k}})$, likewise for $\bar{\Delta}_{\underline{k}}(1)$. If only anisotropy in $\tilde{\omega}_{\underline{k}}(n)$ is absent, then $\tilde{\Delta}_{\underline{k}}(1) = \langle\tilde{\Delta}_{\underline{k}}(1)\rangle (1+C_{\mu}a_{\underline{k}})$, similarly $\bar{\Delta}_{\underline{k}}(1)$, where C_{μ} is some constant greater than unity. This increase in gap anisotropy comes about because the kernel $\lambda_{\underline{kk}'}(m)-\mu^*$ is more anisotropic than $\lambda_{\underline{kk}'}(m)$ itself, at least for the Matsubara frequencies where $\lambda(m) \gtrsim \mu^*$. Typical values for C_{μ} (with $\langle a_{\underline{k}}^2\rangle = .04$) for Al, Sn and Hg are 1.44, 1.21, and 1.13 respectively. It follows that $P_{\Delta}(a)$, defined so that $\bar{\Delta}_{\underline{k}}(1)/\langle\bar{\Delta}_{\underline{k}}(1)\rangle - 1$ has a probability $P_{\Delta}(a)da$ of lying between a and a+da, is merely a uniformly stretched version of P(a). If however anisotropy in $\tilde{\omega}_{\underline{k}}(1)$ is allowed, so that for $\bar{\Delta}_{\underline{k}}(1) = \tilde{\Delta}_{\underline{k}}(1)/(1 + \lambda_{\underline{k}}(0))$ a part of the anisotropy in $\bar{\Delta}_{\underline{k}}(1)$ is washed out, the amount depending on the size of $\lambda(0)$. In addition, P(a) can no longer describe $\bar{\Delta}_{\underline{k}}(1)$. For the small $\langle a_{\underline{k}}^2\rangle$ used here, the resulting difference in shape between $P_{\Delta}(a)$ and P(a) is insignificant, even if $\lambda(0)$ is very large, but the amount of stretching is not, especially for strong coupling where this effect dominates. The entries in brackets under Hg in Table 5-7 show that removing the anisotropy in $\tilde{\omega}_{\underline{k}}(n)$ nearly quadruples R_0^2 and $T_{ca}-T_{ci}$. Even for Al, it makes a difference; R_0^2 increases by 50% without it. But there μ^* is far more important. Table 5-7 shows that with $\mu^* = 0$ there is 50% less anisotropy. It looks as if Markowitz and Kadanoff's simplifications are nowhere good approximations, because for strong coupling anisotropy in $\tilde{\omega}_{\underline{k}}(n)$ plays an essential role, while for weak coupling μ^* influences the gap anisotropy just

Table 5-7

Comparison of the numerical calculations of T_c with the analytical expressions of Markowitz and Kadanoff

Entries in brackets correspond to calculations with $\tilde{\omega}_{\underline{k}}(n)$ replaced by $\langle\tilde{\omega}_{\underline{k}}(n)\rangle$.

N(0)V was taken from Rickayzen[50].

For Pb the calculated, not the tunneling $\alpha^2F(\omega)$, was used and for Nb, spectrum 1

	Hg	Nb	Pb	Sn	Tl	Al ($\mu^* \neq 0$)	Al ($\mu^* = 0$)
$\lambda(0)$	1.62	.98	1.32	.72	.80	.41	.41
T_{ci}	4.15	9.20	7.19	3.73	2.30	1.18	8.34
N(0)V	.35	.29	.39	.25	.28	.18	.27
$\langle a_{\underline{k}}^2\rangle$	.04	.04	.02	.04	.04	.04	.04
R_0^2	.014 (.049)	.023	.0062	.031	.029	.052 (.075)	(.038)
$\frac{T_{ca}-T_{ci}}{T_{ci}}$	.033 (.125)	.056	.014	.095	.084	.31 (.48)	(.145)
$\frac{\langle a_{\underline{k}}^2\rangle}{N(0)V}$	.114	.138	.049	.16	.14	.22	(.148)
$-\frac{1}{\pi}\frac{\partial T_c}{\partial \rho}R_0^2$	.0035 (.012)	.0076	.0016	.014	.011	.031 (.044)	(.018)
$\frac{\pi}{8}\langle a_{\underline{k}}^2\rangle$	.016	.016	.0075	.016	.016	.016	.016

as much. In the intermediate coupling range, although $R_0^2 \sim \langle a_{\underline{k}}^2 \rangle$, the deficiencies of the approximate solution surface in T_c itself.

These discrepancies between the actual $\bar{\Delta}_{\underline{k}}(n)$ and the simple form assumed for the analytical solution are less conclusive than a comparison of the behavior of T_c. Markowitz and Kadanoff find

$$\frac{T_{ca}-T_{ci}}{T_{ci}} = \frac{\langle a_{\underline{k}}^2 \rangle}{N(0)V} \qquad (3\text{-}50(a))$$

where $N(0)V$ is the usual BCS parameter, and

$$\tau\left(\frac{\partial T_c}{\partial c}\right)_{c=0} = -\frac{\pi}{8}\langle a_{\underline{k}}^2 \rangle \qquad (3\text{-}48(b))$$

in contrast to

$$\frac{T_{ca}-T_{ci}}{T_{ci}} = \frac{\partial T}{\partial \rho}\langle a_{\underline{k}}^2 \rangle \frac{\lambda(0)-1}{\lambda(0)+1}, \qquad (3\text{-}49)$$

an approximate expression valid only for very large $\lambda(0)$, and

$$\tau\left(\frac{\partial T_c}{\partial c}\right)_{c=0} = \frac{1}{\pi} R_0^2 \frac{\partial T}{\partial \rho} \qquad (3\text{-}34)$$

in which no approximations are made. Table 5-7 compares the calculated values with the approximate expressions. There is admittedly considerable uncertainty in $N(0)V$, and it may be meaningless to assign such a number to a strong-coupling system, but even so expression (3-50(a)) is very inaccurate. It can be greatly improved by replacing $\langle a_{\underline{k}}^2 \rangle$ by R_0^2. Similarly eqn. (3-48(b)) compares very badly with eqn. (3-34), which is exact.

Again, replacing $\langle a_{\underline{k}}^2 \rangle$ by R_0^2 brings about some improvement, but not in Al. In fact the only system where eqns. (3-50(a)) and (3-48(b)) are at all accurate is in Al with $\mu^*=0$ and with isotropic $\tilde{\omega}_{\underline{k}}$. It would not be worthwhile making the comparison were it not for the fact that these expressions have been widely used to estimate the gap anisotropy. A recent example of inappropriate use is their application to Nb_3Sn[98], a system that probably behaves much like Pb. Using eqn. (3-48(b)) to obtain the gap anisotropy would underestimate it by about 50%.

The formula (3-49) proposed for the strong coupling limit fares no better; it predicts $(T_{ca}-T_{ci})/T_{ci} = .0024$ for Hg. The reason is not the failure of $\partial T_c/\partial\rho$ to remain constant; in Al, for example, with $\langle a_{\underline{k}}^2 \rangle = .09$, T_{ca} is double T_{ci} while $\partial T/\partial\rho$ differs from the isotropic value by only 15%; in Pb $\partial T/\partial\rho$ changes by less than 4% while $\langle a_{\underline{k}}^2 \rangle$ goes from zero to .02. Nor is it the inadequacy of the approximation for R_0^2, a poor one even for $\lambda = 1.62$. The problem is the assumption that $R^2 \approx 1 - \langle\bar{\Delta}_{\underline{k}}(1)\rangle^2/\langle\bar{\Delta}_{\underline{k}}(1)^2\rangle$. This is quite true for c=0, but at intermediate concentrations where the anisotropy is washed out in $\bar{\Delta}_{\underline{k}}(1)$ but not in all the other $\bar{\Delta}_{\underline{k}}(n)$ it fails. Because a given $\bar{\Delta}_{\underline{k}}(n)$ will not be smoothed out until the isotropic part of $\tilde{\omega}_{\underline{k}}(n)$ dominates the anisotropic part, ie until $|\omega_n| + c\tau^{-1} >> |\tilde{\omega}(n)-\omega_n|$ the larger values of n are what contributes most to R^2 at higher concentrations. This means the saturation of T_c is certain to be very slow, since $c\tau^{-1}$ must be far greater than ω_c to remove the anisotropy in the

last Matsubara frequency. Figure 5-15, which shows T_c and R^2 (ie $\partial T_c/\partial c$) versus concentration, reveals that most of the area under $\partial T_c/\partial c$ comes from the very high concentrations where R^2 is nearly zero. Therefore only an equation that takes into account all the terms in the sum for R^2 can hope to represent T_c versus c correctly for $c\tau^{-1} > T_c$. When the separable model is complicated by the inclusion of μ^* and anisotropy in $\tilde{\omega}_{\underline{k}}$, the expressions for $\langle\bar{\Delta}_{\underline{k}}\rangle$ and $\langle\bar{\Delta}_{\underline{k}}^2\rangle$ become very messy, so there may not be much hope of progress in that direction. Interestingly enough, Markowitz and Kadanoff also point out that the frequency cutoff must be handled with great care when impurities are present to get halfway sensible results.

So far nothing much has been said about any experimental evidence for anisotropy except for D(t) in Nb, and some rather general features of the effect on T_c of impurities. The example of Nb illustrates the typical difficulties encountered in an experimental search for anisotropy. In the first place, the evidence is indirect, thus requiring a good theoretical understanding of the phenomenon; in the second place the effect is small, differing by only a few percent from the isotropic value and being of the same order as the experimental error. Finally, the important parameter controlling the washing out of anisotropy, the impurity lifetime can only be known approximately through the residual resistivity. The direct approaches such as tunneling at different crystal orientations do not

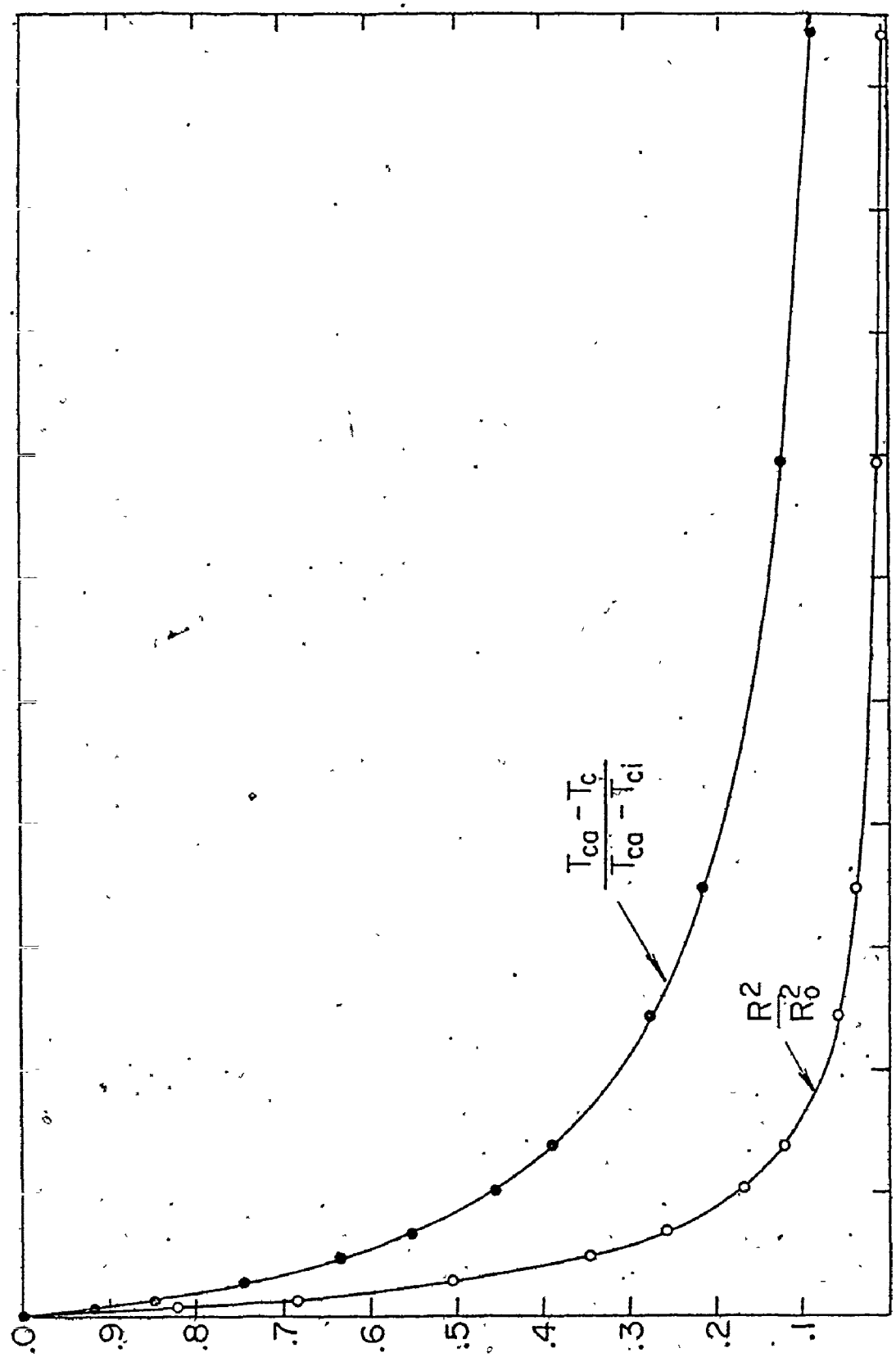

Fig. 5-15 Washing out of anisotropy and saturation of T_c for Hg with a model anisotropy ($\langle a_{\underline{k}}^2 \rangle = .04$). τ_c^{-1} is the impurity lifetime.

lead to completely reproducible results, although they do indicate which superconductors are more anisotropic than others. That is about all that the other kinds of experiments reveal, despite their number and variety, because different experiments on the same superconductor seem to lead to very different estimates of the anisotropy. The reader is referred to a comprehensive review paper[83] and a more recent discussion[16] of the contradictions in the various estimates. Part of the trouble almost certainly lies in the formulas developed by Clem that are used to interpret the experiments. Since his work shares the assumptions of Markowitz and Kadanoff's analytical solution, it shares the defects just demonstrated too. Being the only candidate in the field other than a purely empirical formula[32] it has been applied just as indiscriminately to strong and weak coupling alike. Because an exact numerical solution offers more hope of providing guidelines in the interpretation of experiment, and because so little is known of the details of the anisotropic interaction, it seemed worthwhile to calculate the thermodynamic properties of several systems with different coupling strengths, using the $\alpha^2F(\omega)$ of the isotropic superconductor combined with a model frequency-independent separable anisotropy described by $P(a) = \frac{1}{3}\,\delta(a+2a_m) + \frac{2}{3}\,\delta(a-a_m)$ with a_m chosen to make $\langle a_k^2 \rangle = .04$. Such a series of calculations should show systematically the effects of strong coupling. Table 5-8 and Figures 5-18 and 5-19 display the results obtained for Al, Hg, Nb, Pb, Sn and Tl. No elastic impurity scattering was included, although the computer pro-

grams exist to do it, because almost no experiments were done that demonstrate the washing out of anisotropy as clearly in as much detail as the impurity dependence of T_c; what experiments there are hardly show more than the difference between the clean and dirty limits. Moreover, there is little reason to do such a calculation if impurities make their presence felt only through the reduction of R^2 and the dependence of R^2 on τ^{-1} is the same at all temperatures, in other words the same as at T_c. Although this assumption seems reasonable, especially in view of the temperature dependence found for the gap anisotropy in these calculations, the washing out of anisotropy at very low temperatures where the specific heat is expected to depend on the details of the gap anisotropy remains an open question.

The calculated temperature dependence of the gap anisotropy, or rather the near-absence of temperature dependence, can be explained in terms of scattering by thermal phonons. In systems where there is little weight in the part of $\alpha^2F(\omega)$ below frequencies of order T_c, in other words the region from which the thermal phonons can be excited, one would expect to find little change in R_0^2 with temperature. These calculations verify that conjecture. Between $t = .1$ and $t = 1$, R_0^2 decreases by about .4% for Sn, 2% for Nb, 5% for Pb and 10% for Hg, with about 80% of the decrease occurring above $t = .5$. Since Pb and Hg have about the same $\lambda(0)$, the difference may be ascribed to the unusual weight of the $\alpha^2F(\omega)$ of Hg at low

frequencies. A ten percent difference is in any case not large compared to the experimental uncertainties.

These numerical calculations also show that the negative values for $\delta T_c/\delta\alpha^2F(\omega)$ turn out to be of greater significance in uncovering the special role of thermal phonons in anisotropic systems than in affecting any measurable quantity. Figures 5-17 and 5-16 show these derivatives for Al (model anisotropy) and Pb (realistic anisotropy). In both cases the change of sign, whose position is predicted very well by combining eqn. (3-8) and the coefficient of ω_0^{-1} in eqn. (3-24), falls very low in $\alpha^2F(\omega)$, (.13 meV for Al, .35 meV for Pb), and the coefficients of ω_0^{-1} (0.178 and .011 meV respectively) are so small that these regions of $\alpha^2F(\omega)$ have a totally negligible effect on T_c.

Two anisotropies are included here that correspond to a P(a) different from the one defined earlier. That used for Pb with the calculated $\alpha^2F(\omega)$ (which is somewhat weaker coupling than the tunneling $\alpha^2F(\omega)$) is based on $\lambda_{\underline{k}}(0)$ in the manner described in the next section. Coincidentally, that P(a) is very close to the one used for the other elements, the main difference being a smaller a_m that results in $\langle a_{\underline{k}}^2\rangle = .019$, so that the anisotropy effects in Pb need only be scaled up by a factor of 2 to put them in their place in the series. Since Hg is anomalous among strong-coupling systems because of that large weight low down in $\alpha^2F(\omega)$, it seemed worth having a more normal strong coupling supercon-

ductor for comparison. This procedure turns out to be unnecessary, since the factor of 2 difference in $\langle a_{\underline{k}}^2 \rangle$ accounts for most of the difference between their anisotropy effects, as Table 5-8 shows. Those relatively abundant thermal phonons do not seem to have any effect of measurable size.

The second "non-standard" anisotropy is really the opposite extreme to separable anisotropy, namely a two-band model with very weak interband coupling and one gap far larger than the other. The interaction was defined as

$$(\alpha^2 F(\omega))_{ij} = V_{ij}\, \alpha^2 F(\omega)$$

where $\alpha^2 F(\omega)$ is the same tunneling $\alpha^2 F(\omega)$ for Sn used throughout, i and j label bands 1 and 2, while V_{ij} satisfies

$$V_i = \Sigma V_{ij} W_j$$

$$1 = \Sigma W_i V_i$$

where the W_i are the relative weights of the two bands with the ratio $W_1/W_2 = 3$, and $V_1/V_2 = 2$, $V_{11} = 1.47$, $V_{22} = 1.84$ and $V_{12} = V_{21} = .15$. This V_{ij} was chosen with the 2-band model of Suhl et al[57] in mind, another model simple enough to yield analytical expressions for T_c; but no attempt is made here to verify them, since this calculation was done just as an example of a non-separable potential. A strange feature of the solution was the sign of $\bar{\Delta}_2(n)$, which was negative for all n, while $\bar{\Delta}_1(n)$ looked normal. The ratio $\bar{\Delta}_2(1)/\bar{\Delta}_1(n)$ was only $-.10$, so this may be a feature peculiar to systems with

Table 5-8

Anisotropy effects in the thermodynamics of Tl, Sn, Nb, Hg and Pb with a separable model interaction

	T_c deg K	$H_c(0)$ Gauss	μ^*	ω_c meV	$\Delta C_v(T_c)$ mJ/mole/deg	$-(dH_c/dT)_{T_c}$ Gauss/deg	$C_{es}(T_c)/\gamma k_B T_c$	$\gamma(k_B T_c/H_c)^2$	$D(t)$	$\langle a_k^2 \rangle$	R_o^2	$\frac{T_{ca}-T_{c1}}{T_{c1}}$	$\frac{H_{ca}-H_{c1}}{H_{c1}}$
Tl	2.391	174.5	.12566	33.	58.8	135.	2.686	.159	-.0184	0	0		
	2.593	185.6	.12566		59.9	131.	2.582	.165	-.0230	.04	.028	.084	.064
	*2.39	170.	.1419					.168	∿-.025	.04	∿.028	0	-.03
Nb	9.199	2007.	.11725	86.	134.	417	2.874	.151	-.0080	0	0		
	9.718	2094.	.11725		136.	409	2.794	.164	$\frac{+.0019}{-.0119}$	.04	.022	.056	.043
	*9.20	1.96×10^3	.1313		127	400	2.78	.165	$\frac{+.0005}{-.013}$	.04	∿.022	0	≥.02
Hg	4.154	447.2	.1230	43.	21.7	218	3.369	.134	.0167	0	0		
	4.290	458.0	.1230	21.5	21.5	215	3.273	.137	.0135	.04	.013	.033	.024
	*4.15	443.	.1357					.137	∿.013	.04	∿.013	0	-.01
Sn	3.730	307.0	.11487	55.	10.8	150	2.621	.161	-.022	0	0		
	4.086	329.3	.11498		11.0	145	2.510	.169	-.027	.04	.030	.095	.073
	*3.73	301	.1294					.167	∿-.029	.04	∿.030	0	-.02
	5.445		.11498		13.6	141	2.405			.63	.33	.460	
Pb	7.201	763.8	.1140	65	48.9	221	3.438	.136	.0193	0	0		
	7.304	771.9	.1140		48.8	219	3.397	.137	.0178	.019	.0062	.0143	.0106
	*7.20	760.	.120					.137	<.0177	.019	∿.0062	0	-.01

Rows marked with an asterisk were calculated from derivatives with respect to μ^*. For Tl and Sn $\partial D(.7)/\partial\mu^*$ was roughly estimated as -.15. For Hg and Pb the $\partial D(.7)/\partial\mu^*$ from the Pb tunneling $\alpha^2F(\omega)$ were used. The calculated $\Delta C_v(T_c)$ is probably a slight underestimate (see previous section).

much weaker coupling in one band than the other. Another oddity was that the specific heat jump actually fell below the BCS value. It would have been interesting to see what happened to C_{es} at very low temperature, but the rate of convergence of the iterations was so slow due to the weak interband coupling that the calculation was not practicable. Table 5-8 shows the results obtained from the upper temperatures. About the only generalization that can be made is that because all the results in this section are limited to separable interactions, they are likely to be uninformative and probably misleading if the interaction is not separable. This is meant to be only a word of caution, not an invitation to dismiss all of Table 5-8; the next section gives quantitative arguments that Pb, and therefore probably other nearly-free electron metals, can be very well described with a separable approximation to the anisotropy.

Since there are relatively few experiments that measure directly the difference between the clean and dirty limits by washing out anisotropy, Table 5-8 shows in addition to those limits the differences between the isotropic superconductor, and the anisotropic one with μ^* increased to bring T_{ca} down to T_{ci}. This adjustment to μ^* has no physical meaning, but it does help to answer the important question: For a given T_c, are the other properties consistent with a certain amount of anisotropy or not? The change in μ^* is simply $(T_{ca}-T_{ci})/(\partial T_c/\partial \mu^*)$, and it is used together with $\partial H_c/\partial \mu^*$, or $\partial D(t)/\partial \mu^*$

to get the H_c and D(t) consistent with the observed T_c and the model anisotropy. Because $H_c^{-1}\partial H_c/\partial\langle a_{\underline{k}}^2\rangle$ may differ by about 50% from $T_c^{-1}\partial T_c/\partial\langle a_{\underline{k}}^2\rangle$ while $H_c^{-1}\partial H_c/\partial\mu^*$ and $T_c^{-1}\partial T_c/\partial\mu^*$ are of comparable size, this increase in μ^* does not cancel out the effect of anisotropy in H_c, or to be more exact, it overcompensates for the increase in H_c due to anisotropy by bringing H_c below its isotropic value. This kind of overcompensation occurs throughout the table, suggesting that an anisotropic superconductor will have a larger ratio $\gamma(k_BT_c)^2/H_c^2$ than the corresponding isotropic system. Unfortunately γ is too uncertain for such a comparison to be carried out with the existing experimental data. With other measurable quantities than $H_c(0)$ the derivative with respect to μ^* is more uncertain or unknown, and it would not be possible to make any estimate were it not for the fact that in ΔC_v and D(t), μ^* and anisotropy work together to pull both quantities down in contrast to the situation with H_c. Knowing $\partial D(t)/\partial\mu^*$ for two Nb systems with λ = .98 and .33, as well as for Pb (λ = 1.62) systems which span the whole range of coupling strengths, one can at least get inequalities for these elements where $\partial\Delta C_v(T_c)/\partial\mu^*$ and $\partial D(t)/\partial\mu^*$ is unknown. In Nb, the effect of this increase in μ^* can be estimated for all the thermodynamic properties because direct calculations were done earlier with the same isotropic $\alpha^2F(\omega)$ but two slightly different μ^*.

Comparison of Tables 5-8 and 5-4 shows that after μ^* is adjusted, the D(t) are now in much better agreement with

experiment, while the specific heat jumps are still rather small*, but within experimental uncertainty when the previously explained underestimate in $\Delta C_v(T_c)$ is taken into account. The absolute magnitudes of $\Delta C_v(T_c)$ and H_c have also fallen a little below experiment, but that can be explained by assuming the γ used in the calculation was too small.

It is worth comparing the numerically calculated R_0^2 with those that are deduced from the calculated T_c, H_c and $\Delta C_v(T_c)$ using Clem's and Markowitz and Kadanoff's formulas. For the critical field Clem finds

$$(H_{ca}/H_{ci})^2 = (1 + \langle R_c^2 \rangle) \qquad (5\text{-}7)$$

and for the difference in the specific heat jump

$$\Delta\left(\frac{C_{es}}{\gamma k_B T_c}\right) = -5.70\langle R_c^2 \rangle \qquad (5\text{-}8)$$

where $\langle R_c^2 \rangle$ is his estimate of the gap anisotropy, which in his theory is identical to the anisotropy in $\lambda_{\underline{k}}(0)$. Table 5-9 shows the true value R_0^2 and the R_c^2 deduced by applying eqns. (5-7), (5-8), (3-50(a)) and (3-48(b)) to the numerical results. The estimates based on T_c are reasonable, but those obtained from H_c are too large by a factor of 4 or 5, while those from specific heat jump are out by only 50 or 100%. It is no wonder that the analyses of different experiments with the same superconductor have led to contradictory values for the gap

---

*Since the results for Pb in Table 5-8 were obtained from the calculated $\alpha^2F(\omega)$, not from the tunneling $\alpha^2F(\omega)$ as in Table 5-4, that specific heat jump is certain to be too small. However, the difference between the isotropic and anisotropic specific heat jumps should be correctly estimated in Table 5-8.

Table 5-9

Contradictory estimates of the gap anisotropy

The first two rows are the anisotropy in $\lambda_{\underline{k}}(0)$ and $\tilde{\Delta}_{\underline{k}}$ respectively. Entries in brackets refer to calculations done with $\tilde{\omega}_{\underline{k}}$ replaced by $\langle\tilde{\omega}_{\underline{k}}\rangle$.

	Hg	Nb	Pb	Sn	Tl	Al	Al ($\mu^*=0$)
$\langle a_{\underline{k}}^2\rangle$	.04	.04	.02	.04	.04	.04	.04
R_0^2	.014 (.049)	.023	.0062	.031	.029	.052 (.075)	(.038)
Estimates of R_0^2 based on equations (5-7), (5-8), (3-50(a)), (3-48(b))							
$\frac{N(0)V(T_{ca}-T_{ci})}{T_{ci}}$	.012 (.044)	.016	.0055	.024	.024	.056 (.087)	(.039)
$-\frac{8}{\pi^2} R_0^2 \frac{\partial T}{\partial \rho}$	.0089 (.031)	.019	.0035	.035	.028	.080 (.11)	(.046)
$\frac{2(H_{ca}-H_{ci})}{H_{ci}}$	.048	.086	.021	.15	.13		
$-\Delta(\frac{C_{es}}{\gamma k_B T_c})/5.70$	.017	.013	.0072	.019	.019		

anisotropy. Just where the error lies in Clem's analysis, or why some estimates of the gap anisotropy are better than others is not clear at the moment. His other predictions of anisotropy effects in nonequilibrium processes should therefore also be used with caution.

6. Fermi Surface Harmonics and Anisotropy in Pb

In this section the suitability of the FSH for describing quantities defined at the Fermi surface of Pb is demonstrated and results are presented for the changes in the thermodynamic properties when a realistic calculated anisotropy in the electron phonon interaction is added. There is less connection between the two sets of results than the preceding chapters would seem to suggest, for it turns out that a very simple separable model for the anisotropy describes Pb nearly as well as the complicated first-principles calculation. That does not however detract from the usefulness of the FSH, which do indeed give rather good expansions for the $\lambda_{\underline{k}}(0)$. But to appreciate that result requires a more detailed description of the Fermi surface and the calculated anisotropic interaction.

The electron-phonon interaction, given by eqn. (2-3), is completely specified when the Fermi surface, pseudopotentials, and phonons are known. The phonon frequencies and polarization vectors were obtained from the force constants fitted by Cowley[23] to neutron scattering data. The pseudopotential form factor for the host atoms was taken from the work of Appapillai and Williams[12], and that for the impurity from

the work of Shaw[71] through a local rescreening procedure described by Sorbello[103]. The Fermi surface geometry is given by the pseudopotential model of Anderson and Gold[9] which was fitted to de Haas-van Alphen data. This model also yields the Fermi velocities and the plane-wave mixing coefficients for the electronic wave functions in the four plane-wave approximation. All the imput to this calculation of the interaction is identical to that used previously by Tomlinson and Carbotte[73] to calculate the gap edge at T=0 on the real axis. This allows a very important comparison with the gap on the imaginary axis to be made at the end of the section.

Once the Fermi surface, pseudopotentials and phonons are specified, there are no more adjustable parameters and there is nothing left to do but calculate. The labelling of the disjoint pieces of Fermi surface on the irreducible 48th is shown schematically in Fig. III-1 and the actual Fermi velocities in Fig. 5-20. Near the intersection of the Fermi surface with the Brillouin zone there is considerable distortion, but in the middle of the larger pieces there are relatively large free electron-like areas with the result that the band mass is only 10% less than the free electron value. The Fermi wave vector shows much less variation, changing by about .4 percent over the Fermi surface; it is $\underline{v}_{\underline{k}}$ which causes the weights $dS_{\underline{k}}/|v_{\underline{k}}|$ to increase sharply near the intersection of the Fermi surface with the Brillouin zone. The picture to retain is that of a sphere intersected with narrow bands where no Fermi surface exists.

Table 5-10

Description of the anisotropy of the realistic interaction

Single < > refer to averages within a given region, double << >> to a full Fermi surface average. Quantities at far right in brackets indicate averages obtained by ignoring the anisotropy within the regions.

$\tilde{\lambda}_{\underline{k}}$ ($\tilde{A}_{\underline{k}}$) is the difference between $\lambda_{\underline{k}}(0)$ ($A_{\underline{k}}$) and its expansion in FSH.

Regions	1	2	3	4	Entire Fermi Surface	
Weights	.508	.329	.135	.028	1.0	
$\langle\lambda_{\underline{k}}(0)\rangle$	1.44	1.09	1.53	1.08	1.33	
$\langle A_{\underline{k}}\rangle$	4.15	2.89	4.44	2.83	3.74	
$\langle\lambda_{\underline{k}}(0)\rangle/\langle\langle\lambda_{\underline{k}}(0)\rangle\rangle$	1.09	.82	1.16	.81	1.0	
$\langle A_{\underline{k}}\rangle/\langle\langle A_{\underline{k}}\rangle\rangle$	1.11	.77	1.19	.76	1.0	
$\langle\lambda_{\underline{k}}(0)^2\rangle/\langle\lambda_{\underline{k}}(0)\rangle^2-1$	.0052	.0018	.0022	.0006	.023	(.019)
$\langle A_{\underline{k}}^2\rangle/\langle A_{\underline{k}}\rangle^2-1$	.0035	.0073	.0011	.0014	.034	(.030)
$\langle\tilde{\lambda}_{\underline{k}}^2(0)/\langle\lambda_{\underline{k}}^2(0)\rangle^2-1$	.0001	.0002	.0005	.00003	.0002	(0.)
$\langle\tilde{A}_{\underline{k}}^2/\langle A_{\underline{k}}^2\rangle-1$	.00004	.0007	.0002	.00004	.0001	(0.)
$\langle\Delta_{\underline{k}}\rangle/\langle\langle\Delta_{\underline{k}}\rangle\rangle^{(a)}$	1.059	.878	1.100	.877	1.0	
$\langle\Delta_{\underline{k}}\rangle/\langle\langle\Delta_{\underline{k}}\rangle\rangle^{(b)}$	1.060	.878	1.103	.862	1.0	
$\langle\Delta_{\underline{k}}\rangle/\langle\langle\Delta_{\underline{k}}\rangle\rangle^{(c)}$	1.069	.862	1.106	.845	1.0	
$\langle\Delta_{\underline{k}}^2\rangle/\langle\Delta_{\underline{k}}\rangle^2-1^{(a)}$					.0084	(.0084)
$\langle\Delta_{\underline{k}}^2\rangle/\langle\Delta_{\underline{k}}\rangle^2-1^{(b)}$	.0013	.0011	.0001	.0011	.0098	(.0088)
$\langle\Delta_{\underline{k}}^2\rangle/\langle\Delta_{\underline{k}}\rangle^2{}_{01}{}^{(c)}$					.0109	(.0109)
$\langle\tau_{\underline{k}}^{-1}\rangle/\tau^{-1}$ (Mg)	.87	1.3	.66	1.6		
$\langle\tau_{\underline{k}}^{-1}\rangle/\tau^{-1}$ (Sn)	.98	1.03	1.05	.86		

(continued next page)

Table 5-10 (continued)

(a) $\Delta_{\underline{k}}$ is $\bar{\Delta}_{\underline{k}}(1)$ obtained from a calculation on the imaginary axis with a kernel expanded in the 4 zeroth-order FSH.

(b) $\Delta_{\underline{k}}$ is the gap edge on the real axis at T=0 calculated by Tomlinson and Carbotte.

(c) $\Delta_{\underline{k}}$ is $\bar{\Delta}_{\underline{k}}(1)$ obtained on the imaginary axis from a separable approximation to the kernel based on the mean values of $A_{\underline{k}}$ in the four regions.

For the purpose of calculation the entire Fermi surface was covered with a fine 2×2 degree mesh (the $\underline{k}'$ mesh), and a coarser grid of 31 representative points covered the forty-eighth (the $\underline{k}$ mesh). The latter are the points where $(\alpha^2F(\omega))_{\underline{k}}$ was calculated by summing $(\alpha^2F(\omega))_{\underline{k}\underline{k}'}$ over the $\underline{k}'$ points. The results are shown in Fig. 5-21 for three directions, which make it look as if the frequency-dependence of the anisotropy is very important, since different frequency bins in $(\alpha^2F(\omega))_{\underline{k}}$ appear to be quite different functions of direction. The moments of $(\alpha^2F(\omega))$, $\lambda_{\underline{k}}(0)$ and $A_{\underline{k}}$ tell a different story. The $\lambda_{\underline{k}}(0)$ shown in Fig. 5-22 are smooth functions of θ and ϕ that correlate quite well with the weights $dS_{\underline{k}}/|v_{\underline{k}}|$ (which can be inferred from Fig. 5-20). A similar plot of the $A_{\underline{k}}$ would look identical, although Table 5-10 shows that there are differences in shape that must be attributed to frequency dependence of the anisotropy. In particular, $A_{\underline{k}}$ is slightly more anisotropic than $\lambda_{\underline{k}}(0)$ which suggests that there is more anisotropy at the higher frequencies. Table 5-10 also shows that most of the anisotropy arises from the considerable differences between the mean values of $\lambda_{\underline{k}}(0)$ and $A_{\underline{k}}$ on the four regions of the forty-eighth. Although there may be some distortion near the boundaries of the regions, the badly distorted pieces of Fermi surface carry relatively little weight. It follows that most of the anisotropy could be taken care of by expanding $\lambda_{\underline{k}}(0)$ with only the four zeroth-order FSH, which are just constants

on the four regions. Still, it is interesting to see how well they can be fitted to the remaining anisotropy within each region. The 26 FSH used were numbers 111, 122, 212, 221, 222, 223, 224, 233, 235, 236, 311, 321, 322, 331, 332, 411, 421, 423, 423 and 432, and of course the four constants (see Table III-4). The number of FSH per region is far from proportional to the weight per region, because the smallest regions are naturally the most distorted. This uncomfortable situation does not quite explain the poor performance shown in Table 5-10 for region 3, say, where the difference between $\lambda_{\underline{k}}(0)$ and the expansion in FSH is actually one-quarter of the anisotropy in $\lambda_{\underline{k}}(0)$ itself. Figure 5-23 gives a more informative picture of the behaviour of the FSH expansions. Along arcs of constant θ, along which $\lambda_{\underline{k}}(0)$ is nearly constant, the fit is not so good, but along arcs of constant ϕ, where most of the anisotropy within a given region occurs, the agreement is excellent, especially at the edges of the regions, where the use of $\underline{v}_{\underline{k}}$ rather than trigonometric function of θ and ϕ as arguments for the polynomials was expected to be most successful. At the lower boundary of region 3, where it intersects not the Brillouin zone but a reflection plane, there is a noticeable failure of the FSH. Closer examination of the function being fitted showed that it was not satisfying cubic symmetry everywhere on the boundaries of the forth-eighth, as Fig. 5-23 shows; it does not have zero slope at $\theta = 54°$. Therefore the FSH

could not possibly give a good fit, because cubic symmetry is built into them. (This deficiency in $\lambda_{\underline{k}}(0)$ was caused by the interpolation used to get a smooth test function from the values at the 31 $\underline{k}$-points. This problem is irrelevant to all the other calculations described here.) Such considerations suggest that the FSH will actually fit quantities defined on the Fermi surface better than Table 5-10 indicates.

To get the changes in the thermodynamics caused by anisotropy, a comparison must be made between calculations with and without anisotropy. The isotropic $\alpha^2F(\omega)$ in this section is therefore not the tunneling $\alpha^2F(\omega)$ of section 4 but the average of the calculated $(\alpha^2F(\omega))_{\underline{k}}$, a slightly different function. Figure 5-24 shows that the two $\alpha^2F(\omega)$ are quite close, but that the calculated $\alpha^2F(\omega)$ is a little smaller than the tunneling result: $\lambda(0) = 1.33$ and $A = 3.8$ versus 1.62 and 4.0 respectively. Therefore the quantities calculated from it will be too weak-coupling to compare with experiment. The difference from the tunneling result is however small enough to give confidence in the estimate of the anisotropy in the interaction. It is also small enough that the changes in the thermodynamic properties due to anisotropy can simply be added onto the previously calculated values from the isotropic tunneling $\alpha^2F(\omega)$ to get numbers that can actually be compared with experiment.

As mentioned earlier, the four zeroth-order FSH account for most of the anisotropy in $\lambda_{\underline{k}}(0)$ and $A_{\underline{k}}$, and therefore probably in the gap also. Column (a) of Table 5-11 shows

Table 5-11

Effects of various realistic anisotropies on the thermodynamic properties of Pb

	(a)	(b)	(c)	(d)	(e)	(f)	(g)
$(T_{ca}-T_{ci})/T_{ci}$	.026	.025	.017	.025	.015	.014	.03
$(H_{ca}-H_{ci})/H_{ci}$	.021	.020	.013	.018	.011	.011	.025
$D_a(.7)-D_i(.7)$	-.0021	-.0021	-.0014	-.0023	-.0015	-.0015	-.0025
$\Delta(C_{es}/\gamma T_c)$	-.057*	-.055*	-.038*	-.074*	-.043	-.041	.07*
$\langle a_{\underline{k}}^2 \rangle$	—— not defined——			.029	.019	.018	not defined
R_0^2	.0084	.0081	.0056	.0109	.0063	.0062	.0098
R_E^2 (Sn or Mg)	.008	.008		.0109	.0063	.0062	.013(est.)

(a) Calculation with no approximations except the truncation of the FSH after the first four, ie. the anisotropy is frequency-dependent and not separable. ω_c = 63 meV and μ^* = .10

(b) Same as (a) except that ω_c = 110 meV.

(c) Same as (a) except that μ^* = 0

(d) $(\alpha^2F(\omega))_{\underline{k}\underline{k}'}$ is approximated by $(1+a_{\underline{k}})(1+a_{\underline{k}'})\alpha^2F(\omega)$, where $1+a_{\underline{k}}$ is determined by the mean values of $A_{\underline{k}}$ on the four pieces of the Fermi surface. ω_c = 63 meV and μ^* = .10.

(e) The interaction is approximated as in (d), except that $1+a_{\underline{k}}$ is determined by the mean values of $\lambda_{\underline{k}}$.

(f) Same as (e), but now regions 2 and 4, also 1 and 3 have been combined, so that $a_{\underline{k}}$ takes on two values instead of 4.

(g) Estimate of the anisotropy effects when the anisotropy within each of the four regions is included, based on the assumption that R_0^2 is the same as the value found by Tomlinson[62], and that anisotropy effects are linear in R_0^2 with a proportionality constant obtained from column (a).

*Obtained from columns (e) and (f) on the assumption that the change in $C_{es}/\gamma\, k_B T_c$ is proportional to R_0^2.

the gap anisotropy R_0^2 obtained from these four FSH with the rather small changes caused by anisotropy in T_c, H_c and D(t). The next two columns show that anisotropy effects in Pb, as one would expect from Table 5-2, are not at all sensitive to μ^* and ω_c. Columns (d) and (e) show something much more interesting: a separable model anisotropy with $a_{\underline{k}}$ based on the mean values of $A_{\underline{k}}$ in the four regions when added onto the isotropic calculated $\alpha^2F(\omega)$ gives the same changes in T_c, H_c and D(t) as in column (a), where no approximations are made, to within 15%, while R_0^2 is larger than the exact solution by some 25%. A separable model based on $\lambda_{\underline{k}}(0)$ (column (e)) underestimates the anisotropy effects, since $\lambda_{\underline{k}}(0)$ corresponds to an $\langle a_{\underline{k}}^2 \rangle$ some 33% smaller than that for $A_{\underline{k}}$. In view of previous remarks about the importance of A rather than $\lambda(0)$ in strong-coupling superconductors, this is hardly surprising. After all, when ω_n is of the same order as ω_0, the maximum phonon frequency, the $\lambda_{\underline{k}}(n)$ in eqn. (2-17) will be closer to the first or zeroth moment of $\alpha^2F(\omega)$ than to $\lambda_{\underline{k}}(0)$. Perhaps the opposite behaviour will be seen in weaker coupling systems. It is rather curious that the greatest difference between the exact solution and the separable model based on $A_{\underline{k}}$ is in the prediction of the critical field; that quantity may of course be sensitive to certain details of the anisotropy that would be smeared out by the thermal phonons at higher temperatures. But the discrepancy may also be related to the same problem that caused Clem's estimate of anisotropy effects in H_c to be so inaccurate. One further simplification remains to be discussed.

Table 5-10 and the P(a) for $\lambda_{\underline{k}}(0)$ in Fig. 5-25 show that the regions 1 and 3, also 2 and 4 have regional averages for $\lambda_{\underline{k}}(0)$ so similar that they could be merged from four into two regions. Then $a_{\underline{k}}$ would take on only two values instead of four. Since column (f) of Table 5-11 demonstrates that calculations with this approximation differ by a negligible amount from column (e), the 4-region calculation based on $\lambda_{\underline{k}}(0)$, it seems reasonable to assume that the same would be true if the $A_{\underline{k}}$ were also merged. Therefore an almost trivial model anisotropy suffices to describe the effects of the complicated, non-separable and frequency-dependent realistic interaction. The last two pages in chapter 4 suggest how to verify whether this situation arises because the interaction is truly separable. Table 5-12 compares the actual interactions between the four regions with the values obtained by assuming the interaction is separable with an $a_{\underline{k}}$ based on $\lambda_{\underline{k}}(0)$ or $A_{\underline{k}}$. In other words it compares $\lambda_{\underline{kk}'}(0)$ with $\lambda_{\underline{k}}(0)\lambda_{\underline{k}'}(0)/\lambda(0)$. The difference is seen to be remarkably small, smaller than the difference between the regions even, except for interactions between region 1 and the other regions. The product of the weights $W_i W_j$, which indicates roughly the contribution of the interaction between regions i and j to the average interaction, is however very small where the deviation from separability is largest.

Table 5-12 also shows how good the approximation of the impurity pseudopotential by a constant really is for a Z=2 impurity (Mg) and a Z=4 impurity (Sn). The isovalent im-

Table 5-12

Separability of the calculated interaction for Pb, and validity of the impurity s-wave approximation

Regions i	Regions j	W_iW_j	A_{ij} Exact	A_{ij} Separable	λ_{ij} Exact	λ_{ij} Separable	$\tau_{ij}^{-1}/\langle\langle\tau_{ij}^{-1}\rangle\rangle$ Mg	$\tau_{ij}^{-1}/\langle\langle\tau_{ij}^{-1}\rangle\rangle$ Sn
1	1	.001	.78	.43	.35	.83	2.7	1.8
1	2	.014	3.47	3.07	1.25	1.15	1.3	.8
1	3	.009	1.40	2.13	1.40	.88	.39	.9
1	4	.004	4.15	3.31	1.30	1.22	1.3	.8
2	2	.258	4.50	4.61	1.51	1.57	.81	1.0
2	3	.167	3.42	3.19	1.28	1.17	1.00	.9
2	4	.069	4.75	4.96	1.60	1.68	.63	1.0
3	3	.108	1.83	2.20	.727	.88	1.9	1.2
3	4	.044	3.83	3.42	1.35	1.25	.7	1.0
4	4	.018	4.97	5.32	1.73	1.79	.5	1.1

$$A_{ij}\ (\text{exact}) = \int_i \frac{dS_{\underline{k}}}{|v_{\underline{k}}|} \int_j \frac{dS_{\underline{k}'}}{|v_{\underline{k}'}|} \sum_R \int d\omega\, (\alpha^2 F(\omega))_{\underline{k}R\underline{k}'} / W_i W_j$$

$$A_i = \Sigma W_j A_{ij}$$

$$A_{ij}\ (\text{separable}) = A_i A_j / A$$

$$W_i = \int_i \frac{dS_{\underline{k}}}{|v_{\underline{k}}|}\ , \text{ normalized so that } \sum_{i=1}^{4} W_i = 1$$

λ_{ij} and τ_{ij}^{-1} are defined analogously

purity, Sn, has both a longer lifetime (τ^{-1} is .2 eV versus 17 for Mg) and less anisotropy in $\tau_{\underline{k}}^{-1}$ than does Mg. This is to be expected from the difference between the two $\Delta W(\underline{q})$. For Mg, the pseudopotential is largest at $\underline{q} = 0$, so that

$$\int \frac{dS_{\underline{k}'}}{|v_{\underline{k}'}|} |\Delta W(\underline{k}-\underline{k}')|^2$$

reflects mainly the relative size of $dS_{\underline{k}'}/|v_{\underline{k}'}|$ for $\underline{k}'$ very close to $\underline{k}$, in other words $\underline{k}'$ from the same region as $\underline{k}$, and very little Fermi surface averaging is being done. For Sn in Pb the pseudopotential vanishes at $\underline{q} = 0$ and has a minimum around $q = 2k_F$, so that the integrand will sample $\underline{k}'$ states from regions of all four types with the result that $\tau_{\underline{k}}^{-1}$ is very nearly independent of $\underline{k}$ as shown in Table 5-10. Table 5-11 gives however a single value of R_E^2 which is appropriate for both impurities, even though the preceding considerations suggest that the approximation $R_0^2 \sim R_E^2$ should be very bad for Mg. Since Table 5-10 demonstrates that $\tau_{\underline{k}}^{-1}$ is negatively correlated with $\bar{\Delta}_{\underline{k}}(1)$ for Mg, in contrast to Sn, the identical values of R_E^2 may therefore be dismissed as coincidence.

The argument put forth earlier in Chapter 3 that R_E^2 should be close to R_0^2 because the gap repeats itself over 48 regions each much smaller than the distance over which $|\Delta W(\underline{q})|^2$ changes, appears to hold, at least for isovalent impurities. A similar idea may explain the separability of the kernel, with $|g_{\underline{k}\underline{k}',\lambda}|^2$ playing the same role as $|\Delta W(\underline{q})|^2$. Of course this matrix element is not a smooth and slowly varying

function of $\underline{k}$ and $\underline{k}'$, but considerable averaging is being done, because the quantities in Table 5-12 are not the interaction between two particular pieces i and j but the interaction between all the symmetry-related pieces of type i with all the pieces of type j. This is how part of the $\underline{q}$ dependence of the interaction is averaged out. The frequency average also matters; Figure 5-21 shows that $(\alpha^2 F(\omega))_{\underline{k}}$ at any given frequency is not correlated with $\lambda_{\underline{k}}(0)$. These two averages magnify the part of the anisotropic interaction which is frequency-independent and invariant under the application of all the group operations (to $\underline{k}$ and $\underline{k}'$ independently, not to $\underline{q}$). By combining eqns. (2-3) and (2-10) $\lambda_{\underline{k}\underline{k}'}(m)$ can be rewritten as

$$\lambda_{\underline{k}\underline{k}'}(m) \alpha \int d\omega \sum_{RR'\lambda} \left\{ \frac{F(\bar{\underline{q}},\omega)}{\omega_{\bar{\underline{q}}\lambda}^2 + \omega_m^2} \sum_{nn'} \underline{\xi}^{\lambda}(\bar{\underline{q}}) \cdot \bar{\underline{q}} \, \Delta W(\bar{q}) a^*_{R'\underline{\kappa}_{n'}}(R'\underline{k}') a_{R\underline{\kappa}_n}(R\underline{k}) \right\}^2 \tag{5-12}$$

where $\underline{k}$ and $\underline{k}'$ both lie inside the irreducible 48th. If the integration over frequency and the sums over R and R' reduce all the functions of $\bar{\underline{q}} \equiv R(\underline{k}+\underline{\kappa}_n) - R'(\underline{k}'+\underline{\kappa}_{n'})$ to constants independent of the exact positions of $\underline{k}'$ and $\underline{k}$ in the 48th but possibly depending on which regions they lie in, eqn. (5-12) is reduced to a sum of terms that are products of functions of $\underline{k}'$ and $\underline{k}$, arising from the plane wave mixing coefficients $a_{\underline{\kappa}_n}(\underline{k})$, which are invariant under all the group operations R and R'. This is the origin of the separability. Anisotropy in $dS_{\underline{k}}/|v_{\underline{k}}|$ may further enhance or decrease this anisotropy

(since $dS_{\underline{k}}/|v_{\underline{k}}|$ is correlated with the $a_{\kappa_n}(\underline{k})$) but cannot by itself account for the separability, let alone for any anisotropy. If the averaging over group operations reduced $\lambda_{\underline{k}\underline{k}'}(m)$ to a constant, then no amount of anisotropy in $dS_{\underline{k}}/|v_{\underline{k}}|$ would suffice to produce gap anisotropy, as eqn. (2-17) shows quite trivially. Fermi surface anisotropy is however necessary to get a separable kernel, since no one-plane wave function will ever result in a factor of $a^*_{\kappa_n}(\underline{k})a_{\kappa_{n'}}(\underline{k}')$ that does not simply reduce to a constant.

If the interaction averaged within each region turns out to be separable, it seems logical to ask whether even the remaining anisotropy within each region can be deduced from $A_{\underline{k}}$ or $\lambda_{\underline{k}}(0)$. One way to check this would be to actually do the expansion and compare as in eqn. (4-14), but there is an easier indirect way that also ties together anisotropy on the real axis and anisotropy on the imaginary axis.

Tomlinson and Carbotte calculated the gap edge at T=0 in Pb using a method suggested by Bennett[81] which consists of iterating the isotropic Eliashberg equations to convergence. The solution is then put into the right-hand side of the anisotropic gap equations and iterated only once (because of computer time limitations), thus getting an approximate value for the gap at the 31 $\underline{k}$ points. When these values are averaged within each region, these averages divided by the overall average form exactly the same ratio as those calculated on the

imaginary axis at T_c, using the 4 zeroth-order FSH, as shown in Fig. 5-25 and Table 5-10. This establishes that one iteration on the real axis suffices to get the anisotropy correctly (because eqn. (2-15) was iterated to convergence); also that gap anisotropy on the imaginary axis at T_c can meaningfully be compared with anisotropy on the real axis at T=0, as eqn. (3-42) suggests. This last conclusion is very important, since it justifies a previous anisotropy calculation on the imaginary axis[82] and lays a firm foundation for the many to follow.

The fact that one iteration on the real axis gets the coarser features of the anisotropic gap right strongly suggests that the small remaining anisotropy in the gap edge is correct also. Direct comparison with a fully-converged imaginary axis solution at the same 31 $\underline{k}$-points is of course impossible because the arrays such as $\lambda_{\underline{k}\underline{k}'}(m)$ are so large, even at T_c, but the smallness of the remaining anisotropy permits another procedure. Since the coefficient C_μ mentioned in the previous section, which determines the shape of $\tilde{\Delta}_{\underline{k}}(1) = \langle\tilde{\Delta}_{\underline{k}}(1)\rangle(1 + a_{\underline{k}}C_\mu)$ in the separable model, was found to be relatively insensitive to the amount of anisotropy, the same value of 1.19 found for the solution with only the 4 zeroth-order FSH can probably serve if a little more anisotropy is added. Since $\bar{\Delta}_{\underline{k}}(1) = \langle\tilde{\Delta}_{\underline{k}}(1)\rangle(1 + a_{\underline{k}}C_\mu)/(1 + \lambda_{\underline{k}}(0))$, the variation of the gap within each region can be approximated by setting $a_{\underline{k}} = \lambda_{\underline{k}}(0)/\lambda(0)-1$ while letting $\lambda_{\underline{k}}(0)$ take on the values calculated at the 31 $\underline{k}$-points instead of the 4 averaged values. The 31 ratios $\bar{\Delta}_k(1)/\langle\bar{\Delta}_{\underline{k}}(1)\rangle$ obtained this way (column

(a) of Table 5-13) differ by less than 2% from the corresponding ratios on the real axis (column (b) of Table 5-13). In fact, these approximations can be pushed still further without much loss of accuracy. If the C_μ is obtained not from a kernel expanded in the four zeroth-order FSH as before, but from a kernel of the type $(1 + a_{\underline{k}})(1 + a_{\underline{k}'})\alpha^2F(\omega)$, where $1 + a_{\underline{k}}$ takes on the four different values of $A_{\underline{k}}/A$ on the 4 regions, and then this division by $1 + \lambda_{\underline{k}}(0)$ is repeated, the resulting values (column (c) of Table 5-13) for $\dfrac{\bar{\Delta}_{\underline{k}}(1)}{\langle\bar{\Delta}_{\underline{k}}(1)\rangle}$ compare almost as well with the gap edge as those obtained from a supposedly better C_μ. It seems reasonable that this procedure - obtaining an exact solution and C_μ from the imaginary-axis gap equations at T_c with an approximate partly-averaged kernel, and then getting more detail by using the $\lambda_{\underline{k}}(0)$ from the exact kernel - should make it unnecessary to ever attempt a complete solution on the real axis.

Although these results show that the gap anisotropy calculated on the imaginary axis could be compared with the results of tunneling experiments which are concerned with the gap on the real axis, this discussion will be limited to the thermodynamic properties, which give considerable evidence that provided the tunneling $\alpha^2F(\omega)$ is correct, the amount of anisotropy calculated here is not just within the range of uncertainty in the experimental data but brings the calculated quantities into better agreement with experiment than if there were no anisotropy. Table 5-14 shows how the results from the isotropic tunneling $\alpha^2F(\omega)$ are modified when the anisotropy

Table 5-13

Comparison of gap anisotropy obtained from one iteration on the real axis with present work

Region	θ	ϕ	$\frac{dS_{\underline{k}}}{\lvert v_{\underline{k}} \rvert}$	$\lambda_{\underline{k}}(0)$	$\frac{\Delta_{\underline{k}}}{\langle \Delta_{\underline{k}} \rangle}$ (a)	$\frac{\Delta_{\underline{k}}}{\langle \Delta_{\underline{k}} \rangle}$ (b)	$\frac{\Delta_{\underline{k}}}{\langle \Delta_{\underline{k}} \rangle}$ (c)
1	1	1	.0035	1.09	.88	.889	.895
	5	1	.0087	1.03	.85	.844	.86
	3	23	.0087	1.06	.87	.866	.88
	5	45	.0070	1.07	.87	.866	.88
2	15	13	.0328	1.57	1.11	1.121	1.10
	33	19	.0308	1.54	1.10	1.106	1.09
	15	23	.0387	1.59	1.12	1.121	1.11
	23	23	.0545	1.30	.996	1.009	1.00
	33	23	.0434	1.53	1.10	1.083	1.09
	19	29	.0400	1.40	1.04	1.053	1.04
	27	29	.0494	1.31	1.00	1.023	1.00
	33	33	.0509	1.52	1.09	1.098	1.09
	13	35	.0217	1.62	1.13	1.114	1.12
	23	35	.0356	1.31	1.00	1.023	1.00
	27	39	.0318	1.31	1.00	1.023	1.00
	19	41	.0285	1.41	1.05	1.053	1.04
	13	45	.0077	1.62	1.13	1.114	1.12
	27	45	.0140	1.32	1.01	1.030	1.01
	33	45	.0280	1.52	1.09	1.091	1.09
3	45	23	.0668	1.04	.85	.851	.87
	45	31	.0701	1.09	.88	.889	.89
	41	35	.0585	1.03	.85	.844	.86
	45	39	.0783	1.11	.90	.904	.91
	39	45	.0263	1.07	.87	.859	.88
	53	45	.0289	1.15	.92	.934	.93
4	35	1	.0186	1.55	1.10	1.115	1.11
	45	1	.0174	1.46	1.07	1.077	1.06
	39	5	.0469	1.52	1.09	1.110	1.09
	37	9	.0256	1.57	1.11	1.115	1.10
	45	9	.0191	1.59	1.12	1.110	1.11
	35	13	.0078	1.57	1.11	1.115	1.10

these numbers cannot be compared with experiment because T_{ca} goes up to 7.41 K which is far above the measured values, so that the procedure of section 4 has to be used - increasing μ^* to bring T_{ca} down to experiment (column (c), Table 5-14). If this is done then the critical field falls to a more reasonable value, only one percent above experiment, and the calculated D(t) decreases to .022, slightly below the mean (.023) of the experimental data shown in Fig. 5-4 and Table 5-4. Doubling R_0^2 would pull the calculated D(t) down to .019, which is below all three experiments while setting it to zero would bring D(t) up to .025, well above the average but only barely above the highest measured values. Therefore the magnetization data by itself permits only the conclusion that $R_0^2 < .015$, with the most likely value, corresponding to the average of the three measured D(t), being .008, a little less than that calculated here.

The analysis of the specific heat data is unfortunately not so straightforward because of the previously-mentioned systematic error in the calculation of $\Delta C_v(T)$ near T_c and the uncertainty about $\partial \Delta C_v(T_c)/\partial \mu^*$. Figure 5-26 shows the $C_{es}/\gamma k_B T$ calculated from the isotropic tunneling $\alpha^2 F(\omega)$ together with the data from Refs. 6, 74, and 48. Above $t^2 = .5$, the calculated and experimental curves run nearly parallel up to $t^2 \sim .8$ where the calculated curve bends downwards. The same downward turn is present in the calculations with other elements shown in Figure 5-6, but does not become obvious until plotted

together with experimental data. A linear extrapolation of the isotropic calculated $C_{es}(T)/\gamma k_B T$, which is the best that can be done without repeating the calculation, brings the specific heat jump up to 3.82, not very far above both the experiments shown in the plot, but significantly greater than the mean value of 3.66 obtained from Table 5-4. Column (c) of Table 5-14 shows that the calculated anisotropy effects might be enough to bring the calculated jump down to this average value. Because Figure 5-26 is already crowded enough such an adjustment is not plotted there, but the reader can visualize the effect of an R_0^2 of .010 on the specific heat by looking at Figure 5-19, which shows the effect of an R_0^2 of .013 on the specific heat of Hg. This kind of change in $C_{es}/\gamma k_B T_c$ would improve the agreement at all temperatures. Doubling the anisotropy would pull the calculations well below the experimental average but removing anisotropy altogether brings the jump above any experiment. It is unfortunate that the amount of anisotropy in Pb is so small, because the slight overestimate of D(t) and $\Delta C_v(T_c)$ in the isotropic calculation can be attributed just as well to a small overestimate of the tunneling $\alpha^2F(\omega)$. In Nb for example, the addition of anisotropy had almost the same effect on D(t) as a 5% reduction in $\alpha^2F(\omega)$. (See discussion in Section 4.) The conclusion drawn here that $0 < R_0^2 < .015$ is therefore contingent on very high accuracy in the tunneling $\alpha^2F(\omega)$. It is however in accord with estimates from other experiments[83,16] most of which also find that Pb is of the more anisotropic superconductors.

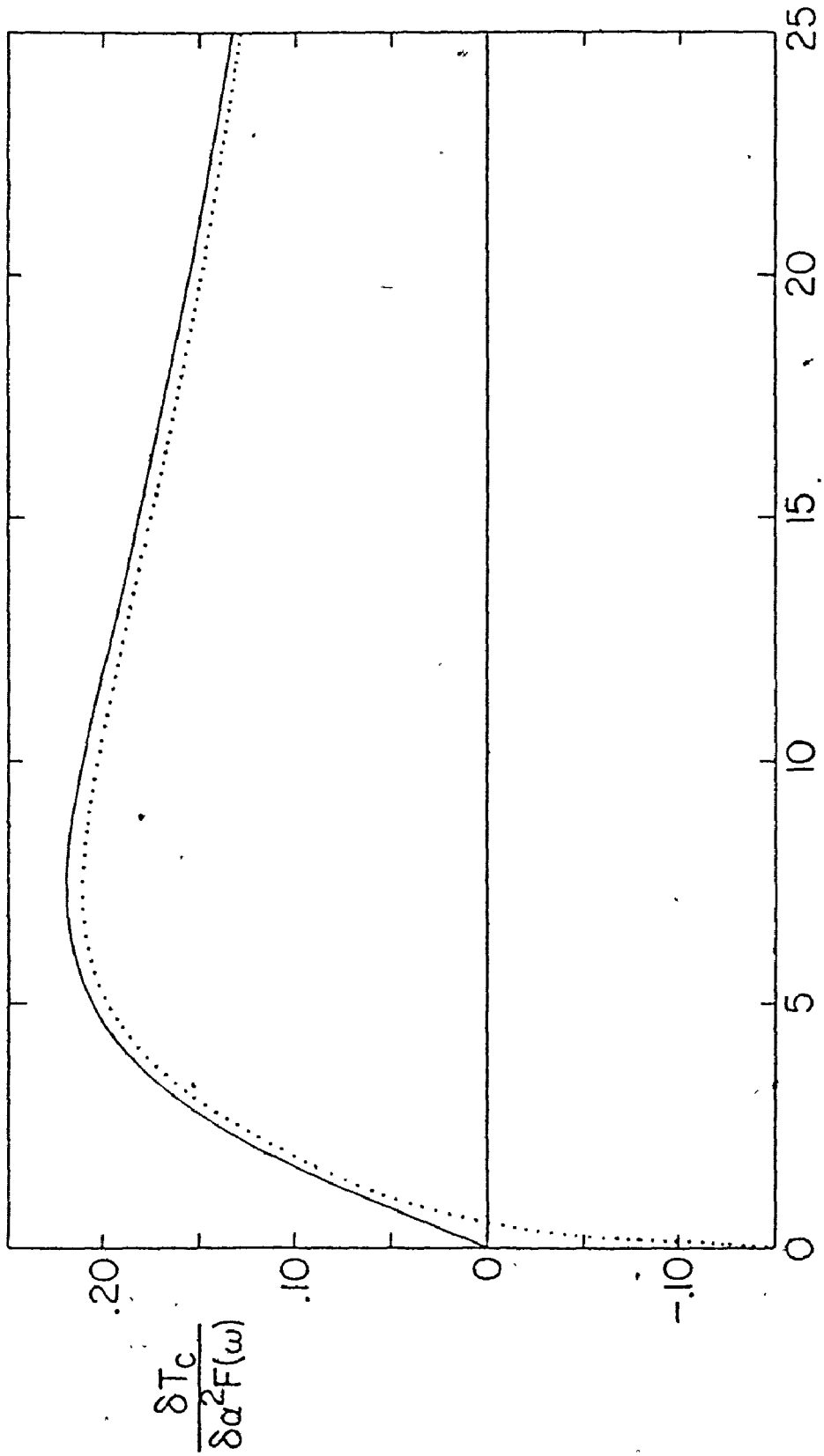

Fig. 5-16 $\delta T_c/\delta \alpha^2 F(\omega)$ for Pb with a realistic anisotropy (------), and no anisotropy (———).

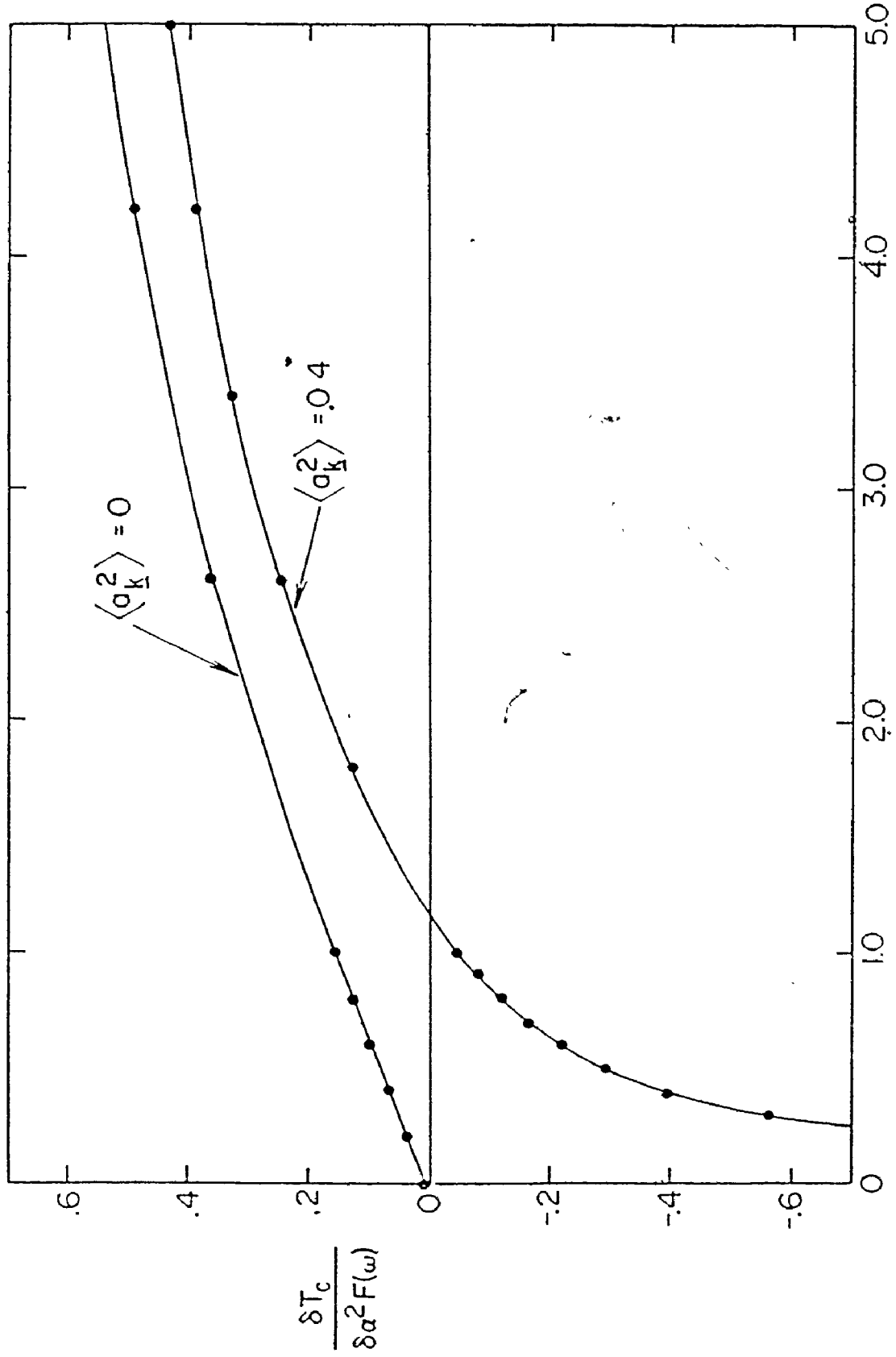

Fig. 5-17 Details at low frequency of $\delta T_c/\delta \alpha^2 F(\omega)$ for Al with a model anisotropy.

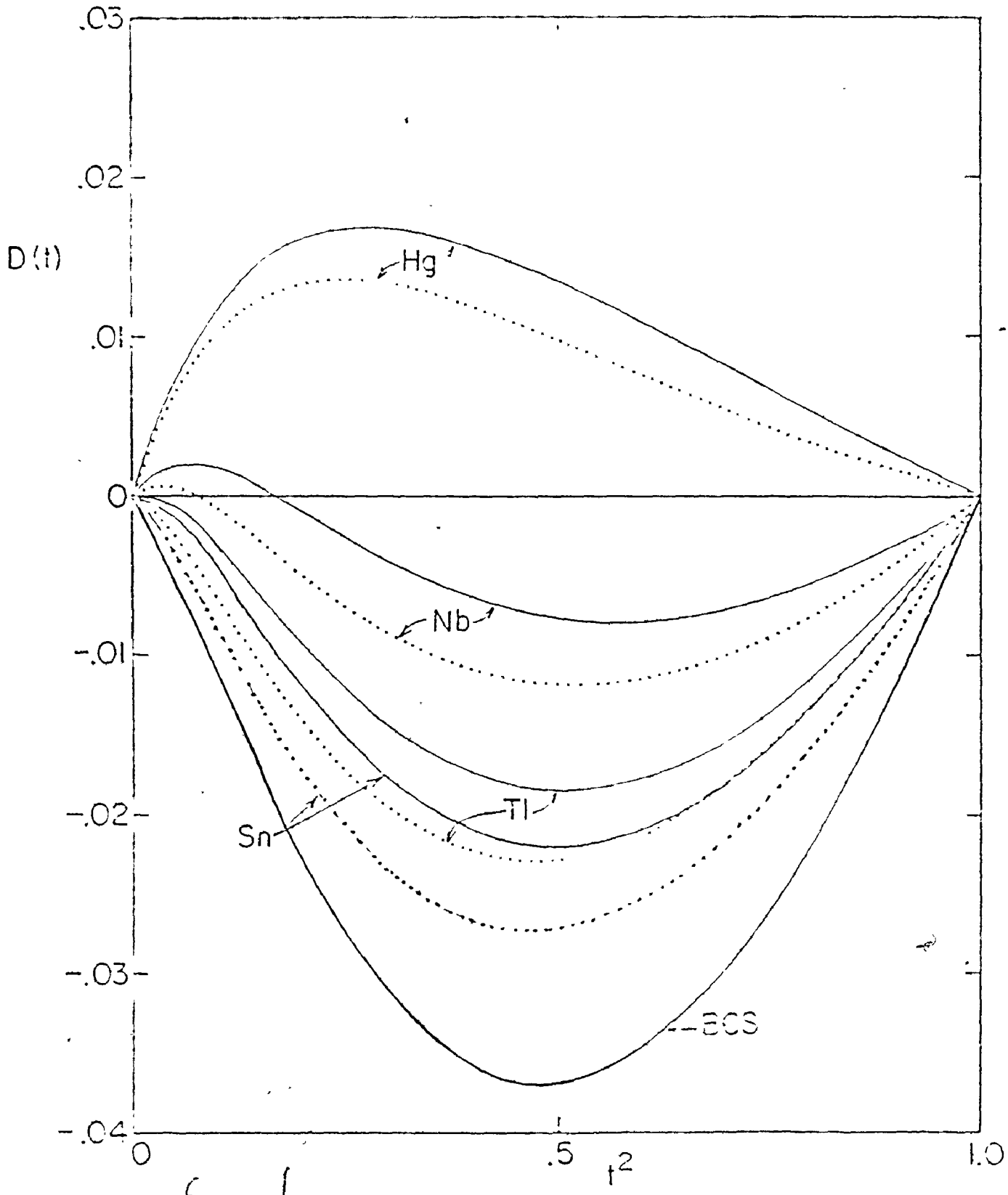

Fig. 5-14 Effect of model anisotropy on D(t) in Hg, Nb, Tl and Sn.

——— isotropic, ····· anisotropic.

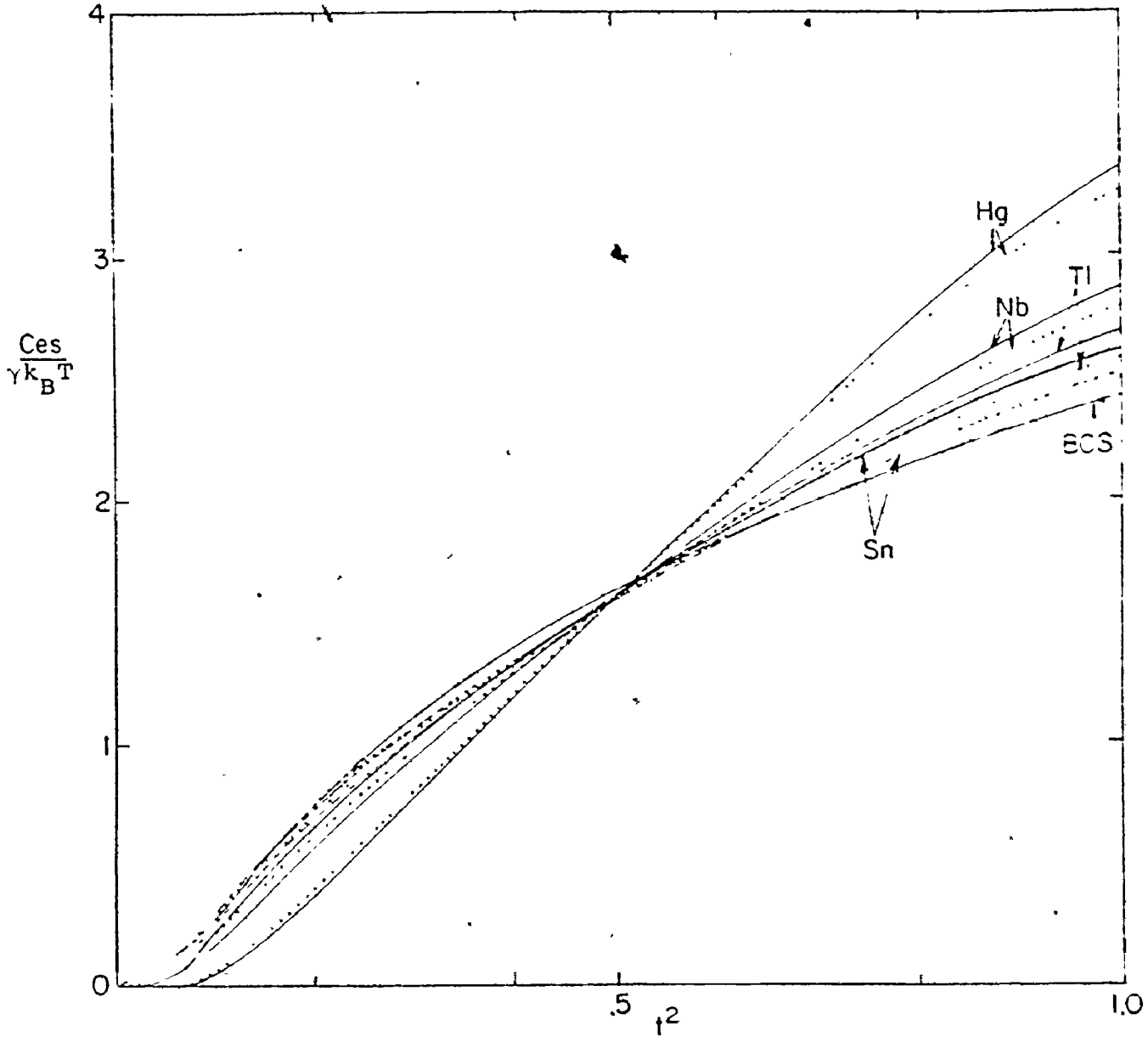

Fig. 5-19 Effect of model anisotropy on $C_{es}/\gamma k_B T$ for Hg, Nb, Tl and Sn.

——— isotropic, ····· anisotropic.

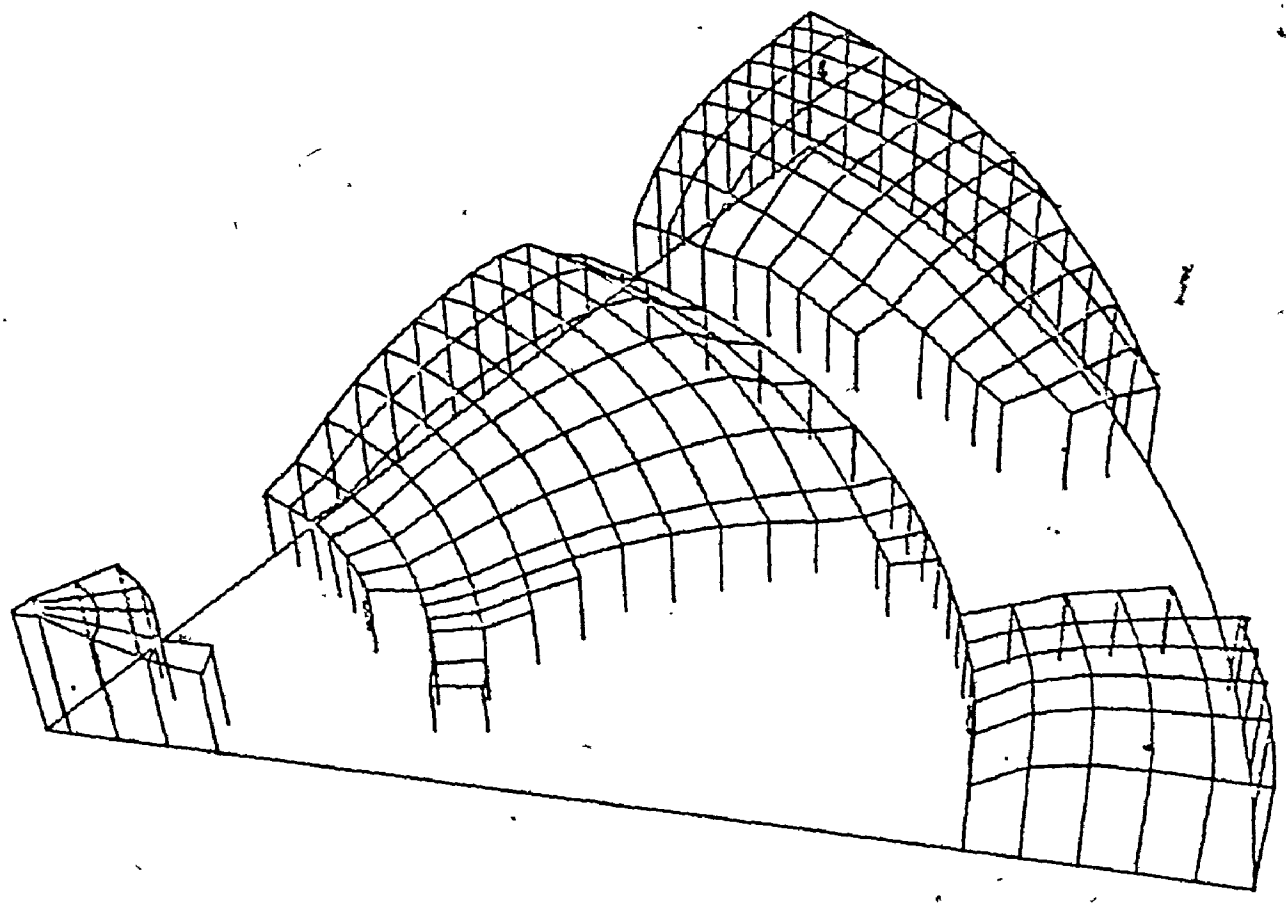

Fig. 5-20 Anistropy in the Fermi velocities on the irreducible 48th.

(001) is at left, (101) at far right.

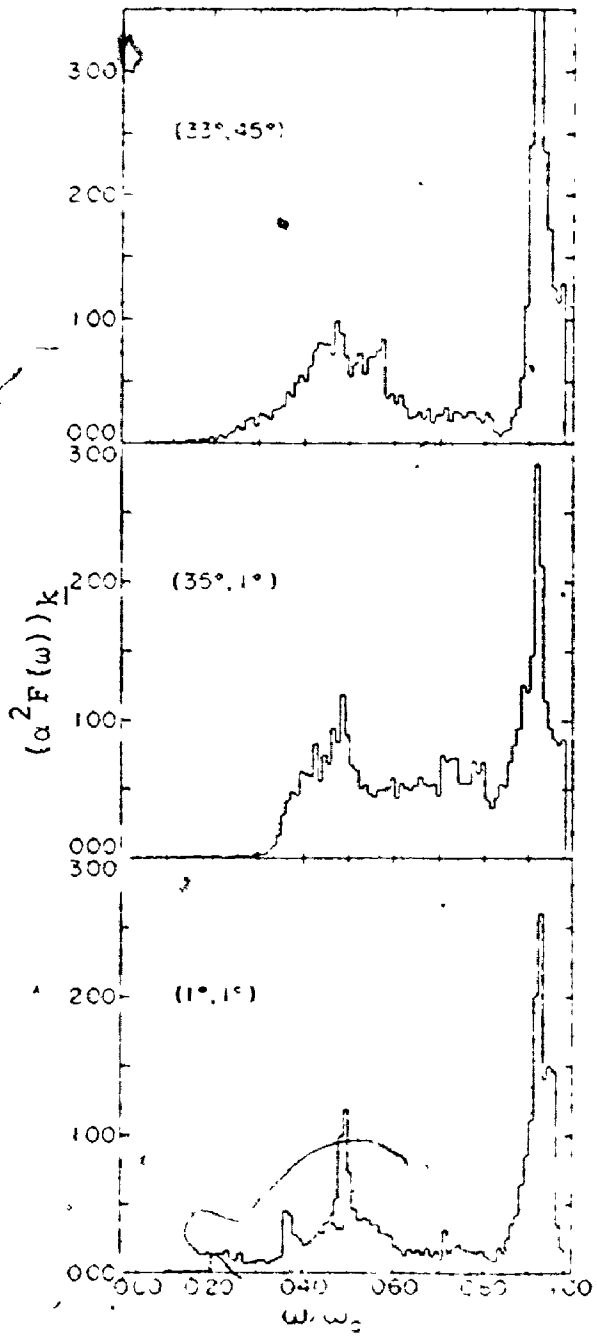

The frequency dependence of the directional spectral weights $\alpha^2 F_{\hat{k}}(\omega)$ for three points on the Pb Fermi surface. The histograms (a), (b), and (c) correspond respectively to $\hat{k}$ in the (1°, 1°), (35°, 1°), and (33°, 45°) direction. Note that the horizontal scale is given as the ratio ω/ω_c with ω_c the maximum phonon frequency in Pb.

Figure 5-21 Directional $\alpha^2F(\omega)$ for Pb. This is taken from Ref. 80.

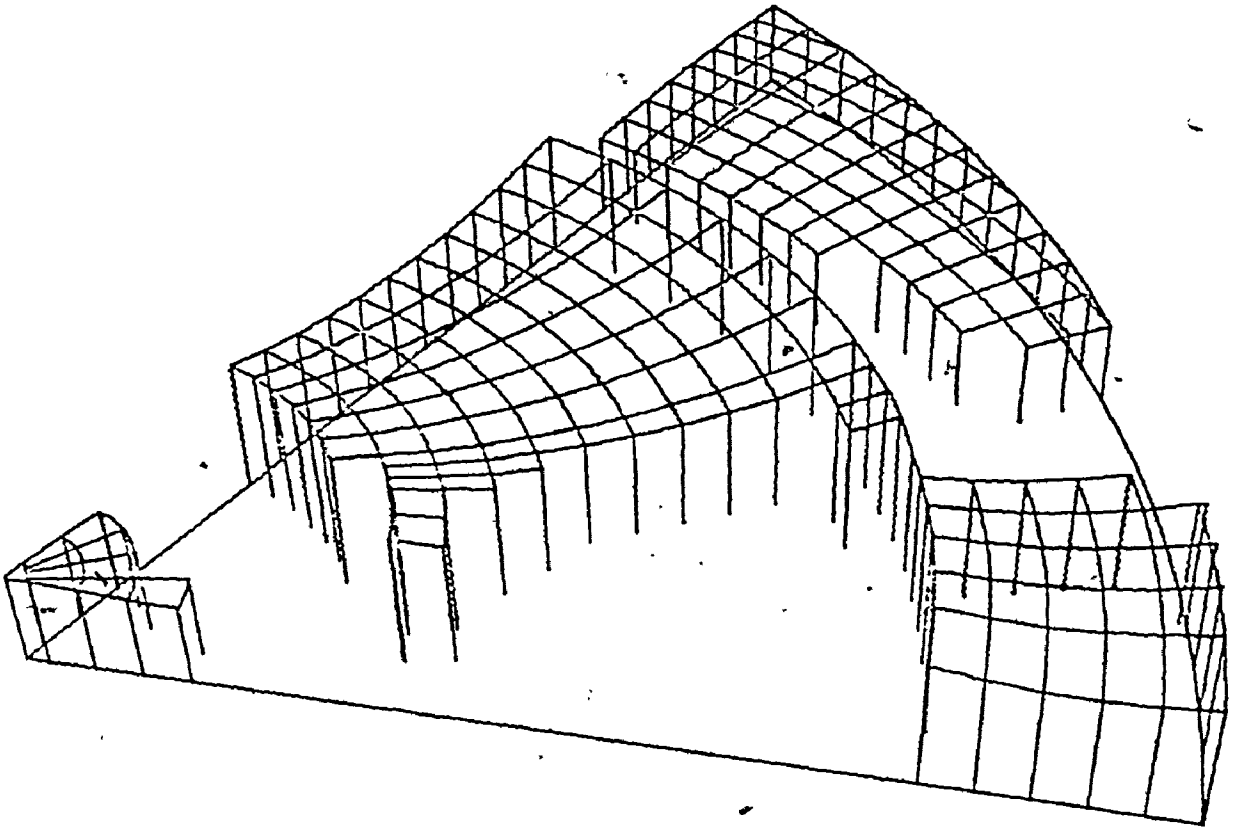

$\lambda_{\underline{k}}(0)$

Fig. 5-22 Anisotropy in $\lambda_{\underline{k}}(0)$ on the irreducible 48th. (001) is at left, (101) at far right

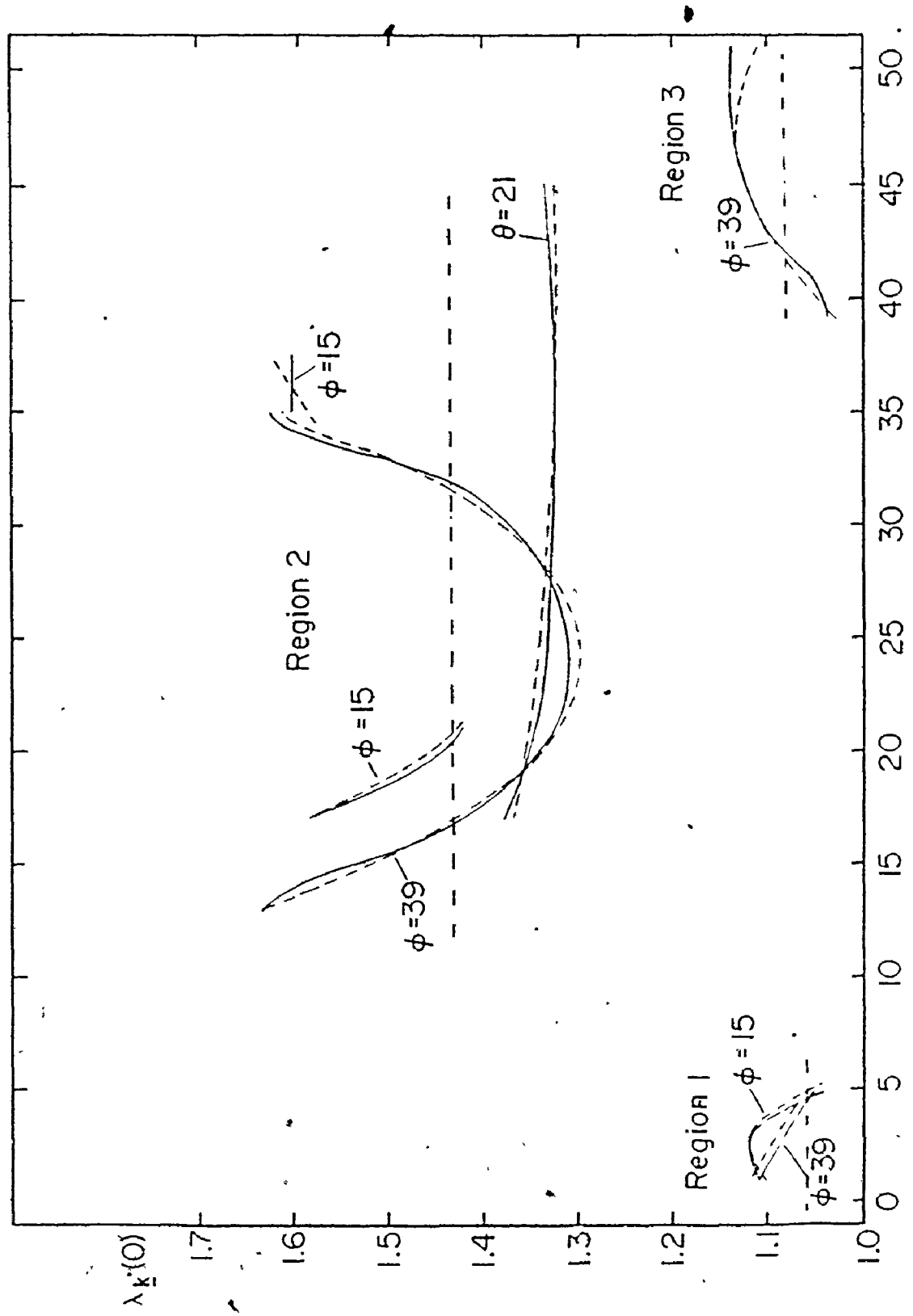

Fig. 5-23 Expansion of $\lambda_{\underline{k}}(0)$ in FSH.

——— Expansion of $\lambda_{\underline{k}}(0)$, ------ original $\lambda_{\underline{k}}(0)$,

-·-·- mean value of $\lambda_{\underline{k}}(0)$ within each region.

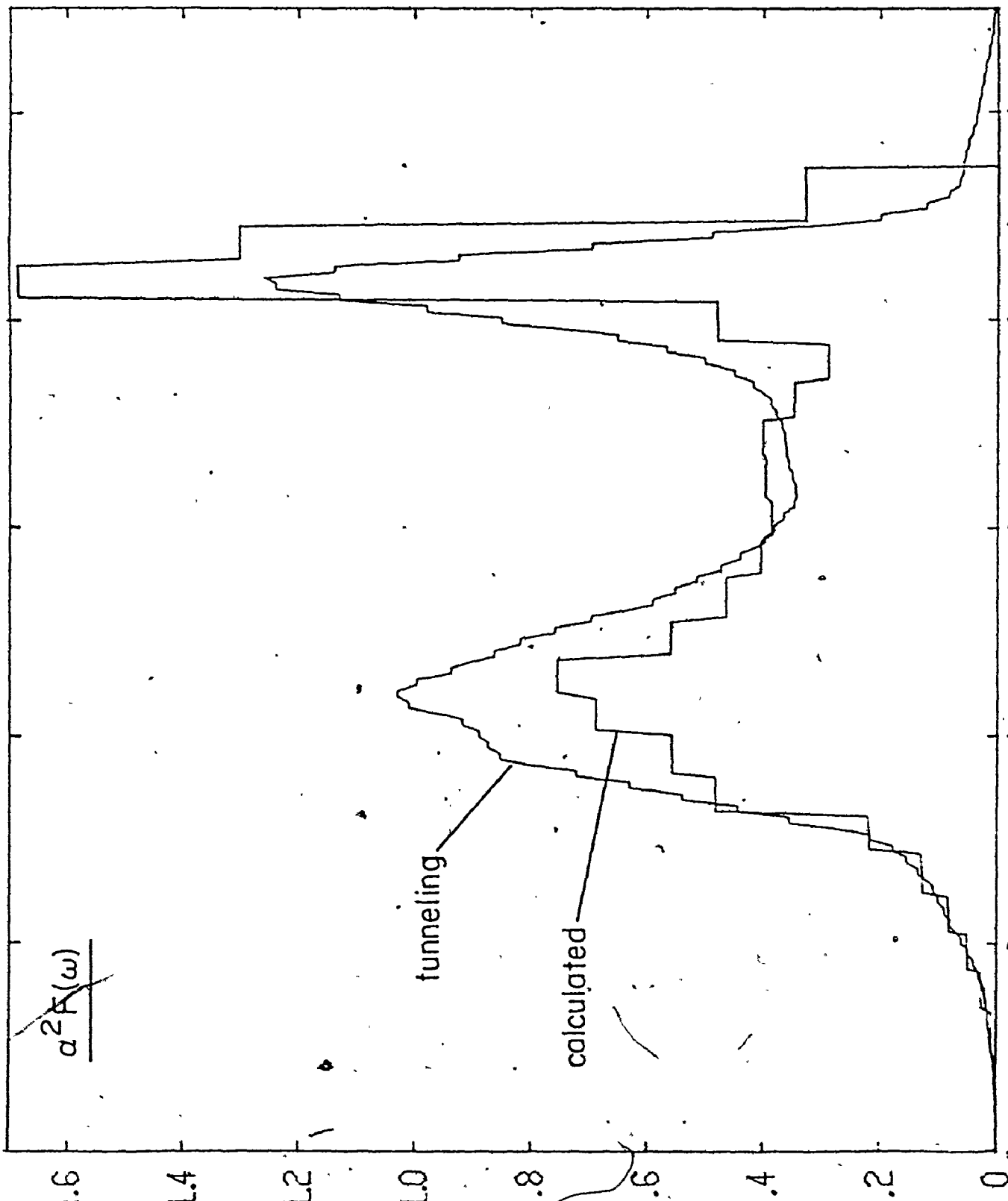

Fig. 5-24 Comparison of tunneling with calculated $\alpha^2F(\omega)$ for Pb.

Fig. 5-25 $P(a)$ and $P_{\Delta}(a)$ for Pb

Horizontal lines are histogram bins:

——— gap on real axis, ------ $\lambda_k(0)$.

Vertical lines are used for average values within the four regions. The height is the weight per region.

——— gap on real axis, ------ $\lambda_{\underline{k}}(0)$,

····· gap on imaginary axis from separable kernel based on $A_{\underline{k}}$.

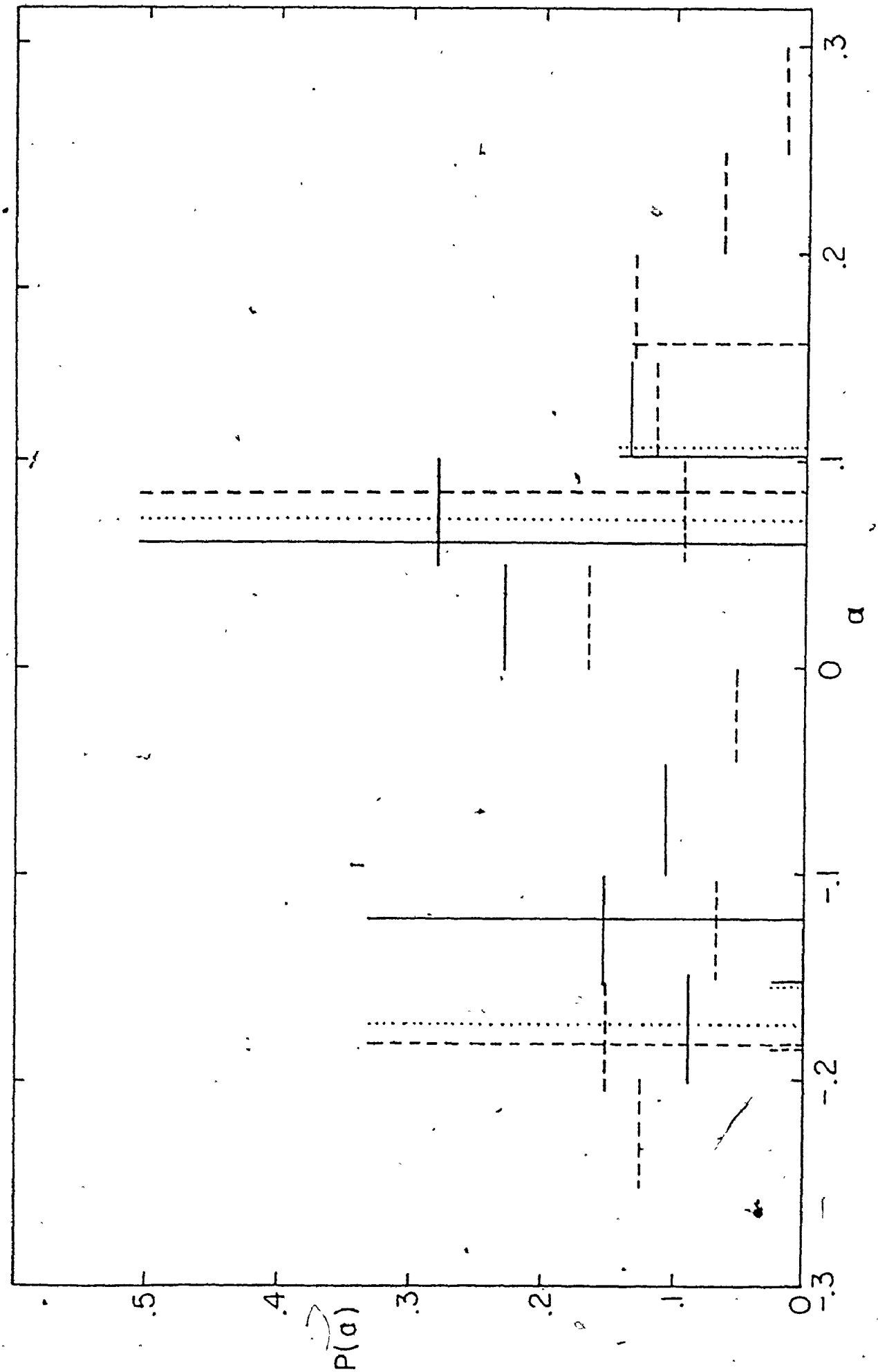
P(a)
.5
.4
.3
.2
.1
0
.3
.2
.1
0
-.1
-.2
-.3
a

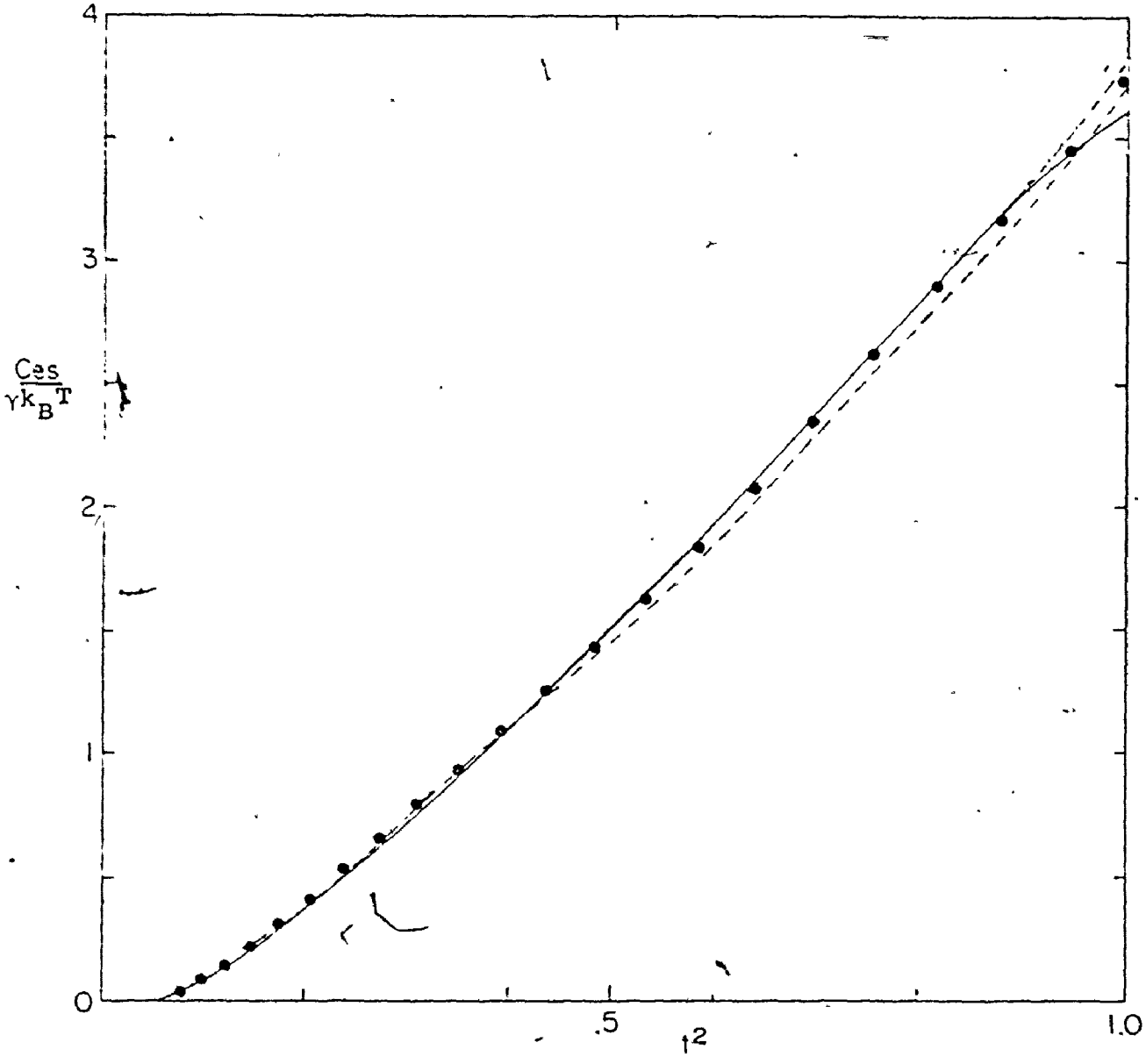

Fig. 5-26 Calculated and experimental specific heat of Pb
------ from Ref. 48 (expt) •••••• Ref. 6 (expt),
——— calculated from isotropic tunneling $\alpha^2 F(\omega)$,
-·-·-· estimated correction to the calculation.

Table 5-14

Addition of anisotropy effects to the quantities calculated from the tunneling $\alpha^2F(\omega)$

	(a)	(b)	(c)
T_c (deg K)	7.19	7.41	7.19
H_c (Gauss)	818	838	811
D(t) (max)	.025	.023	.022
$C_{es}/\gamma k_B T$	3.50(3.82)	3.54(3.76)	>3.35(3.57)
$\gamma(k_B T_c)^2 H_c^2$	.136	.134	.140
$\Delta C_v(T_c)$ (mJ/mole/deg)	58.4 (63.3)	55.6(60.6)	>53(58)
$-(dH_c/dT)_{T_c}$ (Gauss/deg)	241	233	>225

(a) Calculated from isotropic tunneling $\alpha^2F(\omega)$.

(b) Obtained by adding to column (a) the anisotropy effects predicted by column (g) of Table 5-11.

(c) Obtained from column (b) by increasing μ^* to bring T_c down to experiment. The derivatives used were $\partial T_c/\partial\mu^* = -15$, $\partial H_c/\partial\mu^* = -1800$, $\partial D(.7)/\partial\mu^* = -.055$. The inequalities were obtained from $\frac{\partial}{\partial\mu^*}\left(\frac{C_{es}}{\gamma k_B T}\right)$ for Nb ($\lambda = .98$) which is expected to be larger than $\frac{\partial}{\partial\mu^*}\frac{C_{es}}{\gamma k_B T_c}$ for Pb. Quantities in brackets are estimates of the values that would be obtained if the error in the specific heat just below T_c were corrected (see Fig. 5-26).

CHAPTER 6

CONCLUSIONS

The preceding results lead to a number of conclusions about isotropic and anisotropic superconductors. Concerning isotropic systems, it is fair to say that the gap equations on the imaginary axis used with the $\alpha^2F(\omega)$ derived from tunneling and N(0) from the electronic specific heat can, with μ^* as the only adjustable parameter, predict the thermodynamic properties of the simple metals to within the experimental accuracy of a few percent. This holds true both for absolute magnitudes such as $H_c(0)$ and ratios such as the specific heat jump, for strong and weak coupling alike, also for Nb and Nb_3Sn where there has been some doubt that the conventional Eliashberg theory is valid. But there are three small but significant exceptions or troublesome points in the specific heat and the deviation function. First, for the strongest coupling systems ($\lambda(0) > 1.5$) the calculated specific heat difference between the normal and superconducting states is less than the usual expression $\gamma k_B T$ for the normal electronic specific heat below $T/T_c = .2$. For Pb at least, this result seems to agree with experiment; that suggests the problem lies in the expression for the normal state, as

other theoretical work confirms. This difficulty with the calculated specific heat at low temperatures is unfortunate because this is the thermodynamic property most sensitive to gap anisotropy. The other two discrepancies, in the specific heat jump and the deviation function, which depend weakly on the average gap anisotropy, do not provide such conclusive evidence for the existence of gap anisotropy. That all the calculated $D(t)$ (and very likely the specific heat jumps too, but here a small systematic error in the calculation prevents quantitative comparison) lie above the average experimental value, and for some of the weaker coupling systems even above the highest experimental value, is not in itself decisive, because the $\alpha^2F(\omega)$, which were almost all obtained by the same experimental group, could have been overestimated. Thanks to the functional derivatives of T_c, H_c and $D(t)$ with respect to $\alpha^2F(\omega)$, also $\partial T_c/\partial\mu^*$, $\partial H_c/\partial\mu^*$ and $\partial D(t)/\partial\mu^*$, it was possible to estimate the small change in the $\alpha^2F(\omega)$ for Nb needed to pull down $D(t)$ to one of the experiments. In fact, from the thermodynamic properties and the functional derivative alone a very reasonable estimate could be made of the most appropriate $\alpha^2F(\omega)$ for this system. This method of analyzing an $\alpha^2F(\omega)$ is clearly useful in situations where $\alpha^2F(\omega)$ is only known approximately, because even when μ^* is fitted to T_c the other thermodynamic properties are still very sensitive to $\alpha^2F(\omega)$.

The discrepancy between theory and experiment cannot all however be explained by a tendency of the tunneling experiments to overestimate $\alpha^2F(\omega)$. The calculation with Al reproduced exactly the BCS prediction for D(t) and the specific heat, despite the relatively large μ^*; therefore further weakening of the coupling strength in the weakest coupling systems cannot explain the measured D(t). Moreover, for most of the elements studied, there is unambiguous experimental evidence for anisotropy in the saturation of the transition temperature. The conclusions reached from the isotropic calculations can be summarized as follows: The isotropic Eliashberg equations can predict the thermodynamic properties of the simple metals to within a few percent; conversely, they can be used to modify a calculated $\alpha^2F(\omega)$ to get better agreement with experiment. If no such modification is made, there remains a small difference between theory and experiment for which the most likely explanation is gap anisotropy.

A way of estimating the amount of gap anisotropy implied by this discrepancy was the object of the calculations done on Al, Hg, Nb, Sn and Tl with a simple factorable model anisotropy in the electron-phonon interaction chosen to conserve $\alpha^2F(\omega)$, the average interaction. The same model was used for all the elements, to study systematically the way the coupling strength and μ^* modify the effect of the interaction anisotropy on gap anisotropy and on the thermodynamic properties. A separable interaction, although justifiable

on other grounds, was chosen because all earlier theoretical work was done with it. These previous investigations included, however, several approximations which were avoided in the present calculations to obtain an analytical expression. The exact numerical solution of the model shows that these approximations matter in several ways. First, the relationship between anisotropy in the gap and anisotropy in the interaction as measured by the directional $\lambda_{\underline{k}}(0)$ depends significantly on the coupling strength, although the relationship between the gap anisotropy and the change in T_c is very well estimated even for very strong coupling. Secondly, the analytical expressions fail very badly for quantities other than T_c, the worst being the critical field, although it is not known why. Possibly the discrepancies between anisotropy estimates based on these expressions from different types of experiments on the same material have the same cause. The calculations presented here are meant as alternative guide to the interpretation of experiment, since no expression has been derived here except a simple proportionality relationship between the gap anisotropy at any impurity concentration and the rate of change in T_c. This formula is moreover not based on any model or approximation.

Since the separable approximation for the interaction was felt to be inadequate for a real metal, where the interaction was expected to depend on frequency and the momentum

transfer rather than a product of functions of $\underline{k}$ and $\underline{k}'$, a realistic calculation of the interaction and the gap was done in Pb that included these complications. A computer program was written to solve the gap equations in an orthonormal basis appropriate for the Fermi surface, namely the Fermi Surface Harmonics (which turned out to be very good for expanding the $\lambda_{\underline{k}}(0)$), but this program was in the end more complicated than necessary. In Pb most of the gap anisotropy arises from the differences in the mean values on the four disjoint pieces of Fermi surface, which greatly simplifies matters. Moreover, when averaged over frequency (as in the calculation of the $\lambda_{\underline{kk}'}(m)$) the interaction was to a very good approximation separable. In fact, enormous simplifications of the anisotropy in the interaction were possible without affecting the thermodynamic properties. This was quite a surprise, and it certainly has important implications for other kinds of calculations requiring detailed knowledge of the electron-phonon interaction. The very high symmetry (cubic) of Pb is thought to be the cause, for the symmetry averages out everything that is not invariant under group operations. The verification of this idea, and its validity for other metals remain to be investigated.

The singularity in $\delta T_c/\delta\alpha^2F(\omega)$ at $\omega=0$, caused by the thermal phonons washing out anisotropy, was shown by the numerical calculations in Pb to be unimportant. The negative

region in $\delta T_c/\delta\alpha^2F(\omega)$) was at very low frequency where any realistic $\alpha^2F(\omega)$ is expected to be small. The thermal phonons did not cause any significant temperature dependence of the gap anisotropy either for any of the systems studied.

The calculation in Pb also tied together anisotropy in the gap edge on the real axis with anisotropy in $\bar{\Delta}_{\underline{k}}(1)$, the first Matsubara frequency. It was identical to the anisotropy in the gap edge at T=0 calculated on the real axis. Finally, the calculated anisotropy turned out to about the right amount to bring the deviation function and specific heat jump obtained from the isotropic $\alpha^2F(\omega)$ down to experiment. These calculations have therefore been more successful than expected.

APPENDIX I

THE FULL CUBIC GROUP O_h AND GROUP REPRESENTATIONS

The following exposition is greatly condensed, and many important results with no bearing on the construction of FSH were omitted. The most important reference used for this appendix was Tinkham[107].

Definition of a group

A group is a set of elements R_1, R_2, R_3 ... together with an operation called multiplication that associates any ordered pair of elements with another element. This multiplication must satisfy the following conditions:

1. Closure. The product of any two elements also belongs to the set.
2. The associative law holds. $R_1(R_2R_3)$ is the same as $(R_1R_2)R_3$.
3. Existence of the identity element. There is an element E such that ER=RE=R for any R.
4. Existence of inverses. For every element R there is in the group an element R^{-1} such that $RR^{-1} = R^{-1}R=E$.

The set of proper and improper rotations that map a cube or octahedron into itself are the elements of a group if we defined multiplication as "followed by"; e.g. if R_1 = rotation by π about (001) and R_2 = rotation by $\pi/2$ about (010),

then

R_1R_2 = rotation by $\pi/2$ about (010) followed by rotation by π about (001).

A "proper rotation" is what is ordinarily understood by the term "rotation"; an improper rotation is the product of a proper rotation with the inversion operator i which changes the cube into its mirror image. Reflections are particular examples of improper rotations.

The elements of a group may be divided into mutually exclusive subsets called classes as follows.

Definition of a class

The elements belonging to the same class as R are the $R_iRR_i^{-1}$ where the R_i are all the elements of the group.

Some of the class elements will appear more than once in such an enumeration. The identity forms a class by itself. The full cubic group O_h consists of six classes of proper rotations:

E	the identity (1 element)
C_3	rotation by $2\pi/3$ about any [111] axis (8 elements)
C_4^2	rotation by π about any [001] axis (3 elements)
C_2	rotation by π about any [101] axis (6 elements)
C_4	rotation by $\pi/2$ about any [001] axis (6 elements)

and six similar classes of improper rotations.

Definition of a group representation by square matrices

If for every group element R there corresponds a square matrix $\Gamma(R)$ such that $\Gamma(R_1)\Gamma(R_2) = \Gamma(R_1R_2)$ then the $\Gamma(R)$ are

a representation of the group. They need not have the same multiplication table as the group, nor be all different. A seemingly trivial example is the representation where $\Gamma(R)$ is the unit 1×1 matrix. This representation is in fact the most important one in the next two appendices. A group representation is called <u>reducible</u> if there exists a similarity transformation that simultaneously block-diagonalizes (in the same way) all the matrices of the representation. If there is no such similarity transformation then the representation is <u>irreducible</u>. That the irreducible representations are the fundamental quantities follows from the fact that the matrices left strung along the diagonal after block-diagonalization are none other than the irreducible representations. A reducible representation Γ is described by $\Sigma\, C_i \Gamma^{(i)}$ where the $\Gamma^{(i)}$ are irreducible representations, C_i is the number of times that $\Gamma^{(i)}$ appears on the diagonal, and the summation does not mean matrix addition but the "decomposition" of Γ. The number of irreducible representations for a given group is in one sense finite, since it can be shown that the number of elements in the group = $\sum_i \ell_i^2$ where ℓ_i is the dimensionality of irreducible representation $\Gamma^{(i)}$, but in another sense infinite, since sets of matrices differing only by a similarity transformation will have the same multiplication table. (The sum $\sum_i C_i \ell_i^2$ is a sum over inequivalent representations not related by a similarity transformation.) Therefore it is useful to differentiate the distinct irreducible representation by a property remaining invariant under such transformations,

the trace = sum of the diagonal elements. For a given irreducible representation, matrices representing elements belonging to the same class have the same trace, which is called the character of that class. It is therefore possible to summarize the invariant properties of a group and its irreducible representation in an array known as the character table. This is the character table of the full cubic group:

I.R. \ Classes	E	$3C_4^2$	$6C_4$	$6C_2$	$8C_3$	i	$3iC_4^2$	$6iC_4$	$6iC_2$	$8iC_3$
Γ_1	1	1	1	1	1	1	1	1	1	1
Γ_2	1	1	-1	-1	1	1	1	-1	-1	1
Γ_{12}	2	2	0	0	-1	2	2	0	0	-1
Γ_{15}'	3	-1	1	-1	0	3	-1	1	-1	0
Γ_{25}'	3	-1	-1	1	0	3	-1	-1	1	0
Γ_1'	1	1	1	1	1	-1	-1	-1	-1	-1
Γ_2'	1	1	-1	-1	1	-1	-1	1	1	-1
Γ_{12}'	2	2	0	0	-1	-2	-2	0	0	1
Γ_{15}	3	-1	1	-1	0	-3	1	-1	1	0
Γ_{25}	3	-1	-1	1	0	-3	1	1	-1	0

The labelling of the irreducible representation follows the convention of Bouckaert, Smoluchowski and Wigner[17]. In common with all character tables, this one has an equal number of rows and columns, the rows are linearly independent, and the character of E is the dimensionality of the irreducible representation. The upper left-hand corner is the character table of an important subgroup O_h consisting of the proper rotations

only, the octahedral group O.

Definition of basis functions

A set of linearily independent functions $\{\phi_1, \phi_2, \ldots \phi_N\}$ that transform into linear combinations of each other under the group operations generates a representation of the group in the following way (with R operating on the arguments of ϕ_i)

$$R\phi_i = \sum_j \Gamma_{ij}(R)\phi_j \quad . \qquad \text{(I-1)}$$

These ϕ_i are basis functions for the N-dimensional representation Γ, which will in general be reducible. To find how Γ decomposes, it is sufficient to find the trace of $\Gamma(R)$ for any R from all the classes of the group. Since the trace of $\Gamma(R)$ is the sum of the traces of the irreducible representation hidden in Γ, this set of traces must be a linear combination of the rows of the character table, the coefficients of each row being the number of times that particular irreducible representations would appear if Γ were block-diagonalized. Thus it is made apparent for which and for how many of the irreducible representations suitable linear combinations of the ϕ_i can serve as basis functions. There are systematic ways of finding these linear combinations, but in practice it is easier to guess at them.

It is the basis functions of the irreducible representations Γ_1 and Γ_{15} that are of special interest. The first row of the character table implies that a set of basis functions

for Γ_1 consists of a single function which remains invariant under all group operations. Comparison of equation (I-1) with the character table shows that there are 3 basis functions for Γ_{15} and that they transform among themselves under the group operations like {x,y,z}. Therefore the basis functions for Γ_1 are appropriate to expand the gap and the kernel of the Eliashberg equations, and those for Γ_{15} are appropriate for transport properties. The Γ_{15} functions are not used anywhere in this thesis. They are included because it was convenient to obtain them at the same time as the others.

APPENDIX II

CONSTRUCTION OF GLOBAL FSH

The machinery of the last chapter was set up to construct from linear combinations of terms like $x^i y^j z^k$† ($i,j,k \geq 0$) functions that transform like Γ_1 and Γ_{15}. The key to the method lies in equation (I-1) and the character table. To see how they are used, it is simpler to do a specific example, the decomposition of the representation generated by some 4th order polynomials. The functions $\{x^i y^j z^k$, $i+j+k = 4\}$ can be separated into subsets that will not be scrambled by any group operation: $\{x^4, y^4, z^4\}$, $\{x^2y^2, y^2z^2, x^2z$ $\{xyz^2, yzx^2, zxy^2\}$, $\{xy^3, yx^3, \ldots$etc.$\}$. Each of these sets is used to find the trace of the $\Gamma(R)$ that they define by equation (I-1) for some convenient element R from each of the five classes of O. Because of redundancy it is unnecessary to use the full character table when the functions are all even or all odd under inversion. From class C_4^2, choose (arbitrarily) rotation by π about (001) = R from class C_5, choose rotation by $\pi/2$ about (001) = R_2,

---

†In appendices II and III, x,y,z instead of the actual arguments v_x, v_y, v_z of the FSH are used for typographical convenience. The reader will have to do some double-think to forget that $x^2+y^2+z^2$ is constant.

from C_2 choose rotation by π about (110) = R_3,

from C_3 choose rotation by $2\pi/3$ about (11I) = R_4.

Then for the set $\{x^4, y^4, z^4\}$ a table can be constructed whose entries are $\Gamma_{ii}(R)$:

Table II-1

Character of the representation generated by $\{x^4, y^4, z^4\}$

	$\Gamma_{ii}(E)$	$\Gamma_{ii}(R_1)$	$\Gamma_{ii}(R_2)$	$\Gamma_{ii}(R_3)$	$\Gamma_{ii}(R_4)$
x^4	1	1	0	0	0
y^4	1	1	0	0	0
z^4	1	1	1	1	0
	3	3	1	1	0

(If different operations had been chosen from the classes, the zeroes and ones would be transposed within each column without altering their sum, the trace.)

The sum of the columns is the trace of Γ for each class. By inspection, this is the sum of the first and third rows of the character table, implying $\Gamma = \Gamma_1 + \Gamma_{12}$. The Γ_1 basis function is obviously $x^4+y^4+z^4$. With more effort, a pair of basis functions for Γ_{12} are found to be x^4-y^4 and $2z^4-y^4-x^4$.

It is clear that the decomposition of the representation generated by $x^iy^jz^k$ depends not on the identity of integers i j k but on questions such as, Are they all even? Are two equal and even while one is odd?, etc. The decomposition of Γ and the

basis functions for the 10 possible $x^i y^j z^k$ are listed in Table II-2. The decomposition of the representations generated by all the $x^i y^j z^k$ of a given order are listed in Table II-3.

Table II-2

Basis functions and irreducible representations obtainable from $x^i y^j z^k$

i	j	k	Irreducible Representations	Basis functions[T]
even	= even	= even	Γ_1	iii
even	= even	≠ even	Γ_1	iik+iki+kii
			Γ_{12}	kii-iki, 2iik-iki-kii
even	≠ even	≠ even	Γ_1	ijk+kij+jki+jik+ikj+kji
			Γ_2	ijk+kij+jki-jik-ikj-kji
			Γ_{12}	ijk+ikj-(jik+kij),2(jki+kji)-(ijk+ikj)-(jik+kij)
			Γ_{12}	jik+jki-(ijk+kij),2(ikj+kij)-(jik+jki)-(ijk+kji)
even	= even	odd	Γ_{15}	kii,iki,iik
even	= even	odd	Γ_{15}	kij+kji, ikj+jki, ijk+jik
			Γ_{25}	kij-kji, jki-ikj, ijk-jik
even	odd	= odd	Γ'_{25}	kii,iki,iik
even	odd	≠ odd	Γ'_{15}	kij-kji,jki-ikj, ijk-jik
			Γ'_{25}	kij+kji, ikj+jki, ijk+jik

(continued next page)

Table II-2 (continued

i	j	k	Irreducible Representations	Basis functions†
odd	≠ odd	≠ odd	Γ_1'	ijk+kij+jki-jik-ikj-kji
			Γ_2'	ijk+kij+jki+jik+ikj+kji
			Γ_{12}'	ijk+ikj-(jik+kij),2(jki+kji)-(ijk+ikj)-(jik+kij)
			Γ_{12}'	jik+jki-(ijk+kji),2(ikj+kij)-(jik+jki)-(ijk+kji)
odd	= odd	≠ odd	Γ_2'	ijk+iki+kii
			Γ_{12}'	kii-iki, 2iik-iki-kii
odd	= odd	= odd	Γ_2'	iii

†In this condensed notation, 2iik-iki-kii stands for $2x^iy^iz^k-x^iy^kz^i-x^ky^iz^i$.

Table II-3

Irreducible representations

generated from all the $x^i y^j z^k$ of a given order

Order		Cumulative number of Γ_{15}	Cumulative number of Γ_1	†Cumulative number of Kubic harmonics transforming like Γ_1
0	Γ_1		1	1
1	Γ_{15}	1		
2	$\Gamma_1+\Gamma_{12}+\Gamma'_{25}$		2	1
3	$\Gamma'_2+2\Gamma_{15}+\Gamma_{25}$	3		
4	$2\Gamma_1+2\Gamma_{12}+\Gamma'_{15}+2\Gamma'_{25}$		4	1
5	$\Gamma'_2+\Gamma'_{12}+4\Gamma_{15}+2\Gamma_{25}$	7		
6	$3\Gamma_1+\Gamma_2+3\Gamma_{12}+2\Gamma'_{15}+4\Gamma'_{25}$		7	2
7	$2\Gamma'_2+2\Gamma'_{12}+6\Gamma_{15}+4\Gamma_{25}$	13		
8	$4\Gamma_1+\Gamma_2+5\Gamma_{12}+4\Gamma'_{15}+6\Gamma'_{25}$		11	3

†The number of Kubic harmonics of given order of type Γ_1 is one for all even orders less than 10, except for 2, for which there are none.

APPENDIX III

CONSTRUCTION OF LOCAL FSH FOR A FERMI SURFACE WITH SEVERAL DISJOINT PIECES

In Appendix II explicit functional forms were listed for the basis functions of all irreducible representations instead of just Γ_1 and Γ_{15}. This was done because they are the most convenient building blocks for local FSH. In the previous appendix sets of $\{x^i y^j z^k,\ i+j+k = \text{constant}\}$ were used to generate reducible representations, which when broken down, revealed for which irreducible representation the set of $x^i y^j z^k$ were basis functions. Here the process is repeated using sets consisting of $\{\phi_j^{(i)}(x,y,z)\delta_\mu,\ j = 1, \ell_i,\ \mu = 1, N_R\}$ where $\phi_j^{(i)}(x,y,z)$ is the jth partner of the ℓ_i-dimensional irreducible representation $\Gamma^{(i)}$, δ_μ is unity (zero) if (x,y,z) lies inside (outside) the piece of Fermi surface labelled by the crystallographic axis μ, and N_R the number of symmetry-related pieces. A particular example is the 18-member set $\{x\delta_{00\pm1},\ y\delta_{00\pm1},\ z\delta_{00\pm1}, x\delta_{0\pm10}, y\delta_{0\pm10}, z\delta_{0\pm10}, x\delta_{\pm100},\ y\delta_{\pm100},\ z\delta_{\pm100}\}$ which consists of the partners of a Γ_{15} basis confined to the pieces of Fermi surface related by symmetry to region 1 of Fig. . For this set construct Table III-1 on the same principles as Table II-1, but now including the improper rotations as well since the basis functions of the new irreducible representation may now have different definitions on pieces related by inversion such as δ_{100} and $\delta_{\bar{1}00}$.

Zeroes appear wherever the group operation maps δ_μ into some other piece; elsewhere the entries are identical to those in the Γ_{15} row of the character table of the full cubic group. The representation reduces to $2\Gamma_{15} + \Gamma_{25} + (\Gamma_1+\Gamma_{12}+\Gamma'_{15}+\Gamma'_{25})$ where the unbracketed terms are those where the basis function of the new irreducible representation is defined in the same way on δ_μ and $\delta_{\bar{\mu}}$ and the others are those where they are defined with opposite signs on δ_μ and $\delta_{\bar{\mu}}$. Hence the old (x,y,z) basis functions generate one Γ_1 and two Γ_{15} irreducible representation basis functions for region 1. The new Γ_1 function is $x(\delta_{100}-\delta_{\bar{1}00}) + y(\delta_{010}-\delta_{0\bar{1}0}) + z(\delta_{001}-\delta_{00\bar{1}})$. The z-component of the new Γ_{15} functions is $z(\delta_{001}+\delta_{00\bar{1}})$ and $z(\delta_{100}+\delta_{\bar{1}00}+\delta_{010}+\delta_{0\bar{1}0})$. Any basis function of Γ_{15} would have produced the same decomposition, and similar new Γ_1 and Γ_{15} basis functions. Therefore, if this procedure is repeated for region 1 with typical global basis functions of the other nine irreducible representations, the origin of all the irreducible representations of Γ_1 and Γ_{15} for region 1 can be found. Such information for all four regions is summarized in Table III-2. The brackets have the same meaning as in the paragraph referring to Table III-1. The numerical coefficient is the number of new irreducible representations that can be constructed from the old ones. Combining Tables III-2 and II-3 gives the number of FSH of a given order for each region.

The number of basis functions is larger for those regions of lower symmetry, because high symmetry puts more con-

straints on the possible basis functions. In region 2 for example, the Γ_1 basis functions need be invariant under only reflection in the plane x=y, whereas in region 1 they must be invariant under eight group operations.

Tables III-2 and II-3, together with the knowledge of the operations under which the basis functions are invariant, is generally sufficient to construct the local F.S.H.. Table III-4 lists some of the lower order ones. The Γ_1 basis functions of odd order show with particular clarity how they were constructed from the old global Γ_2' and Γ_{15} and Γ_{25}' basis functions. (Γ_{12}' does not appear until 5th order.) The origin of the other functions listed is sometimes less clear because some are linear combinations of functions generated from different global basis functions. For example, the 2nd order Γ_1 functions in region 1 are not so obviously related to the old Γ_1 and Γ_{12} from which they originated. The linear combinations were usually chosen for the maximum simplicity of the functional form on the 48th.

In evaluating the expansion coefficients of a quantity with full cubic symmetry, only the definition of the basis function on the irreducible 48th matters. The definitions on the other pieces are included as verification of the full cubic symmetry of the basis functions extended outside the 48th.

To evaluate the expansion coefficients of a quantity transforming like the z component of the basis for Γ_{15}, such as those involved in transport problems, the definition of the FSH need be known only on the region described by

planes y = 0 and x = z. Table III-2 implies that such a function can be constructed from a linear combination of the x, y, and z components of a Γ_{25} global representation. Table II-2 gives the functional forms of these components and also says whether or not a Γ_{25} representation exists for a given set of exponents i, j k. When the functional form is known, it becomes clear that the required linear combination is the y component alone. Functions 423 and 446 in Table III-4 are examples contructed from Γ_{25} basis functions. To obtain the functional forms on the pieces $\delta\mu$ related by symmetry to region 4, the same group operation that maps region 4 into $\delta\mu$ is applied to the linear combination of Γ_{25} components that is used in region 4. For example, R_1 maps δ_{101} into δ_{011} and the y component of a Γ_{25} basis function into the x component.

Fig. III-1, the irreducible 16th for the z component.

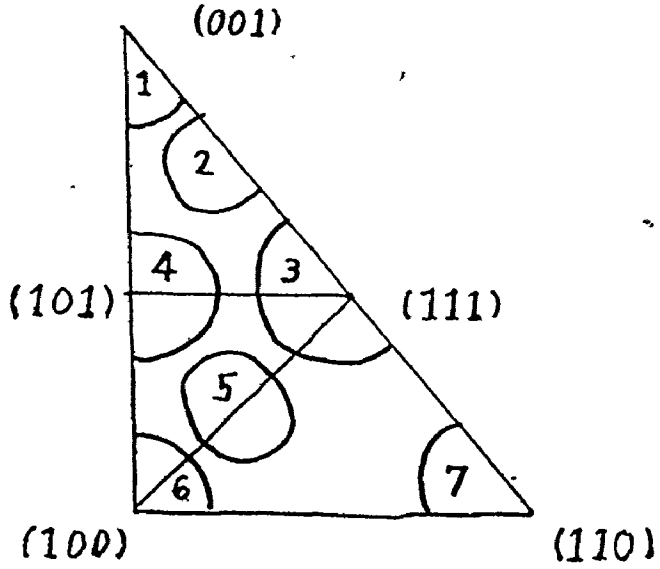

Fig. III-1

Labelling of the pieces of Fermi surface in the irreducible 16th. The uppermost triangle is the irreducible 48th. (The regions are not drawn to scale. See Fig. 5-20)

In using Table III-4, it should be kept in mind that any linear combination of basis functions for a given region and order is also the basis function of an irreducible representation. For example, the second 2nd-order function for region 1 could just as well be $(x^2+y^2+2z^2)(\delta_{001}+\delta_{00\bar{1}})+(x^2+z^2+2y^2)(\delta_{010}+\delta_{0\bar{1}0})+(y^2+z^2+2x^2)(\delta_{100}+\delta_{\bar{1}00})$. The particular linear combination given in Table III-4 is therefore to a certain degree arbitrary.

For the lowest orders, guess-work will generally suffice to construct the FSH. Still, some general principles are worth discussing. Consider the functional form that a Γ_1 basis function must have in region 4. It must be invariant under the following operations: reflection in the

Table III-1

The character of the reducible representation generated by global Γ_{15} basis functions on the pieces related by symmetry to region 1.

	$\Gamma_{ii}(E)$	$\Gamma_{ii}(R_1)$	$\Gamma_{ii}(R_2)$	$\Gamma_{ii}(R_3)$	$\Gamma_{ii}(R_4)$	$\Gamma_{ii}(i)$	$\Gamma_{ii}(iR_1)$	$\Gamma_{ii}(iR_2)$	$\Gamma_{ii}(iR_3)$	$\Gamma_{ii}(iR_4)$
$(x,y,z)\delta_{001}$	3	-1	1	0	0	0	0	0	1	0
$(x,y,z)\delta_{00\bar{1}}$	3	-1	1	0	0	0	0	0	1	0
$(x,y.z)\delta_{010}$	3	0	0	0	0	0	1	0	0	0
$(x,y,z)\delta_{0\bar{1}0}$	3	0	0	0	0	0	1	0	0	0
$(x,y,z)\delta_{100}$	3	0	0	0	0	0	1	0	0	0
$(x,y,z)\delta_{\bar{1}00}$	3	0	0	0	0	0	1	0	0	0
	18	-2	2	0	0	0	4	0	2	0

Table III-2

Origins of Γ_1 and Γ_{15} irreducible representations for each of the four regions in terms of the old global irreducible representations

Region \ I.R.	Γ_1	Γ_{15}
1	$\Gamma_1\ \Gamma_{12}$	$2\Gamma_{15}\ \Gamma_{25}$
	(Γ_{15})	$(\Gamma_1\ \Gamma_{12}\ \Gamma'_{15}\ \Gamma'_{25})$
2	$\Gamma_1\ \Gamma_{12}\ \Gamma'_{15}\ 2\Gamma'_{25}$	$\Gamma'_1\ 2\Gamma'_2\ 3\Gamma'_{12}\ 5\Gamma_{15}\ 4\Gamma_{25}$
	$(\Gamma'_2\ \Gamma'_{12}\ 2\Gamma_{15}\ \Gamma_{25})$	$(2\Gamma_1\ \Gamma_2\ 3\Gamma_{12}\ 4\Gamma'_{15}\ 5\Gamma'_{25})$
3	$\Gamma_1\ \Gamma'_{25}$	$\Gamma'_2\ \Gamma'_{12}\ 2\Gamma_{15}\ \Gamma_{25}$
	$(\Gamma'_2\ \Gamma_{15})$	$(\Gamma_1\ \Gamma_{12}\ \Gamma'_{15}\ 2\Gamma'_{25})$
4	$\Gamma_1\ \Gamma_{12}\ \Gamma'_{25}$	$\Gamma'_2\ \Gamma'_{12}\ 3\Gamma_{15}\ 2\Gamma_{25}$
	$(\Gamma_{15}\ \Gamma_{25})$	$(\Gamma_1\ \Gamma_2\ 2\Gamma_{12}\ 2\Gamma'_{15}\ 2\Gamma'_{25})$

Table III-3

Number of FSH of type Γ_1 and Γ_{15} of a given order for all four regions.

Order \ Region	Γ_1 1	2	3	4	Total	Number of Kubic harmonics of type Γ_1
0	1	1	1	1	4	1
1	1	2	1	1	5	0
2	2	4	2	3	11	0
3	2	6	3	3	14	0
4	4	9	4	6	23	1
5	4	12	5	6	27	0

Order \ Region	Γ_{15} 1	2	3	4	Total
0	1	2	1	1	4
1	2	5	2	3	12
2	3	10	4	5	22
3	5	16	6	9	35
4	7	24	9	12	52
5	10	33	12	18	73

Table III-4

Listing of FSH of Type Γ_1 and Γ_{15} of lower order

The number of functions listed for each region is roughly proportional to the weight of each region as listed in Table .

For Γ_1 functions of odd order, and Γ_{15} functions of even order, $\delta\mu$ is an abbreviation of $(\delta\mu-\delta\bar{\mu})$; conversely, for Γ_1 functions of even order and Γ_{15} functions of odd order, $\delta\mu$ stands for $(\delta\mu+\delta\bar{\mu})$, unless both $\delta\mu$ and $\delta\bar{\mu}$ are written out.

Zeroth order Γ_1 functions are simply unity on all the pieces related by symmetry to a given region.

Γ_1 BASIS FUNCTIONS

Region 1	μ = 100, 010, 001	Value on 48th (001)
	1st order	
111	$z\delta_{001}+y\delta_{010}+x\delta_{100}$	z
	2nd order	
121	$z^2\delta_{001}+y^2\delta_{010}+x^2\delta_{100}$	z^2
122	$(x^2+y^2)\delta_{001}+(x^2+z^2)\delta_{010}+(y^2+z^2)\delta_{100}$	x^2+y^2
	3rd order	
131	$z^3\delta_{001}+y^3\delta_{010}+x^3\delta_{100}$	z^3
132	$z(x^2+y^2)\delta_{001}+y(x^2+z^2)\delta_{010}+x(y^2+z^2)\delta_{100}$	$z(x^2+y^2)$
	4th order	
141	$z^4\delta_{001}+y^4\delta_{010}+x^4\delta_{100}$	z^4
142	$(x^4+y^4)\delta_{001}+(x^4+z^4)\delta_{010}+(y^4+z^3)\delta_{100}$	x^4+y^4
143	$z^2(x^2+y^2)\delta_{001}+y^2(x^2+z^2)\delta_{010}+x^2(y^2+z^2)\delta_{100}$	$z^2(x^2+y^2)$
144	$x^2y^2\delta_{001}+x^2z^2\delta_{010}+y^2z^2\delta_{100}$	x^2y^2

Region 2

The label is μ,ν where μ = nearest 4 fold axis, ν = nearest 3-fold axis, μ = 001, 0±10, ±100; and ν = 111, $\bar{1}\bar{1}1$, $\bar{1}11$, $1\bar{1}1$.

In the summation impossible combinations such as μ = 001, ν = $\bar{1}\bar{1}\bar{1}$ are understood to be excluded.

	1st order	Value on 48th (001,111)
211	$z\Sigma\delta_{001,\nu}+y\Sigma\delta_{010,\nu}+x\Sigma\delta_{100,\nu}$	z
212	$(x+y)(\delta_{001,111}-\delta_{001,\bar{1}\bar{1}1})$	x+y
	$+(x-y)(\delta_{001,1\bar{1}1}-\delta_{001,\bar{1}11})$	
	$+(z+x)(\delta_{010,111}+\delta_{0\bar{1}0,1\bar{1}1})$	
	$+(z-x)(\delta_{010,\bar{1}11}+\delta_{0\bar{1}0,\bar{1}\bar{1}1})$	
	$+(y+z)(\delta_{100,111}+\delta_{\bar{1}00,\bar{1}11})$	
	$-(y-z)(\delta_{\bar{1}00,\bar{1}\bar{1}1}+\delta_{\bar{1}00,1\bar{1}1})$	
	2nd order	
221	$z^2\Sigma\delta_{001,\nu}+y^2\Sigma\delta_{010,\nu}+x^2\Sigma\delta_{100,\nu}$	z^2
222	$(x^2+y^2)\Sigma\delta_{001,\nu}+(x^2+z^2)\Sigma\delta_{010,\nu}$	x^2+y^2
	$+(y^2+z^2)\Sigma\delta_{100,\nu}$	
223	$xy(\delta_{001,111}+\delta_{001,\bar{1}\bar{1}1}-\delta_{001,1\bar{1}1}-\delta_{001,\bar{1}11})$	xy
	$+yz(\delta_{100,111}+\delta_{\bar{1}00,\bar{1}11}-\delta_{\bar{1}00,\bar{1}\bar{1}1}-\delta_{001,1\bar{1}1})$	
	$+zx(\delta_{010,111}+\delta_{0\bar{1}0,1\bar{1}1}-\delta_{010,\bar{1}11}-\delta_{0\bar{1}0,\bar{1}\bar{1}1})$	
224	$\Sigma\,\delta_{\mu,111}(x+y+z)^2+\Sigma\delta_{\mu,\bar{1}11}(-x+y+z^2)$	$(x+y+z)^2$
	$+\Sigma\,\delta_{\mu,\bar{1}\bar{1}1}(-x-y-z)^2+\Sigma\,\delta_{\mu,1\bar{1}1}(x-y+z)^2$	

Region 2 (continued)

	3rd order	Value on 48th
231	$z^3\Sigma\delta_{001,\nu}+y^3\Sigma\delta_{010,\nu}+x^3\Sigma\delta_{100,\nu}$	z^3
232	$z(x^2+y^2)\Sigma\delta_{001,\nu}+y(x^2+z^2)\Sigma\delta_{001,\nu}$ $+x(y^2+z^2)\Sigma\delta_{100,\nu}$	$z(x^2+y^2)$
233	$z^2(x+y)(\delta_{001,111}-\delta_{001,\bar{1}\bar{1}1})$ $+z^2(x-y)(\delta_{001,1\bar{1}1}-\delta_{001,\bar{1}11})$ $+y^2(z+x)(\delta_{010,111}+\delta_{0\bar{1}0,1\bar{1}1})$ $+y^2(z-x)(\delta_{010,\bar{1}11}+\delta_{0\bar{1}0,\bar{1}\bar{1}1})$ $+x^2(y+z)(\delta_{100,111}+\delta_{\bar{1}00,\bar{1}11})$ $-x^2(y-z)(\delta_{\bar{1}00,\bar{1}\bar{1}1}+\delta_{100,1\bar{1}1})$	$z^2(x+y)$
234	$(x^3+y^3)(\delta_{001,111}-\delta_{001,\bar{1}\bar{1}1})$ $+(x^3-y^3)(\delta_{001,1\bar{1}1}-\delta_{001,\bar{1}11})$ $+(z^3+x^3)(\delta_{010,111}+\delta_{0\bar{1}0,1\bar{1}1})$ $+(z^3-x^3)(\delta_{010,\bar{1}11}+\delta_{0\bar{1}0,\bar{1}\bar{1}1})$ $+(y^3+z^3)(\delta_{100,111}+\delta_{\bar{1}00,\bar{1}11})$ $-(y^3-z^3)(\delta_{\bar{1}00,\bar{1}\bar{1}1}+\delta_{\bar{1}00,1\bar{1}1})$	x^3+y^3
235	$xyz\sum_{\mu}(\delta_{\mu,111}+\delta_{\mu,\bar{1}\bar{1}1}-\delta_{\mu,\bar{1}11}-\delta_{\mu,1\bar{1}1})$	xyz
236	$(x(z^2-y^2)+y(z^2-x^2))(\delta_{001,111}-\delta_{001,\bar{1}\bar{1}1})$ $+(x(z^2-y^2)-y(z^2-x^2))(\delta_{001,1\bar{1}1}-\delta_{001,\bar{1}11})$ $+(x(y^2-z^2)+z(y^2-x^2))(\delta_{010,111}+\delta_{0\bar{1}0,1\bar{1}1})$ $-(x(y^2-z^2)-z(y^2-x^2))(\delta_{0\bar{1}0,\bar{1}\bar{1}1}+\delta_{010,\bar{1}11})$ $+(y(x^2-z^2)+z(x^2-y^2))(\delta_{100,111}+\delta_{\bar{1}00,\bar{1}11})$ $-(y(x^2-z^2)-z(x^2-y^2))(\delta_{\bar{1}00,\bar{1}\bar{1}1}+\delta_{\bar{1}00,1\bar{1}1})$	$x(z^2-y^2)+y(z^2-x^2)$

Region 2 (continued)

	4th order	Value on 48t
241	$z^4\Sigma\delta_{001,\nu}+y^4\Sigma\delta_{010,\nu}+x^4\Sigma\delta_{100,\nu}$	z^4
242	$(x^4+y^4)\Sigma\delta_{001,\nu}+(x^4+z^4)\Sigma\delta_{010,\nu}$ $+(y^4+z^4\Sigma\delta_{100,\nu}$	x^4+y^4
243	$(x^3y+y^3x)(\delta_{001,111}+\delta_{001,\bar{1}\bar{1}1}-\delta_{001,1\bar{1}1}-\delta_{001,\bar{1}11})$ $+(y^3z+z^3y)(\delta_{100,111}+\delta_{\bar{1}00,\bar{1}11}-\delta_{\bar{1}00,\bar{1}\bar{1}1}-\delta_{100,1\bar{1}1})$ $+(z^3x+x^3z)(\delta_{010,111}+\delta_{0\bar{1}0,1\bar{1}1}-\delta_{010,\bar{1}11}-\delta_{0\bar{1}0,\bar{1}\bar{1}1})$	x^3y+y^3x
244	$\Sigma\delta_{\mu,111}(x^3y+y^3x+z^3x+x^3z+y^3z+z^3y-r_ir_j^3-r_i^3r_j)_{i,j\neq\mu,i\neq j}$ $+\Sigma\delta_{\mu,\bar{1}11}(-x^3y-y^3x-z^3x-x^3z+y^3z+z^3y-r_ir_j^3-r_i^3r_j)_{i,j\neq\mu,i\neq j}$ $+\Sigma\delta_{\mu,\bar{1}\bar{1}1}(+x^3y+y^3x-z^3x-x^3z-y^3z-z^3y-r_ir_j^3-r_i^3r_j)$ $\quad i,j\neq\mu,i\neq j$ $+\Sigma\delta_{\mu,1\bar{1}1}(-x^3y-y^3x+z^3x+x^3z-y^3z-z^3y-r_ir_j^3-r_i^3r_j)$ $\quad i,j\neq\mu,i\neq j$	y^3z+z^3y $+z^3x+x^3z$
245	$x^2y^2\Sigma\delta_{001,\nu}+y^2z^2\Sigma\delta_{100,\nu}+x^2z^2\Sigma\delta_{010,\nu}$	x^2y^2
246	$z^2(x^2+y^2)\Sigma\delta_{001,\nu}+y^2(x^2+z^2)\Sigma\delta_{010,\nu}+x^2(y^2+z^2)\Sigma\delta_{100,\nu}$	$z^2(x^2+y^2)$
247	$z^2xy(\delta_{001,111}+\delta_{001,\bar{1}\bar{1}1}-\delta_{001,\bar{1}11}-\delta_{001,1\bar{1}1})$ $+y^2xz(\delta_{010,111}+\delta_{0\bar{1}0,1\bar{1}1}-\delta_{010,\bar{1}11}-\delta_{0\bar{1}0,\bar{1}\bar{1}1})$ $+x^2yz(\delta_{100,111}+\delta_{\bar{1}00,\bar{1}11}-\delta_{\bar{1}00,\bar{1}\bar{1}1}-\delta_{100,1\bar{1}1})$	z^2xy

Region 3

$\mu = 111,\ 1\bar{1}1,\ \bar{1}\bar{1}1,\ \bar{1}11$

		Value on 48 (1 1 1)
	1st order	
311	$(x+y+z)\delta_{111}+(-x+y+z)\delta_{\bar{1}11}+(x-y+z)\delta_{1\bar{1}1}$ $+(-x-y+z)\delta_{\bar{1}\bar{1}1}$	$x+y+z$
	2nd order	
321	$(x^2+y^2+z^2)\Sigma\delta_{\mu}$	$x^2+y^2+z^2$
322	$(xy+yz+zx)\delta_{111}+(-xy+yz-zx)\delta_{\bar{1}11}$ $+(xy-yz-zx)\delta_{\bar{1}\bar{1}1}+(-xy-yz+zx)\delta_{1\bar{1}1}$	$xy+yz+xz$
	3rd order	
331	$xyz(\delta_{111}+\delta_{\bar{1}\bar{1}1}-\delta_{\bar{1}11}-\delta_{1\bar{1}1})$	xyz
332	$(x+y+z)^3\delta_{111}+(-x+y+z)^3\delta_{\bar{1}11}+(x-y+z)^3\delta_{1\bar{1}1}$ $+(-x-y+z)^3\delta_{\bar{1}\bar{1}1}$	$(x+y+z)^3$
333	$x(y^2+z^2)(\delta_{111}+\delta_{1\bar{1}1}-\delta_{\bar{1}11}-\delta_{\bar{1}\bar{1}1})$ $+y(x^2+z^2)(\delta_{111}+\delta_{\bar{1}11}-\delta_{1\bar{1}1}-\delta_{\bar{1}\bar{1}1})$ $+z(x^2+y^2)(\delta_{111}+\delta_{1\bar{1}1}+\delta_{\bar{1}11}+\delta_{\bar{1}\bar{1}1})$	$[x(y^2+x^2)$ $+y(x^2+z^2)$ $+z(x^2+y^2)]$
	4th order	
341	$(x^4+y^4+z^4)\Sigma\delta_{\mu}$	$x^4+y^4+z^4$
342	$(x^2y^2+y^2z^2+z^2x^2)\Sigma\delta_{\mu}$	$x^2+y^2z^2+x^2z^2$
343	$(z^2xy+x^2yz+y^2zx)\delta_{111}+(-z^2xy+x^2yz-zxy^2)\delta_{\bar{1}11}$ $+(z^2xy-x^2yz-y^2zx)\delta_{\bar{1}\bar{1}1}+(-xyz^2-yzx^2+zxy^2)\delta_{1\bar{1}1}$	$z^2xy+x^2yz+y^2$
344	$(x+y+z)^4\delta_{111}+(-x+y+z)^4\delta_{\bar{1}11}$ $+(-x-y+z)^4\delta_{\bar{1}\bar{1}1}+(x-y+z)^4\delta_{1\bar{1}1}$	$(x+y+z)^4$

Region 4

	$\mu = 110,\ 1\bar{1}0,\ 101,\ \bar{1}01,\ 011,\ 0\bar{1}1$	Value on 48th (101)
	1st order	
411	$(x+y)\delta_{110}+(x-y)\delta_{1\bar{1}0}+(x+z)\delta_{101}-(x-z)\delta_{\bar{1}01}$ $+(y+z)\delta_{011}-(y-z)\delta_{0\bar{1}1}$	$x+z$
	2nd order	
421	$(x^2+y^2)(\ _{110}+\ _{1\bar{1}0})+(y^2+z^2)(\ _{011}+\ _{1\bar{1}0})$ $+(x^2+z^2)(\delta_{101}+\delta_{\bar{1}01})$	x^2+z^2
422	$z^2(\delta_{110}+\delta_{1\bar{1}0})+y^2(\delta_{101}+\delta_{\bar{1}01})+x^2(\delta_{011}+\delta_{0\bar{1}1})$	y^2
423	$xy(\delta_{110}-\delta_{1\bar{1}0})+xz(\delta_{101}-\delta_{\bar{1}01})+yz(\delta_{011}-\delta_{0\bar{1}1})$	xz
	3rd order	
431	$(x^3+y^3)\delta_{110}+(x^3-y^3)\delta_{1\bar{1}0}+(x^3+z^3)\delta_{101}$ $-(x^3-z^3)\delta_{\bar{1}01}+(y^3+z^3)\delta_{011}-(y^3-z^3)\delta_{0\bar{1}1}$	x^3+z^3
432	$(x(y^2+z^2)+y(x^2+z^2))\delta_{110}+(x(y^2+z^2)-y(x^2+z^2))\delta_{1\bar{1}0}$ $+(x(y^2+z^2)+z(x^2+y^2))\delta_{101}-(x(y^2+z^2)-z(x^2+y^2))\delta_{\bar{1}01}$ $+(y(x^2+z^2)+z(x^2+y^2))\delta_{011}-(y(x^2+z^2)-z(x^2+y^2))\delta_{0\bar{1}1}$	$[x(y^2+z^2)$ $+z(x^2+y^2)]$
433	$(x(z^2-y^2)+z(x^2-y^2))\delta_{101}-(x(z^2-y^2)-z(x^2-y^2))\delta_{\bar{1}01}$ $+(x(y^2-z^2)+y(x^2-z^2))\delta_{110}+(x(y^2-z^2)-y(x^2-z^2))\delta_{1\bar{1}0}$ $+(z(y^2-x^2)+y(z^2-x^2))\delta_{011}+(z(y^2-x^2)-y(z^2-x^2))\delta_{0\bar{1}1}$	$[x(z^2-y^2)$ $+z(x^2-y^2)]$
	4th order	
441	$z^4(\delta_{110}+\delta_{1\bar{1}0})+y^4(\delta_{101}+\delta_{\bar{1}01})+x^4(\delta_{011}+\delta_{0\bar{1}1})$	y^4
442	$(x^4+y^4)(\delta_{110}+\delta_{1\bar{1}0})+(x^4+z^4)(\delta_{101}+\delta_{\bar{1}01})$ $+(y^4+z^4)(\delta_{011}+\delta_{0\bar{1}1})$	x^4+
443	$z^2(x^2+y^2)(\delta_{110}+\delta_{1\bar{1}0})+y^2(x^2+z^2)(\delta_{101}+\delta_{\bar{1}01})$ $+x^2(y^2+z^2)(\delta_{011}+\delta_{0\bar{1}1})$	$y^2(x^2+z^2)$
444	$x^2y^2(\delta_{110}+\delta_{1\bar{1}0})+x^2z^2(\delta_{101}+\delta_{\bar{1}01})+y^2z^2(\delta_{011}+\delta_{0\bar{1}1})$	x^2z^2
445	$xyz^2(\delta_{110}-\delta_{1\bar{1}0})+xzy^2(\delta_{101}-\delta_{\bar{1}01})+yzx^2(\delta_{011}-\delta_{0\bar{1}1})$	xzy^2
446	$(x^3y+y^3x)(\delta_{110}-\delta_{1\bar{1}0})+(x^3z+z^3x)(\delta_{101}-\delta_{\bar{1}01})$ $+(y^3z+z^3y)(\delta_{0}\ \ -\ )$	x^3z+z^3x

Γ_{15} BASIS FUNCTIONS

Region 1		Value in Region 1 (001)	Region 6 (100)
	Zeroth order		
101	δ_{001}	1	0
	1st order		
111	$z\delta_{001}$	z	0
112	$z(\delta_{010}+\delta_{100})$	0	z
	2nd order		
121	$z^2\delta_{001}$	z^2	0
122	$(x^2+y^2)\delta_{001}$	x^2+y^2	0
123	$xz\delta_{100}+ yz\delta_{010}$	0	xz
	3rd order		
131	$z^3\delta_{001}$	z^3	0
132	$z^3(\delta_{010}+\delta_{100})$	0	z^3
133	$z(x^2+y^2)\delta_{001}$	$z(x^2+y^2)$	0
134	$z(x^2+y^2)(\delta_{010}+\delta_{100})$	0	$z(x^2+y^2)$
135	$zx^2\delta_{100}+zy^2\delta_{010}$	0	zx^2
	4th order		
141	$z^4\delta_{001}$	z^4	0
142	$z^2(x^2+y^2)\delta_{001}$	$z^2(x^2+y^2)$	0
143	$(x^4+y^4)\delta_{001}$	x^4+y^4	0
144	$x^2y^2\delta_{001}$	x^2y^2	0
145	$zx^3\delta_{100}+zy^3\delta_{010}$	0	zx^3
146	$z^3x\delta_{100}+z^3y\delta_{010}$	0	z^3x
147	$y^2xz\delta_{010} + x^2yz\delta_{100}$	0	x^2yz

Region 1 (continued)

		Value in Region 1 001	Region 6 100
	5th order		
151	$z^5\delta_{001}$	z^5	0
152	$z^5(\delta_{010}+\delta_{100})$	0	z^5
153	$z^3(x^2+y^2)\delta_{001}$	$z^3(x^2+y^2)$	0
154	$z^3(x^2+y^2)(\delta_{010}+\delta_{100})$	0	$z^3(x^2+y^2)$
155	$z(x^4+y^4)\delta_{001}$	$z(x^4+y^4)$	0
156	$z(x^4+y^4)(\delta_{100}+\delta_{010})$	0	$z(x^4+y^4)$
157	$zx^2y^2\delta_{001}$	zx^2y^2	0
158	$zx^2y^2(\delta_{100}+\delta_{010})$	0	zx^2y^2
159	$zx^4\delta_{100}+zy^4\delta_{010}$	0	zx^4
1510	$z^3x^2\delta_{100}+z^3y^2\delta_{010}$	0	z^3x^2

Region 2 μ=nearest 4-fold axis, ν=nearest 3-fold axis
μ=001,0±10,±100, ν=111,$\bar{1}$11,1$\bar{1}$1,$\bar{1}\bar{1}$1

		Region 2 (001,111)	Region 5 (100,111)
	Zeroth order		
201	$\Sigma\delta_{\mu,\nu}$ $(\mu \neq 001)$	0	1
202	$\Sigma\delta_{\mu,\nu}$ $(\mu \neq \pm 100, 0\pm 10)$	1	0
	1st order		
211	$z\Sigma\delta_{\mu,\nu}$ $(\mu \neq 001)$	0	z
212	$z\Sigma\delta_{001,\nu}$	z	0
213	$(x+y)(\delta_{001,111}-\delta_{001,\bar{1}\bar{1}1})$ $+(x-y)(\delta_{001,1\bar{1}1}-\delta_{001,\bar{1}11})$	x+y	0
214	$x(\delta_{010,111}+\delta_{0\bar{1}0,1\bar{1}1}-\delta_{0\bar{1}0,\bar{1}\bar{1}1}$ $-\delta_{010,\bar{1}11})+y(\delta_{100,111}+\delta_{\bar{1}00,\bar{1}11}$ $-\delta_{100,1\bar{1}1}-\delta_{\bar{1}00,\bar{1}\bar{1}1})$	0	x
215	$x(\delta_{100,111}-\delta_{\bar{1}00,\bar{1}\bar{1}1}+\delta_{100,1\bar{1}1}$ $-\delta_{\bar{1}00,\bar{1}11})+y(\delta_{010,111}-\delta_{0\bar{1}0,\bar{1}\bar{1}1}$ $+\delta_{010,\bar{1}11}-\delta_{0\bar{1}0,1\bar{1}1})$	0	y

Region 2 (continued)

	2nd order	Value in Region 2	Value in Region 5
221	$(x^2+y^2)\Sigma\delta_{\mu,\nu}$ ($\mu \neq 001$	0	x^2+y^2
222	$z^2\Sigma\delta_{\mu,\nu}$ ($\mu \neq 001$)	0	z^2
223	$(x^2+y^2)\Sigma\delta_{\mu,\nu}$ ($\mu \neq \pm 100, 0\pm 10$)	x^2+y^2	0
224	$z^2\Sigma\delta_{\mu,\nu}$ ($\mu \neq \pm 100, 0\pm 10$)	z^2	0
225	$x^2(\delta_{100,111}+\delta_{100,1\bar{1}1}+\delta_{\bar{1}00,\bar{1}11}+\delta_{\bar{1}00,\bar{1}\bar{1}1})+y^2(\delta_{010,111}+\delta_{010,\bar{1}11}+\delta_{0\bar{1}0,1\bar{1}1}+\delta_{0\bar{1}0,\bar{1}\bar{1}1})$	0	x^2
226	$xy(\delta_{001,111}+\delta_{001,\bar{1}\bar{1}1}-\delta_{001,\bar{1}11}-\delta_{001,1\bar{1}1})$	xy	0
227	$xy(\delta_{010,111}+\delta_{100,111}+\delta_{0\bar{1}0,\bar{1}\bar{1}1}+\delta_{\bar{1}00,\bar{1}\bar{1}1})-\delta_{010,\bar{1}11}-\delta_{100,1\bar{1}1}-\delta_{0\bar{1}0,1\bar{1}1}-\delta_{\bar{1}00,\bar{1}11})$	0	xy
228	$xz(\delta_{001,111}+\delta_{001,1\bar{1}1}-\delta_{001,\bar{1}11}-\delta_{001,\bar{1}\bar{1}1})+yz(\delta_{001,111}+\delta_{001,\bar{1}11}-\delta_{001,1\bar{1}1}-\delta_{001,\bar{1}\bar{1}1})$	xz+yz	0
229	$xz(\delta_{100,111}+\delta_{100,1\bar{1}1}-\delta_{\bar{1}00,\bar{1}11}-\delta_{\bar{1}00,\bar{1}\bar{1}1})+yz(\delta_{010,111}+\delta_{010,\bar{1}11}-\delta_{0\bar{1}0,1\bar{1}1}-\delta_{0\bar{1}0,\bar{1}\bar{1}1})$	0	xz
2210	$yz(\delta_{100,111}+\delta_{\bar{1}00,\bar{1}11}-\delta_{100,1\bar{1}1}-\delta_{\bar{1}00,\bar{1}\bar{1}1})+xz(\delta_{010,111}+\delta_{0\bar{1}0,1\bar{1}1}-\delta_{010,\bar{1}11}-\delta_{0\bar{1}0,\bar{1}\bar{1}1})$	0	yz

Region 2 (continued)

		Value in Region 2	Value in Region 5
	3rd order		
231	$z^3\Sigma\delta_{\mu\nu}$ $(\mu \neq 001)$	0	z^3
232	$z(x^2+y^2)\Sigma\delta_{\mu\nu}$ $(\mu \neq 001)$	0	$z(x^2+y^2)$
233	$z^3\Sigma\delta_{001,\nu}$	z^3	0
234	$z(x^2+y^2)\Sigma\delta_{001,\nu}$	$z(x^2+y^2)$	0
235	$z^2(x+y)(\delta_{001,111}-\delta_{001,\bar{1}\bar{1}1})$ $+z^2(x-y)(\delta_{001,1\bar{1}1}-\delta_{001,\bar{1}11})$	$z^2(x+y)$	0
236	$(x^3+y^3)(\delta_{001,111}-\delta_{001,\bar{1}\bar{1}1})$ $+(x^3-y^3)(\delta_{001,1\bar{1}1}-\delta_{001,\bar{1}11})$	x^3+y^3	0
237	$x^3(\delta_{010,111}+\delta_{0\bar{1}0,1\bar{1}1}-\delta_{0\bar{1}0,\bar{1}\bar{1}1}$ $-\delta_{010,\bar{1}11})+y^3(\delta_{100,111}+\delta_{\bar{1}00,\bar{1}11}$ $-\delta_{100,1\bar{1}1}-\delta_{\bar{1}00,\bar{1}\bar{1}1})$	0	y^3
238	$x(y^2+z^2)(\delta_{010,111}+\delta_{0\bar{1}0,111}$ $-\delta_{0\bar{1}0,\bar{1}\bar{1}1}-\delta_{010,\bar{1}11})$ $+y(x^2+z^2)(\delta_{100,111}+\delta_{\bar{1}00,\bar{1}11}$ $-\delta_{100,1\bar{1}1}-\delta_{\bar{1}00,\bar{1}\bar{1}1})$	0	$y(x^2+z^2)$
239	$x^3(\delta_{100,111}-\delta_{\bar{1}00,\bar{1}\bar{1}1}+\delta_{100,1\bar{1}1}$ $-\delta_{\bar{1}00,\bar{1}11})+y^3(\delta_{010,111}-\delta_{0\bar{1}0,\bar{1}\bar{1}1}$ $+\delta_{010,\bar{1}11}-\delta_{0\bar{1}0,1\bar{1}1})$	0	x^3
2310	$x(y^2+z^2)(\delta_{100,111}-\delta_{\bar{1}00,\bar{1}\bar{1}1}$ $+\delta_{100,1\bar{1}1}-\delta_{\bar{1}00,\bar{1}11})$ $+y(x^2+z^2)(\delta_{010,111}-\delta_{0\bar{1}0,\bar{1}\bar{1}1})$ $+\delta_{010,\bar{1}11}-\delta_{0\bar{1}0,1\bar{1}1})$	0	$x(y^2+z^2)$
2311	$z^2(x-y)[\delta_{100,111}-\delta_{010,111}$ $-\delta_{\bar{1}00,\bar{1}\bar{1}1}+\delta_{0\bar{1}0,\bar{1}11}-\delta_{\bar{1}00,\bar{1}11})$ $+z^2(x+y)(\delta_{010,\bar{1}11}-\delta_{\bar{1}00,\bar{1}11}$ $+\delta_{100,1\bar{1}1}-\delta_{0\bar{1}0,1\bar{1}1})$	0	$z^2(x-y)$

Region 2 (continued)		Value in Region 2	Value in Region 5
	3rd order (continued)		
2312	$zx^2(\delta_{100,111}+\delta_{100,1\bar{1}1}+\delta_{\bar{1}00,\bar{1}11}+\delta_{\bar{1}00,\bar{1}\bar{1}1})$ $+zy^2(\delta_{010,111}+\delta_{010,\bar{1}11}+\delta_{0\bar{1}0,\bar{1}\bar{1}1}+\delta_{0\bar{1}0,1\bar{1}1})$	0	zx^2
2313	$(xy^2+yx^2)(\delta_{001,111}-\delta_{001,\bar{1}\bar{1}1})$ $+(-xy^2-yx^2)(\delta_{001,\bar{1}11}-\delta_{001,1\bar{1}1})$	xy^2+yx^2	0
2314	$(xy^2+yx^2)(\delta_{100,111}+\delta_{010,111}-\delta_{\bar{1}00,\bar{1}\bar{1}1}-\delta_{0\bar{1}0,\bar{1}\bar{1}1})$ $+(-xy^2+yx^2)(\delta_{010,\bar{1}11}+\delta_{\bar{1}00,\bar{1}11}-\delta_{100,1\bar{1}1}-\delta_{0\bar{1}0,1\bar{1}1})$	0	xy^2+yx^2
2315	$xyz(\delta_{001,111}+\delta_{001,\bar{1}\bar{1}1}-\delta_{001,\bar{1}11}-\delta_{001,1\bar{1}1})$	xyz	0
2316	$xyz(\delta_{100,111}-\delta_{100,\bar{1}1}+\delta_{\bar{1}00,\bar{1}\bar{1}1}-\delta_{0\bar{1}0,1\bar{1}1})+\delta_{010,111}-\delta_{010,\bar{1}11}+\delta_{0\bar{1}0,\bar{1}\bar{1}1}-\delta_{0\bar{1}0,1\bar{1}1})$	0	xyz

Region 3		Value in Region 3 (111)
	Zeroth order	
301	$\Sigma\delta_\mu$	1
	1st order	
311	$z\Sigma\delta_\mu$	z
312	$(x+y)\ \delta_{111}-(x+y)\delta_{\bar{1}\bar{1}\bar{1}}+(x-y)\delta_{1\bar{1}1}+(-x+y)\delta_{\bar{1}11}$	x+y

Region 3 (continued)		Value in region 3
	2nd order	
321	$z^2\Sigma\delta_\mu$	z^2
322	$(x^2+y^2)\Sigma\delta_\mu$	x^2+y^2
323	$xy(\delta_{111}+\delta_{\bar{1}\bar{1}1}-\delta_{\bar{1}11}-\delta_{1\bar{1}1})$	xy
324	$z(x+y)(\delta_{111}-\delta_{\bar{1}\bar{1}1})+z(x-y)(\delta_{1\bar{1}1}-\delta_{\bar{1}11})$	$z(x+y)$
	3rd order	
331	$z^3\Sigma\delta_\mu$	z^3
332	$z(x^2+y^2)\Sigma\delta_\mu$	$z(x^2+y^2)$
333	$(x^3+y^3)\delta_{111}-(x^3+y^3)\delta_{\bar{1}\bar{1}1}$ $+(x^3-y^3)\delta_{1\bar{1}1}+(-x^3+y^3)\delta_{\bar{1}11}$	x^3+y^3
334	$z^2(x+y)\delta_{111}-z^2(x+y)\delta_{\bar{1}\bar{1}1}$ $+z^2(x-y)\delta_{1\bar{1}1}+z^2(-x+y)\delta_{\bar{1}11}$	$z^2(x+y)$
335	$(xy^2+yx^2)(\delta_{111}-\delta_{\bar{1}\bar{1}1})+(-xy^2+yx^2)(\delta_{\bar{1}11}-\delta_{1\bar{1}1})$	$xy(y+x)$
336	$xyz(\delta_{111}+\delta_{\bar{1}\bar{1}1}-\delta_{\bar{1}11}-\delta_{1\bar{1}1})$	xyz
	4th order	
341	$z^4\Sigma\delta_\mu$	z^4
342	$z^2(x^2+y^2)\Sigma\delta_\mu$	$z^2(x^2+y^2)$
343	$(x^4+y^4)\Sigma\delta_\mu$	x^4+y^4
344	$x^2y^2\ \Sigma\delta_\mu$	x^2y^2
345	$z^2xy(\delta_{111}+\delta_{\bar{1}\bar{1}1}-\delta_{\bar{1}11}-\delta_{1\bar{1}1})$	z^2xy
346	$(x^3y+y^3x)(\delta_{111}+\delta_{\bar{1}\bar{1}1}-\delta_{\bar{1}11}-\delta_{1\bar{1}1})$	x^3y+y^3x
347	$z(x^3+y^3)(\delta_{111}-\delta_{\bar{1}\bar{1}1})+z(x^3-y^3)(\delta_{1\bar{1}1}-\delta_{\bar{1}11})$	$z(x^3+y^3)$
348	$z^3(x+y)(\delta_{111}-\delta_{\bar{1}\bar{1}1})+z^3(x-y)(\delta_{1\bar{1}1}-\delta_{\bar{1}11})$	$z^3(x+y)$
349	$(y^2zx+x^2zy)(\delta_{111}-\delta_{\bar{1}\bar{1}1})+(y^2zx-x^2zy)(\delta_{1\bar{1}1}-\delta_{\bar{1}11})$	$xyz(x+y)$

Region 3 (continued)		Value in region 3
	5th order	
351	$z^5 \Sigma\delta_\mu$	z^5
352	$z^3(x^2+y^2)\Sigma\delta_\mu$	$z^3(x^2+y^2)$
353	$z(x^4+y^4)\Sigma\delta_\mu$	$z(x^4+y^4)$
354	$(x^5+y^5)(\delta_{111}-\delta_{\bar{1}\bar{1}1})+(x^5-y^5)(\delta_{1\bar{1}1}-\delta_{\bar{1}11})$	x^5+y^5
355	$z^2(x^3+y^3)(\delta_{111}-\delta_{\bar{1}\bar{1}1})+z^2(x^3-y^3)(\delta_{1\bar{1}1}-\delta_{\bar{1}11})$	$z^2(x^3+y^3)$
356	$z^4(x+y)(\delta_{111}-\delta_{\bar{1}\bar{1}1})+z^4(x-y)(\delta_{1\bar{1}1}-\delta_{\bar{1}11})$	$z^4(x+y)$
357	$(xy^4+yx^4)(\delta_{111}-\delta_{\bar{1}\bar{1}1})-(xy^4-yx^4)(\delta_{\bar{1}11}-\delta_{1\bar{1}1})$	xy^4+yx^4
358	$(x^3y^2+y^2x^2)(\delta_{111}-\delta_{\bar{1}\bar{1}1})-(x^3y^2-y^3x^2)(\delta_{\bar{1}11}-\delta_{1\bar{1}1})$	$x^3y^2+y^3x^2$
359	$z^2(xy^2+yx^2)(\delta_{111}-\delta_{\bar{1}\bar{1}1})-z^2(xy^2-yx^2)(\delta_{\bar{1}11}-\delta_{1\bar{1}1})$	$xyz^2(x+y)$
3510	$xyz\,(x^2+y^2+z^2)(\delta_{111}+\delta_{\bar{1}\bar{1}1}-\delta_{\bar{1}11}-\delta_{1\bar{1}1})$	$xyz(x^2+y^2+z^2)$
3511	$xyz^3(\delta_{111}+\delta_{\bar{1}\bar{1}1}-\delta_{\bar{1}11}-\delta_{1\bar{1}1})$	xyz^3
3512	$x^2y^2z\Sigma\delta_\mu$	x^2y^2z

Region 4 $\mu = 101, \bar{1}01, 110, 1\bar{1}0, 011, 0\bar{1}1$		Value in Region 4	Value in Region 7
	Zeroth order		
401	$\delta_{101}+\delta_{\bar{1}01}+\delta_{011}+\delta_{0\bar{1}1}$	1	0
	1st order		
411	$z(\delta_{101}+\delta_{\bar{1}01}+\delta_{011}+\delta_{0\bar{1}1})$	z	0
412	$z(\delta_{110}+\delta_{1\bar{1}0})$	0	z
413	$y(\delta_{011}-\delta_{0\bar{1}1})+x(\delta_{101}-\delta_{\bar{1}01})$	x	0
	2nd order		
421	$x^2(\delta_{101}+\delta_{\bar{1}01})+y^2(\delta_{011}+\delta_{0\bar{1}1})$	x^2	0
422	$(y^2+z^2)(\delta_{101}+\delta_{\bar{1}01})$ $+(x^2+z^2)(\delta_{011}+\delta_{0\bar{1}1})$	y^2	0
423	$(z^2-x^2)(\delta_{101}+\delta_{\bar{1}01})$ $+(z^2-y^2)(\delta_{011}+\delta_{0\bar{1}1})$	z^2-x^2	0
424	$xz(\delta_{101}-\delta_{\bar{1}01})+yz(\delta_{011}-\delta_{0\bar{1}1})$	xz	0
425	$z(x+y)(\delta_{110}-\delta_{\bar{1}\bar{1}0})+z(x-y)(\delta_{1\bar{1}0}-\delta_{\bar{1}10})$	0	$z(x+y)$
	3rd order		
431	$z^3(\delta_{101}+\delta_{\bar{1}01}+\delta_{011}+\delta_{0\bar{1}1})$	z^3	0
432	$z(x^2+y^2)(\delta_{101}+\delta_{\bar{1}01}+\delta_{011}+\delta_{0\bar{1}1})$	$z(x^2+y^2)$	0
433	$z^3(\delta_{110}+\delta_{1\bar{1}0})$	0	z^3
439	$z(x^2+y^2)(\delta_{110}+\delta_{1\bar{1}0})$	0	$z(x^2+y^2)$
435	$y^3(\delta_{011}-\delta_{0\bar{1}1})+x^3(\delta_{101}-\bar{1}01)$	x^3	0
436	$y(x^2+z^2)(\delta_{011}-\delta_{0\bar{1}1})$ $+x(y^2+z^2)(\delta_{101}-\delta_{\bar{1}01})$	$x(y^2+z^2)$	0
437	$zy^2(\delta_{101}+\delta_{\bar{1}01})+zx^2(\delta_{011}+\delta_{0\bar{1}1})$	zy^2	0
438	$xy^2(\delta_{101}-\delta_{\bar{1}01})+x^2y(\delta_{011}-\delta_{0\bar{1}1})$	xy^2	0
439	$xyz(\delta_{110}-\delta_{1\bar{1}0})$	0	xyz

APPENDIX IV

PROOF THAT THERMAL PHONONS ARE THE ORIGIN OF THE NEGATIVE $\delta T_c/\delta\alpha^2F(\omega)$ IN ANISOTROPIC SUPERCONDUCTORS

It is convenient to write the real part of the linearized form of eqn. (2-32) in the following way (using the identity (2-30) to express $\mathrm{Im}\Delta k(\omega)$ in terms of Re $\Delta_{\underline{k}}(\omega)$):

$$\tilde{\rho}(T)\,\frac{\mathrm{Re}\,\Delta_{\underline{k}}(\omega)}{\omega} = \int \frac{dS_{\underline{k}'}}{|v_{\underline{k}'}|}\int_{-\infty}^{\infty} d\omega' \Big[\int_0^{\infty} d\Omega\,(\alpha^2F(\Omega))_{\underline{k}\underline{k}'}\,(f(-\omega')+n(\Omega))$$

$$\Big(\frac{1}{\omega'+\Omega+\omega}+\frac{1}{\omega'+\Omega-\omega}\Big)$$

$$-\frac{1}{2}\,\mu^*\tanh\frac{\omega'}{2k_BT_c}\Big]\mathrm{Re}\,\frac{\Delta_{\underline{k}'}(\omega')}{\omega'} - \mathrm{Re}\Big(\frac{\Delta_{\underline{k}}(\omega)}{\omega}\Big)\mathrm{Re}\,(\omega Z_{\underline{k}}(\omega))$$

$$+\frac{1}{\pi}\,\mathrm{Im}\,(\omega Z_{\underline{k}}(\omega))\int_{-\infty}^{\infty} d\omega'\,\frac{\mathrm{Re}\,\Delta_{\underline{k}}(\omega')/\omega'}{\omega'-\omega} \qquad \text{(IV-1)}$$

where

$$\omega Z_{\underline{k}}(\omega) = \omega - \int \frac{dS_{\underline{k}'}}{|v_{\underline{k}'}|}\Big[\int_0^{\infty} d\Omega\,(\alpha^2F(\Omega))_{\underline{k}\underline{k}'}\int_{-\infty}^{\infty} d\omega''\,(n(\Omega)+f(-\omega''))$$

$$\Big(\frac{1}{\omega''+\Omega+\omega+i\delta}-\frac{1}{\omega''+\Omega-\omega-i\delta}\Big) \qquad \text{(IV-2)}$$

and as usual, only the variation in the eigenvalue which passes through zero at T_c will be considered. Eqn. (IV-1) is of the form

$$\tilde{\rho}(T)\,\mathrm{Re}\,\frac{\Delta_{\underline{k}}(\omega)}{\omega} = \int \frac{dS_{\underline{k}'}}{|v_{\underline{k}'}|} \int_{\infty}^{\infty} d\omega'\ \mathrm{Re}\,\frac{\Delta_{\underline{k}'}(\omega')}{\omega'} \sum_{i=1}^{3} K^{(i)}_{\underline{k}\underline{k}'}(\omega,\omega') \qquad \text{(IV-3)}$$

where

$$K^{(1)}_{\underline{k}\underline{k}'}(\omega,\omega') = \int_0^{\infty} d\Omega\,(\alpha^2F(\Omega))_{\underline{k}\underline{k}'}\,(f(-\omega')+n(\Omega))\left(\frac{1}{\omega'+\Omega+\omega}+\frac{1}{\omega'+\Omega-\omega}\right)$$

$$-\frac{1}{2}\,\mu^*\tanh\frac{\omega'}{2k_BT_c}$$

$$K^{(2)}_{\underline{k}\underline{k}'}(\omega,\omega') = -\delta(\omega-\omega')\,\delta(\underline{k}-\underline{k}')\,\mathrm{Re}(\omega Z_{\underline{k}}(\omega))$$

$$K^{(3)}_{\underline{k}\underline{k}'}(\omega,\omega') = \frac{1}{\pi}\,\delta(\underline{k}-\underline{k}')\,\frac{\mathrm{Im}(Z_{\underline{k}}(\omega))}{\omega'-\omega}\,.$$

From the theory of homogeneous Fredholm equations of the second kind it follows that the infinitesimal change in T_c due to a variation of the kernel is proportional to

$$\int_{-\infty}^{\infty} d\omega \int_{-\infty}^{\infty} d\omega' \int \frac{dS_{\underline{k}}}{|v_{\underline{k}}|} \int \frac{dS_{\underline{k}'}}{|v_{\underline{k}'}|}\,\hat{\Delta}_{\underline{k}}(\omega) \sum_{i=1}^{3} \delta K^{(i)}_{\underline{k}\underline{k}}(\omega,\omega')\ \mathrm{Re}\,\frac{\bar{\Delta}_{\underline{k}'}(\omega')}{\omega'} \qquad \text{(IV-4)}$$

where $\hat{\Delta}_{\underline{k}}(\omega)$ is the solution of the adjoint of eqn. (IV-1), and a denominator $(\partial\tilde{\rho}/\partial T)_{T_c}$ has been omitted.

If $\delta(\alpha^2F(\omega))_{\underline{k}\underline{k}'} = \varepsilon\,\delta(\omega-\omega_0)$, then

$$\delta K^{(1)}_{\underline{k}\underline{k}'}(\omega,\omega') = (f(-\omega')+n(\omega_0))\left(\frac{1}{\omega'+\omega_0+\omega}+\frac{1}{\omega'+\omega_0-\omega}\right) \qquad \text{(IV-5)}$$

$$\delta K^{(2)}_{\underline{k}\underline{k}'}(\omega,\omega') = \delta(\omega-\omega')\,\delta(\underline{k}-\underline{k}')\int_{-\infty}^{\infty} d\omega''\,(f(-\omega'')+n(\omega_0))\left(\frac{1}{\omega''+\omega_0+\omega} - \frac{1}{\omega''+\omega_0-\omega}\right) \tag{IV-6}$$

and

$$\delta K^{(3)}_{\underline{k}\underline{k}'}(\omega,\omega') = \frac{1}{\pi}\,\delta(\underline{k}-\underline{k}')\int_{\infty}^{\infty} d\omega''\,(f(-\omega'')+n(\omega_0))\,(-\pi\delta(\omega''+\omega_0+\omega) - \pi\delta(\omega''+\omega_0-\omega))/(\omega'-\omega)$$

$$= -\delta(\underline{k}-\underline{k}')\,(2n(\omega_0)+f(\omega+\omega_0)+f(\omega_0-\omega))/(\omega'-\omega)\,. \tag{IV-7}$$

In eqns. (IV-6) and (IV-7) the identity

$$\frac{1}{\omega+i\delta} = -i\pi\delta(\omega) + P\,\frac{1}{\omega}$$

was used.

At this stage the limit $\omega_0/k_B T_c \to 0$ can be taken, since it is now clear how $\Sigma K^{(i)}$ can be expanded in powers of ω_0 ; in particular, it is obvious that the only source of terms proportional to ω_0^{-1} is $n(\omega_0)$, as was to be proved. There are no other inverse powers of ω_0 present.

The mathematical methods used here differ significantly from those pioneered by Appel[13] for isotropic superconductors. He did not introduce an eigenvalue $\tilde{\rho}(T)$ explicitly, working directly with T_c instead, and chose a different kernel:

$$\mathrm{Re}\{Z^{-1}(\omega)K^{(1)}(\omega+i\delta,\omega')\}.$$

Since $\delta \mathrm{Re} Z^{-1}(\omega)$ and $\delta \mathrm{Im} Z^{-1}(\omega)$ were very awkward to evaluate, he approximated them in such a way that the low-frequency phonons did not cancel out, leading to an incorrect functional derivative that turned negative as in an anisotropic superconductor instead of going linearly to zero.

BIBLIOGRAPHY

1. P. B. Allen, Phys. Rev. 13, 1416-27 (1976).
2. C. Chou, D. White and H. L. Johnston, Phys. Rev. 109, 788-796 (1958).
3. H. A. Leupold and H. A. Boorse, Phys. Rev. 134, A1322-8 (1964).
4. S. Alterovitz, Phys. Rev. 13, B121-5 (1976).
5. L. J. Vieland and A. W. Wicklund, Phys. Rev. 166, 424-31 (1968).
6. J. E. Neighbor, J. F. Cochran and C. A. Shiffman, Phys. Rev. 155, 384-7 (1967).
7. R. W. Shaw, D. E. Mapother and D. C. Hopkins, Phys. Rev. 120, 88-91 (1960).
8. M. Ishikawa and L. E. Toth, Phys. Rev. B 1856-61 (1971).
9. J. R. Anderson and A. V. Gold, Phys. Rev. 139, A1459 (1963).
10. P. W. Anderson, J. Phys. Chem. Solids 11, 26-30 (1959).
11. H. R. O'Neal and N. E. Phillips, Phys. Rev. 137, A748-59 (1965).
12. M. Appapillai and A. R. Williams, J. Phys. F3 (1973).
13. J. Appel, Phys. Rev. 156, 421-32 (1967).
14. J. Bardeen and M. Stephen, Phys. Rev. 136, A1485-7 (1964).
15. G. Bergmann and D. Rainer, Z. Phys. 263, 59-68 (1973).

16. J. L. Bostock and M. L. A. MacVicar, Proceedings of the international discussion meeting held at Vienna (1976). ed. H. W. Weber, Plenum Press, New York (1977).

17. L. P. Bouckaert, R. Smoluchowski and E. Wigner, Phys. Rev. 50, 58-67 (1936).

18. W. H. Butler, P. B. Allen, Proceedings of the second Rochester Conference on d- and f-band Metals, ed. D. H. Douglass, Plenum Press, New York, pp 73-121 (1976).

19. W. S. Corak and C. B. Satterthwaite, Phys. Rev. 102, 662-6 (1956).

20. G. V. Chester, Phys. Rev. 103, 1693-99 (1956).

21. J. R. Clem, Phys. Rev. 148, 392-401 (1966).

22. J. R. Clem, Annals of Physics 40, 268-95 (1966).

23. E. R. Cowley, Sol. St. Comm. 14, 587 (1964).

24. G. M. Eliashberg, JETP 43, 1005-7 (1962).

25. N. L. Muench, Phys. Rev. 99, 1814-20 (1955).

26. D. E. Farrell and B. S. Chandrasekhar, Phys. Rev. Lett. 38, 788-91 (1977).

27. T. F. Stromberg and C. A. Swenson, Phys. Rev. Lett. 9, 370-4 (1962).

28. M. D. Fiske, J. Phys. Chem. Solids 2, 191-8 (1957).

29. W. R. Fehlner and S. H. Vosko, Can. J. Phys. 54, 2159-69 (1976).

30. E. Maxwell and O. S. Lutes, Phys. Rev. 95, 333-8 (1954).

31. H. Gamari-Searle and B. R. Coles, Proc. Phys. Soc. 86, 1199-1204 (1965).

32. D. U. Gubser, Phys. Rev. B6, 827-31 (1972).

33. C. R. Leavens, Sol. State Comm. 17, 1499-1504 (1975).

34. C. R. Leavens and J. P. Carbotte, J. Low Temp. Phys. 14, 195-211 (1974).

35. C. R. Leavens, J. Phys. F (Metal Phys.) 7, 1911-22 (1977).

36 D. Markowitz and L. P. Kadanoff, Phys. Rev. 131, 563-75 (1963).

37. J. E. Schirber and C. A. Swenson, Phys. Rev. 123, 115-22 (1961).

38. C. H. Hinrichs and C. A. Swenson, Phys. Rev. 123, 1106-14 (1961).

39. B. J. C. van der Hoeven, Jr. and P. H. Keesom, Phys. Rev. 135, A631-7 (1964).

40. D. K. Finnemore and D. E. Mapother, Phys. Rev. 140, A507-18 (1965).

41. Superconductivity, ed. R. D. Parks, Marcel Dekker Inc. New York (1969).

42. D. K. Finnemore, D. E. Mapother and R. W. Shaw, Phys. Rev. 118, 127-9 (1960).

43. J. F. Cochran, Annals of Physics 19, 186-218 (1962).

44. B. M. Powell, P. Martel and A.D.B. Woods, Can. J. Phys. 55, 1601 (1977).

45. C. A. Bryant and P. H. Keesom, Phys. Rev. 123, 491-9 (1961).

46. V. Novotny and P. P. M. Meincke, J. Low Temp. Phys. 18, 147-57 (1975).

47. D. K. Finnemore, T. F. Stromberg and C. A. Swenson, Phys. Rev. 149, 231-43 (1966).

48. G. Chanin and J. P. Torre, Phys. Rev. B5, 4357-64 (1972).

49. D. Rainer and G. Bergmann, J. Low Temp. Phys. 14, 501-19 (1974).

50. G. Rickayzen, Theory of Superconductivity, John Wiley and Sons Inc. (1965).

51. A. Brown, M. W. Zemansky and H. A. Boorse, Phys. Rev. 92, 52-8 (1953).

52. C. A. Shiffman, J. F. Cochran and M. Garber, J. Phys. Chem. Solids 24, 1369-73 (1963).

53. J. Ferreira da Silva, E. A. Burgemeister and Z. Dokoupil, Physica 41, 409-39 (1969).

54. T. Ohtsuka and Y. Kimura, Physica 55, 562-70 (1971).

55. J. M. Corsan and A. J. Cook, Phys. Letters 28A, 500-01 (1969).

56. Scalapino and Wilkins, in Ref. 41.

57. H. Suhl, B. T. Matthias and L. R. Walker, Phys. Rev. Lett. 3, 552 (1959).

58. C. Guo-Kuang, L. Ti-Hang and K. Wei-Yen, Acta Physica 21 (1965).

59. R. D. Worley, M. W. Zemansky and H. A. Boorse, Phys. Rev. 99, 447-58 (1955).

60. D. White, C. Chou and H. L. Johnston, Phys. Rev. 109, 797-802 (1958).

61. R. A. French, Cryogenics 8, 301-8 (1968).

62. P. G. Tomlinson and J. P. Carbotte, Phys. Rev. B13, 4738-44 (1976).

63. J. I. Budnick, Phys. Rev. 119, 1578-86 (1960).

64. J. E. Gueths, C. A. Reynolds and M. A. Mitchell, Phys. Rev. 150, 346-55 (1966).

65. J. R. Clement and E. H. Quinnell, Phys. Rev. 92, 258-67 (1953).

66. H. Rohrer, Helv. Phys. Acta 33, 675-705 (1960).

67. T. Tsuneto, Prog. Theor. Phys. 28, 857-69 (1962).

68. H. J. Vidberg and J. W. Serene , private communication.

69. P. Hohenberg, Sov. Phys. JETP 18, 834-9 (1964).

70. M. D. Reeber, Phys. Rev. Lett. 4, 198 (1960).

71. R. W. Shaw, Phys. Rev. 174, 769 (1968).

72. H. Suhl, B. T. Matthias and L. R. Walker, Phys. Rev. Lett. 3, 552- (1959).

73. P. G. Tomlinson and J.P. Carbotte, Phys. Rev. B13, 4738-44 (1976).

74. D.L. Decker, D. E. Mapother and R.W. Shaw, Phys. Rev. 112 1888 (1958).

75. J. R. Clement and E. H. Quinnell, Phys. Rev. 85, 502 (1952).

76. R. Viswanathan, H. L. Luo and L. J. Vieland, Proc. LT 13 Low Temperature Physics Conference, 472-4 (1974).

77. T. Tsuneto, Prog. Theor. Phys. 28, 857-69 (1962).

78. H. J. Vidberg, J. W. Serene, private communication.

79. Y. Wada, Phys. Rev. 135, A1481-97 (1964).

80. P. G. Tomlinson and J. P. Carbotte, Can. J. Phys. 55, 751 (1977).

81. A. J. Bennett, Phys. Rev. 140, A1902 (1965).

82. M. Peter, J. Ashkenazi and M. Dacorogna, Helvetica Physica Acta, 50, 267-78 (1977).

83. A. G. Sheplev, Soviet Physics USPEKHI 11, 690-711 (1969).

84. L. Yun Lung Shen, N. M. Senozan and N. E. Phillips, Phys. Rev. Lett. 14, 1205-6 (1965).

85. M. L. A. MacVicar and R. M. Rose, J. Applied Phys. 39, 1721-7 (1968).

86. G. J. Sellers, A. C. Anderson and H. K. Birnbaum, Phys. Letters, 44A, 173-4 (1973).

87. B. Mühlschlegel, Z. Phys. 155, 313 (1959).

88. C. R. Leavens, Solid State Comm. 15, 1329-32 (1974).

89. H. A. Boorse, A. T. Hirschfeld and H. Leupold, Phys. Rev. Lett. 5, 246 (1960).

90. C. A. Bryant and P. H. Keesom, Phys. Rev. Lett. 4, 460 (1960).

91. W. H. Butler, H. G. Smith and N. Wakabayashi, Phys. Rev. Lett. 39, 1004-7 (1977).

92. J. Bostock, W. N. Cheung, R. M. Rose and M.L. A. MacVicar, To appear in Proc. of the Int. Conf. on Transition Metals, (Toronto) (1977).

93. B. M. Powell, P. Martel and A. D. B. Woods, Phys. Rev. 171, 727 (1968).

94. R. Carin, P. Goy, R. Herrmann and S. Hess, preprint.

95. G. Grimvall, Physica Scripta 14, 63-78 (1976).

96. H. K. Leung, J. P. Carbotte, D. W. Taylor and C. R. Leavens, J. Low Temp. Phys. 24, 25-34 (1976).

97. P. Horsch and H. Rietschel, Z. Phys. 27, 153-160 (1977).

98. M. Gurtvitch, A. K. Ghosh, C. L. Snead and M. Strongin, Phys. Rev. Lett. 39, 1102-3 (1977).

99. B.C.J. van der Hoeven and P. H. Keesom, Phys. Rev. 134, A1320-1 (1964).

100. A. T. Hirshfeld, H. A. Leupold and H. A. Boorse, Phys. Rev. 127, 1501-7 (1962).

101. C. R. Leavens and J. P. Carbotte, Annals of Phys. 70, 338-76 (1972).

102. J. P. Carbotte, Proceedings of LT13 Low Temperature Physics Conference, 587-98 (1974).

103. R. S. Sorbello, J. Phys. F4, 503 (1974); J. Phys. F4, 1665 (1974).

104. J. Daams and J. P. Carbotte, submitted to Can. J. Phys.

105. D. Rainer, private communication.

106. H. Widom, Lectures on Integral Equations, Van Nostrand Reinhold (1969) pg. 23

107. M. Tinkham, Group Theory and Quantum Mechanics, McGraw-Hill (1964).

108. M. J. Zuckerman and D. M. Brink, Phys. Lett. 4, 76 (1963).

109. D. E. Mapother, Phys. Rev. 126, 2021-9 (1962).